THE ENVIRONMENTS OF RADIO GALAXIES

Richard Martin Prestage

Presented for the Degree of Doctor of Philosophy

at the University of Edinburgh

February 1985

This thesis has been composed by myself and consists entirely of my own work except where specifically indicated in the text.

ABSTRACT

An investigation into the environments of a large number of radio galaxies is described. These are drawn from radio complete samples, with no initial knowledge of source environment required. Instead, an objective method is used to parameterise this quantity, which is then compared with the sources' radio and optical properties.

The main source of objects is an all-sky sample, defined at high frequency, which provides an opportunity to investigate some less well studied members of the radio-source population. As a preliminary study, U.K. Schmidt plates are used to look for optical counterparts for 34 sample members, which have no reliable identifications. VLA observations are made of 71 sources, comprising all objects between $+10^{\circ} > \delta > -46^{\circ}$ which are not known to be compact. These data allow unambiguous morphological classifications to be made for the lower-redshift sources for which clustering analyses are performed.

The environment parameter used is the angular cross-correlation amplitude, corrected for the effects of redshift using the galaxy luminosity function. Results for radio sources correlated with the Lick counts are presented; for a number of objects deeper U.K. Schmidt material is also considered. Particular attention is paid to the origin and magnitude of possible sources of error in the measurement of cluster strength.

Compact sources are found not to appear in regions of enhanced galaxy density. This is stong evidence against 'unified' models for these objects. For extended sources, there is a correlation between the local galaxy density and the radio structure. FRI galaxies appear in regions of generally enhanced galaxy density. FRII sources are typically found in environments similar to those of "ordinary" members of the galaxy population, although some FRII sources do appear in richer environments. In terms of local environment there is no definite distinction between the classical and non-classical double sources.

Surface photometry of 29 sample members is presented and discussed. Both the total magnitude and the optical structure of a source are found to be closely related to its local environment. FRI galaxies, in rich environments, are bright and have large characteristic sizes, while FRII galaxies are fainter and less extended. A number of good examples of mergers are found, and in each case the associated radio structure is of type FRI. Correlations with optical spectral type are also presented.

The implications of these results for the morphology of radio galaxies is discussed.

ACKNOWLEDGEMENTS

I would particularly like to thank John Peacock, my supervisor, for his constant advice, encouragement and enthusiasm throughout the course of this project.

The observations described in Chapters Three and Six were made in conjunction with John Peacock and Simon Lilly respectively. I would like to thank them both for their friendly collaboration, and for introducing me to the art of making radio and optical observations. I acknowledge the U.S. National Radio Astronomy Observatory for the allocation of time to perform the VLA observations, and also PATT for observing time on the AAT.

The work described in Chapters Two and Five could not have been performed without the excellent facilities of the U.K. Schmidt Unit, and I would like to thank all involved in the provision of the plate material and running of the plate library. Thanks must go to Sue Tritton, for her advice and assistance in image classification; and of course to the staff of the COSMOS measuring machine, for providing the data for analysis. I am also grateful to Paul Hewett, for his endless patience and advice, in all COSMOS matters and in the field of Schmidt plates and correlation functions in general.

My thanks are due to the many people who helped with computing matters, and especially to Steve Heathcote and Colin Aspin, who provided two excellent graphics packages, and answered many calls to amend them.

Finally, I would like to thank all the people not mentioned above who gave me advice, assistance and encouragement during the course of this thesis; in particular Malcolm Longair, Lance Miller, Gerry Gilmore, and Philip Godwin.

CONTENTS

Chapter 1 : INTRODUCTION

There have been many investigations into the properties of radio sources in recent years. These have grown, from initial investigations into a narrow sub-set of the properties (e.g. radio structure and luminosity; Fanaroff and Riley 1974), to investigations into many more and varied aspects of the radio source population (e.g. total radio and optical luminosities, nuclear radio and X-ray luminosities, optical line strengths and optical colours; Fabbiano et al. 1984). The results of these studies have been the discovery of a number of correlations, found over a wide range of both physical scale and observing frequency. Many of these correlations, such as, for example, that between the presence of optical emission lines (from regions of physical extent ~ tens of kpc) and the radio structure (hundreds of kpc in size), are not obviously due to a simple direct relation. Links between properties such as these are commonly thought to be due to the nature of the 'central engine' of the source, conventionally a massive black hole, which in this case provides both the non-thermal ionising radiation responsible for the emission lines, and the energy supply to the radio lobes. The question then to be answered is how conditions outside the central nucleus can modify the basic phenomenon in such a way as to cause the range of properties which we see. It is becoming apparent that much of this modification may be due to interactions of the host galaxy with its immediate environment, either by the mediation of an inter-galactic medium (IGM), or directly via interactions with close neighbours.

To further our understanding of these effects, a quantitative measure of the local environment of a large number of radio sources is clearly required. The majority of the work described in this

thesis has been to provide such a quantity, and to consider in detail its relationship to other properties, for members of a large sample of radio galaxies.

In the remainder of this chapter, a more detailed discussion of topics relevant to this thesis is given. In particular, since radio structure is one of the primary properties under consideration, the classification scheme for this quantity is presented. The optical spectra of radio galaxies are probably the most readily available indicator as to the nuclear properties of these objects, and have been used as such here; a brief description of the study most relevant to this work - that of Hine and Longair (1979) - is also given. Then follows a consideration of previous investigations into the local environment of radio sources, together with a brief discussion of the interpretation of the findings. In the light of all of the above, the main aims of the thesis are presented, together with the layout of the remaining chapters. Finally, the main samples of radio sources used here are described.

1.1 : Radio Source Structure

The structure of a radio source is clearly one of its most basic properties; a detailed discussion is given by Miley (1980). Briefly, the main characteristics are as follows.

The majority of powerful radio sources, selected at low frequency, exhibit a double structure, with radio emission emanating from two components, symmetrically disposed with respect to the parent galaxy (or quasar), and with roughly the same intensity in each 'lobe'. The typical component separation in these objects is of the order of 100 to 500kpc, although some sources are as large as

6Mpc in extent. Often, one or both source components contains a compact 'hot-spot', usually situated towards its leading edge. These hot-spots have typical physical sizes ~ 10kpc, and thus are not nearly as compact as the milliarcsecond sources found within galactic nuclei. Hot-spots are generally found in the most powerful sources, and are relatively weaker or absent in intrinsically weak objects. Many double sources also posess a compact 'core', with a flat spectrum, associated with the galactic nucleus or quasar. In some cases, radio jets are observed extending from this nucleus towards one of the radio lobes.

As well as the these simple double sources, more complex radio morphologies are found. These include 'bent double' sources, and sources which exhibit double structure, but in which the peaks of surface brightness are found nearer the centre of the source. Also found are 'radio-trail' sources, in which the bulk of the emission originates from an extended trail, extending like a 'wake' behind the associated galaxy.

Finally, there are the 'compact' sources. An operational definition for these objects is that they are less than one arcsec in size, and hence information on their structure comes generally from VLBI, and studies of their spectra and variablility. In angular size, they range from less than 10^{-3} arcsec, and there is often evidence for structure on a variety of scales. Many of these sources have flat high-frequency spectra, are of angular size $\theta \sim 10^{-3}$ arcsec, and exhibit synchrotron self-absorption at frequencies $\nu > 1$GHz. Due to their flat spectra, this class of source is much better represented in surveys made at higher frequencies.

Quantitative methods to parameterise radio source structure are hard to formulate, due both to the difficulty of application (where

available data have a wide range of dynamic range and linear resolution), and to the intrinsically large range in source structure. A convenient classification system was however introduced by Fanaroff and Riley (1974) with the intention of distinguishing double sources from the more complex sources. Their definition is based on the linear separation of the regions of highest brightness on opposite sides of the central galaxy (or quasar), compared to the total extent of the source measured from the lowest contour; any central component being excluded. If this ratio is greater than 0.5, the source is classified as class II (FRII), otherwise it is class I (FRI). This definition clearly depends upon the angular resolution and sensitivity of available structural information; it is usually reasonably unambiguous however, and is operational in separating the more complex sources.

When compared to total radio luminosity, Fanaroff and Riley found a striking division by FR class; all the lower luminosity sources ($P_{178} < 2 \times 10^{25} WHz^{-1}sr^{-1}$) from a sample of 3CR radio sources fell into the FRI class, while essentially all the more powerful sources were classified as FRII. This division remains one of the strongest correlations between radio source properties, although it is not strictly obeyed by all sources (see for example Fig. 4.11).

Within class II, it is often useful to make a further distinction between those sources in which the radio maxima take the form of intense hot-spots at the leading edges of the radio lobes, and those in which they do not. The former are often termed 'classical double' sources (see e.g. Longair and Riley 1979), with the 'others' consisting of sources with only ill-defined hot-spots, hot-spots in only one lobe, and so on. While this classification is not as quantitative as the FR classification it is a useful distinction to make; classical double sources are the objects which

provide the most extreme physical conditions which models must explain. Unfortunately, the FRII/classical double descriptions are frequently used interchangeably (compare for example the classifications used in the studies of Longair and Seldner, 1979, and Stocke, 1979), with the result that the precise definition implied is not clear. We will use these terms strictly according to the definitions given above (although note that the classical/non-classical double classification is often difficult to make). The majority of the investigations described below consider simply the FR class of the source, although the classical doubles are often the most extreme members of the FRII category.

1.2 : The Optical Spectra of Radio Galaxies

It has been noted that strong emission-line spectra are found much more frequently amongst powerful radio galaxies (e.g. 3CR) than is the case for normal galaxies. Much work has been devoted to investigating the optical spectra of these systems; their general properties, and their relationship to other active nuclei (e.g. Seyfert galaxies) are now fairly well known (see e.g. Osterbrock, 1978). This is obviously one property of the radio source which might be expected to reveal many clues as to the physical processes occuring in these systems. Unfortunately, many of the spectra available for large samples of radio galaxies are without absolute line-strengths, or are even confined to those simply taken to obtain redshifts. This has made it difficult to perform quantitative studies of such samples, and the majority of investigations made so far have been qualitative only.

One of the first studies of this sort was that of Hine and Longair (1979). They studied a complete sample of 76 3CR radio

galaxies, comprising essentially all sources with $V < 19.5$, $S_{178} > 9$ Jy, and $\delta > 10^{o}$. These galaxies were classified spectroscopically on the basis of information in the literature into two classes, A and B. Class A galaxies exhibit strong [OII]3727 emission lines; many also show other strong lines such as [OIII]5007 and [NeIII]3869. These galaxies show many similarities to the Seyfert galaxies; approximately two-thirds have narrow emission line widths $\sim 500 kms^{-1}$ (as Type 2 Seyferts), while the remainder have broad emission lines similar to Type 1 Seyfert galaxies. Class B galaxies are defined as having only the weak absorption-line spectra typical of giant elliptical galaxies, or else very weak [OII]3727 lines. It should be noted that this classification was made in a subjective manner; it is likely that some galaxies classified on the basis of more recent spectral information would be placed in a different spectral class (e.g. see Fabbiano et al. 1984).

Hine and Longair found in their sample a correlation between the percentage of galaxies with class A spectra and redshift, in the sense that the fraction of galaxies showing strong emission lines increased with redshift. After a careful consideration of possible selection effects they concluded that this was a real effect, and was hence caused by a correlation with radio luminosity. They investigated this and correlations with other properties in the sample, with the following results.

A) Class A galaxies are stronger radio emitters than class B galaxies. Specifically, for low radio luminosities, only 10-15% of radio galaxies exhibit strong emission line spectra, whilst at the highest radio luminosities, this fraction reaches ~ 70%.

B) There is no correlation between the radio luminosity of the central component and the spectral class, apart from that introduced by result A. Nor is there an independent correlation between the relative intensity of the core and the spectral type. However, for

class A galaxies, sources with the broadest lines have the greatest fraction of their radio luminosity in the central component.

C) Class A radio galaxies are almost exclusively associated with classical double sources, whereas class B objects can be associated with radio morphology of all types, including classical double structure.

These results have a natural interpretation in the 'beam model' of radio sources (e.g. Blandford and Rees, 1974). In this model, collimated jets from the nucleus supply energy to the distant 'working-surfaces', where the beams interact with the ambient inter-galactic medium. The energy is converted here into relativistic electrons; the synchrotron emission from these regions is seen as the intense hot-spots. These relativistic electrons subsequently expand laterally, to form the diffuse 'tail regions' around the hot-spots, so that for there to be a significant probability of observing the hot-spots, there must be a continuous flow of energy from the nucleus. Hine and Longair suggest that sources which have the greatest rate of energy supply from the nucleus (as evidenced by high-luminosity hot-spots) will also exhibit more strongly other forms of nuclear activity - e.g. optical emission lines. Sources with strong central radio components might also be expected to have greater non-thermal optical and ultraviolet radiation, resulting in ejection of material from the nucleus with greater velocities, and also in increased turbulant motions. This would explain the greater breadth of the permitted recombination lines in these objects. Alternatively, the stronger central radio components might require higher gas pressures to collimate the beams of relativistic material from the nucleus. If part of this confinement was associated with ram pressure, then higher velocities might be associated with the dynamics of these clouds.

The third result, that essentially all galaxies with class A spectra are associated with classical double sources is perhaps the most difficult to explain. Hine and Longair interpret this as evidence that the structure in the nucleus must be maintained throughout the life-time of the system. Coupling this with the requirement of a continuous, collimated beam supplying energy to the outer components suggests that in these systems a steady state has been reached, which persists for periods of longer than 10^7 years. Hine and Longair speculate that this may be possible only for the most massive radio galaxies.

1.3 : The Local Environment of Radio Galaxies

Initial analyses of the local environment of radio galaxies concentrated upon sources for which this quantity was already known - e.g. those found in Zwicky and Abell clusters. Investigations such as these (Burns and Owen, 1977; McHardy, 1979) lead to the conclusion that sources found within clusters generally came from the morphologically more complex, lower-luminosity end of the population. These studies had the drawback, however, that they did not consider systematically the cluster environments of sources drawn from complete and unbiassed radio samples. One of the first attempts to approach the problem from this angle was that of Longair and Seldner, (LS; 1979). In their study, LS used the amplitude of the cross-correlation function of galaxies about a radio source to parameterise its 'cluster environment'. They were then able to correlate this amplitude with other source properties, for objects drawn from a well-defined sample. The main results of this work were as follows:

A) Weak radio galaxies ($P_{178} \sim 10^{22} - 10^{24}$ WHz^{-1}sr^{-1}) exhibit clustering properties similar to that found for galaxies in general;

i.e. there is no evidence that they are anything other than random members of the normal galaxy population.

B) The average clustering of galaxies about radio galaxies having $P_{178} \sim 10^{24} - 10^{25}$ WHz^{-1}sr^{-1} is about a factor of 4-5 greater than that for galaxies in general. These sources lie at the lower end of the luminosity range associated with extended, powerful radio sources and exhibit FRI morphology.

C) The most luminous radio galaxies, with FRII morphology, also lie in regions of enhanced galaxy density, but with enhancements only ~ twice that of galaxies in general. However, when split into 'classical-doubles' and 'non-classical doubles', this result appears due to the non-classical doubles (with enhancement factors ~ 4); the classical double radio galaxies do not appear to lie in regions of enhanced galaxy density. As discussed by Hine and Longair, these are the sources which also exhibit strong emission-line spectra. (It should be noted here that this result is based on a small number of high-reshift sources, and so must be considered very uncertain.)

At first sight, these results again appear to form a consistent picture for the radio source phenomenon. The weakest radio emitters may be considered simply as normal galaxies, with supernovae rates sufficiently great to result in 10-100 times as much radio emission as our own Galaxy. There would then be no reason for them to exhibit any abnormal clustering properties. The occurence of extended radio sources must depend upon the presence of some ambient medium, since this is required to provide the working surface with which the beams interact. It is therefore not suprising that these sources do appear to belong to regions of enhanced galaxy density, since it is known that the density of the IGM is high in these regions.

How then do we explain the suggestion that classical double sources do not appear in these regions of enhanced galaxy density?

Longair and Seldner suggest that these objects are galaxies that are sufficiently massive to contain their own extended gaseous atmospheres in their own gravitational potential wells. In this case it must be the accretion of the galaxy's own atmosphere onto the nucleus which provides the fuel for the energy source. The absence of these systems in rich clusters is presumably then due to the motion of the galaxy with respect to the centre of mass of the cluster. The motion will disrupt the collimated flow of relativistic material, and hence result in the production of a more complex source. This picture provides an alternative explanation of the result of Hine and Longair. In this case, the powerful double sources' own atmosphere provides the gas responsible for the emission lines. Ram pressure sweeping by the intra-cluster gas would then explain the absence of these lines in cluster sources.

The work of Longair and Seldner has a number of drawbacks, however. Chief amongst these, as discussed by LS, is the small number of sources used in the analysis. The results for radio galaxies of various morphological types depends upon only 27 sources, of which only 15 are FRIIs. Thus, in any event, confirmation with a larger number of sources is desirable.

In addition however, there is the possibility of a number of systematic effects in the analysis. In calculating the correlation function amplitude, LS used an assumed power-law slope of $\gamma = 1.77$, and a constant angular counting radius of 1 degree. Recent results for other types of radio source suggest that a larger value for the power-law index might be appropriate. If so, the use of an incorrect value of γ would lead to a systematic error in the observed correlation amplitude with redshift. Also, since the variation in metric radius corresponding to $\theta = 1^{o}$ between $z = 0.02 - 0.1$ is large, different physical areas are being sampled in each case.

Since redshift is correlated with morpholgical type, these effects may lead to a systematic difference in the mean value for different types of radio galaxy.

Whether or not these effects are present, there is one further point not discussed in detail by LS. This is the possibility that a specific type of radio source might appear in a range of cluster environments. This must be true to some extent since, for example, some powerful double sources (e.g. Cygnus A, 3C295) are known to lie in rich clusters. If this is the case, this has serious implications for the straightforward interpretation of the results discussed above.

1.4 : Aims of the Thesis

The above discussion reveals that a number of questions concerning the relationship between radio source structure, nuclear properties and environment remain to be answered. In particular, a detailed clustering investigation, with allowance for the effects described above, is required, to place the analysis of Longair and Seldner upon a secure footing. If detailed spectral information were also available for these sources, the relationships between radio source structure, emission line properties and cluster environment could be studied in more detail. Optical imaging and photometric data for the sources would also be useful, as it would allow absolute magnitude and size measurements to be made. As well as being of interest as intrinsic source parameters, these may be taken as indicators of the presence of galaxy merging, which is also expected to be related to the galaxy environment. Finally, the environment of flat-spectrum (compact) sources has largely not been considered, since these sources are not well represented in surveys

defined at low frequencies. If these are essentially the same class of object as the steep-spectrum sources, the difference being due to projection effects (as suggested by Orr and Browne (1982)), then we might expect their local environments to be similar. Alternatively, if the lack of large-scale structure is due to the absence of a confining medium, we might also expect this to be tied in to the question of environment. An investigation of these sources would therefore be of great interest.

Various groups (e.g. Burns and Gregory 1982) are investigating the properties of radio sources in clusters. However, as these are usually performed by selection of radio sources due to their cluster membership, or even by specific radio observations of clusters, these studies have two drawbacks; firstly, the sample definitions are biased by the difficulty of defining a complete sample, and secondly the majority of sources studied are relatively weak. The study of a complete radio-selected sample of sources, as performed in this thesis, is the only way of investigating the whole range of cluster membership, for the most powerful sources.

The observational pursuit of these investigations is described in the next five Chapters of the thesis.

Chapter Two describes work undertaken to improve the identification content of the high-frequency all-sky sample, described below, which forms the basic source list for the objects under study. This is achieved both via the consideration of improved radio data, and by an optical investigation of some of the 'empty fields' and less secure identifications in the literature.

In Chapter Three, new radio data for the all-sky sample members between declinations $+10^{\circ}$ and -46° are presented. These include not

only the lower redshift sources whose structure is required for correlation with other parameters, but also the higher redshift sources, for which a knowledge of structure is desirable for a variety of other reasons.

Chapters Four and Five describe the work undertaken to define the cluster environment of the sample members. This is undertaken not only for the main sample, but also for a number of fainter sources, in order to provide a broad base for comparison. In Chapter Four, the galaxy data used are the Lick counts, while in Chapter Five the results of some investigations using U.K. Schmidt plates are presented.

In Chapter Six, the results of an optical imaging and photometric study of a number of sources is described. The correlations between source structure, cluster environment and optical spectra for these sources are also discussed.

Finally, in Chapter Seven, the various different results from earlier chapters are summarised, and the possible causes of the observed relationships discussed. Suggestions for future work are also presented.

1.5 : The Radio Source Samples

In the study of the properties of any set of objects, it is well known that the basis of any investigation must be a well-defined sample. For historical reasons, the best-studied samples to date have been drawn from the low-frequency surveys made in the northern hemisphere; the obvious example being the ubiquitous "3CR complete sample" (see Jenkins Pooley and Riley 1977), defined by

$$S_{178} > 10\text{Jy}$$
$$\delta > 10^{o}$$
$$|b| > 10^{o}$$

and recently improved and extended by Laing, Riley and Longair (LRL 1983). Intense observational effort has meant that this sample is extremely complete, both in identification and redshift content, and it has provided the basis for many earlier investigations of the properties of radio sources. In its most recent (LRL) form this sample contains 173 sources, and is estimated to be 96 percent complete for sources with angular sizes less than 10 arcmin. At the time of publication, 162 sources were considered firmly identified, with 137 having known redshifts.

This sample does however have two limitations. Firstly, by its definition at low frequency, it tends to exclude the "flat-spectrum" or "compact" radio sources, which represent a much greater fraction of the radio source population at high frequencies. Secondly, its restriction to the Northern hemispere ($\delta > 10^{o}$) means that it includes sources from only half the area of sky available for study (i.e. with $|b| > 10^{o}$).

In order to remedy this situation, Peacock and Wall (1981), and Wall and Peacock (WP; 1985) have constructed two new samples, from sources drawn from surveys made at Parkes (Wall 1977) and Bonn (Pauliny-Toth 1977). These are defined at the higher frequency of 2.7GHz.

The first sample, a Northern-hemisphere sample, is defined by

$$S_{2.7} > 1.5\text{Jy}$$
$$\delta > 10^{o}$$
$$|b| > 10^{o}$$

This sample contains 168 sources, and is a direct analogue of the

LRL sample at high frequency. For this sample (not least due to the overlap with 3CR) the identification and redshift content is high, with 156 identifications, and 108 measured redshifts.

The second sample, again defined at 2.7GHz, is an all-sky sample, containing 233 sources satisfying:

$$S_{2.7} > 2\text{Jy}$$
$$|b| > 10^{o}$$

As a result of the new radio and optical data presented here, and also through CCD observations (Wall, in preparation) 224 members now have optical identifications. Of these, 172 also have redshifts.

The particular importance of this sample is its all-sky coverage (10sr). Since lowering the flux density limit at fixed redshift simply increases the number of lower-luminosity nearby sources, the sample contains essentially all nearby powerful sources. It is therefore the best we can do for any observations, such as galaxy clustering, where a redshift limit must be imposed. The complete sample is listed in Appendix A, and it is this sample which provides the main source of objects studied in this thesis.

Chapter 2 : OPTICAL IDENTIFICATIONS OF SOUTHERN SAMPLE MEMBERS

2.1 : Introduction

The task of finding the optical counterparts of extragalactic radio sources has become more straightforward in recent years. Radio structures and positions of high accuracy from synthesis telescopes together with the very deep optical data available from solid-state detectors have allowed essentially complete optical identifications to be obtained for statistical samples of bright extragalactic sources (see e.g. Gunn et al. 1981). For a variety of reasons, this work has been most successfully performed in the Northern hemisphere. In this chapter, the results are presented of a programme to complete as far as possible the identification of sources in the WP sample, using existing optical data.

This sample is of particular importance in constraining the properties of the powerful radio source population. Much of the work in this thesis can only be performed at comparatively low redshift. In order to consider as many as possible of the more powerful sources, we must therefore cover as much of the sky as possible. In addition, knowledge of the properties of powerful nearby sources is important for comparison with the higher-redshift objects of fainter samples. While faint samples may be expanded to include arbitrarily large numbers of sources, bright samples are fundamentally restricted by the occurence of nearby sources. It is thus important that our knowledge of these intrinsically rare sources is as complete as possible; hence the interest in an all-sky sample.

A critical assessment (prior to Wall and Peacock, 1985) of the

identification content of their 233-source sample revealed 34 sources (generally in the Southern hemisphere) which had no secure identification. This was either because the field of the source had only been examined to the depth of the Palomar Sky Survey (P.S.S.), and no suitable candidate found, or because the suggested identifications in the literature had not been checked for close positional agreement. For a large fraction of these sources, the radio data presented in Chapter Three provides the first high-resolution estimates of the expected position of the identification. The availability of such data is very important; many of these sources have suggested identifications which are 15 - 20 years old, and which have never been checked in the light of more recent high-accuracy positional data. Accordingly, the optical fields of the 34 sources were examined, either on U.K. Schmidt plates (usually J film copies) or on PSS glass copies, and optical positions measured for candidate identifications. The high density of background objects on the U.K. Schmidt plates presents some difficulties for unambiguous identifications, and in Section 2.2 a method is discussed for assessing the reliability of identifications, appropriate to an inhomogeneous collection of objects such as those considered here. The results of this analysis are presented in Section 2.3, and the identification rate discussed in Section 2.4. Finally, Section 2.5 relates these identifications to the optical data on the sample as a whole.

2.2 : Identification Procedure

2.2.a Radio Positions

For fourteen of the objects considered here, the observations presented in this thesis provide the first available high-resolution

radio maps. Details of these observations are presented in the next chapter; here we are simply concerned with the expected position of the optical counterpart of the source. For compact sources, or extended sources where a compact core has been detected, the situation is simple; the optical identification and core are expected to coincide to the errors of measurement. The case of extended sources with no obvious core is more difficult; however Laing et al. (1983) have shown that ~ 96 pecent of all their extended sources (with $\theta > 5$ arcsecs), which have detected core components, have their identifications within 0.2θ of the source midpoint. We have therefore assumed this to be the expected position of any optical identification, with an assigned r.m.s. deviation of 0.1θ.

For a further fourteen sources, high resolution radio data were already available (Perley, VLA calibrator list; Ulvestad et al. 1981). All these sources are known to be compact, and hence the expected identification position is again known to high accuracy. For the remaining six sources, the only available positions are low resolution radio centroids from the Molonglo telescope (Hunstead, 1972; Large et al., 1981). Although these are known to high accuracy, they will not always be a correct estimate of the identification position (e.g. if the source is asymmetric). The effect of this on the identification process is discussed in Section 2.2.d.

2.2.b Candidate Selection and Measurement

The positions of all objects within ~ 1 arcmin of the radio source were obtained relative to 8 S.A.O. stars, using a Packman x-y Machine, and the CHART and ASTROM reduction programs of Starlink. The selection of the correct optical counterpart to the radio source

is complicated by errors in both the radio and optical positions; the density of objects on U.K.S.T. plates is high, ($\sim 10^{-3}$ per square arcsec), and thus unrelated background objects may fall within the error circle. In most cases, the error in the optical position is either the dominant or an important fraction of the total error, so some care was taken to estimate these errors accurately.

There are two main causes of uncertainty in the optical positions:

1) Random and systematic errors in measurement of the candidate objects and the standard stars;

2) Uncertainties in the co-ordinate transformation due to errors in the catalogued positions of the S.A.O. stars.

In order to allow for the systematic effects, and to estimate the magnitudes of the various errors, each plate was measured in two orientations, 180^{o} apart. For each plate the two sets of measurements, designated N and S, were reduced separately, and the difference N-S was then calculated for the R.A. (in arcsecs on the sky) and dec of each object. The distributions of these quantities are shown in Fig. 2.1, for the 63 optical candidates whose positions were initially measured. These plots should reveal any systematic errors in the positioning of the x-y carriage as a non-zero mean, while the standard deviation measures the combined random errors. In practice, the means for the two distributions are small in comparison with the standard deviations. In fact, there is no evidence that the two standard deviations differ; the Kolmogorov-Smirnov test indicates that both distributions may be fitted by a Gaussian with a standard deviation of 0.83 arcsec (and

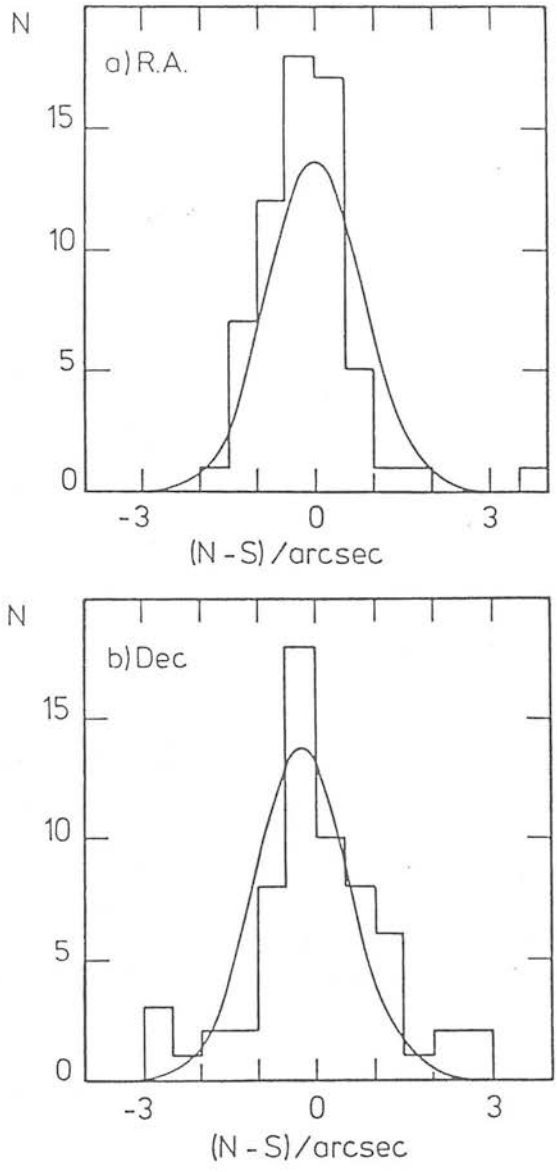

Figure 2.1. Distribution of the difference N-S in arcsec of the optical positions for the 63 candidate objects measured: (a) RA, (b) declination. The curves shown are normal distributions with standard deviation 0.83 arcsec, and means of (a) 0.0 and (b) -0.25 arcsec.

mean -0.25 arcsec and 0.0 arcsec for R.A. and dec respectively). Thus if we adopt as our final position the mean of the N and S measurements, this will eliminate the (small) systematic errors, and reduce the r.m.s. random error to $(0.83/\sqrt{2}) = 0.6$ arcsec in each co-ordinate.

This analysis does not allow for errors in the co-ordinate frame. Random errors in the (α, δ) positions of the S.A.O. stars show up as non-zero residuals between the calculated and catalogued positions of the standard stars. The r.m.s. residual was typically 1 arcsec, which leads to an r.m.s. error in the average co-ordinate frame of $1/\sqrt{7}$ arcsec. Adding this in quadrature to the random measuring error yields an overall r.m.s. error of 0.7 arcsec in each co-ordinate. Finally, Sullivan and Argue (1980) have detected systematic errors of up to 0.5 arcsec in S.A.O. positions; a correction has been made for those cases where the effect (as shown in their Fig. 2) is significant.

The above treatment assumes that all objects can be measured to the same degree of accuracy; in fact for some especially extended or faint objects, this was unlikely to be the case. For these sources (0008-42, 0859-25, 1308-22, 1549-79) an error of 1 arcsec in each co-ordinate was adopted.

2.2.c Image Types and Magnitudes

The candidate identifications were classified as follows: those objects which were obviously non-stellar were classified as galaxies, denoted by G in Table 2.1. Those which were stellar in appearance are denoted by SO, while those (usually near the plate limit) which could not easily be classified are denoted by G?. (The assumption that faint objects are likely to be galaxies is dealt

with in Section 2.5.)

The magnitudes given were estimated by visual comparison with the standard sequences of Hawkins (1980) for the U.K. Schmidt film copies and Sandage (1953) (see also Johnson and Sandage 1956) for the P.S.S. The accuracy is probably no better than 1 magnitude.

2.2.d Association Analysis

We now derive an expression for the probability that a suggested identification is indeed the true optical counterpart of the radio source. Similar analyses have been performed to assess identifications for large homogeneous radio samples (e.g. de Ruiter, Willis and Arp 1977). The present case differs from these, since we are not dealing with a collection of objects selected according to any uniform criteria.

For each candidate object, we calculate the value of the dimensionless difference in radio and optical positions;

$$r = \left[\frac{(\Delta\alpha)^2}{\sigma_\alpha^2} + \frac{(\Delta\delta)^2}{\sigma_\delta^2} \right]^{\frac{1}{2}} \qquad (2.1)$$

where $\Delta\alpha$ and $\Delta\delta$ are the measured position differences between the radio source and the optical candidate, and $\sigma_\alpha^2=\sigma_{\alpha OPT}^2 + \sigma_{\alpha RAD}^2$, $\sigma_\delta^2=\sigma_{\delta OPT}^2 + \sigma_{\delta RAD}^2$, where the σs are the standard deviations in the right ascensions and declinations of the objects, as described above.

Having obtained the value of r for each candidate object, we now have two conflicting possibilities;

1) that the object is a confusing background object, which by

chance happens to lie at a distance r from the radio position,

2) that the object is the true optical counterpart of the radio source, which appears to lie at a distance r due to the uncertainties in the radio and optical positional measurements. (As is usual in this type of work, the assumption is made that the optical and radio positions would coincide in the absence of errors; in fact this may be incorrect when the radio position used is a centroid. Possible difficulties of this sort are discussed below.)

If the probability of (2) is very much greater than that of (1), then the object must be the true identification. This may be quantified as follows.

Let P(id/r) and P(c/r) be the probabilities that, given an object at r, it is the true identification or a confusing object respectively. Let P(id) be the probability that the true object is in fact visible on the plate, and let the probability that a confusing object is visible on the plate be P(c). P(c) = 1, since confusing objects do appear.

Now if P(r/id) and P(r/c) are the probabilities that an object will appear at r, given that it is the true identification or a confusing object respectively, then by the theorem of total probability we have;

$$P(id/r) = \frac{P(id)P(r/id)}{P(id)P(r/id)+P(c)P(r/c)} \qquad (2.2)$$

$$P(c/r) = \frac{P(c)P(r/c)}{P(id)P(r/id)+P(c)P(r/c)} \qquad (2.3)$$

Since P(id/r)+P(c/r)=1, we have

$$\frac{P(id/r)}{1-P(id/r)} = \frac{P(id)}{P(c)} \frac{P(r/id)}{P(r/c)} = P(id).LR(r) \qquad (2.4)$$

where LR(r) is the likelihood ratio, i.e. the ratio of the probability densities of an identification and a confusing object at r. P(r/id) is given by the Rayleigh distribution;

$$P(r/id) = r\exp(-r^2/2) \qquad (2.5)$$

P(r/c) depends on N_0, the background density of objects on the plate as bright or brighter than the one under consideration, and is given by;

$$P(r/c) = 2\pi r N_0 \sigma_\alpha \sigma_\delta \qquad (2.6)$$

although if (as is usual) we are considering only the nearest object, then P(r/c) is multiplied by $\exp(-\pi r \sigma_\alpha \sigma_\delta N_0)$. To find N_0 precisely is hard, since background objects may cluster; in practice independent estimates of N0 agreed to within ~ 20 percent.

Now, the probability that the optical counterpart does not appear on the plate

$$[1-p(id)] = \prod_i [1-P_i(id/r_i)] \qquad (2.7)$$

where the Pi's are the probability that the i'th object lying at r is the true identification, and the product is taken over all the objects on the plate. (Obviously as r becomes large, P quickly tends to zero.)

Hence

$$P(id) = 1 - \prod_i [1-P_i(id/r_i)] \qquad (2.8)$$

and therefore $P(id) \geqslant P(id/r)$, so that (4) yields

$$P(id/r) \geqslant 1-1/LR(r) \qquad (2.9)$$

Also $P(id) \leqslant 1$, hence

$$1-1/LR(r) \leqslant P(id/r) \leqslant \frac{1}{1 + 1/LR(r)} \qquad (2.10)$$

We can thus estimate P(id/r), independent of assumptions about P(id). De Ruiter et al. (1977) were dealing with a complete sample for which P(id) could be estimated, leading to closer constraints on P(id/r). In the present case, the above expression is preferrable, which yields $P(id/r) \simeq 1 - 1/LR(r)$ for large LR, independent of P(id).

This expression has the great practical advantage that the correct estimation of the radio errors is not crucial. In the expression for LR(r), the positional errors are assumed to be Gaussian, which was found to be the case for our optical measurements, but which need not apply to the radio positions. If the positions for one object are abnormally in error, then the position difference will be many standard deviations, corresponding to a low formal probability of association. However, for a low background density, LR will still be high, and we will conclude that the object cannot be a chance association, implying that the positional errors were underestimated.

An additional complication with this analysis occurs when the

radio positions used are obtained from an instrument of low resolution. When maps of ~ 1 arcsec resolution are available, the derivation of the expected position for the optical counterpart is relatively straightforward, as described in Section 2.2.a. However, for 6 of the 34 sources, the only available observations are from the Molonglo radio telescope, which has a beam of ~ 1 arcmin. For these sources, the position quoted is a centroid, on which the formal errors may be only a few arcsec; but for an asymmetric source, the optical position and radio centroid may differ considerably. The quoted errors in the centroids have been used here to derive values of LR for the optical candidates. If LR is large, there is no difficulty - the candidate is very unlikely to coincide by chance with the centroid, so we can assume that the identification is correct and that the source is compact/symmetric. Conversely, if LR is low when a centroid position is used, the identification need not be incorrect - such cases must be considered separately.

2.3 : Results

Of the 34 sources investigated, 5 could be immediately classified as empty fields, with no objects near to a high accuracy radio position. For two of these objects (0500+01, 1005+07), for which only P.S.S. material was available, this simply confirmed results already in the literature (Shaffer 1978, Bozyan 1979); although 0500+01 had previously only been inspected on paper prints. Of the remaining three empty fields, two, (0022-42,2008-06) were ones for which no previous inspection had been made and one, 0114-21, was a confirmation on a U.K.Schmidt copy of an empty field as found on the P.S.S. (Bozyan 1979).

For the remaining 29 sources, data on optical candidates are listed in Table 2.1, which contains the positions and likelihood ratios of the closest objects to each source (finding charts for all these objects are shown in Plate 2.1, page 37). The following quantities are given, in columns 1 to 12:

1) Parkes identification number

2) Any other name by which the source is known

3) Reference to earlier identification work; reference to radio position (see key following Table)

4) Identifier of candidate on finding chart

5)&6) R.A. and dec for candidate object

7)&8) The differences $\Delta\alpha$ and $\Delta\delta$ for the candidate in the sense radio-optical in arcsec. on the sky

9) "r"

10) LR(r)

11) The candidate object type, as described in Section 2.2

12) The J magnitude of the candidate. (For objects identified on Palomar copies, indicated by an asterisk, the magnitude given is the V magnitude.)

Additional notes on the individual sources are as follows:

0105-16. This is a confirmation of the suggested identification of Moseley et al. (1970). The object is not visible on the Palomar O plate; on the E plate it appears at the centre of a faint ($\frac{7}{8}$ 20th mag) cluster of galaxies.

0117-15. The suggested identification of Moseley et al. (1970) appears 56 arcsecs east and 15 arcsecs south. We find two possible

Table 2.1: The Optical Data

(1)	(2)	(3)	(4)	(5)	(6)	(7)	(8)	(9)	(10)	(11)	(12)
0008-42		LU1;PL	-	00 08 21.96	-42 10 04.0	-7.5	13.4	15.14	0.000	G?	22.0
0023-26	OB-238	-;PL	-	00 23 08.96	-26 18 48.7	-0.6	-0.6	0.91	1840.	G	20.5
0105-16	3C32	MBD;*	-	01 05 48.82	-16 20 20.0	-0.7	-2.0	1.73	58.32	G	20.1*
0117-15	3C38	MBD;*	A	01 17 59.60	-15 35 55.7	-2.0	-5.6	2.81	2.545	G?	21.0*
			B	01 17 59.74	-15 36 00.7	-4.0	-0.6	1.93	20.16	G?	21.0*
0157-31	OC-397	BBE;*	-	01 57 58.35	-31 07 57.2	2.1	0.0	0.51	51.13	SO	19.6
0213-13	3C62	BE;*	-	02 13 12.27	-13 13 25.3	-0.7	1.3	0.90	700.0	G	18.0*
0235-19	OD-149	ML;*	-	02 35 24.77	-19 45 31.7	-2.1	-0.8	0.42	32.83	G?	21.3
0347+05	4C05.16	SH;*	-	03 47 06.81	05 43 08.1	-2.5	3.0	5.21	0.008	SO	18.2*
0407-64		HN;LA	A	04 07 57.43	-65 52 46.8	2.9	-1.3	0.93	8.413	SO	18.0
			B	04 07 58.84	-65 52 41.9	-6.7	-6.3	2.99	0.793	G?	20.0
0409-75		AP;LA	A	04 09 57.80	-75 15 04.0	7.0	5.0	3.18	0.180	G?	22.5
			B	04 09 58.92	-75 15 05.9	2.0	6.9	2.31	0.769	G?	22.5
0442-28	OF-271	BCE;*	-	04 42 37.78	-28 15 22.5	2.5	6.7	0.65	13.82	G	18.4
0625-35		BCE;*	-	06 25 20.23	-35 27 21.8	0.5	1.6	1.85	2100.	G	15.0
0834-19	OJ-158.1	-;UL	A	08 34 55.82	-19 41 13.5	4.7	-11.9	15.81	0.000	SO	19.4
			B	08 34 56.32	-19 41 21.2	-2.4	-4.2	5.98	0.000	G?	22.5
0858-27	OJ-297	RK;UL	-	08 58 31.47	-27 56 32.8	0.5	-0.2	0.46	215.2	SO	16.2
0859-25	OJ-299	BZ;*	A	08 59 36.42	-25 43 23.9	1.0	-2.6	0.48	6.103	G	22.2
			B	08 59 36.61	-25 43 41.7	-1.6	15.2	2.70	0.302	G	22.0
			C	08 59 37.18	-25 43 35.7	-9.3	9.2	2.31	3.140	SO	20.3
1015-31	OL-327	BZ;PL	-	10 15 53.38	-31 29 11.7	0.1	0.3	0.49	400.4	G?	21.2
1017-42		BB;*	A	10 17 56.47	-42 36 23.2	0.2	-0.3	0.40	197.6	SO	19.0
			B	10 17 57.24	-42 36 25.7	-8.3	2.2	9.98	0.000	SO	19.6
			C	10 17 57.65	-42 36 18.6	,13.3	-4.9	16.36	0.000	SO	19.0
1306-09	OP-10	HM;*	-	13 06 02.01	-09 34 31.8	1.0	-1.3	2.18	98.27	G?	20.5*
1308-22	3C283	MBD;UL	-	13 08 57.30	-22 00 43.8	1.4	-2.9	2.96	5.909	G?	22.5
1518+04	4C04.51	CL;*	-	15 18 44.73	04 41 05.5	-7.2	-6.3	1.59	23.07	G	18.2
1549-79		-;HN2	A	15 49 25.71	-79 05 18.8	5.7	-4.3	4.11	0.010	G	20.7
			B	15 49 28.31	-79 05 17.9	-1.7	-5.3	2.53	4.147	G	19.8
1622-25	OS-237.8	-;PL	-	16 22 43.47	-25 20 53.8	8.7	2.3	12.82	0.000	G?	21.3
1740-51		-;LA	A	17 40 26.81	-51 43 22.2	1.8	-2.8	1.46	2.706	G	20.2
			B	17 40 27.18	-51 43 35.1	-1.7	10.1	4.80	0.000	SO	18.7
1932-46		LU2;*	-	19 32 18.24	-46 27 20.4	-2.2	4.4	1.37	10.42	G	19.9
1938-15	OV-164	WYN:LA	A	19 38 23.87	-15 31 44.4	6.6	10.4	2.71	0.305	SO	19.6
			B	19 38 23.94	-15 31 40.4	5.6	6.4	2.24	1.063	SO	18.5
			C	19 38 24.45	-15 31 34.4	-1.9	0.5	0.70	1.709	G?	22.5
2032-35	OW-354	LU1;*	A	20 32 37.02	-35 04 32.9	1.7	-0.1	0.48	14.01	G?	22.5
			B	20 32 37.08	-35 04 29.7	1.0	-3.3	0.96	10.14	G?	22.5
2106-41		-;PL	-	21 06 19.40	-41 22 33.7	0.1	0.4	0.53	830.2	SO	20.0
2135-20	OX-258	-;PL	-	21 35 01.31	-20 56 03.6	0.1	-0.1	0.26	807.4	G	20.4
2150-52		LU3;HN2	-	21 50 46.87	-52 04 50.4	12.0	26.5	15.27	0.000	SO	18.0

key to references:

* = Chapter Three

AP = Anguita et al., 1977.

BB = Burbidge & Burbidge, 1972.

BCE= Bolton et al., 1965.

BE = Bolton & Ekers, 1966.

BZ = Bozyan, 1979.

CL = Clarke et al., 1966.

FM = Fomalont & Moffet, 1971.

HM = Hoskins et al., 1974.

HN1= Hunstead, 1971.

HN2= Hunstead, 1972.

LA = Large et al., 1981

LU1= Lu, 1970a.

LU3= Lu, 1974.

MBD= Moseley et al., 1970.

ML = Mills, 1960.

PL = V.L.A. Calibrator list.
(Perley, priv. comm.)

RK = Radevich & Kraus, 1971.

SCH= Schmidt, 1977.

SH = Shaffer, 1978.

UL = Ulvestad et al. 1981.

WS = Westerlund & Smith, 1966.

WW = Wills & Wills, 1966.

WYN= Wyndham, 1965.

candidates, which appear to lie in a small group at the extreme limit of the Palomar plates, slightly fainter on the E plate than the O. We cannot make a definite statement as to which of our candidates is the identification, although candidate B is rather more likely than A. However, since it is probable that the candidates are physically associated (i.e. in the same cluster) and have similar types and magnitudes, we feel that this source can be considered as definitely identified. This identification has been confirmed by Wall (private communication) using CCD data.

0347+05. This source was previously classified as an empty field by Shaffer (1978). The observations of Chapter Three show that the source is a wide double; however, the candidate object is displaced too far from the source midpoint to be considered correct in this sense. It is sufficiently near one radio component for the object to be considered as a D2 source, but the likelihood ratio in this case is still small. As only Palomar plate material has been examined for this source, it is possible that the correct identification lies below the plate limit.

0409-75. We confirm the finding of Anguita and Pedreros (1977) that the identification of Westerlund and Smith (1966) is incorrect. The true identification is uncertain; our candidate appears to lie on the edge of a faint cluster of galaxies slightly to the south of the radio position.

0625-35. The identification is a confirmation of that suggested by Bolton et al. (1965). The identification is with a galaxy which appears to be the dominant member of a nearby cluster. The galaxy has two stellar images superposed.

0858-27. This is a confirmation of the identification of Radevich

and Kraus (1971) with a stellar object. Wills & Wills (1976) discarded the identification as it had the spectrum of a galactic star. However, the object is seen on the U.K. Schmidt plate to be a stellar object with a field star superimposed.

1549-79. Candidate B for this identification is rather extended in the North-South direction, with less dense nebulosity to the south of a denser, slightly irregular compact region.

1938-15. Ulvestad et al. (1981) give positions for three compact features in this source, none of which coincide with any optical object. Our object C (suggested by Wyndham 1965), however, lies between their components A and C, which form an 8 arcsec double. If component B, which lies some 20 arcsec is unrelated, then this is likely to be the identification.

2032-35. Again, we have two candidate identifications with similar likelihood ratios; as for 0117-15 we consider the source to be definitely identified.

2150-52. This object is that suggested by Lu (1974); we consider the identification unlikely to be correct, although no closer object has been found.

2.4 : Discussion

As noted in Section 2.2.d, the interpretation of the data in Table 2.1 depends partly on the structural information available. We may distinguish 3 cases:

1) Definite identifications. Here LR is high (an arbitrary division has been made at LR = 10) and the probability of the optical object lying at the radio position by chance is small, confirming both the identification and the accuracy of the radio position.

2) Definite empty fields. Either LR is small (here < 0.1) when the radio position is based on high-resolution observations, or there are no nearby objects at all.

3) Uncertain identifications. Either LR $\sim$ 1 based on a high resolution radio position, or LR < 10, but based on a radio centroid position. In these latter cases we cannot be sure the source is compact, and the identification may be offset from the centroid position.

From consideration of the values for the likelihood ratios for the candidate objects, we find that, for 17 of the 29 remaining sources, one of the candidate objects is definitely the identification. This includes three of the previously unexamined sources. Of the 18 sources with suggested identifications in the literature, however only nine were found by our analysis to be correct; three were found to be incorrect. This is not entirely suprising, since the objects chosen for investigation here were those for which previous identifications had not been checked for positional agreement; but it does highlight the need for such checks to be carried out.

Of eight sources whose identifications are considered uncertain from their values of LR, only 1308-22 has been observed, at high resolution, to be compact. With LR $\sim$ 8, this is probably the correct identification. Inspection of the radio structure of 0859-25

(Chapter Three) suggests that candidate A for this source (LR ~ 6) is also correct. In fact, the remaining six sources turn out to be those for which only radio centroid positions are available. It is therefore interesting to compare the results presented here, with those of an earlier version of this work (Prestage and Peacock 1983), performed before the observations of Chapter Three were available. Of the five objects in that analysis with only centroid positions, and LR < 10, four are considered here to be definitely identified, in the light of the new radio data. It therefore seems likely that the majority of the remaining sources will turn out to have been correctly identified, when high resolution data become available.

We may thus summarize these results as follows:

Definite identifications

0023-26	0235-19	1015-31	1932-46
0105-16	0442-28	1017-42	2032-35
0117-15	0625-35	1306-09	2106-41
0157-31	0858-27	1308-22	2135-20
0213-13	0859-25	1518+04	

No identification

0008-42	0347+05	0834-19	1622-25
0022-42	0500+01	1005+07	2008-06
0114-21			

Identification uncertain

0407-65	1549-79	1938-15
0409-75	1740-51	2150-52

2.5 : Conclusions

The results presented here have essentially completed the identification data for the WP 233 source sample. Including the CCD observations of Wall (in preparation) there now remain only 9 objects which are empty fields so that 96% of the sample is now identified. The status of the uncertain sources will remain in doubt until high resolution radio data becomes available. In light of a comparison with an earlier version of this work however, it seems likely that the majority of them will turn out to be correctly identified.

A guide to the nature of the faint identifications of uncertain type may be obtained from the magnitude distributions for the whole sample, which are shown in Fig. 2.2. This gives the distributions of V magnitude for all definite galactic and stellar identifications in the 233 source sample, divided according to their radio spectra into two classes; "steep" ($\alpha_{27}^{5} \geqslant 0.5$) and "flat" ($\alpha_{27}^{5} < 0.5$). All of the identifications of uncertain type in the 34 source sample are steep-spectrum sources, and are fainter than 19.5th mag. Since the majority of these sources are galaxies (Fig. 2.2.a.), and further since the distribution for stellar objects peaks around 17.5th mag. and falls sharply thereafter, the faint identifications seem likely to be distant galaxies. Similar trends in the magnitude distributions are also found in samples such as 3CR (see Gunn et al. 1981), but there are some interesting differences in the present case. For both galaxies and stellar objects there is a bias in the 2-Jy sample towards brighter magnitudes. This point is discussed in detail by Wall and Peacock (1985); essentially, the 2-Jy sample contains a far higher proportion of low-redshift objects than does 3CR, reflecting the increased steepness of the radio luminosity function at high redshift. Although the 2-Jy sample is of similar

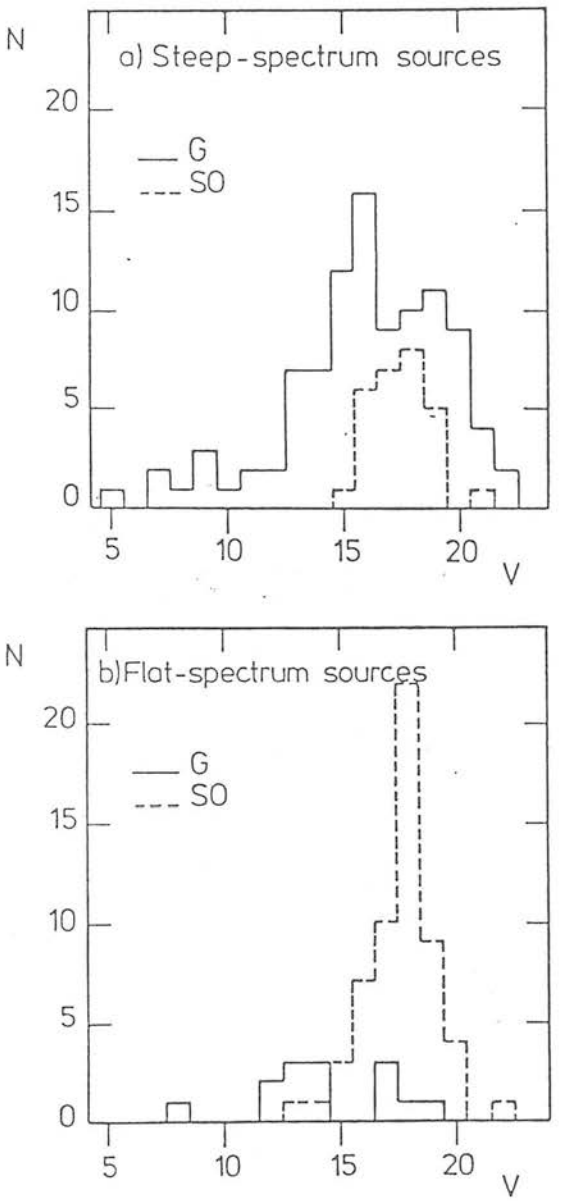

Figure 2.2. Magnitude distributions for the 196 identifications of definite type in the 233-source all-sky sample, associated with (a) steep- and (b) flat-spectrum sources.

depth to 3CR, the difference is sufficient to produce the movement towards low redshift. This fact has certainly helped us to achieve a high identification rate here, despite the fact that efficient detectors such as CCDs were not used.

Plate 2.1.

Finding photographs 7.5-arcmin square for the 29 sources with candidate identifications. (For completeness, finding photographs for all candidate identifications are presented, although for some objects these are already available.) North is to the top, east to the left. In all cases SSO Test film copies were used, apart from the following sources, for which Palomar plates were used:

0105-16(E)
0117-15(O)
0213-13(E)
0347+05(E)
1306-09(E)

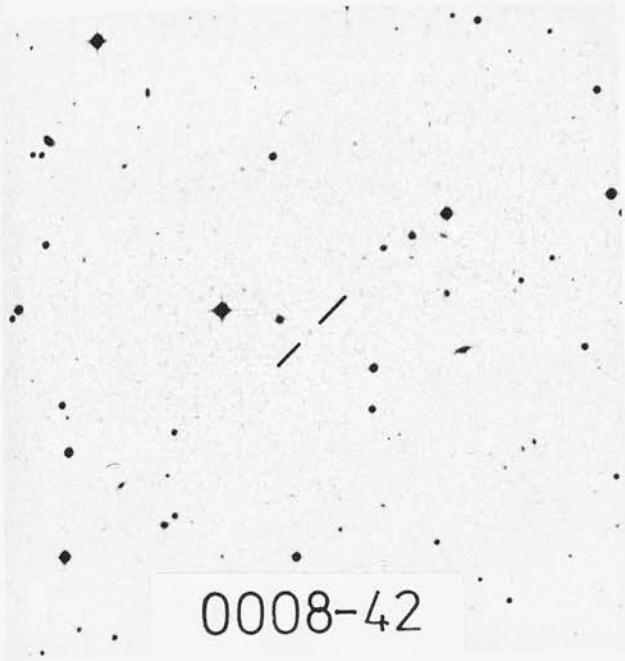

0008-42

0023-26

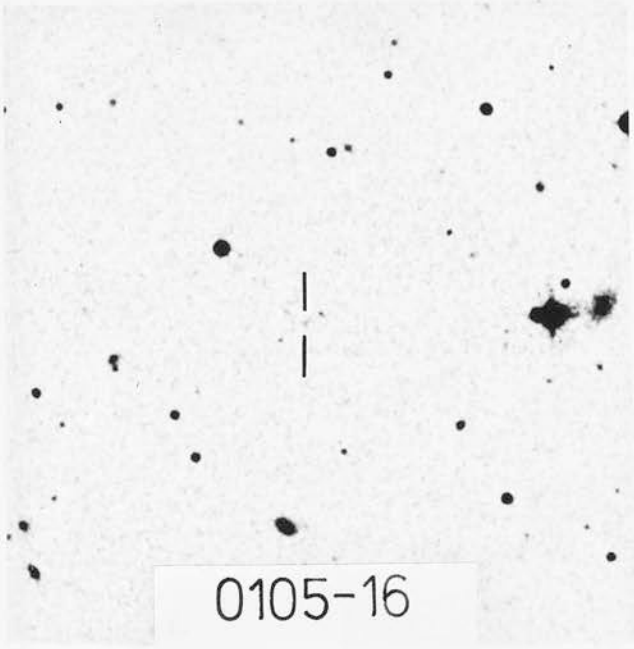

0105-16

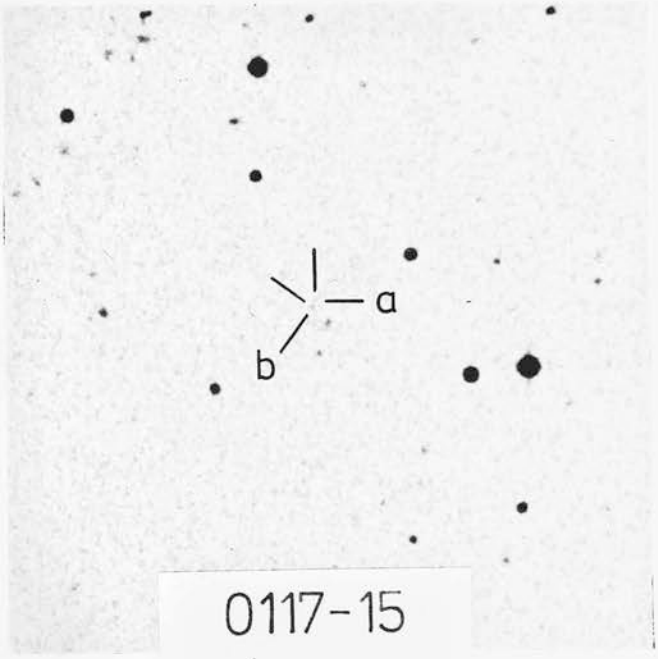

0117-15

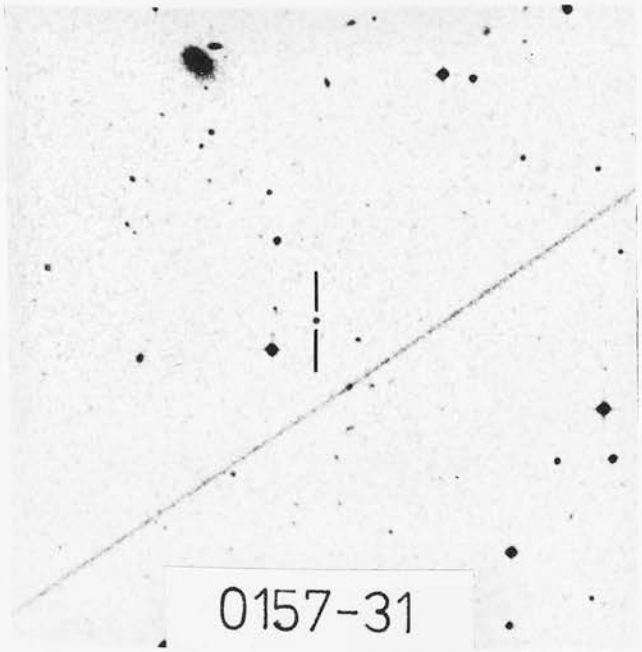

0157-31

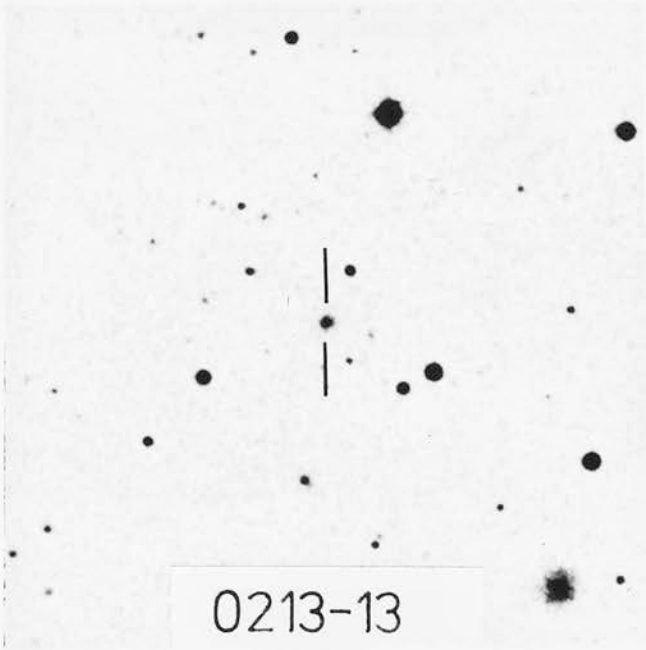

0213-13

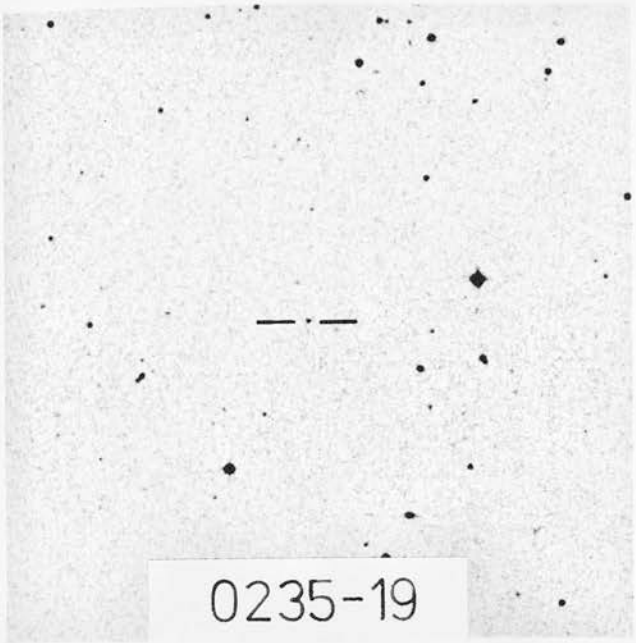

0235-19

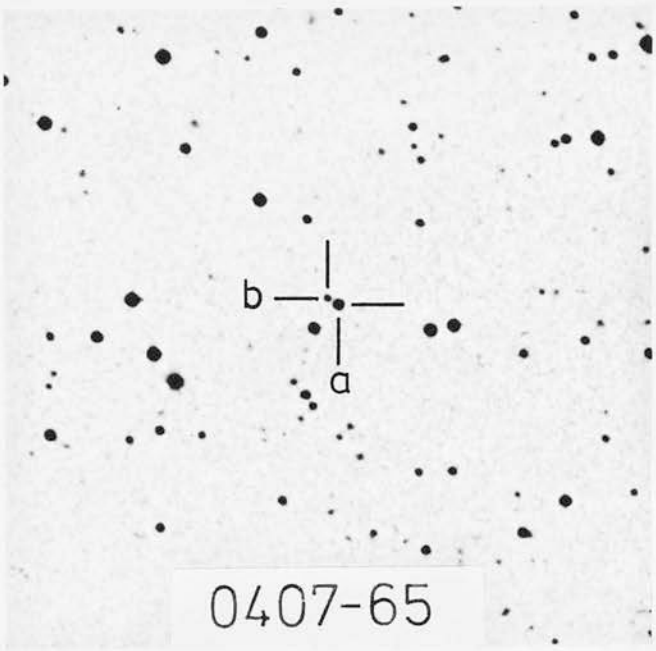

0407-65

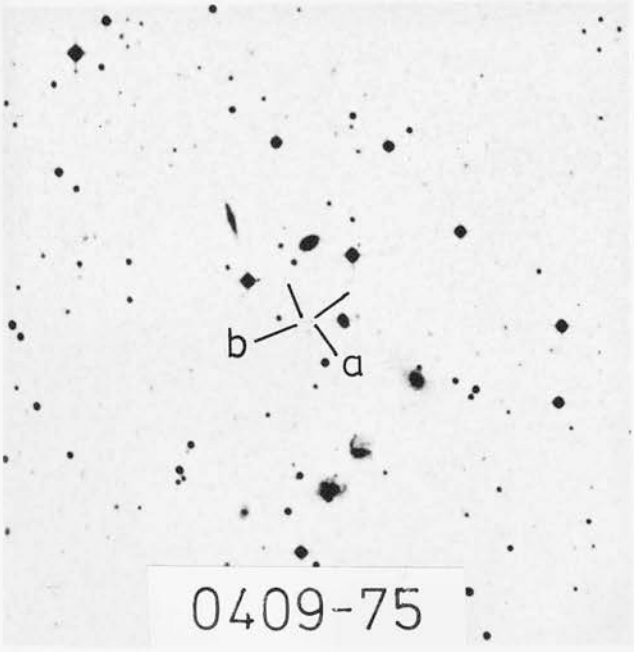

0409-75

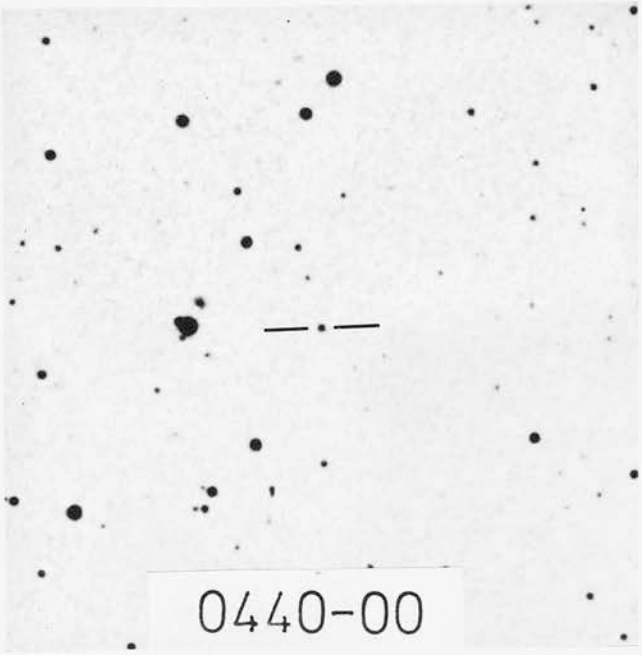

0440-00

0442-28

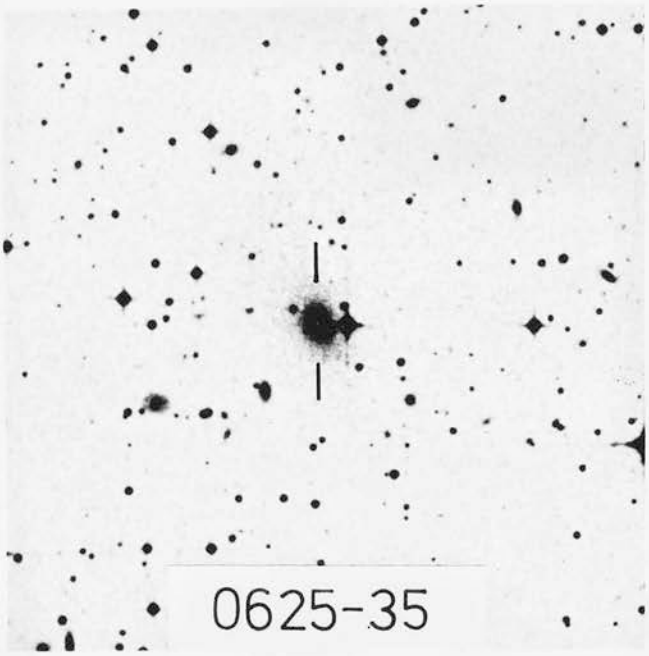

0625-35

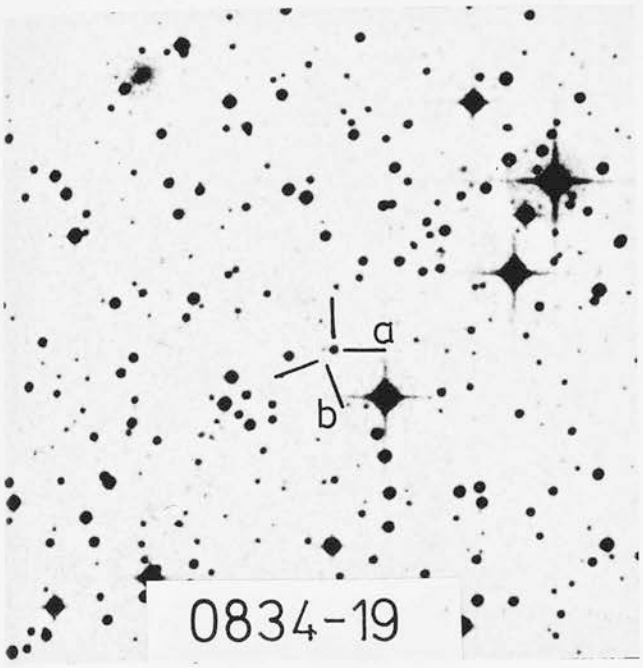
a
b
0834-19

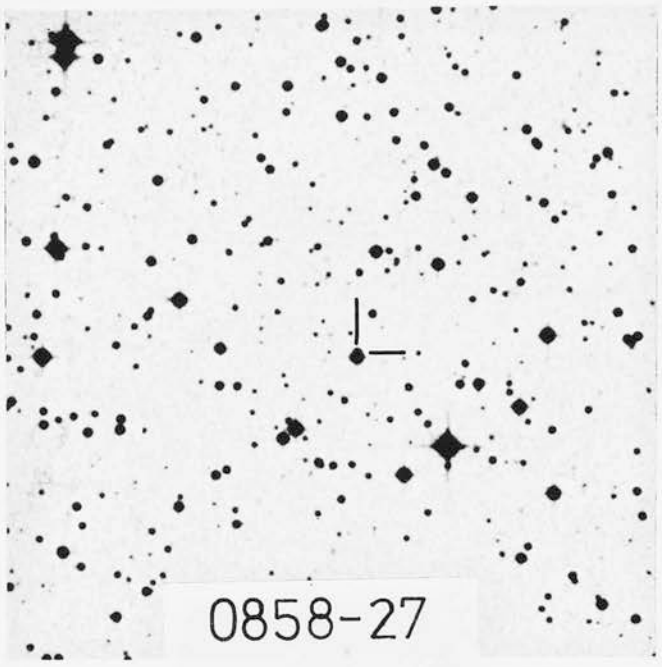
0858-27

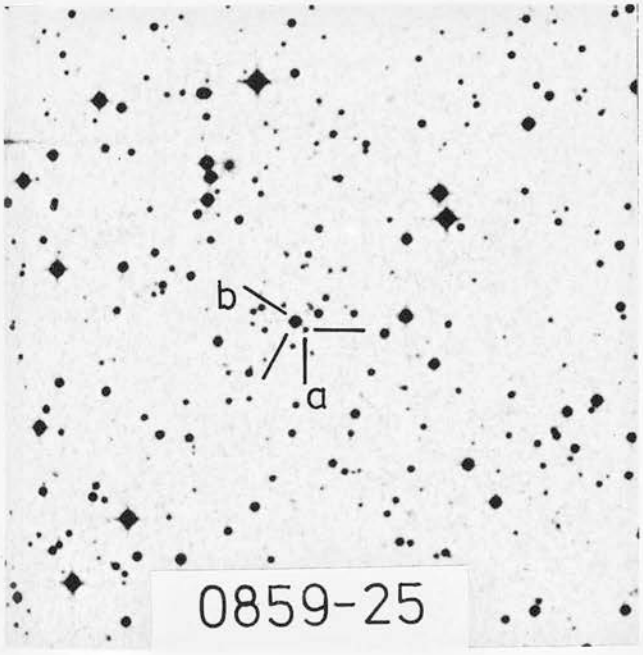
b
a
0859-25

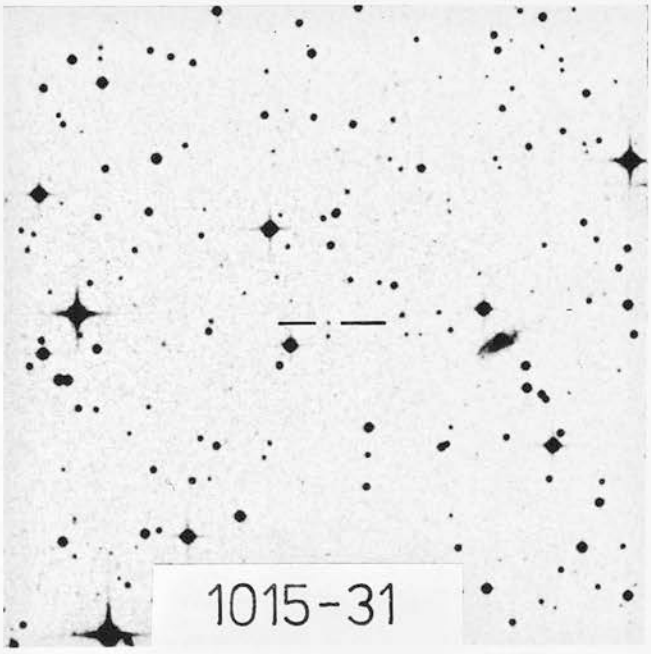
1015-31

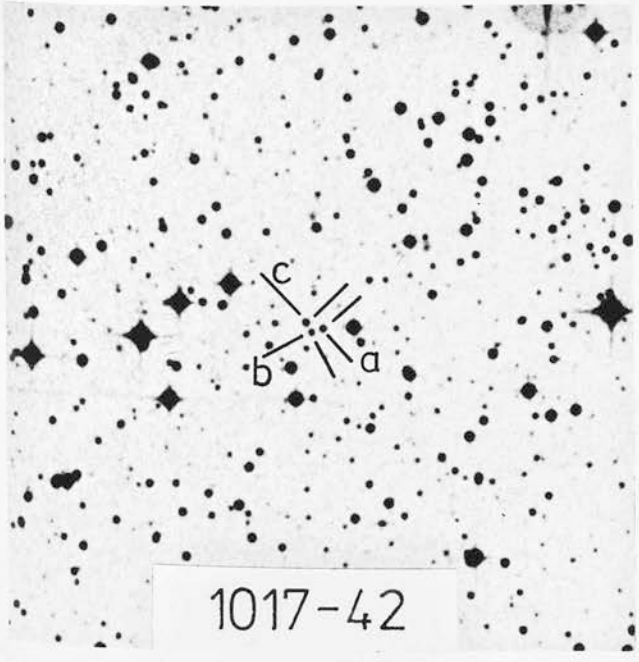
c
b
a
1017-42

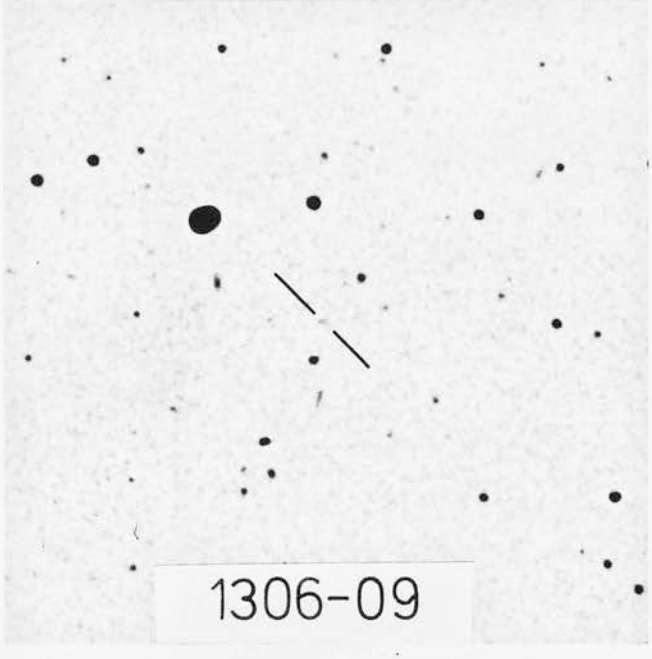
1306-09

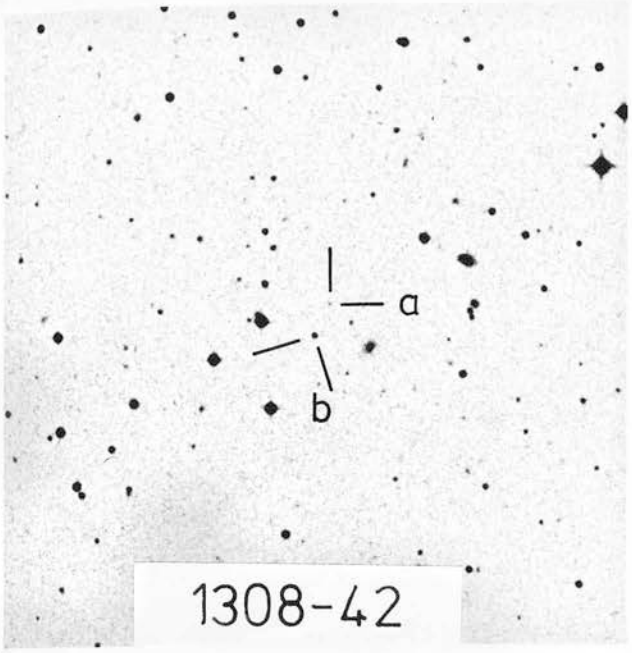

1308-42

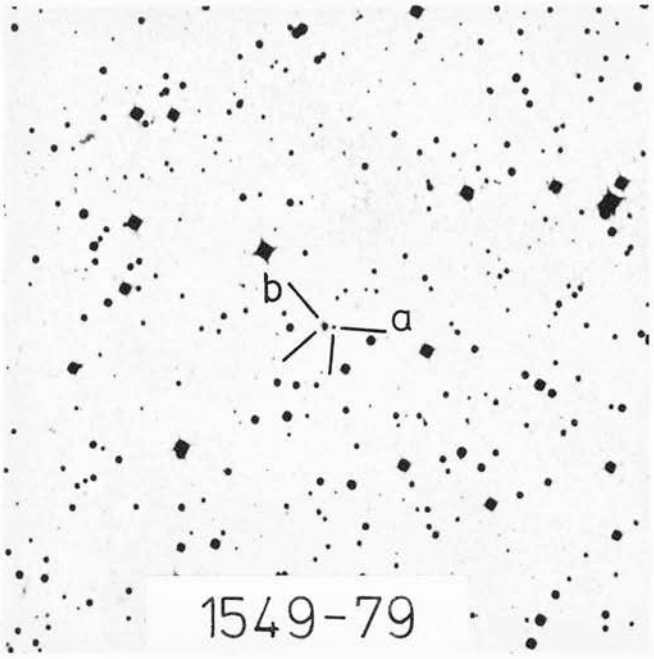

1549-79

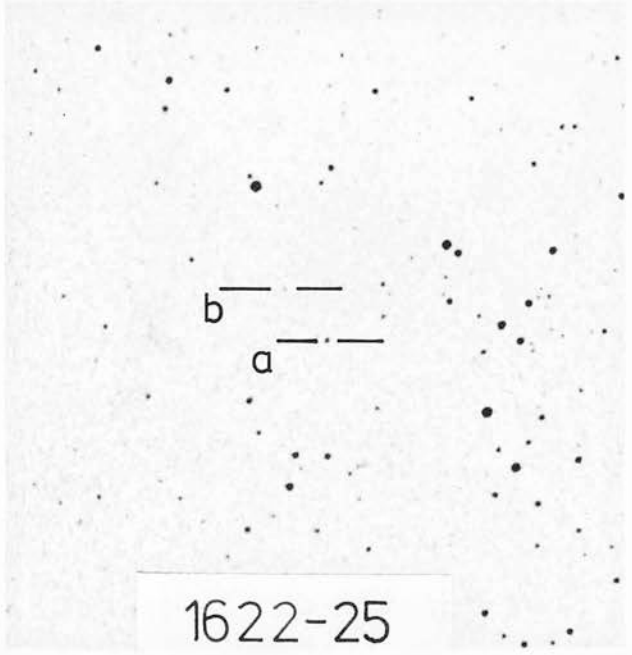

1622-25

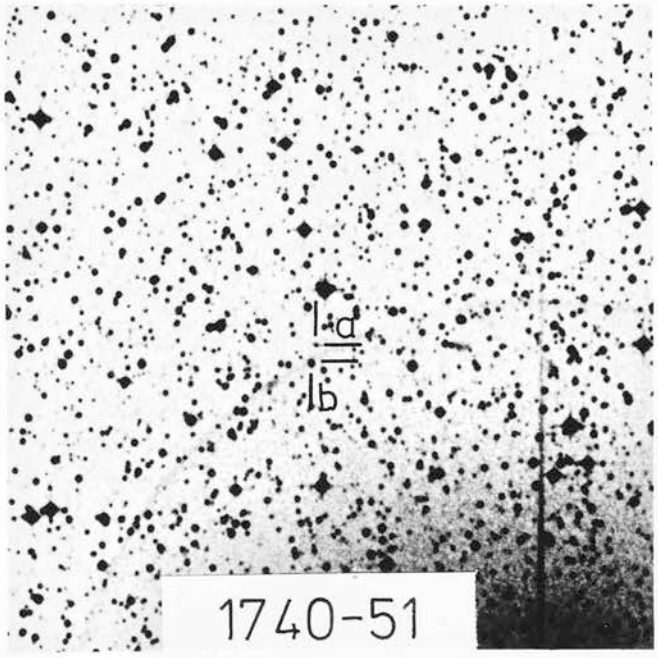

1740-51

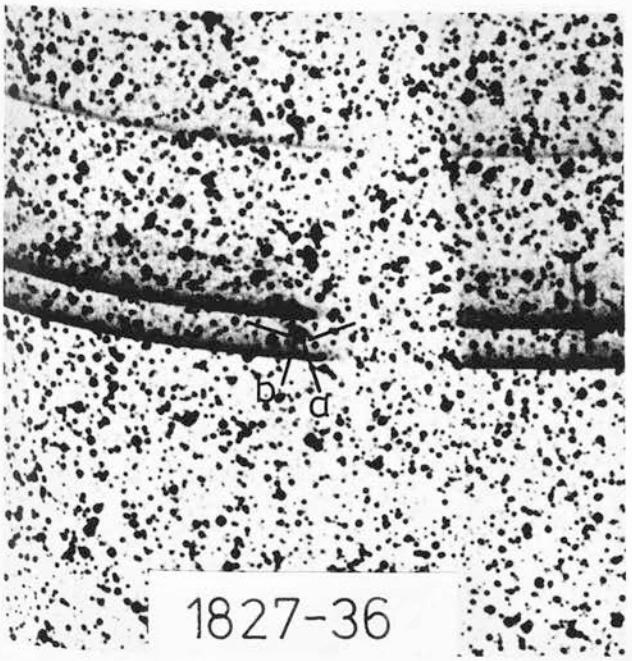

1827-36

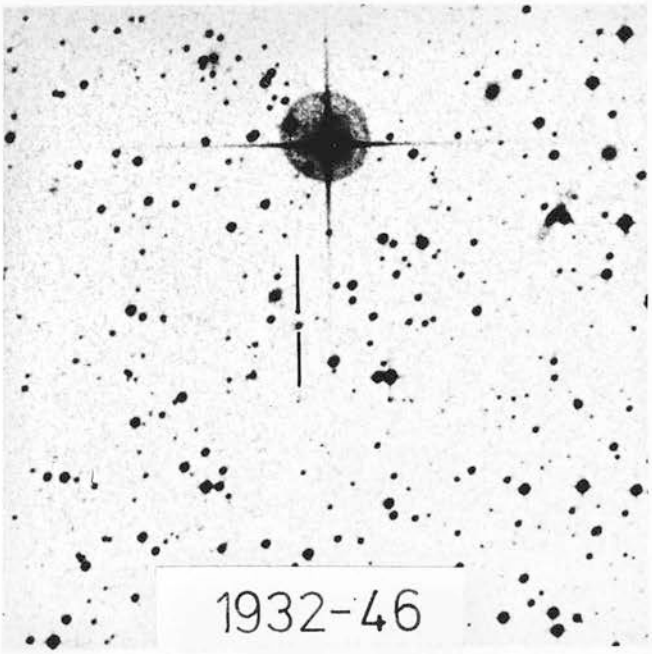

1932-46

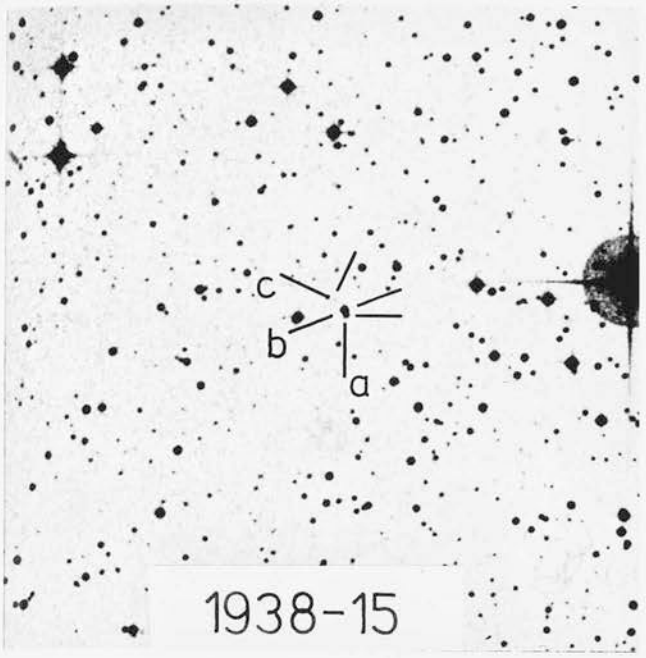
c
b
a
1938-15

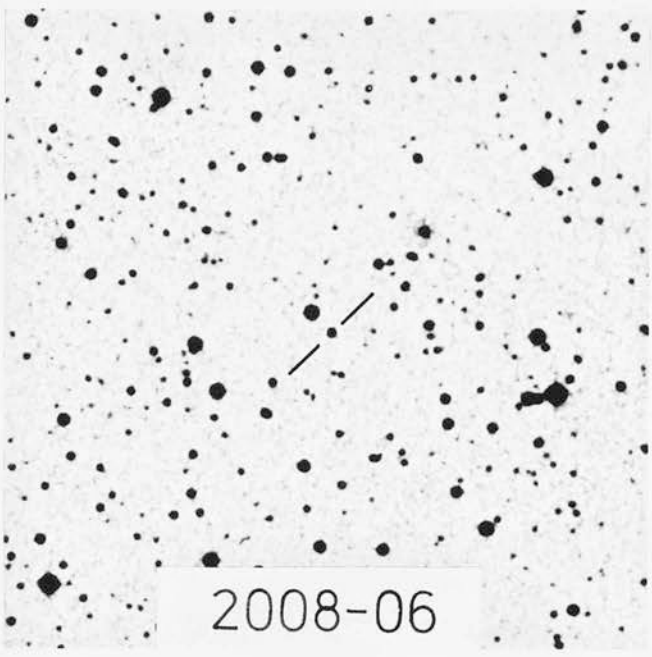
2008-06

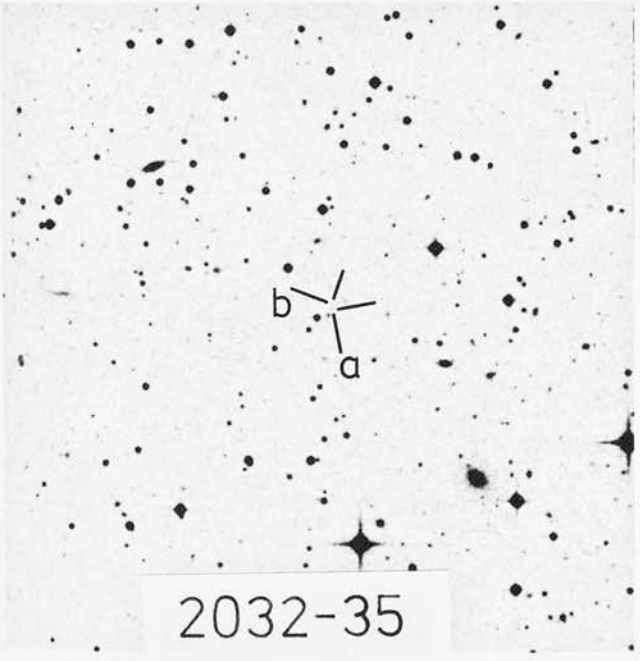
b
a
2032-35

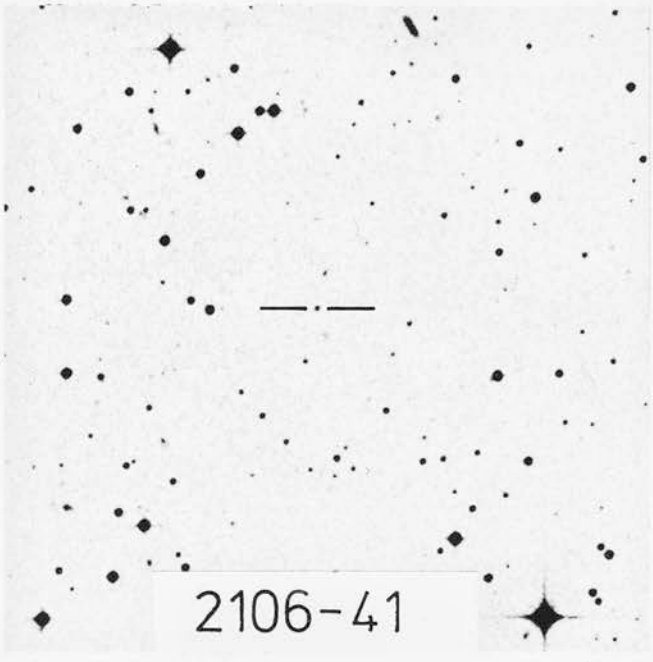
2106-41

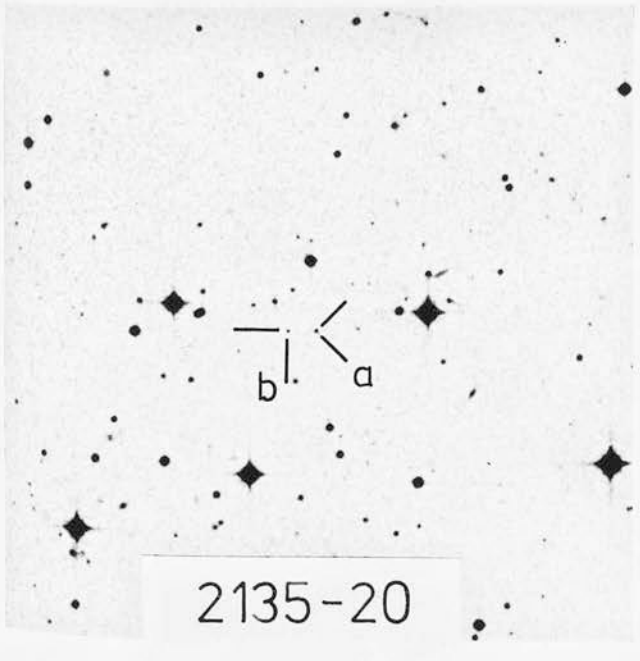
b
a
2135-20


2211-17

Chapter 3 : RADIO OBSERVATIONS OF SOUTHERN SAMPLE MEMBERS

3.1 : Introduction

High resolution radio maps of the sources in the WP all-sky sample are highly desirable, for a number of reasons. Of particular interest, as has been discussed, is the fact that many properties of radio sources (e.g. the presence of optical emission lines) are correlated with source structure. To investigate the nature of any such effects, and in particular, to investigate the correlations with environment and optical structure, high-resolution radio maps are thus essential. In addition, from a practical viewpoint, structural data is required to confirm some of the more ambiguous optical identifications (Chapter Two). In this chapter, observations made with the VLA are described, which were designed to complete as far as possible the mapping (at reasonably high resolution) of all members of the WP sample.

For all northern ($\delta > 10^{o}$) members of the sample, high resolution (Cambridge 5km) maps were already available, either from previous investigations, or from the work of Peacock and Wall (1982). For many of the remainder however, data on structure was either of low resolution, or non-existent. In the range $+10^{o} > \delta > -46^{o}$ (the southern limit of the VLA) the WP sample contains 117 sources. Of these, 46 were either known to be compact (Perley, 1982; Ulvestad et al., 1981), or were assumed to be so (i.e.they have flat spectra). This left a total of 71 sources. These sources, excluding Cen A and For A, (and together with two more initially considered for but subsequently not included in the WP complete sample) comprise the sample described here.

In the following section, the observations and their reduction are described. The results, including maps of the resolved sources are presented in Section 3.3. In Section 3.4., the structures of a number of sources are discussed.

3.2 : The Observations

The observations were made in March 1983, using the VLA in its C configuration. This provides minimum and maximum antenna spacings of 0.063 and 2.8km respectively. The observations were made in one 24 hour period using the "snapshot" mode, with one 7-8 minute observation per source, at both 1.4 and 5GHz, using bandwidths of 50 and 25Mhz respectively. The weather conditions at the start of the run were rather poor; in particular snow in the dishes affected the sensitivity (especially at 5GHz) for the first few hours. In addition, scheduling constraints - basically the requirement that low declination sources be observed on the meridian - meant that a few sources were observed while within about 10 degrees of the sun. Two of these were subsequently reobserved by the VLA staff; details of the the affected sources are described in section 3.3. Finally, for a few of the more extended sources additional UV coverage was obtained by A. Downes; these data were concatenated with the observations already made.

3.2.a Calibration

Nineteen observations were made, evenly spaced throughout the run, of a number of calibrator sources, including the primary flux standard 3C286, which was assumed to have a flux of 14.70Jy and 7.50Jy at 1.4 and 5GHz. Prior to calibration, the amplitudes and r.m.s. of each antenna pair, vector averaged over each calibrator

observation were inspected, and any suspect correlators flagged out of the data. After flagging, a small number of good antennas near the centre of the array were selected, and the calibrator sources used to calculate the gain solutions. These are empirical values for the complex gains at each antenna, which are applied to take out instrumental and slowly-varying atmospheric phase errors. Let us denote a visiblilty measurement Vjk as:

$$Vjk = Ajk \exp[i\theta jk] \tag{3.1}$$

For a good amplitude and phase calibrator (a point source with an accurately known position, and flux density S), one knows that after calibration,

$$Vjk = S \tag{3.2}$$

that is, the visibility amplitude is equal to the flux density, and the visibility phase is zero. If Vjk,corr is the visibility measurement with only corrections applied (e.g. for antenna shadowing), then

$$Ajk,corr[\exp(i\theta jk,corr)] = S.GjGk[\exp\ [i(\theta j + \theta k)]] + Ejk \tag{3.3}$$

The V.L.A. reduction program ANTSOL uses the N(N-1)/2 visibility measurements of N antennas to solve for the N complex Gi's, using a combination of interative and non-linear least squares solutions, and assuming that the closure errors, Ejk, are zero. In practice, once the calibration parameters are determined, the closure errors Ejk are a mixture of noise and systematic failures in the assumptions underlying this method of calibration (i.e. the "calibrator" might be partially resolved). The closure errors for

each calibrator were inspected and found to be good, with errors seldom above 10%, 10^{o} and never above 20%, 20^{o} for the 1.4GHz data. Similar results were obtained for the 5GHz data, apart from the first four calibrators (covering approximately 6 hours), for which the closure gains and phases were very poor.

Using the above solution for the gains the flux of each calibrator was calculated, on the assumption of a constant gain throughout the run, by comparison with the absolute flux of 3C286. This is important, to allow for the fact that many of the compact calibrator sources are highly variable. The resultant fluxes were well consistent with the VLA calibrator manual nominal values, apart from the first three calibrators, which were all rather low (by a factor of ~ 1.6 at 1.4GHz, and ~ 3 at 5GHz). Accordingly, the calculated fluxes of all the calibrators were used, apart from the first three sources, for which the nominal values were reinserted.

Having checked the solutions and obtained the fluxes, the calibration was applied to the data. Gain solutions were calculated from the calibrators for all antennas, and these were applied to each source using a boxcar average of all calibrators within two hours of the source.

3.2.b Mapping

All the processing of the initial UV data to produce the final maps was carried out using the standard AIPS package of the VLA. After some initial data-processing on site, the majority of the reduction was performed using the ROE Starlink VAX 11/780. For the majority of the sources, the following procedure was applied. The UV data were sorted, mapped and cleaned using the default values for most parameters. Typical values used were maps of 256 x 256 cells

with cell sizes of 1 arcsec for the 5GHz data, and 4 arcsec for the 1.4GHz data. The 5GHz data were generally untapered, while a 12kλ taper was applied to the 1.4GHz data. (For some of the larger sources, a heavier taper was used, to increase the sensitivity to low-surface brightness structure; the cell size in these cases was also increased.) The cleaned maps thus produced were then used to self-calibrate the original UV data. In the initial iteration, the calibration was applied to the phase only, weighted by amplitude. This whole process was then repeated, with amplitude and phase self-calibrations applied, until the maximum dynamic range given the limitations of the initial data was obtained.

For a number of the more extended sources, some problems occured due to the undersampling of the UV plane; this is discussed in more detail below.

3.3 : Results

3.3.a Unresolved Sources

All sources observed were initially mapped, in an attempt to detect possible faint outer structure. Ten sources were unresolved at both 1.4 and 5GHz, i.e. there was no evidence in the visibility data for any extended structure. For these sources, positions and intensities were determined by fitting a Gaussian profile to the clean map. The fitting procedure also attempts to deconvolve the clean beam; this gives an estimate of the size of the largest Gaussian which would be consistent with the data. While this may be an underestimate, if low-surface brightness structure is present, it does give an indication of the likely largest angular size (LAS) for the majority of the emission.

The fitting procedure results in positions of high accuracy, typical errors of one or two hundredths of an arcsecond being obtained. This however, is only the formal error in the position of the fitted Gaussian with respect to the map. Much larger errors may be introduced by fluctuations in the ionosphere and troposphere. Experience at the VLA suggests that the accuracy in the C array is ~0.3 arcseconds in R.A.; the error in dec is similar at high declinations, becoming a factor of two worse by -20^{o}, and progressively worse for more southerly sources.

The results for these sources are give in Table 3.1. The key to the columns is as follows:

(1) IAU type name.

(2) Other name.

(3) & (4) R.A. and Dec as described above.

(5) Total 5GHz flux denisity (Jy).

(6) Total 1.4GHz flux density (Jy).

(7) LAS of source as described above (arcseconds).

3.3.b Extended Sources

For an additional 10 sources, the 5GHz data revealed structure consisting of one or more basically isolated and essentially unresolved components. These sources were reduced in a similar manner to those above, to derive results for the individual components. The positions and flux densities of these components are given in Table 3.2, together with some notes on source structure.

The remaining 51 sources comprise those with significant resolved emission at either one or both frequencies. The data for these sources is presented primarily in the form of contour maps, in Figures 1-51 (page 58).

Table 3.1: Compact Source Parameters

(1)	(2)	(3)	(4)	(5)	(6)	(7)
0159-11	3C57	01 59 30.33	-11 46 58.9	1.52	2.50	< 2
0454-46		04 54 24.13	-46 20 31.6	1.21	2.33	< 5
0858-27	OJ-297	08 58 31.50	-27 56 33.0	1.96	1.48	< 1
1005+07	3C237	10 05 22.05	07 44 58.7	1.84	6.20	< 2
1151-34	OM-386	11 51 49.47	-34 48 48.2	2.43	5.79	< 2
1215-45		12 15 27.48	-45 43 50.4	1.87	4.56	< 4
1306-09	OP-10	13 06 02.08	-09 34 33.1	1.68	4.29	< 3
1308-22	3C283	13 08 57.35	-22 00 46.5	1.05	5.08	< 2
1424-41		14 24 46.67	-41 52 52.9	2.24	2.82	< 2
2223-05	3C446	22 23 11.07	-05 12 18.2	3.67	5.18	< 1

The quality of the final maps which can be produced from "snapshot" data such as these depends critically upon the angular scale of the source emission. The smaller sources, while barely resolved at 1.4GHz, are well sampled at 5GHz, and for these sources 5GHz data only are presented. Conversely, for the larger sources, the limited UV coverage means that the 5GHz data is not sufficiently sampled to allow a reliable map to be produced; for these sources only the lower-frequency maps are shown. This problem also effects to a lesser extent the 1.4GHz observations of the larger sources; in such cases a considerable fraction of the total single-dish flux may be lost. However, maps are still shown where these contain significant smaller scale structure. For intermediate sources, the most appropriate map is presented, unless the alternate frequency provides significant additional information, in which case both maps are shown. For four sources (0003-00, 0034-01, 0035-02 and 0038+09), the 5GHz data were affected by the presence of the sun. Two of these (0003-00, 0034-01) were subsequently reobserved; these observations are used here. 0035-02 was not reobserved, and the 5GHz data was discarded. The original 5GHz data for 0038+09 has been presented, although the map may well contain some spurious artefacts.

The considerations described above mean that a complete compilation of compact source parameters cannot be made at both frequencies. However positions, and where possible flux densities of source components are given in Table 3.2. The treatment of the various components is as follows. For sources with no obviously distinct regions of emission, the positions of the peaks of surface brightness of the source are given. Such positions are designated as 'peak' in the Table. Since the surface brightness values of the peaks are obtained simultaneously to the positions, these are also given in the Table; however care in interpreting these values should be used, since they are critically dependent upon the size of the

Table 3.2: Component Parameters for the Extended Sources

(1)	(2)	(3)	(4)	(5)	(6)	(7)	(8)	(9)	(10)	(11)	(12)
0003-00	peak	5.0	00 03 48.80	-00 21 06.0	0.02	1.10	1.39	3.31	3.40	< 10	slightly resolved in p.a. 10deg.
	opt	(5)	00 03 48.70	-00 21 06.6							
0034-01	peak	5.0	00 34 30.47	-01 25 35.0	1.0	0.27	-	1.54	2.15	57	
	peak	5.0	31.00	53.0	1.0	0.11	-				
	opt	(2)	00 34 30.52	-01 25 44.3							
0035-02	peak	1.4	00 35 47.19	-02 24 07.7	4.0	2.52	5.14	-	5.14	85	
	opt	(2)	00 35 47.26	-02 24 09.2							
0038+09	core	5.0	00 38 14.84	09 46 59.0	1.0	0.13	0.08	1.84	2.42	66	
	peak	5.0	13.82	47 23.0	1.0	0.16	-				
	peak	5.0	14.83	46 35.0	1.0	0.12	-				
	opt	(2)	00 38 15.01	09 47 01.0							
0039-44	c.c.	5.0	00 39 46.73	-44 30 26.2	0.02	0.21	0.21	0.53	2.07	6	two unresolved components
	c.c.	5.0	47.28	28.2	0.02	0.32	0.32				
	opt	(9)	00 39 46.70	-44 30 27.8							
0043-42	c.c.	5.0	00 43 51.61	-42 23 19.0	2.0	0.71	1.00	2.44	4.22	145	
		1.4				1.48	1.48				
	c.c.	5.0	44 00.64	25 01.0	2.0	0.24	0.41				
		1.4				0.55	0.55				
	opt	(2)	00 43 55.00	-42 24 13.6							
0045-25	peak	5.0	00 45 05.42	-25 33 33.0	0.75	0.33	-	0.86	4.00	~170	
		1.4				1.63	-				
	opt	(11)	00 45 07.80	-25 33 42.0							
0055-01	core	5.0	00 55 01.60	-01 39 40.0	1.5	0.07	0.03	1.29	4.38	150	
	opt	(2)	00 55 01.41	-01 39 40.6							
0105-16	core	5.0	01 05 48.77	-16 20 22.0	1.0	0.01	0.01	1.10	3.64	83	
	Np	5.0	46.48	13.0	1.0	0.16	0.47				
	Sf	5.0	50.58	32.0	1.0	0.19	0.62				
	opt	(*)	01 05 48.82	-16 20 20.0							
0117-15	peak	5.0	01 17 59.25	-15 36 05.5	1.0	0.27	-	1.50	4.29	20	
	peak	5.0	59.66	35 57.0	1.0	0.79	-				
	opt	(*)	01 17 59.74	-15 36 00.7							
0123-01	core	1.4	01 23 27.41	-01 36 16.7	0.15	0.05	0.05	-	3.25	~600	*
	p	1.4	09.98	38 20.0	4.0	0.07	0.47				
	Sf	1.4	30.00	39 28.0	4.0	0.10	2.07				
	Nf	1.4	31.87	34 04.0	4.0	0.10	0.65				
	opt	(4)	01 23 27.48	-01 36 17.2							
0131-36	p	1.4	01 31 09.6	-36 44 01	20.0	0.05	1.43	-	4.23	800	
	f	1.4	32 02.1	45 37	8.0	0.26	2.80				
	opt	(2)	01 31 43.63	-36 44 55.6							
0157-31	peak	5.0	01 57 58.51	-31 07 47.8	1.0	0.39	-	1.33	2.84	40	
	peak	5.0	58.58	08 07.0	1.0	0.20	-				
	opt	(*)	01 57 58.35	-31 07 57.2							
0213-13	core	5.0	02 13 12.22	-13 13 24.0	1.5	0.02	0.02	1.54	4.39	90	
	p	5.0	9.75	24.0	1.5	0.34	0.95				
		1.4				1.76	-				
	f	5.0	14.27	30.0	1.5	0.13	0.57				
		1.4				1.03	-				
	opt	(*)	02 13 12.27	-13 13 25.3							
0235-19	p	5.0	02 35 23.27	-19 45 31.0	1.0	0.12	0.43	1.28	4.32	53	
	f	5.0	25.96	34.0	1.0	0.38	0.85				
	opt	(*)	02 35 24.77	-19 45 31.7							
0240-00	peak	5.0	02 40 07.07	-00 13 30.0	1.0	0.77	-	1.86	5.07	~130	
		1.4				3.86	-				
	opt	(5)	02 40 07.00	-00 13 30.0							
0255+05	peak	1.4	02 55 00.00	05 51 20.0	4.0	0.21	-	-	5.08	~430	*
	opt	(4)	02 55 03.01	05 49 20.7							
0305+03	peak	5.0	03 05 48.97	03 55 14.0	1.0	0.93	-	3.15	6.98	230	
		1.4				1.63	-				
	opt	(2)	03 05 49.07	03 55 13.1							
0325+02	core	5.0	03 25 18.19	02 23 20.6	0.01	0.13	0.13	0.64	3.80	235	
		1.4				0.15	-				
	peak	5.0	12.2	22 30	5.0	0.02	0.30				
		1.4				0.22	-				
	peak	5.0	23.8	24 17	5.0	0.01	0.20				
		1.4				0.25	-				
	opt	(2)	03 25 18.25	02 23 20.4							

Table 3.2: Continued

(1)	(2)	(3)	(4)	(5)	(6)	(7)	(8)	(9)	(10)	(11)	(12)
0347+05	c.c.	5.0	03 47 06.64	05 43 11.1	0.01	0.27	0.34	1.07	2.91	62	Np component slightly
		1.4				1.00	1.00				resolved; Sf component
	c.c.	5.0	07.37	42 11.0	0.01	0.64	0.73				extended in p.a. 0deg.
		1.4				1.91	1.91				
	opt	(*)	03 47 06.81	05 42 08.1							
0349-27	Sp	1.4	03 49 19.08	-27 55 24.0	5.0	0.29	1.14	-	4.17	415	
	Nf	1.4	40.95	- 52 09.0	5.0	0.79	3.03				
	c.c.	1.4				0.79	1.00				
	opt	(2)	03 49 31.85	-27 53 30.4							
0404+03	peak	5.0	04 04 48.13	03 32 48.0	1.0	1.01	-	1.65	5.22	380	
		1.4				2.78	-				
	peak	1.4	32.77	36 16.7	4.0	0.15	-				
	opt	(2)	04 04 38.54	03 34 27.2							
0405-12	core	5.0	04 05 27.45	-12 19 32.6	0.02	0.78	0.87	1.41	2.88	42	
	S	5.0	27.16	45.0	1.0	0.10	0.22				
	N	5.0	27.57	15.0	1.0	0.20	0.32				
	opt	(5)	04 05 27.46	-12 19 32.3							
0442-28	peak	5.0	36.38	14 39.0	1.5	0.36	-	2.11	6.19	110	
		1.4				1.31	-				
	peak	5.0	39.56	15 52.5	1.5	0.25	-				
		1.4				1.22	-				
	opt	(*)	04 42 37.78	-28 15 22.5							
0453-20	peak	5.0	04 53 13.85	-20 38 54.5	0.75	0.26	-	1.72	4.21	37	*
	opt	(*)	04 53 14.12	-20 38 59.2							
0518-45	core	5.0	05 18 23.59	-45 49 37.9	0.06	0.85	0.92	4.73	54.2	480	
		1.4				1.25	-				
	c.c	5.0	00.24	48 50.9	5.0	2.15	2.84				
		1.4				8.91	-				
	c.c	5.0	40.42	50 35.9	5.0	0.42	-				
	c.c	5.0	42.33	35.9	5.0	0.29	-				
	peak	1.4	40.41	26.0	5.0	3.02	-				
	opt	(2)	05 18 24.10	-45 49 45.0							
0521-36	peak	5.0	05 21 12.90	-36 30 14.0	1.0	1.97	-	6.59	15.8	50	
	peak	5.0	13.56	18.0	1.0	1.52	-				
	opt	(2)	05 21 13.00	-36 30 14.0							
0625-35	c.c.	5.0	06 25 20.27	-35 27 20.2	0.02	0.73	0.85	1.04	4.55	270	
	peak	1.4				1.62	-				
	opt	(*)	06 25 20.23	-35 27 21.8							
0634-20	N	1.4	06 34 22.0	-20 26 28	8.0	0.48	3.60	-	8.22	900	
	S	1.4	24.3	40 04	8.0	1.79	4.62				
	opt	(2)	06 34 23.10	-20 32 18.0							
0806-10	core	5.0	08 06 30.31	-10 18 49.5	1.5	0.04	0.02	1.28	3.88	137	
		1.4				0.42	-				
	Sp	5.0	29.19	19 42.0	1.5	0.19	1.00				
		1.4				1.15	-				
	Nf	5.0	31.73	17 57.0	1.5	0.08	0.28				
		1.4				0.74	-				
	opt	(*)	08 06 30.21	-10 18 49.5							
0825-20	core	5.0	08 25 03.60	-20 16 27.0	0.03	0.04	0.04	1.15	3.79	14	three slightly
	c.c.	5.0	03.17	22.5	0.01	0.70	0.74				resolved components
	c.c.	5.0	04.00	34.7	0.01	0.30	0.33				
	opt	(1)	08 25 03.40	-20 16 31.0							
0859-25	peak	5.0	08 59 35.19	-25 43 14.0	1.0	0.34	0.47	1.52	5.44	56	
	peak	5.0	37.78	39.0	1.0	0.57	0.70				
	opt	(*)	08 59 36.42	-25 43 23.9							
0915-11	peak	5.0	09 15 41.09	-11 53 16.0	1.0	1.22	-	12.1	39.2	~250	
	peak	5.0	41.30	52 55.0	1.0	2.10	-				
	opt	(2)	09 15 41.20	-11 53 04.4							
0945+07	peak	1.4	09 44 59.32	07 38 57.0	3.0	0.46	-	-	7.49	245	
	peak	1.4	45 13.65	39 15.0	3.0	1.43	-				
	opt	(2)	09 45 06.61	07 39 17.1							
1017-42	c.c.	5.0	10 17 56.20	-42 36 28.9	0.01	0.82	-	1.10	4.10	13	two overlapping
	c.c.	5.0	56.77	18.0	0.01	0.20	-				components
	opt	(*)	10 17 56.47	-42 36 23.2							
1136-13	peak	5.0	11 36 37.94	-13 34 01.8	0.75	0.43	-	1.68	4.45	31	
	peak	5.0	38.55	07.0	0.75	0.54	-				
	opt	(5)	11 36 38.51	-13 34 05.9							

Table 3.2: Continued

(1)	(2)	(3)	(4)	(5)	(6)	(7)	(8)	(9)	(10)	(11)	(12)
1216+06	core	5.0	12 16 50.00	06 06 08.9	0.01	0.29	0.29	-	1.60	530	
	core	1.4				0.22	-				
	opt	(2)	12 16 50.02	06 06 08.5							
1246-41	peak	5.0	12 46 03.55	-41 02 17.0	1.0	0.34	-	1.08	3.86	45	
	opt	(2)	12 45 54.00	-41 01 42.0							
1251-12	core	5.0	12 51 58.57	-12 17 51.9	0.10	0.08	0.08	-	8.17	~240	*
	opt	(4)	12 51 58.85	-12 17 53.5							
1318-43	peak	1.4	13 18 22.91	-43 25 30.0	8.0	0.43	-	-	5.19	~1050	
	opt	(2)	13 18 17.35	-43 26 34.3							
1333-33	core	1.4	13 33 47.05	-33 42 40.0	4.0	0.16	-	-	3.63	~700	
	peak	1.4	44.48	12.0	4.0	0.25	-				
	peak	1.4	50.58	43 16.0	4.0	0.26	-				
	opt	(2)	13 33 47.30	-33 42 40.0							
1355-41	core	5.0	13 55 57.16	-41 38 18.0	1.0	0.08	0.08	1.22	4.16	66	
	c.c	5.0	55.02	03.0	1.0	0.29	-				
	c.c	5.0	55.64	37 59.0	1.0	0.07	-				
	peak	1.4				1.80	-				
	c.c	5.0	59.57	38 33.0	1.0	0.35	0.51				
	peak	1.4				1.52	-				
	opt	(5)	13 55 57.27	-41 38 19.3							
1453-10	core	5.0	14 53 12.10	-10 56 38.4	0.02	0.12	0.12	1.30	4.05	35	components slightly resolved
	Np	5.0	11.58	27.7	0.02	0.22	0.25				
	Sf	5.0	12.58	59.9	0.02	0.39	0.93				
	opt	(5)	14 53 12.22	-10 56 39.9							
1514+07	peak	5.0	15 14 17.00	07 12 17.0	1.0	0.31	-	1.08	5.34	100	
		1.4				2.43	-				
	opt	(2)	15 14 17.00	07 12 16.7							
1518+04	c.c.	5.0	15 18 44.77	04 41 05.9	0.03	0.98	0.98	1.07	4.31	60	two unresolved components
		1.4				4.10	4.10				
	c.c.	5.0	46.82	40 14.9	0.03	0.09	0.09				
		1.4				0.21	0.21				
	opt	(*)	15 18 44.73	04 41 05.5							
1559+02	peak	1.4	15 59 44.19	02 06 40.0	4.0	0.53	-	-	8.19	325	
	peak	1.4	16 00 01.80	05 56.0	4.0	1.19	-				
	opt	(2)	15 59 55.67	02 06 12.3							
1602+01	peak	5.0	16 02 12.51	01 26 01.0	0.75	0.31	-	1.02	4.08	20	
	peak	5.0	13.30	25 55.8	0.75	0.30	-				
	opt	(10)	16 02 13.00	01 25 59.0							
1648+05	peak	5.0	16 48 36.08	05 04 44.0	2.0	0.25	3.91	11.5	45.2	210	
	peak	5.0	43.58	16.0	2.0	0.75	7.56				
	opt	(2)	16 48 39.98	05 04 35.0							
1717-00	peak	1.4	17 17 45.00	-00 55 59.0	4.0	1.63	-	-	46.8	300	
	peak	1.4	59.40	35.0	4.0	2.28	-				
	opt	(2)	17 17 53.29	-00 55 49.5							
1932-46	peak	5.0	19 32 16.58	-46 27 11.0	1.0	0.35	-	3.57	11.2	34	
	peak	5.0	19.48	21.0	1.0	1.61	-				
	opt	(*)	19 32 18.24	-46 27 20.4							
1938-15	peak	5.0	19 38 24.55	-15 31 35.4	1.0	1.23	-	2.13	6.58	< 18	resolved in p.a. 40deg.
	opt	(*)	19 38 24.45	-15 31 34.4							
1949+02	peak	5.0	19 49 41.40	02 22 38.0	1.5	0.23	0.59	1.75	5.64	215	*
		1.4				1.50	-				
	peak	5.0	46.30	45.5	1.5	0.06	-				
	peak	5.0	47.90	48.5	1.5	0.15	-				
	peak	1.4	47.57	49.0	4.0	0.98					
	opt	(2)	19 49 44.57	02 22 37.1							
2032-35	S	5.0	20 32 37.04	-35 04 48.0	1.0	0.25	0.42	1.68	5.54	35	
	N	5.0	37.28	18.0	1.0	1.11	1.26				
	opt	(*)	20 32 37.02	-35 04 32.9							
2058-28	peak	5.0	20 58 38.59	-28 13 42.0	3.0	0.06	-	1.26	4.88	~555	*
	peak	5.0	40.41	14 15.0	3.0	0.02	-				
	peak	5.0	36.32	12 26.0	3.0	0.02	0.25				
	peak	1.4				0.27	-				
	peak	5.0	43.74	14 46.0	3.0	0.03	0.87				
	peak	1.4				0.27	-				
	opt	(8)	20 58 38.68	-28 13 44.1							

Table 3.2: Continued

(1)	(2)	(3)	(4)	(5)	(6)	(7)	(8)	(9)	(10)	(11)	(12)
2104-25	peak	1.4	21 04 26.80	-25 38 34.0	4.0	0.62	-	-	11.1	~525	*
	peak	1.4	30.64	37 18.0	4.0	0.73	-				
	opt	(3)	21 04 29.20	-25 37 51.0							
2135-14	core	5.0	21 35 01.16	-14 46 27.0	0.02	0.12	0.12	1.23	3.85	180	
	Np	5.0	34 56.83	12.0	2.5	0.18	0.63				
	Sf	5.0	35 04.58	37.0	2.5	0.05	0.47				
	opt	(5)	21 35 01.21	-14 46 27.3							
2211-17	peak	5.0	22 11 41.77	-17 15 42.0	1.5	0.09	-	2.29	8.11	130	
	peak	5.0	42.71	17 19.5	1.5	0.10	-				
	opt	(*)	22 11 42.60	-17 16 31.0							
2221-02	peak	1.4	22 21 11.76	-02 17 00.0	8.0	0.11	-	-	2.81	600	
	peak	1.4	13.37	-02 16 36.0	8.0	0.27	-				
	peak	1.4	17.64	25 56.0	8.0	0.46	-				
	opt	(2)	22 21 14.66	-02 21 26.8							
2250-41	c.c.	5.0	22 50 11.77	-41 13 42.6	0.75	0.38	0.30	0.86	3.70	17	some lsb emission between components
	c.c.		13.24	44.7	0.75	0.45	0.45				
	opt	(6)	22 50 12.22	-41 13 44.8							
2314+03	c.c.	5.0	23 14 01.89	03 48 55.5	0.5	0.19	-	0.91	4.45	7	two unresolved components
	c.c.	5.0	02.37	55.0	0.5	0.73	-				
	opt	(10)	23 14 02.31	03 48 54.9							
2331-41	Sp	5.0	23 31 44.76	-41 42 07.3	0.75	0.55	-	1.20	4.45	25	
	Nf	5.0	46.30	41 56.8	0.75	0.25	-				
	opt	(7)	31 31 45.43	-41 42 02.6							

References for optical positions:

(*) = This Thesis.
(1) = Bolton & Kinman, 1966.
(2) = Burbidge & Crowne, 1979.
(3) = Christiansen et al., 1977.
(4) = Griffin, 1963.
(5) = Hewitt & Burbidge, 1980.
(6) = Hunstead, 1971.
(7) = Lu, 1970.
(8) = Schilizzi, 1975.
(9) = Savage, 1976.
(10) = Smith & Spinrad, 1980.
(11) = de Vaucouleurs et al., 1976.

beam in comparison to the source structure. For sources where separate regions of emission are present, total component flux densities are given, as well as the component position; these cases are distinguished by a positional designation (e.g. Np, Sf). Finally, where possible, flux densities of compact source components (c.c.) are also given.

The positions of peak surface brightness for extended emission were determined using a cursoring routine on the map. For well defined positions, the quoted error corresponds to one pixel; in more diffuse regions, a larger error results due to the difficulty of defining the peak. Positions for compact components were again determined by Gaussian fitting, with a similar accuracy as for the unresolved sources. Again, in all cases the effects of atmospheric phase errors should be added, as described above.

Flux densities for resolved components were determined by summation over the relevant area of the map; for core components an attempt has been made to subtract the contribution of extended emission where possible. Identical values for peak surface brightness (Jy/beam) and total flux density (Jy) for a component indicate that it is unresolved. The total flux density in the mapped region has also been given, although this has been omitted for sources which were grossly undersampled.

Finally, the optical identification of each source has been marked with a cross on the countour maps (except for those sources for which a compact core is present); the positions of the optical counterparts are also given in the Table.

The key to the columns for Table 3.2 is as follows:

(1) IAU name.

(2) Source component.

(3) Frequency of observation in GHz; ref. for optical position.

(4) & (5) R.A. and Dec of component.

(6) Error of position in arcseconds.

(7) Peak surface brightness (Jy/beam).

(8) Component flux density (Jy).

(9) & (10) Total 5GHz/1.4GHz flux density in map (Jy).

(11) LAS of source in arcseconds.

(12) Comments on source structure (an asterisk indicates that the source is discussed further below).

3.4 : Discussion

The sources mapped in Figs. 1-51 provide a number of good examples of the classifications discussed in Chapter One, from good 'classical doubles' (e.g. 0043-42), through FRIIs (0131-36) to FRIs (0915-11). For the purposes of this thesis, the main aim of these observations was to enable such FR classifications to be obtained for the lower-redshift objects, for which the clustering analysis was to be performed. These are presented in Chapters Four and Five; and in the remainder of this chapter we will simply consider the structure of some of the more complex low-redshift objects. One of these, 1949+02, has an unusual region of low surface brightness emission. Another, 0453-20, is a possible example of a source with precessing jets. Finally, there are five low-redshift galaxies with rather complex radio structure.

3.4.a 0453-20

This source has been identified with a 14th mag elliptical galaxy (Bolton et al., 1965); our 5GHz map is shown in Fig. 22. The morphology of this source is rather unusual; a ridge of high surface brightness crosses the identification position, with subsidiary ridges of emission on either side. This structure is very similar to the low-resolution 1.4GHz map of 2300-189 presented by Hunstead et al. (1984). This is a 17th mag object (z = 0.13) described by them as a QSO, but originally described as an N galaxy. Higher-resolution maps of 2300-189 reveal that the emission is of the form of two oppositely directed curved jets (with 'S' shaped symmetry); this is explained by Hunstead et al. as being due to the ejection of the jets along an axis which is precessing, probably under the tidal influence of a nearby galaxy. A higher resolution map of 0453-20 would be of interest, to see whether such a model would also fit these data.

3.4.b 1949+02

The identification of this source (3C403) is with a 15.4 mag E galaxy (Clarke et al., 1966). Previous radio observations (Fomalont, 1971) have shown this source to have a simple double structure. However, our 5GHZ map (Fig. 44a) reveals that the eastern lobe contains two hot-spots. The 1.4GHz map confirms the presence, less well defined by the 5GHz observations, of symmetric regions of low surface brightness emission, oriented at an angle of approximately 40 degrees to the axis of the hot-spots. The appearance of this object is remarkably similar to that of 3C52 (Leahy and Williams, in preparation). They suggest that such source distortion may be created if the source axis has changed in the past. The old 'cocoon' of material from the previous jet might then provide a channel into

which the backflow from the present hot-spot may be deflected.

3.4.c Low-Redshift Radio Galaxies

There are five low-redshift ($z < 0.04$) galaxies in the sample which have unusually complex radio morphology. The optical counterparts of these sources are in four cases 'dumb-bell' galaxies, with two E galaxies within a common extended envelope. All of these sources are also associated with groups or clusters of a greater or lesser richness. Brief descriptions of these sources are given below.

0123-01 (3C40). Low resolution (~ 3-4 arcmin) maps of this source have been presented by Schilizzi et al. (1972) and Schilizzi and McAdam (1975). It has been described as having "two main peaks, an extended arc-like structure to the north, and an extension to the west of the southern peak" (Schilizzi et al., 1972). The optical identification has been made with the double galaxy NGC 545-547 (Mills, 1960), a pair of closely spaced 13th mag elliptical galaxies, classified as cD4 by Matthews et al. (1964). Schilizzi et al. (1972) also noted that a third 13th mag elliptical galaxy, NGC541, lay within their radio contours. All these objects are members of the Abell cluster A194 (richness class 0); accurate positions have been measured by Griffin (1963), and are listed in Table 3.3.

Our higher resolution map (Fig. 9) provides some new information. Firstly, the observation of a compact core suggests that the main radio source is associated with the galaxy NGC547, rather than the dumb-bell system as a whole. Secondly, the emission to the west of the main source is resolved into a separate 'head-tail' source, associated with NGC541.

Table 3.3: Optical Positions for Objects in the Fields of Low-Redshift Radio Galaxies

0123-01	(1)	01 23 11.17	-01 38 20.9		(NGC 541)
		01 23 26.00	-01 35 59.5	in common	(NGC 545)
		01 23 27.48	-01 36 17.2	envelope	(NGC 547)
0255+05	(1)	02 55 02.95	05 49 37.02	in common	
		02 55 03.01	05 49 20.74	envelope	
1251-12	(1)	12 50 58.85	-12 17 53.5	in common	
		12 51 59.05	-12 17 14.3	envelope	
2058-28	(2)	20 58 38.68	-28 13 44.1		
2104-25	(3)	21 04 29.2	-25 37 51	in common	
		21 04 30.2	-25 37 51	envelope	

(1) position from Griffin (1963)

(2) position from Schilizzi (1975)

(3) position from Christiansen et al. (1977)

CCD observations (Chapter Six) show that the two galaxies NGC545-7 are embedded in a common outer isophote. Detailed optical observations of this system have been made by Arp and Bertola (1971) and Simkin (1977), and reveal a prominant optical bridge connecting NGC545-7 with NGC541, as first noted by Zwicky and Humason (1964). Simkin (1977) has found that this region has a (B-V) colour and continuum spectrum consistent with it being composed primarily of stars comparable to those in the outer regions of the galaxies it connects. It is interesting to note that the head-tail source lies in same direction as the optical bridge; however the suggestion of Simkin that in fact the radio emission in this region is emanating from "Minkowski's object", a peculiar galaxy ~ 55 arcsec east of NGC541, is not supported by our observations.

0255+05 (3C75). This source is associated with a 15th mag dumb-bell galaxy (Maltby et al., 1963), the dominant member of the Abell cluster A400, (richness class 1). It has been described by Matthews et al. (1964) as "ED2 + ED1 in common envelope"; and the cluster is cited as the standard by Bautz and Morgan (1970) for their BM class II-III. The CCD observations of Chapter Six reveal that the two galaxies are symmetrically disposed upon either side of the centre of spherically symmetric faint outer isophotes. Accurate positions for the two objects, obtained by Griffin (1963) are listed in Table 3.3.

No obvious core emission has been detected for this source (Fig. 15), although this might be hidden by the jet emission. The radio structure is of the 'twin-tail' type, (Simon, 1978) although it is rather complex. The eastern tail bends sharply north after about 50kpc and then back eastwards, while the more smoothly curved western tail bends more sharply westwards after 150kpc, before petering out into low-surface-brightness emission.

1251-12 (3C278). The identification of this source with the close pair of galaxies NGC 4782-4783 was first made by Mills et al. (1958), and has been discussed by Maltby et al. (1963). The system is classified as "DE2 + DE2 in common envelope" by Matthews et al. (1964). The positions of Griffin (1963) are given in Table 3.3; again, the observation of a strong radio core for this source (Fig. 34a) indicates an association with the southern galaxy of the pair. The optical observations of this system is discussed in more detail in Chapter Six. At 5GHz the source appears as a twin-tail; with the eastern tail terminating in a rather extended, low surface brightness region. At 1.4GHz, a more diffuse halo surrounds the whole source.

2058-28. This source has been observed at ~ 1 arcmin resolution by Christiansen et al. (1977), who also discuss previous radio observations. An accurate position for the 16th mag E galaxy identification (Bolton, et al., 1964) has been given by Schilizzi (1975). Our 5GHz map (Fig. 46a) reveals a basic double structure; a compact core is associated with the identification, while a 50kpc long jet extends towards the southern lobe, terminating rather abruptly before reaching it. The southen lobe appears extended approximately perpendicular to this jet, and the lower resolution 1.4GHz map (Fig 46b) reveals extended low-surface brightness structure in this region. In addition, there is an extended diffuse region extending northwards from the east side of the northen lobe.

2104-25. This final source has also been observed by Christiansen et al. (1977). As discussed by them, the identification with a 17th mag E galaxy by Bolton (1965) is incorrect. Our observations confirm that the true identification is with a 13.5 mag dumb-bell galaxy, as suggested by Christiansen et al. They suggest that the arc-like structure to the south might be a separate

head-tail source. However, our observations indicate that it is in fact associated with the double source; tails of emission extend north-westwards from both lobes, the northern one rapidly degenerates, while the southern one appears to bend southwards, and then experiences a rapid increase in brightness and extends some 350kpc to the south east, before again petering out in low-surface-brightness structure.

Figures 1.- 51.

Contour maps of the extended sources in the sample. Each map contains eight equally spaced positive logarithmic contours; in each case the highest contour level has been set to the peak surface brightness in the map (Jy or mJy/beam). The ratio of the highest to lowest contour levels is also given, and the intervening levels may be calculated from these quantities.

For example, for a source with a peak surface brightness of 3Jy/beam, and a contour ratio of 50:1, the contour levels are set to

$$C_n = 3/50 \times (50^{\frac{n-1}{7}}), \quad n = 1\text{-}8$$

$$= 0.06 \times (1.0,\ 1.7,\ 3.1,\ 5.3,\ 9.4,\ 16.4,\ 28.6,\ 50)\ \text{Jy/beam}$$

In addition, one negative contour of absolute value equal to the lowest positive contour has been plotted.

The clean beam (FWHM) is indicated by a shaded ellipse.

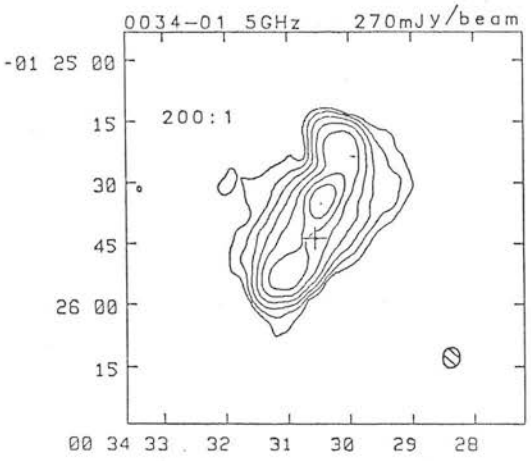

Figure 1. A 5GHz map of 0034-01

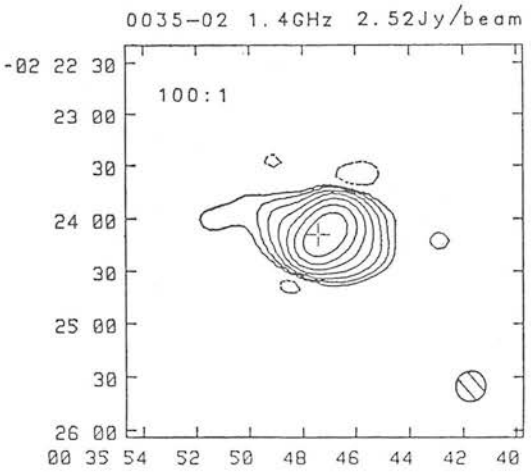

Figure 2. A 1.4GHz map of 0035-02

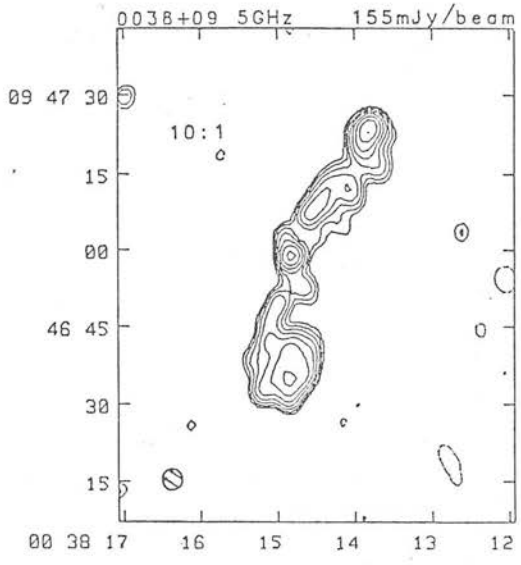

Figure 3. A 5GHz map of 0038+09

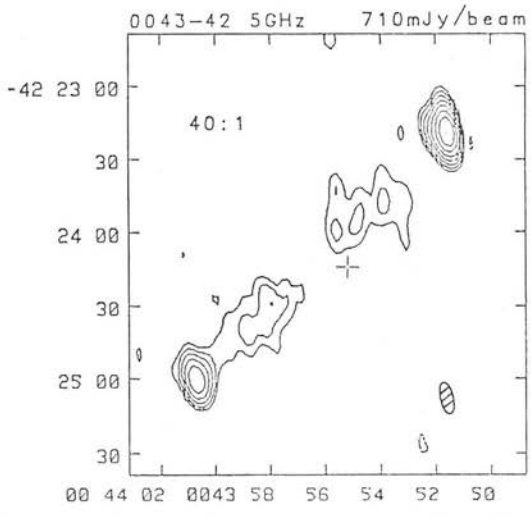

Figure 4. A 5GHz map of 0043-42

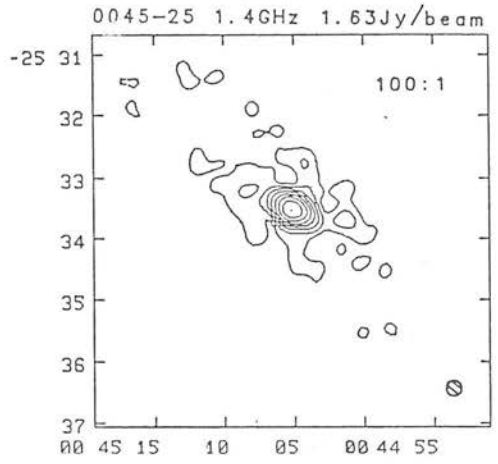

Figure 5. A 1.4GHz map of 0045-25

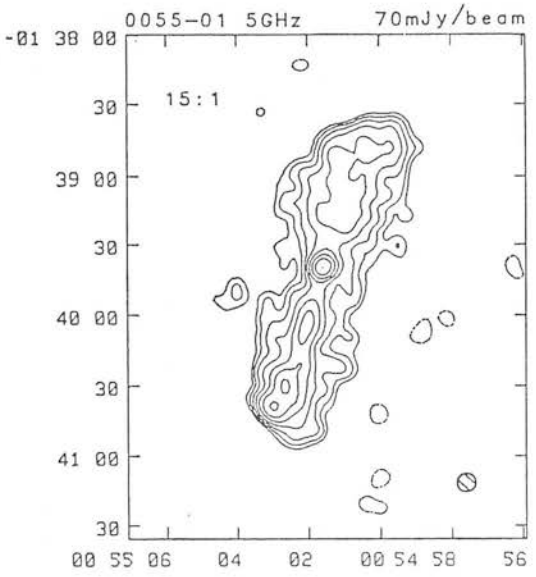

Figure 6. A 5GHz map of 0055-01

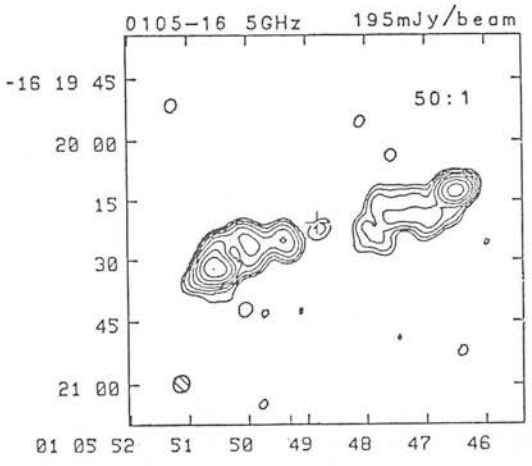

Figure 7. A 5GHz map of 0105-16

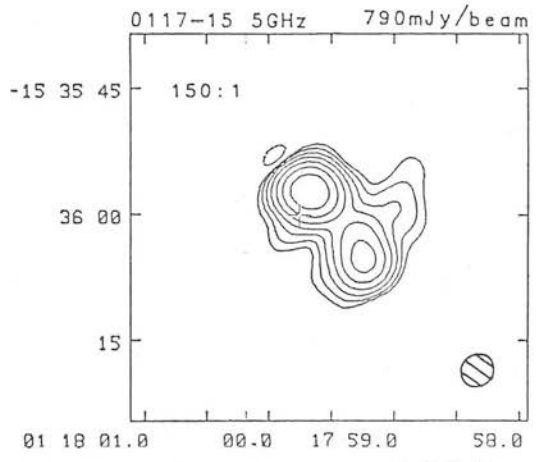

Figure 8. A 5GHz map of 0117-15

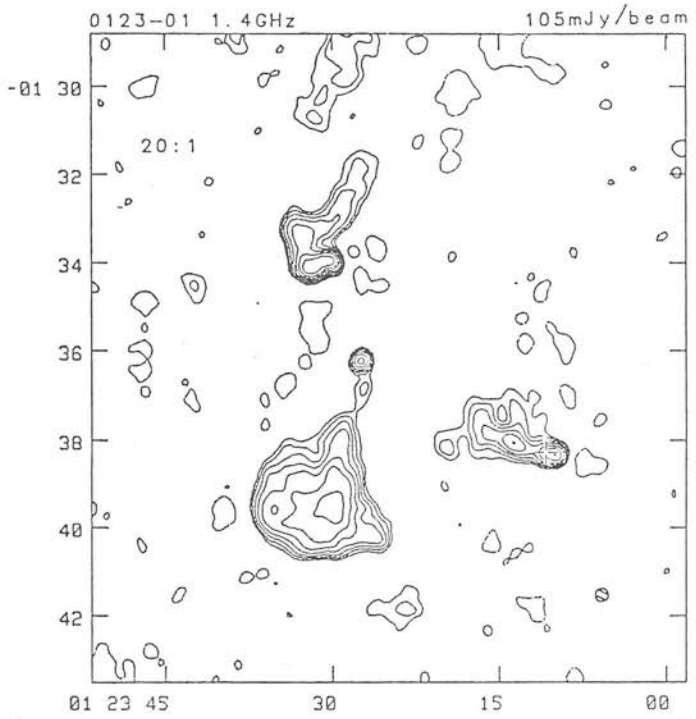

Figure 9. A 1.4GHz map of 0123-01

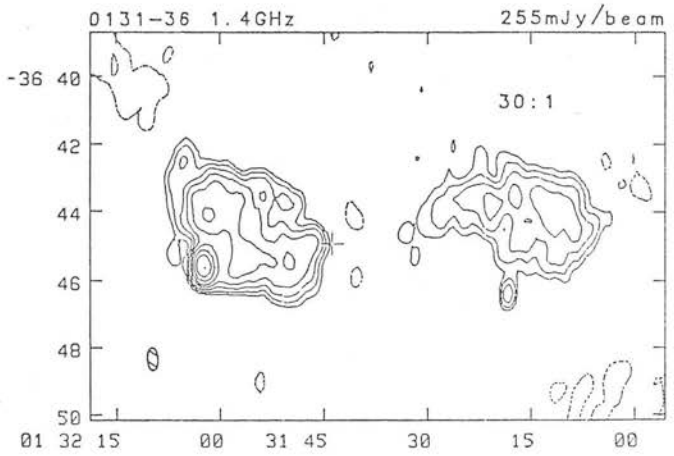

Figure 10. A 1.4GHz map of 0131-36

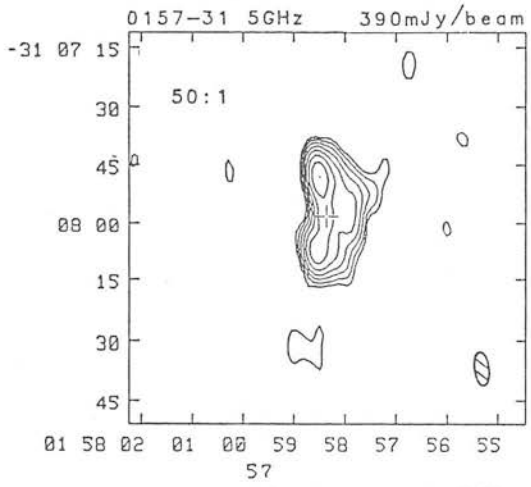

Figure 11. A 5GHz map of 0157-31

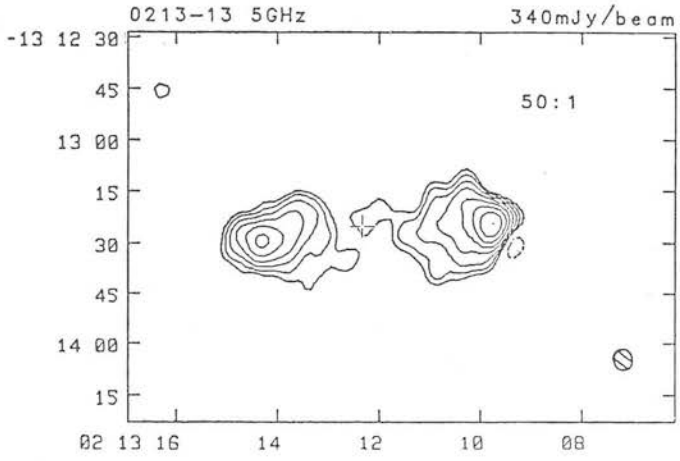

Figure 12. A 5GHz map of 0213-13

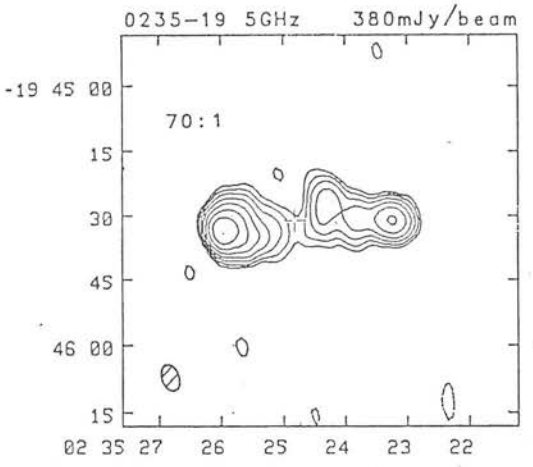

Figure 13. A 5GHz map of 0235-19

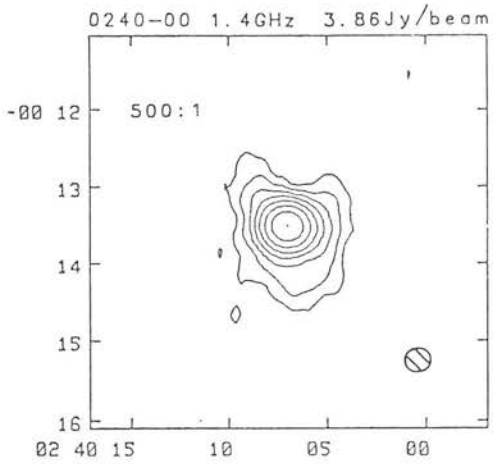

Figure 14. A 1.4GHz map of 0240-00

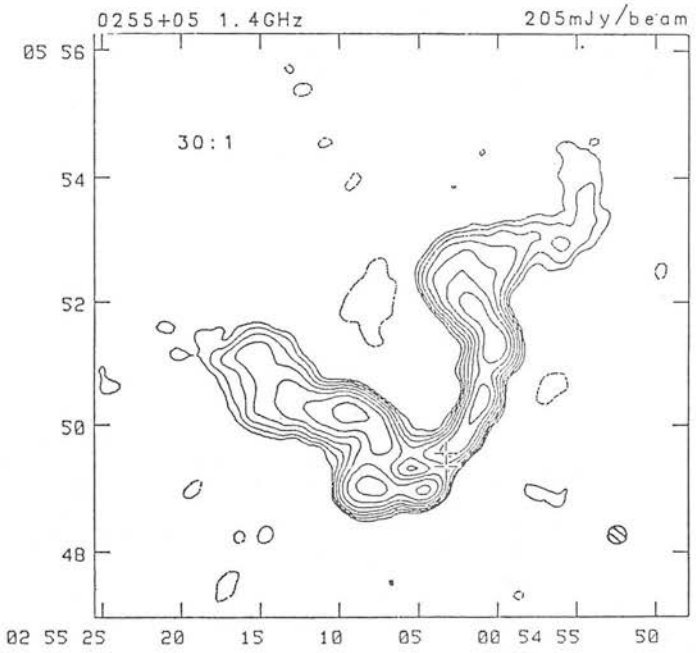

Figure 15. A 1.4GHz map of 0255+05

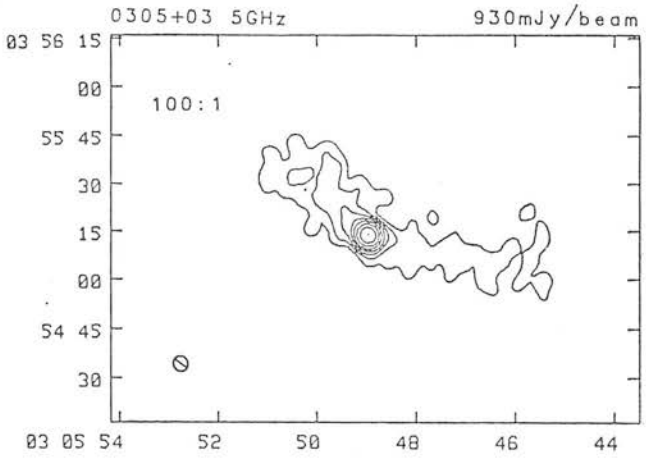

Figure 16a. A 5GHz map of 0305+03

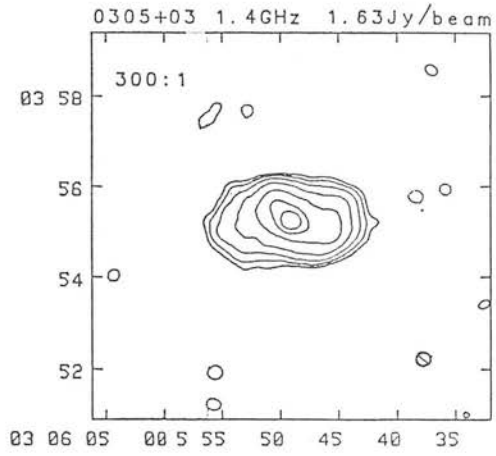

Figure 16b. A 1.4GHz map of 0305+03

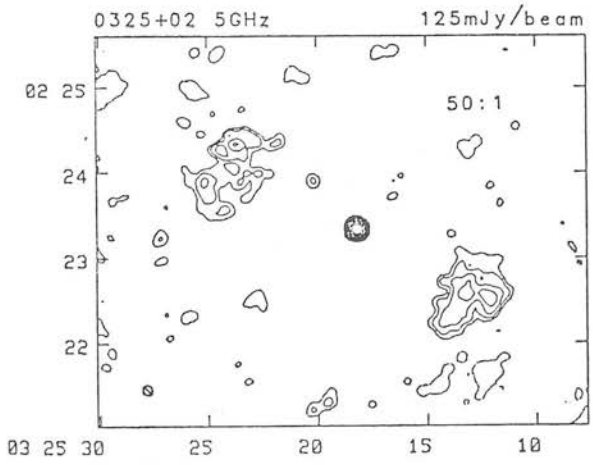

Figure 17a. A 5GHz map of 0325+02

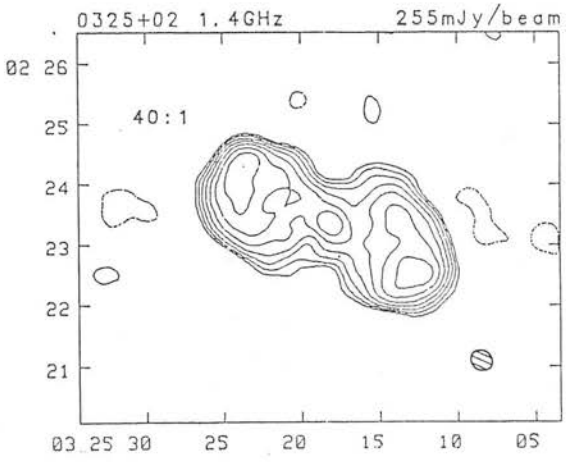

Figure 17b. A 1.4GHz map of 0325+02

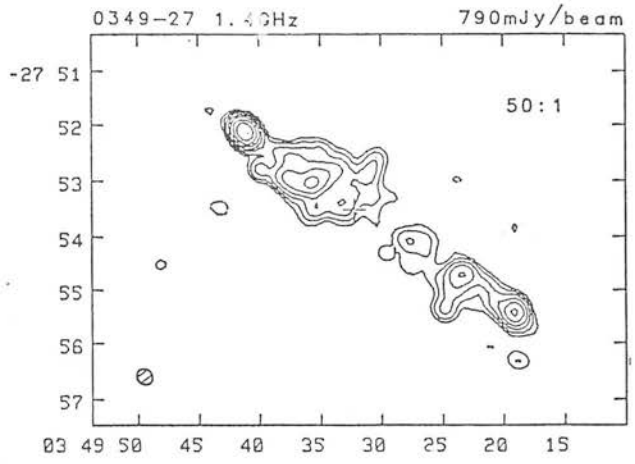

Figure 18. A 1.4GHz map of 0349-27

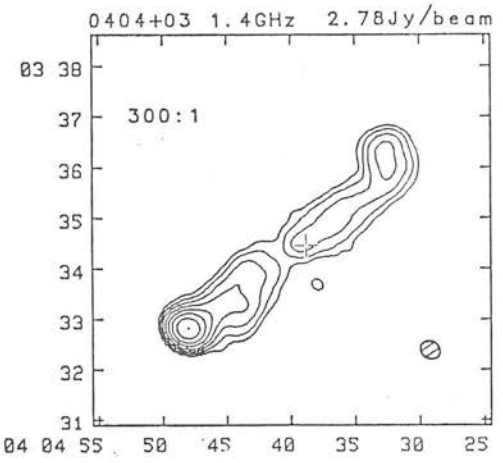

Figure 19. A 1.4GHz map of 0404+03

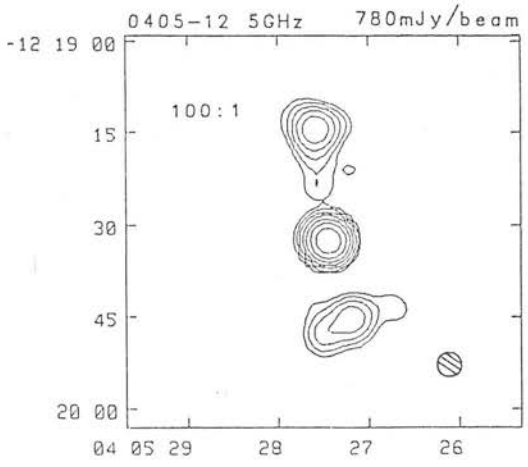

Figure 20. A 5GHz map of 0405-12

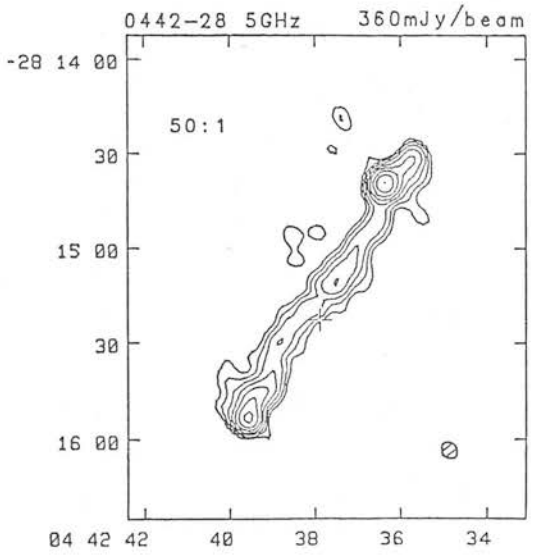

Figure 21. A 5GHz map of 0442-28

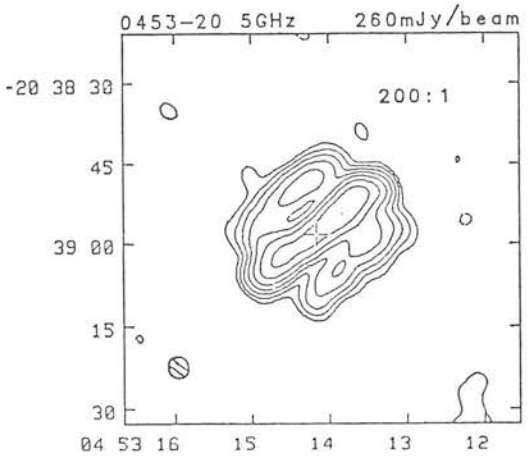

Figure 22. A 5GHz map of 0453-20

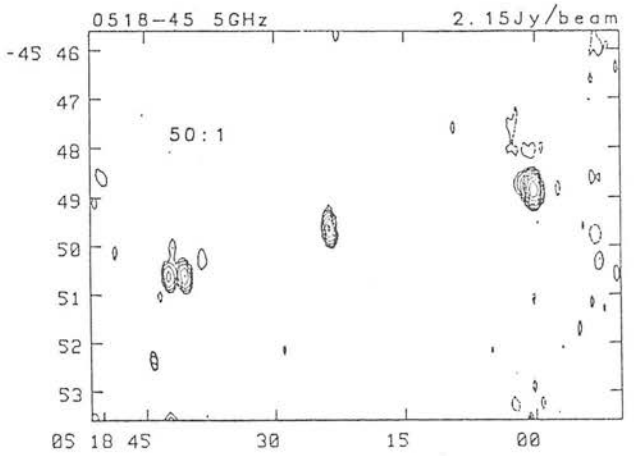

Figure 23a. A 5GHz map of 0518-45

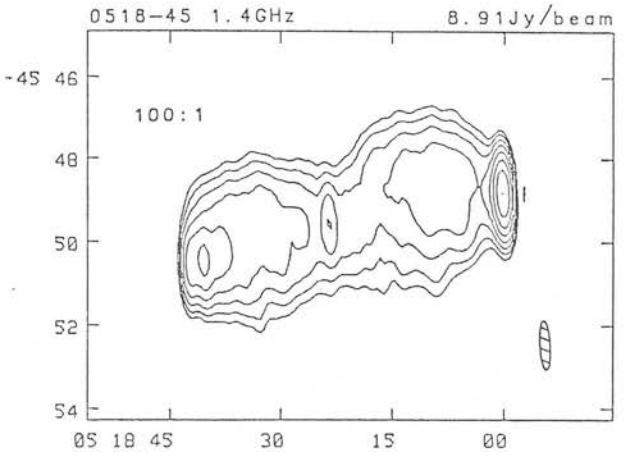

Figure 23b. A 1.4GHz map of 0518-45

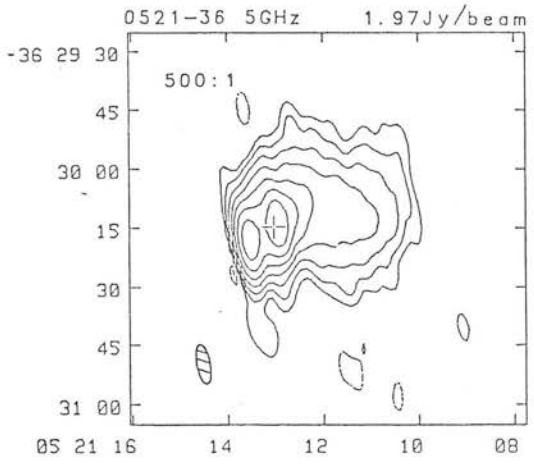

Figure 24. A 5GHz map of 0521-36

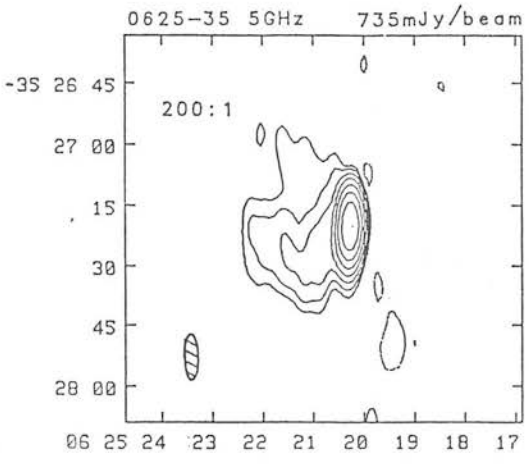

Figure 25a. A 5GHz map of 0625-35

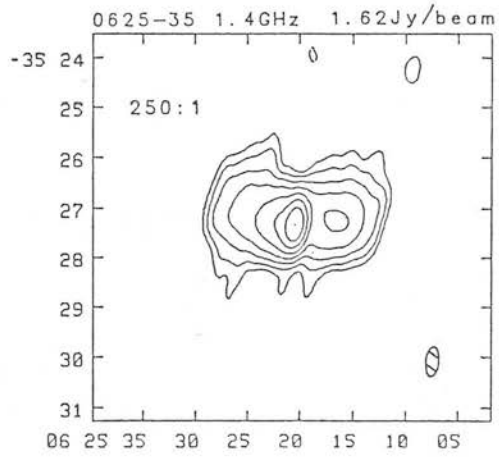

Figure 25b. A 1.4GHz map of 0625-35

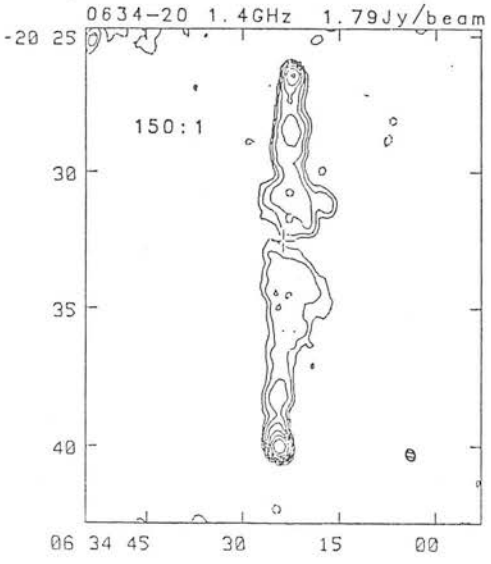

Figure 26. A 1.4GHz map of 0634-20

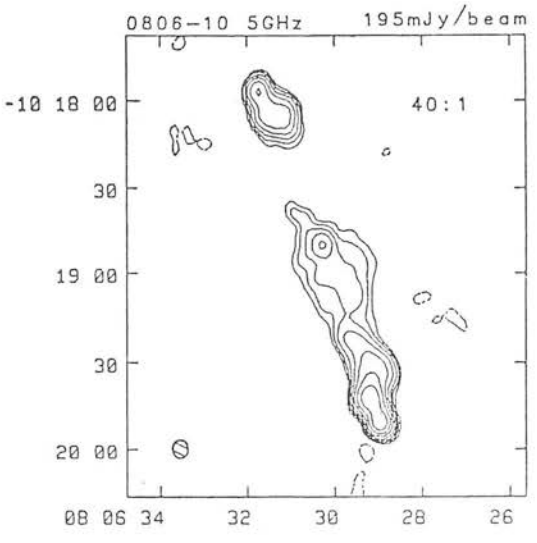

Figure 27. A 5GHz map of 0806-10

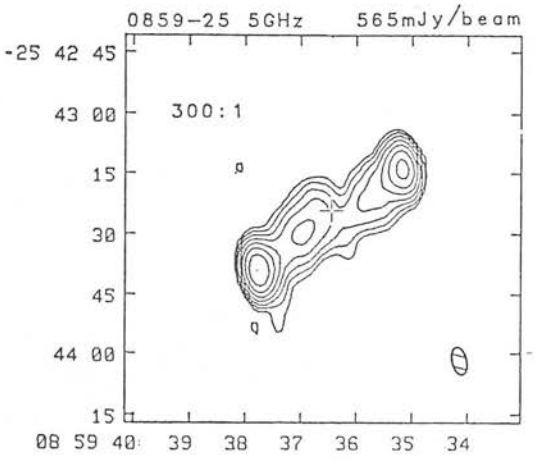

Figure 28. A 5GHz map of 0859-25

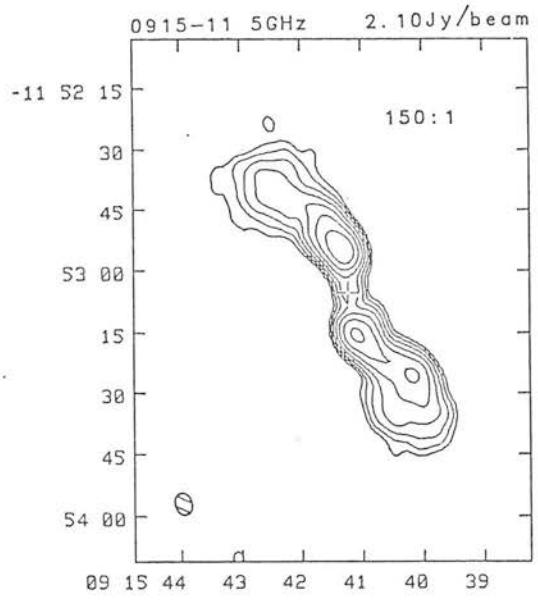

Figure 29a. A 5GHz map of 0915-11

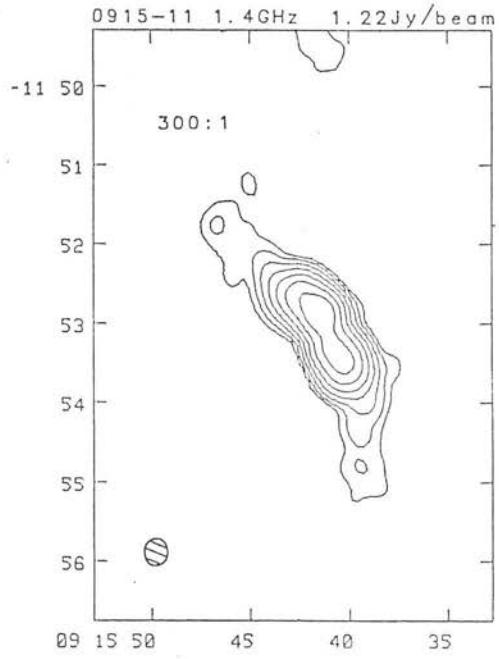

Figure 29b. A 1.4GHz map of 0915-11

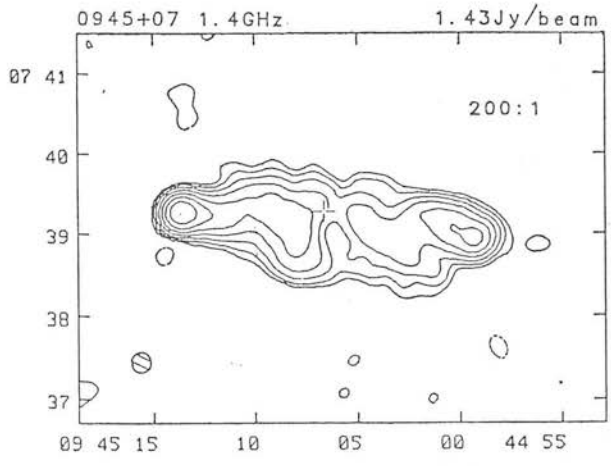

Figure 30. A 1.4GHz map of 0945+07

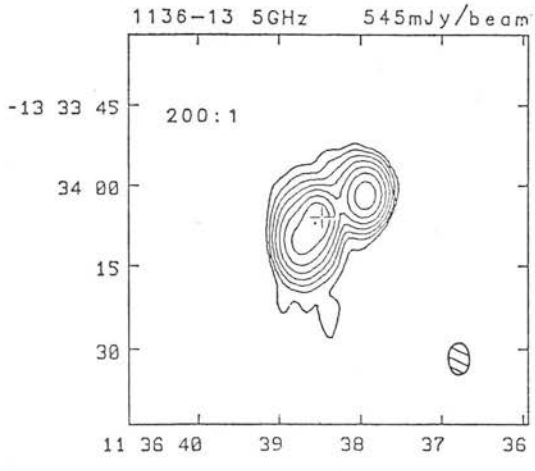

Figure 31. A 5GHz map of 1136-13

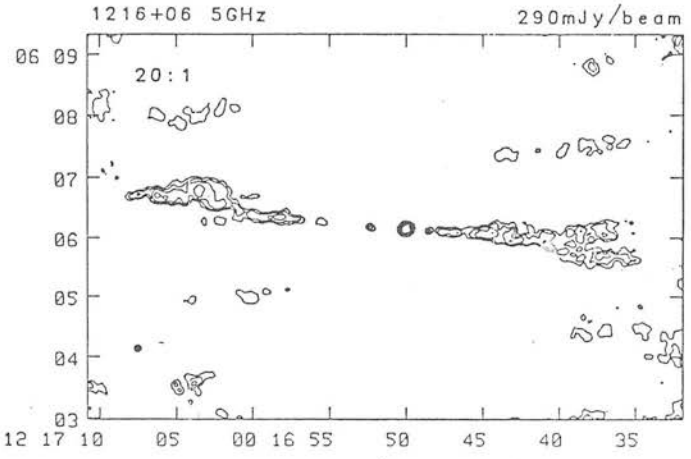

Figure 32a. A 5GHz map of 1216+06

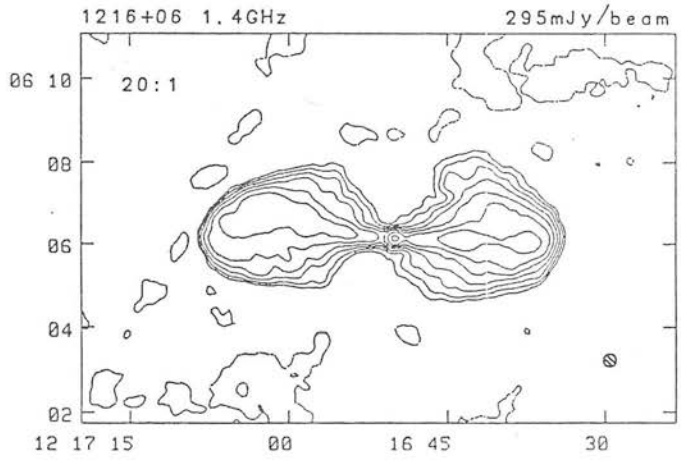

Figure 32b. A 1.4GHz map of 1216+06

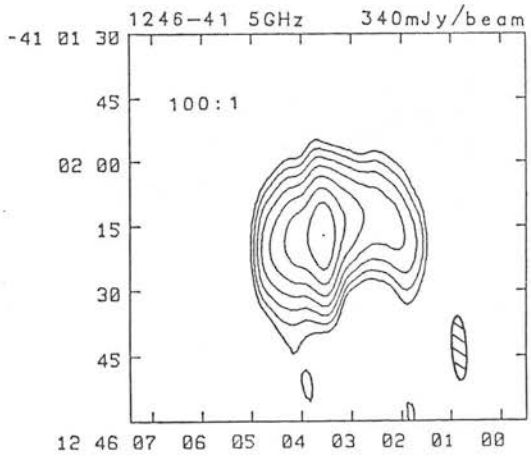

Figure 33. A 5GHz map of 1246-41

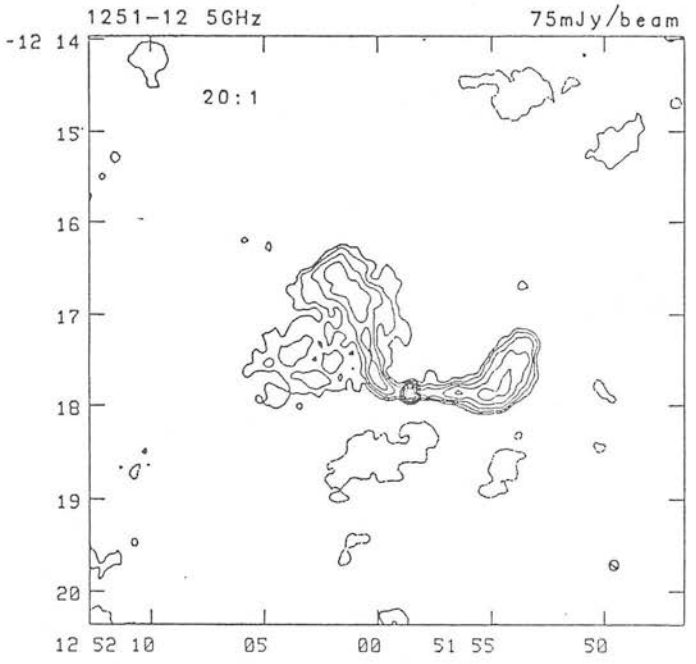

Figure 34a. A 5GHz map of 1251-12

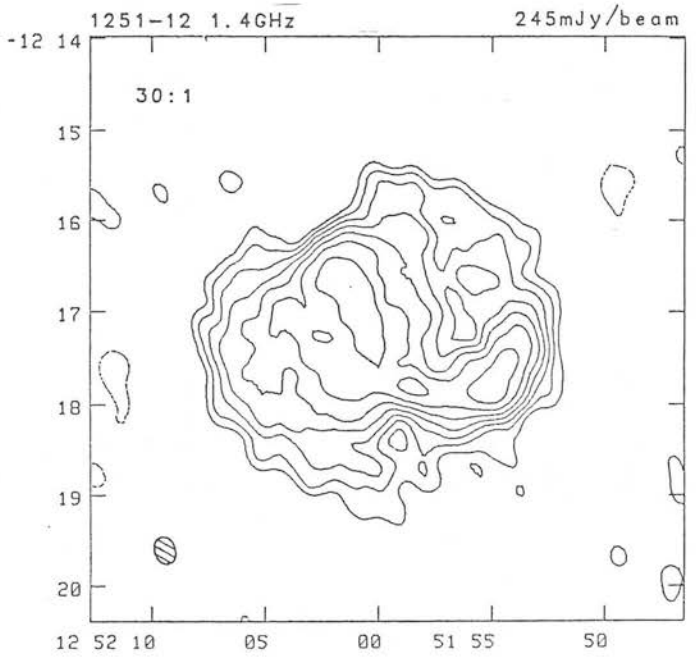

Figure 34b. A 1.4GHz map of 1251-12

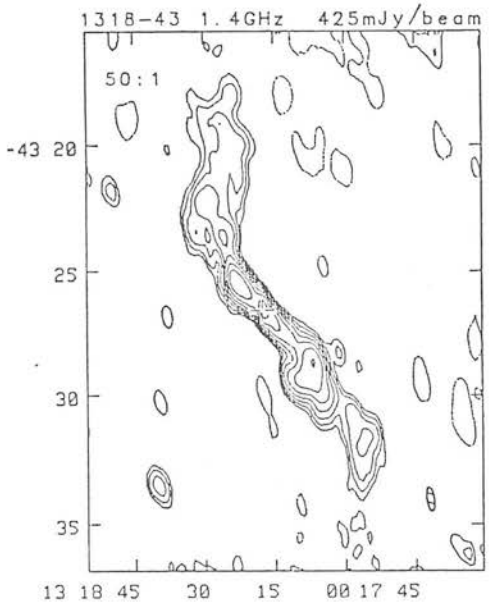

Figure 35. A 1.4GHz map of 1318-43

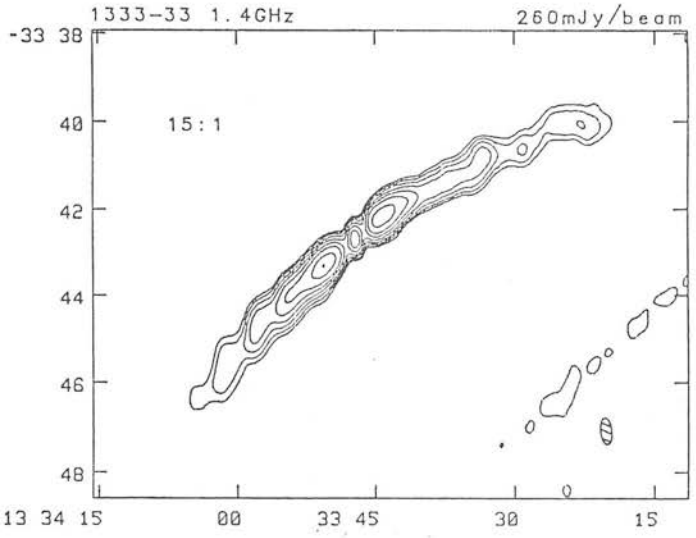

Figure 36. A 1.4GHz map of 1333-33

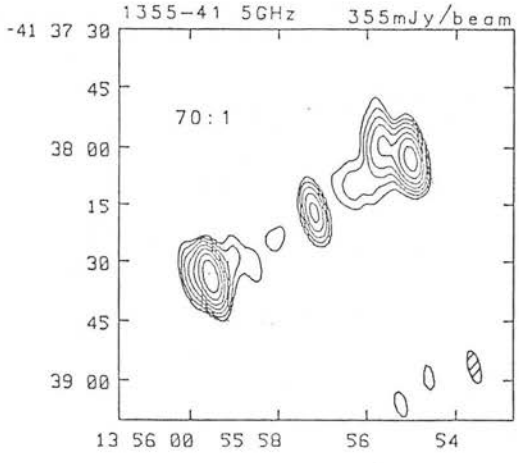

Figure 37. A 5GHz map of 1355-41

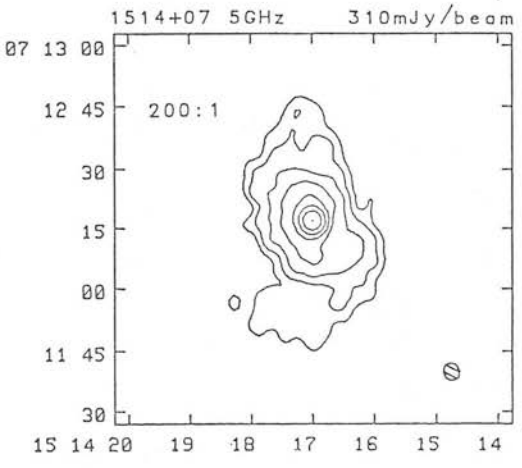

Figure 38. A 5GHz map of 1514+07

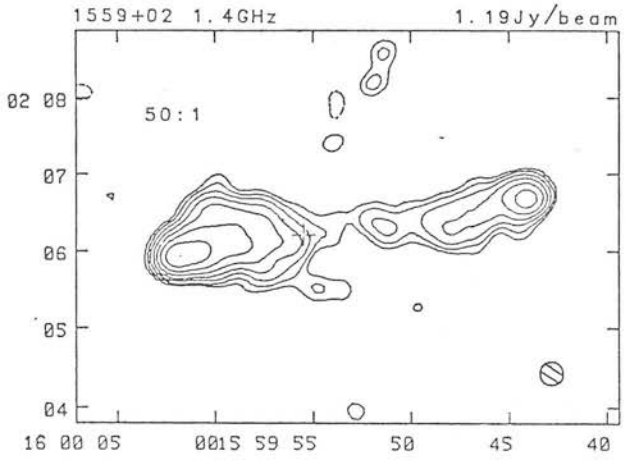

Figure 39. A 1.4GHz map of 1559+02

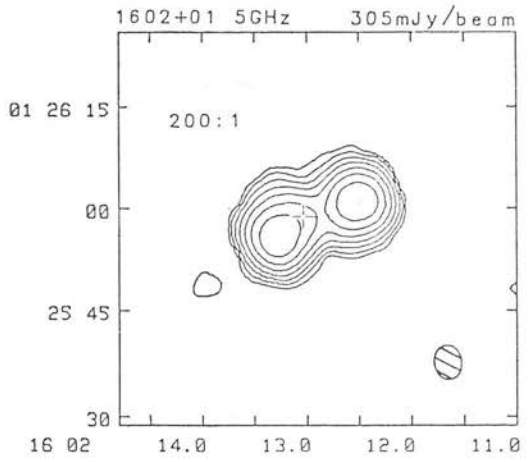

Figure 40. A 5GHz map of 1602+01

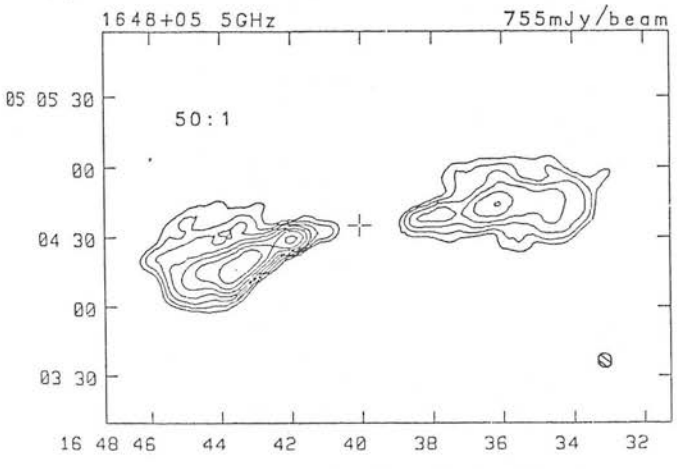

Figure 41. A 5GHz map of 1648+05

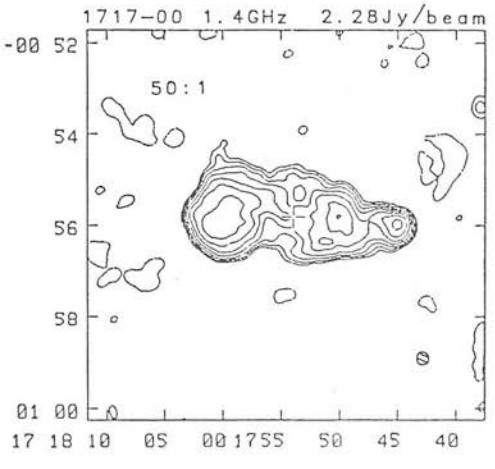

Figure 42. A 1.4GHz map of 1717-00

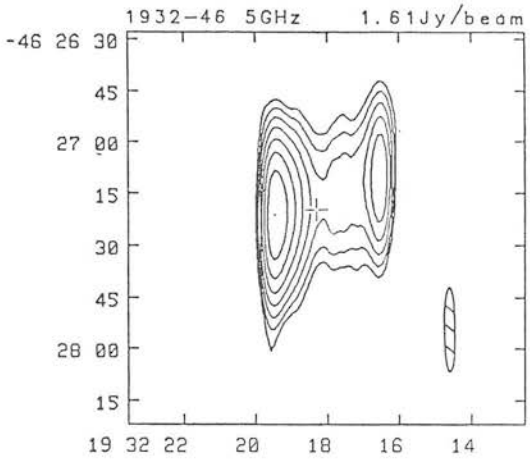

Figure 43. A 5GHz map of 1932-46

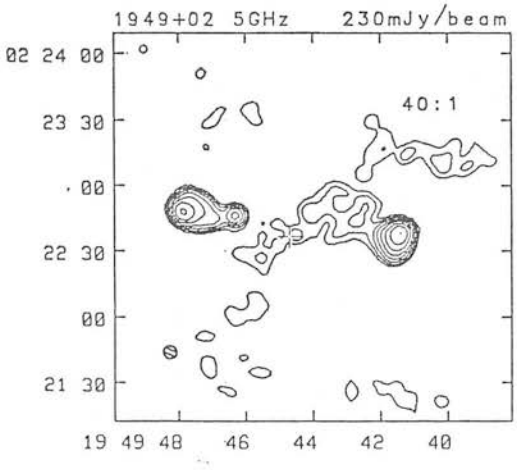

Figure 44a. A 5GHz map of 1949+02

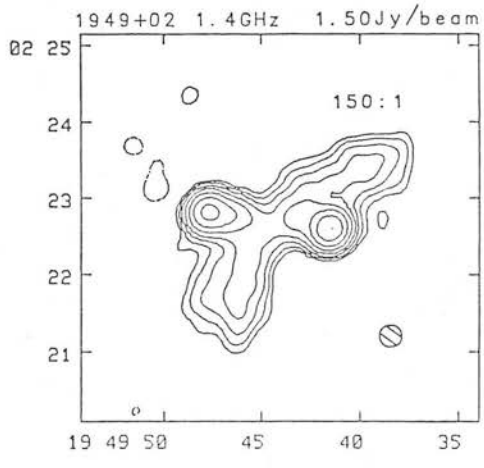

Figure 44b. A 1.4GHz map of 1949+02

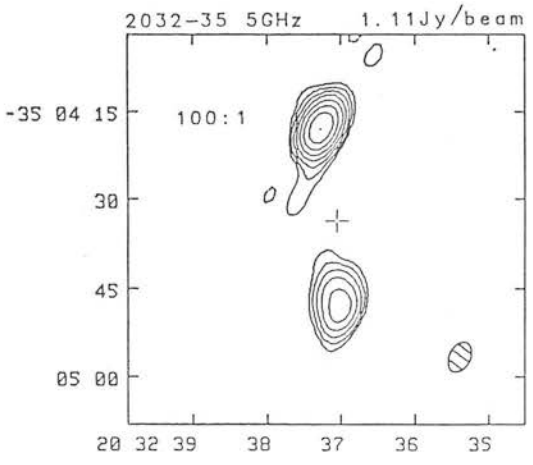

Figure 45. A 5GHz map of 2032-35

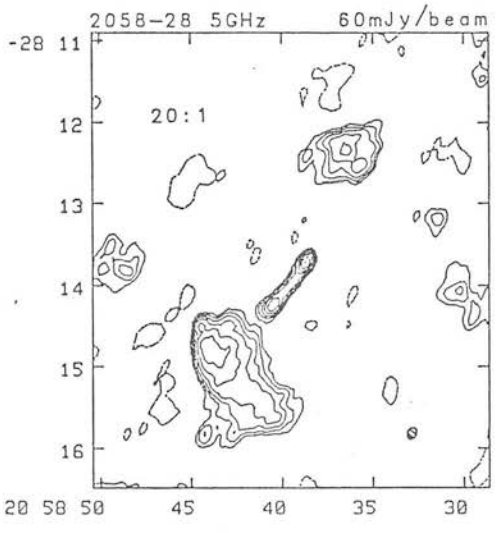

Figure 46a. A 5GHz map of 2058-28

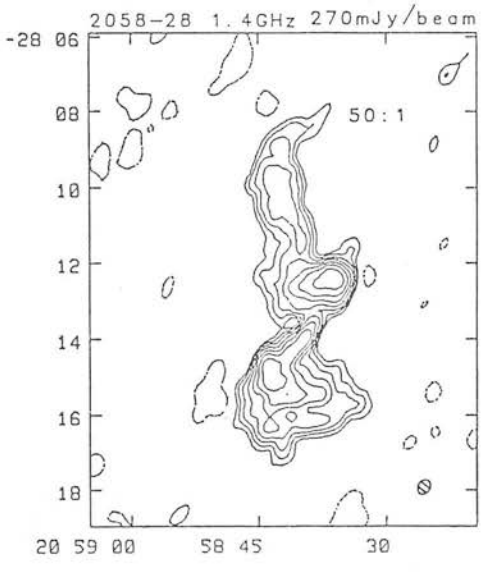

Figure 46b. A 1.4GHz map of 2058-28

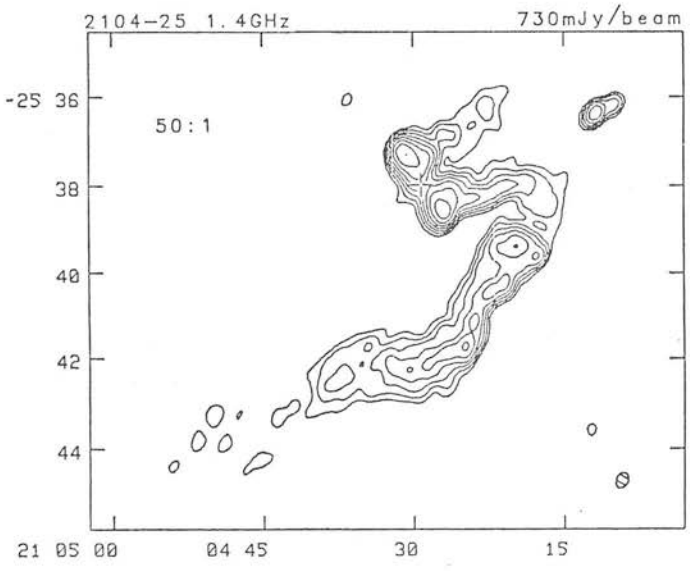

Figure 47. A 1.4GHz map of 2104-25

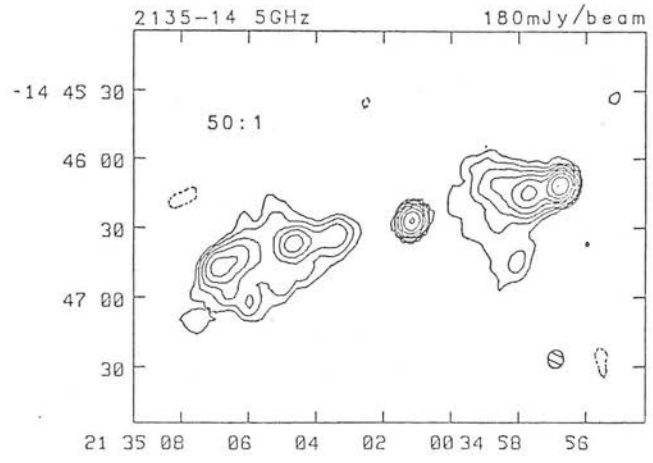

Figure 48. A 5GHz map of 2135-14

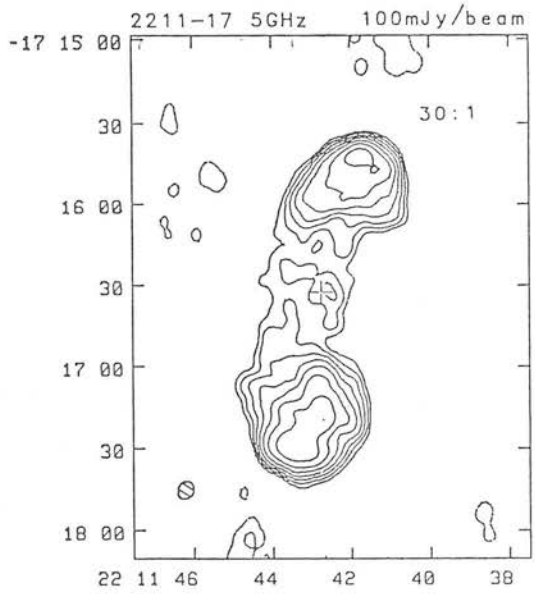

Figure 49. A 5GHz map of 2211-17

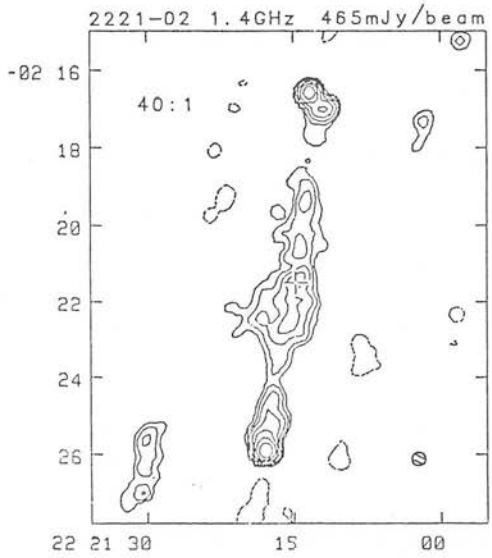

Figure 50. A 1.4GHz map of 2221-02

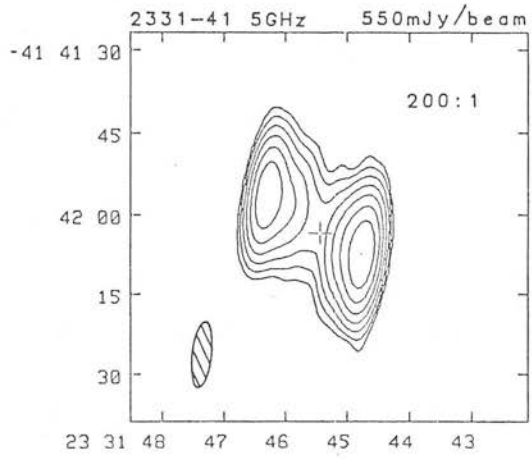

Figure 51. A 5GHz map of 2331-41

Chapter 4 : RADIO SOURCES AND CLUSTERING (1)

4.1 : Introduction

In this, and the following chapter, the clustering environment of galaxies about powerful radio sources is discussed. The method of Longair and Seldner (LS, 1979), with some modifications, is applied to various radio-source samples, to derive objective measures for the clustering environment of individual sources. The relationships between this and various other radio source parameters are then investigated, and the physical implications of these results considered.

In Chapter Five, the results derived from a number of U.K. Schmidt plates are presented. However, the number of sources which may be investigated in this way is small; we thus need to make use of already available galaxy catalogues to collect data for large numbers of sources. The best available data-set is still the Lick catalogue of galaxy number counts, used by LS in their initial investigation. For a number of reasons a re-analysis of these data is now worthwhile.

Firstly, the availablilty of the WP sample, covering the whole sky, means that the whole of the area covered by the Lick counts can be used. The extension, from $+10^{\circ}$ to -23°, essentially doubles the area of sky in which sources from complete samples can be analysed. Consideration of sources from other radio catalogues (e.g. that of Kuhr et al. 1981, and the Parkes catalogue) also increases the number of objects which may be analysed. While these sources have less detailed information available than those in the complete

samples, in a statistical study such as this they are still of value. The final sample used here represents an increase in numbers by a factor of ~ 5 in comparison to LS.

Secondly the definition of these samples at high frequencies includes, as has been discussed, a number of "flat-spectrum" sources, which were not considered in the work of LS. Information of the clustering environment of these sources provides an excellent non-radio parameter for the comparison of their properties with those of the steep-spectrum objects.

Finally, there are some important differences in the analysis as performed here in comparison to that of LS. These include the use of more recent galaxy luminosity functions, and a constant metric distance in the evaluation of the clustering parameter. Both these factors remove potential systematic effects in the LS analysis, and may thus be expected to have some effect on the results derived. Also, a more detailed consideration of the values for individual sources has had important consequences upon the interpretation of the results.

In this chapter the analysis of radio source environments using the Lick galaxy counts, without reference to any deeper plate material is considered, and the basic results presented. A brief description of the method is given in Section 4.2, and some desirable properties of a clustering parameter discussed. Section 4.3 describes the basic galaxy number-count data - the Lick counts. The application of the method to this data-set is described in Section 4.4, along with a discussion of the random errors affecting individual sources, and possible systematic effects. In Section 4.5, the radio samples are presented. The results for sources of known redshift are given in Section 4.6, while the results for a sample of

objects of estimated redshift are given in Section 4.7 Finally, Section 4.8 summarises the main points arising - a detailed discussion of the results, and their interpretation, is delayed until Chapter Five, where a comparison is made between results derived using the Lick and U.K. Schmidt galaxy samples.

4.2 : The Clustering Parameter

In order to investigate properties of radio sources in terms of their "local environments", we need a simple parameter which is a good statistic to describe that environment. In practice, this parameter is generally most easily defined in terms of the local number density of galaxies in the vicinity of the source. How do we derive such a number? With only two dimensional data available (a sample of galaxies down to some faint magnitude limit m_o) we are faced with two problems. Firstly, putting a similar cluster at different distances will result in a different number of galaxies actually observed above the sample limit. Secondly, without redshift information, we are faced with the problem of unassociated foreground (and background) galaxies seen in projection along the line of sight. One method to avoid these difficulties is to attempt to isolate galaxies by their apparent magnitudes or sizes (e.g. Stocke 1979). Such methods however are difficult to apply, and clearly require such information (e.g. an apparent magnitude for each individual galaxy) to be available. An alternative method to surmount these difficulties is that proposed and described in some detail by Longair and Seldner.

In their paper, LS parameterise the distribution of galaxies in terms of the three-dimensional cross-correlation function of galaxies about the radio source. This is defined in the usual way

as:

$$n(r)dV = \rho[1 + \xi(r)]dV \qquad (4.1)$$

where $n(r)$ is the number of galaxies in volume element dV at a distance r from the radio source, and ρ is the mean number density of galaxies. $\xi(r)$ is the cross-correlation function, assumed to have a power-law form:

$$\xi(r) = Br^{-\gamma} \qquad (4.2)$$

The amplitude B is directly related to the number of excess galaxies near the source, which is the parameter we require. Longair and Seldner showed how knowledge of the galaxy luminosity function could be used to convert an observed angular correlation function into this distance-independent spatial amplitude. In particular they showed that if the spatial correlation function is of the form given above, then at a redshift z this will produce an observed angular correlation function

$$\omega_z(\theta) = A_z\theta^{-(\gamma-1)} \qquad (4.3)$$

where

$$A(z) = H(z)B \qquad (4.4)$$

and $H(z)$ is a function which can be calculated for a given galaxy luminosity function. In other words, if we measure a value of A, we can calculate the value of $H(z)$ appropriate to that redshift, and then obtain a value of the spatial amplitude B. In this method, the correlation function approach allows (in a statistical way) for the presence of unrelated "field" galaxies, while the conversion from A

to B via H(z) allows for the effects of the magnitude limits on the "observability" of clustering.

In studying the cluster environment of radio sources as described above, we may consider two separate, but related questions. Firstly, in terms of their cluster environment, is there any evidence that these objects are anything other than "ordinary" members of the galaxy population? (By ordinary, we mean objects selected at random from the whole population, which may itself exhibit a non-random distribution.) If this is the case, we may then consider how the cluster environment of each source is related to its radio properties.

In order to show that our objects may or may not be considered to be ordinary members of the galaxy population, we must compare their environments to that which we would expect around an "average" galaxy. In this case the correlation function approach as described above is an excellent way to proceed, since the correlation function for galaxies in general is well known. We use $\gamma = 1.77$ (the value found for the autocorrelation of normal galaxies), and calculate the mean value of B for our sample. Individual objects might show different values of γ if, for example, a power-law of the above form were fitted to ringcounts made around each source. However, this would also be the case for ordinary galaxies. The correlation function makes no assumption as to the physical origin of any non-randomness which may appear in the distribution, and makes no differentiation between "cluster" and "field" galaxies. A galaxy which happens in one realisation of the distribution to lie in a region of higher than average density simply produces a "positive contribution" to the value of ξ. Thus the correlation function is more usefully thought of as a property of the sample as a whole, than considered individually for each object.

If however (as is the case), we find that our radio sources are not ordinary members of the galaxy population, we may wish to change our null hypothesis somewhat. For example, if we find that the mean value of B is similar to that for galaxies which lie in the centre of Abell clusters, we may wish to assume that all our radio sources lie in clusters of some strength. The correlation function parameter is still a perfectly valid measure of this strength, but we may note two points.

Firstly, in calculating the two point correlation function about the radio source, the object itself is excluded from the sum of excess neighbours (see Peebles, 1980). If the radio source is truly in a physical association, (e.g. a poor group) then the radio galaxy, as possibly a dominant member of that group, will itself contribute to the cluster potential well (which will determine the density of the IGM). Thus excluding it from the statistic will introduce a bias into the measured value of the cluster 'strength', if considered as a measure of the IGM density. In most cases, this effect will be small, since we hope that the number of neighbours observed will be well in excess of one. We may avoid the problem by recasting the method slightly. If we consider the galaxies in the vicinity of the radio source to be a cluster, whose centre is near the radio source, and which has a power-law distribution of number density, we can use the above method to calculate the amplitude of the power-law including the radio source in the sum. (the method will still assume that some of the galaxies near the source are actually "field galaxies", but this effect will be negligible.) In this case however, the value of B may not be directly compared to that for galaxies in general.

Secondly, it might be appropriate to consider a larger value for the power-law exponent, as for example is appropriate for Abell

clusters (Bahcall, 1977). If we could measure ξ directly, (from three-dimensional data), an incorrect value of γ would simply lead to a constant multiplicative error in B. However, using the H(z) conversion, an incorrect γ will lead to a systematic variation with z, if a constant angular integration distance is used. (This effect is discussed in more detail in section 4.4.d.) In their analysis, Longair and Seldner used a constant radius of 1^{o} in calculating A. In our analysis, we have integrated the angular excess only out to a distance corresponding to 1Mpc at the redshift of the source. In addition to the removal of the potential systematic effect, use of a counting radius which does not extend substantially beyond the main body of the cluster should increase the signal to noise of the measurement for more distant sources.

4.3 : The Galaxy Counts

The Lick Observatory counts of galaxies (Shane and Wirtanen 1967) are a compilation of the numbers of galaxies in cells 10 arcmin square, counted to a limiting magnitude $m \sim 19$, over the whole of the sky north of $\delta = -23^{o}$. The original counts were compiled from 1246 Kodak 103a-O plates taken with the Carnegie 20inch Astrograph. The observations were made with generally one plate per field, taken under similar observing conditions, with the field centres spaced so that each $6^{o} \times 6^{o}$ plate had at least one degree overlap with adjacent plates. The counts were performed by eye, the counter scanning across the plates in 10arcmin steps, with the acceptance criterion for images being based on "the observer's confidence that the images represent galaxies".

In their original paper, Shane and Wirtanen presented the counts summed into 36 one degree square areas for each plate. In addition

to the raw counts, they presented two sets of "correction factors", designed to reduce the counts from each plate to a uniform limiting magnitude. For the set of plates as a whole, a "field correction factor" was presented, to allow for non-uniformity (including the effects of vignetting) of the limiting magnitude over each plate. In addition, a composite "plate correction factor" was given for each plate. This was designed to allow for the effects of atmospheric extinction, date of counting, identity of counter, exposure time and emulsion batch. A smoothing factor and a normalisation factor were also applied. These corrections to the counts were calculated largely independently of the observed values. For example, the atmospheric extinction correction was calculated from a known value for the extinction at the zenith, and an assumed limiting magnitude - number relation. While factors such as the date of counting could only be determined from a knowledge of the counts, in this case the correction was determined from comparisons of repeat counts of the same plate.

In 1977 Seldner et al. (henceforth SSGP) presented a new reduction of the Lick counts. In this paper, the counts were presented in the original 10 arcmin square cells. In addition, SSGP provided new correction factors to reduce the count to a uniform system. In this analysis, the field correction factor was calculated for each of the 1296 separate cells on the plate by dividing the mean count over all cells on all plates, by the mean count of the cell of interest over all plates. The plate correction factors were calculated in a purely empirical manner from the observed counts. 1246 plate correction factors were sought which made the counts in overlapping regions of adjacent plates as consistent as possible. These 1246 factors were found simultaneously, using an iterative least-squares technique, weighting the individual overlap regions by the number of galaxies in those regions. This process thus simply

made the assumption that the counts in overlap regions should be identical, all things being equal, and attempted to achieve this; external information, such as the identity of the counter, was not utilised. The final plate correction factors correspond to a combination of the Shane and Wirtanen personal, counting date, emulsion and smoothing factors. The atmospheric and galactic extinction factors were calculated by a least-squares fit of the counts to a simple cosecant model. Finally, a normalisation factor was calculated so that the sum of counts corrected via the field, plate and atmospheric correction factors equalled the sum of the raw counts.

It should be noted that while these correction factors statistically reduce the mean count to a uniform limiting magnitude, this is not equivalent to correcting to a uniform magnitude for clustering estimates. However, in the majority of cases, these correction factors are small, and hence only have a minor effect upon the result. Also, since the correction factors are independent of the positions of the radio sources, we do not expect any systematic effects to occur. Errors in the corrected counts will simply increase the random spread in the values of B derived. Results using the counts in their corrected form are presented here; the results derived from the raw counts were not found to significantly differ.

4.4 : The Method

4.4.a Derivation of A

The derivation of B from the Lick counts was performed in a similar manner to that of LS. For the two-dimensional correlation

function, we have;

$$N(\theta)d\Omega = Ng[1 + \omega(\theta)]d\Omega \qquad (4.5)$$

where

$$\omega(\theta) = A\theta^{-\delta} \qquad (4.6)$$

and $\delta = \gamma - 1$.

As in LS, we assume spherical symmetry. As the data are too poor to determine A and δ simultaneously (e.g. from ringcounts), we will assume δ, and determine A from the integral of the above equation. From 4.5 and 4.6 we have

$$\int N(\theta)d\Omega = \int Ngd\Omega + NgA\int\theta^{-\delta}\, d\Omega \qquad (4.7)$$

We will write this as

$$Nobs = Nbc + NgAJ \qquad (4.8)$$

(where $J = \int\theta^{-\delta}d\Omega$). Here Nobs is the total number of galaxies observed within θ of the source position, and Nbc is the expected number of background objects in the same area. We can write this as

$$A = (Nobs-Nbc)/NgJ = Nt/NgJ \qquad (4.9)$$

where Nt is our "best guess" of the number of sources physically associated with the source position. (From this equation, we can see that A is a measure of the ratio of the surface number density of galaxies associated with the source, compared to the field number density; the integral J taking into account the effect of the area used and the radial profile of the associated-galaxy distribution.)

Due to the binned nature of the data, the above integral cannot be performed analytically; at large redshifts, it becomes difficult to construct counts over an exactly circular area. Accordingly, the following method was used to calculate A. Firstly, the position of the source on the plate with the nearest plate centre was found. The counts from all bins with centres within X^{o} (usually corresponding to 1Mpc at the distance of the source) were then included in the summation to find Nobs. The value of Ng was estimated from the mean of all bins in an annulus, usually between $3-5^{o}$ away from the source. Finally, the value of J over an identical area as used for Nobs was calculated numerically, and the value of A obtained.

This method will result in slightly different areas used for each source, due to variations in position with respect to the bin centres. The effect of this however will be shown to be negligilbe in comparison with the other sources of error in A.

The value of θ = 1Mpc has been chosen for a variety of reasons. For high redshifts, values of θ corresponding to linear radii much less than 1Mpc become smaller than the size of the individual bins. Conversely, at low redshifts, larger values for the linear distance correspond to impractically large angular diameters if we wish the background normalisation to be made at a reasonable distance from the source. We are thus constrained by the data to a value of this order. This is a reasonable value however; it is large enough to encompass all but the most extended radio sources, and is also sufficient to include the main body of any possible surrounding cluster, without extending past the distance where such clusters provide a useful signal.

4.4.b Error Analysis

In their analysis, LS did not explicitly estimate the error associated with A. Because the values are subject to large random errors however, and are also a function of redshift, an accurate error estimate (especially when considering individual sources) was considered essential.

From equation 4.9, we can see that the error in A can be found directly from the percentage errors in Ng and Nt. For a random distribution of objects, the error in Ng would be given simply from Poisson statistics. Because galaxies are clustered, however, the r.m.s. variation is increased. The standard error in Ng was thus calculated from the standard error in the counts in the bins used to calculate Ng. This has the advantage that the effects of plate corrections, etc. are empirically included in the error estimate.

The error in Nt is rather less straightforward. In the absence of field galaxies Nt, the number of galaxies "associated" with the radio source, could be measured exactly. (This value might have some variation from source to source for sources with, for example, similar IGM densites; either due to genuine differences, or because of fluctuations in the number of associated galaxies appearing above the plate limit. Allowance for this "cosmic scatter" will not be made here.) In practice however, we can only get Nt by observing Nobs galaxies and assuming Nbc of them are an unassociated background contamination. Again Nobs is a precise number; hence the error in determining Nt is solely due to the uncertainty in estimating the number of unrelated objects in the area used.

To calculate the error in this number, a set of areas each identical to that used in the Nobs summation was distributed over

the plate, and the number in each area found. The standard deviation of the sample for these areas was then used as the error in Nt. (Note that the mean number from this sample was not used for Nbc, as this was more accurately determined from Ng. The small error in the actual value for Nbc used, due to the error in Ng is much less than the r.m.s., as calculated above, and was not included.)

The above values were then combined to find the resultant error in A. This was then used to calculate the error in B directly via the conversion using H(z). Thus the error quoted in B includes only the random error implicit in the measuring process, and does not allow for a) cosmic scatter in the value of Nt, nor b) errors in B introduced by uncertainties in the value of H(z).

4.4.c The Conversion from A to B

The conversion function H(z) allows for the variation in the number of galaxies of fixed absolute magnitude which are observed to have a given apparent magnitude due variations in the source distance. For a magnitude limited sample, the H(z) function is given by (LS Eqn. 19):

$$H(z) = \frac{I_\gamma}{Ng} \left(\frac{D}{1+z}\right)^{3-\gamma} \Phi(m_o,z) \qquad (4.10)$$

where I_γ is a definite integral, D the proper distance to the source, and Ng the surface number density of galaxies. $\Phi(m_o,z)$ is the integral number of galaxies per unit volume which at redshift z are observed to be brighter than the apparent magnitude limit m_o. To calculate this function, we need to assume not only values of H_o and Ω_o, but also the form of the luminosity function for galaxies, galaxy K-corrections, and so on. The work of various authors over recent years has produced a wide range of values for these basic

galaxy parameters (see e.g. Ellis 1982; Shanks 1984). Many combinations of the different parameters (e.g. the luminosity "characteristic magnitude", M*, and normalisation ϕ *) may produce similar observational results, i.e. number-magnitude counts, which themselves are not constant from group to group. Accordingly, the H(z) function must be considered rather uncertain. For this analysis, values for the various parameters were taken from the literature; the validity of the combinations were checked by using them to predict number-magnitude counts for comparison with observed results. Since much of the recent work has been performed in the J passband, the initial selection was made at this wavelength.

The "standard" model parameters are listed in Table 4.1. A Schechter luminosity function was assumed, galaxies being distributed between five morphological types, each with (in principle) its own characteristic magnitude and slope. K-corrections were taken from Ellis (1982). For the Schmidt plates used in Chapter Five, the effects of thresholding were also included. The absolute normalisation ϕ* was chosen to match the observed counts at bright magnitudes; the standard model gives an excellent fit to J ~ 20 for the counts in Shanks (1984). No allowance was made for the effects of luminosity evolution, which increases the observed counts at faint magnitudes; this will be negligible for the Lick counts, and also for all but the most distant Schmidt plate sources, where the correction would in any case be uncertain.

The inverse of the standard H(z) function (i.e. B = (1/H).A), calculated using a magnitude limit appropriate to the Lick counts, is shown in Fig. 4.1.a. Also shown are the effects of two simple variations to the parameters; that of changing M* by $\pm$ 0.3 magnitudes, and that of changing α to -1.0. In each case an appropriate adjustment to ϕ* has been made, to preserve the fit to

Table 4.1: The H(z) Function Standard Parameters

$H_o = 50 kms^{-1} Mpc^{-1}$, $\Omega_o = 1.0$

waveband J = SRC J (COSMOS galaxy samples)

B (Lick galaxy sample)

galaxy K-corrections: from Ellis (1982)

galaxy luminosity function: Schechter (1976) form.

galaxy morphological types:	E/S0,	Sab,	Sbc,	Scd,	Sdm
relative proportions:	0.35	0.20	0.20	0.15	0.10

characteristic absolute mag: Mj* = -21.2 (all types)

Mb* = -21.0 (all types)

luminosity function slope : -1.25

normalisation : 0.0022 Mpc^{-3}

COSMOS standard parameters: threshold = 10%, seeing = 0.5 arcsec

Msky = 22.5

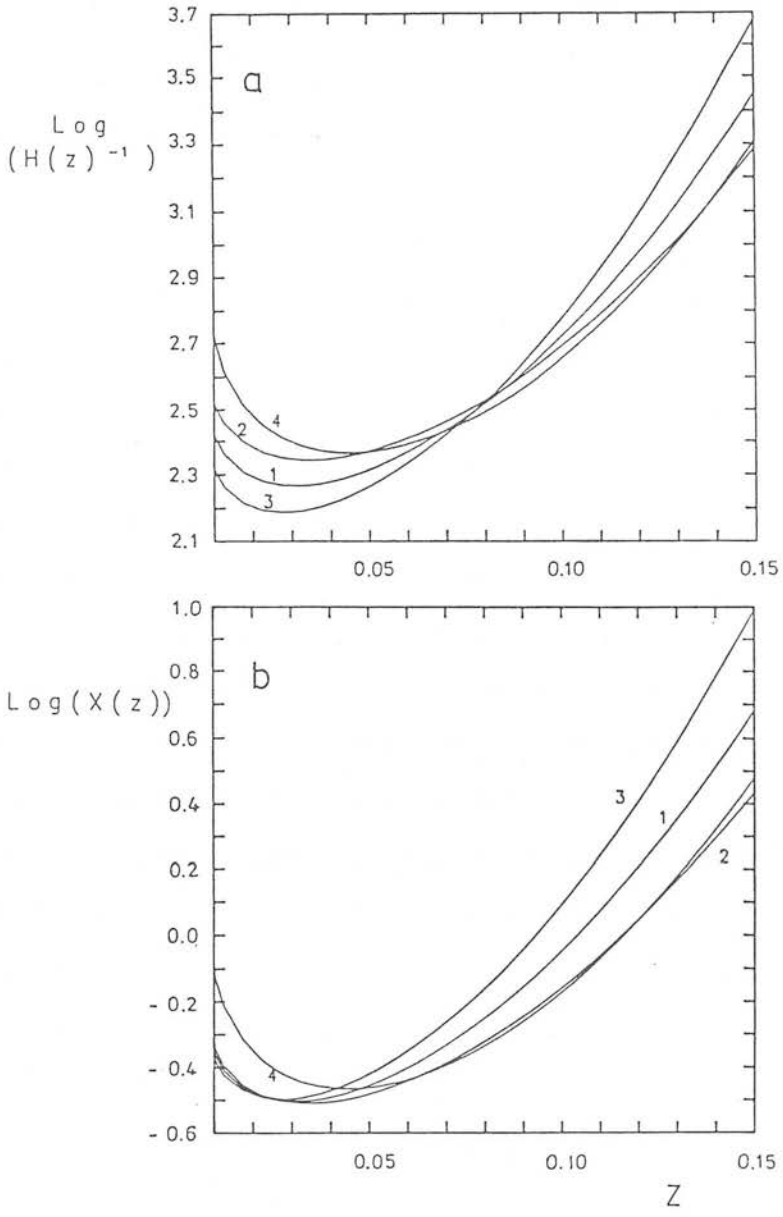

Figure 4.1. a) The inverse of the H(z) function appropriate to the Lick counts, for four variations about the standard function parameters.

1) standard values 2) $M^* = -21.3$

3) $M^* = -20.7$ 4) $\alpha = -1.0$

b) as (a) for the X(z) function.

the observed number-magnitude counts. The affect on H(z) is largest at low and high values of z; the variations however are not nearly as extreme as those demonstated by LS, for their form of the luminosity function.

Since we wish to compare the value of the correlation amplitude B obtained for a radio source to that expected for a 'normal' galaxy, we also need to know this quantity - its value may be obtained from the auto-correlation function for galaxies in general. This is defined for a galaxy sample in an identical way as the cross-correlation function for specific objects, except that in this case counts are made using each galaxy in turn as the centre. The amplitude of the spatial auto-correlation function for a sample may be considered to represent the "average" value for galaxies in that sample. This spatial amplitude (Bgg) may be obtained from an observed angular correlation amplitude (Agg), in a similar manner to that described above for individual objects. In this case however, we must average equation 4.10 over all galaxies in the sample. Thus we have:

$$Bgg = Q \cdot Agg \qquad (4.11)$$

where

$$Q = \frac{\int H(z)n(z)dz}{\int n(z)dz} \qquad (4.12)$$

Here n(z) is the number of galaxies with redshifts between z and z+dz, also calculated from the input model parameters.

Groth and Peebles (1977) obtained for the galaxies in the Lick sample a value of Agg = 0.068. This converts to a value of Bgg = 40, using the standard model parameters to evaluate Eqn. 4.12. Note

however, that varying the H(z) parameters will also affect this value. It is therefore appropriate to consider, rather than H(z), the function X(z) defined by

$$Bgg^*/Bgg = X(z)Agg^*/Agg \qquad (4.13)$$

(i.e. X = Q/H).

The variation of X with z for the above three cases is shown in Fig. 4.1.b. It can be seen that the systematic variations introduced by variations in the galaxy luminosity function have been reduced over the range $0.02 < z < 0.1$ to less than ~ 30% for varying M*, and ~ 70% for the change in α . This represents a reasonable upper limit to the systematic error which would occur in a comparison between objects at these two redshifts.

Finally, it should be noted that this analysis assumes that there are no unknown selection effects in the Lick counts. These include the possible use of a surface brightness - angular size limit rather than a true magnitude limit in the compilation of the counts (Phillips et al. 1981), or the possibility of stellar contamination. These effects may modify the X(z) function, but are difficult to quantify; for this reason, no attempt has been made to derive results for many different forms for X(z). Any results which depend solely upon the comparison of high and low-redshift sources, corrected in this manner, should be treated with caution.

4.4.d The Effect of Incorrect γ

There has been some indication (see e.g. Yee and Green 1984, Stockton 1984) that the value of γ for some types of radio source is rather larger (~ 2.5) that that of galaxies in general. It is therefore instructive to consider the effect of an incorrect choice

for this quantity upon the final result.

Suppose that we have observed an excess number of galaxies ΔN around a source.

Firstly, consider the simplified case in which we can actually integrate the correlation function over a sphere in three-dimensional space. Then

$$\Delta N = \int \rho B r^{-\gamma} dV = \int \rho B r^{-\gamma} 4\pi r^2 dr \qquad (4.14)$$

$$\Rightarrow \quad \Delta N = \frac{4\pi}{3-\gamma} \rho B r^{3-\gamma} \qquad (4.15)$$

so that, if the correct values are B_o and γ_o, use of an incorrect value of of the power-law index, γ_1, will result in an incorrect value of the amplitude, B_1, with the ratio of observed to true value given by:

$$\frac{B_1}{B_o} = \frac{(3-\gamma_1)}{(3-\gamma_o)} r^{-(\gamma_1-\gamma_o)} \qquad (4.16)$$

We can thus see the requirement to use a constant metric distance in evaluating B. In this case, an incorrect value of γ simply leads to a constant multiplicative error in B. If however, we use a constant angular radius, a systematic error will occur. Putting $r \propto 1/z$, we get

$$\frac{B}{B_o} \propto z^{(\gamma_1-\gamma_o)} \qquad (4.17)$$

Thus having γ wrong by ~ 0.5 would lead to a systematic change in the observed value of B over the range z = 0.02 to 0.1 of $\sim\sqrt{5} \simeq 2$.

An effect of this magnitude would be sufficient to account for a large part of the LS result.

In practice, we must perform the integration over a cone defined by the two-dimensional data, as discussed by LS. From their equation 15, we find:

$$\Delta N = \int d\Omega \Phi(m_o, z) \theta^{1-\gamma} D^{3-\gamma} (1+z)^{\gamma-3} B I_\gamma \tag{4.18}$$

putting $d\Omega = 2\pi\theta d\theta$ we get;

$$\Delta N = \frac{2\pi}{3-\gamma} \theta^{3-\gamma} D^{3-\gamma} (1+z)^{\gamma-3} I_\gamma B \tag{4.19}$$

but for a fixed metric distance $x = \theta D/(1+z)$;

$$\Delta N = \frac{2\pi}{3-\gamma} \Phi B x^{3-\gamma} I_\gamma \tag{4.20}$$

so that now

$$\frac{B_1}{B_o} = \frac{I_{\gamma_o}}{I_{\gamma_1}} \frac{(3-\gamma_1)}{(3-\gamma_o)} x^{(\gamma_1-\gamma_o)} \tag{4.21}$$

for x fixed (at 1Mpc), the variation of B_1/B_o depends on two factors

$$\frac{B_1}{B_o} \propto (3-\gamma_1), \quad \frac{B_1}{B_o} \propto \frac{1}{I_{\gamma_1}} \tag{4.22}$$

and for a given (true) value of B_o and γ_o, the observed value of the spatial amplitude (B_1) varies with the assumed power-law index (γ_1) as

$$\frac{B_1}{B_o} \propto \frac{(3-\gamma_1)}{I_{\gamma_1}} \tag{4.23}$$

A plot of this function, for γ_1 varying from 1 to 3 is shown in Fig. 4.2. The shape of this curve is independent of the true value of γ, which only changes the normalisation. The position of the peak is determined by the relative strengths of $1/I_{\gamma_1}$, which allows for the conic volume used, and the value of $(3-\gamma_1)$, which results from the constraint that the integral number of galaxies is fixed. It is remarkable that this function should peak at $\gamma_1 = 1.84$, so near the observed value ($\gamma = 1.77$) for galaxies in general.

As long as $\gamma \sim 2$ for all sources, variations of γ between sources should not introduce a large variation in the value of B derived.

4.5 : The Radio Samples

Clearly, for an investigation such as this, where the results for individual sources may have large random errors, it is important to include as many sources as possible in the analysis. Accordingly, as well as the main WP sample, sources from a number of other bright radio samples were considered. Equally important however, is the necessity for any sample used to be complete, both in terms of identification content and redshift. For example, if sources in clusters are associated with more obvious cD galaxies, then use of an incomplete sample would introduce a serious bias. Similarly, if those radio sources for which redshifts were more readily available were those which lay within Abell clusters, then a bias would again be introduced. Candidates were initially taken from the two complete samples; the WP sample and the Northern sample. Selection of sources from within these samples was made initially on the basis of redshift alone; the limit $0.01 < z < 0.15$ being imposed. This is not necessarily the range over which H(z) is well known, but it covers

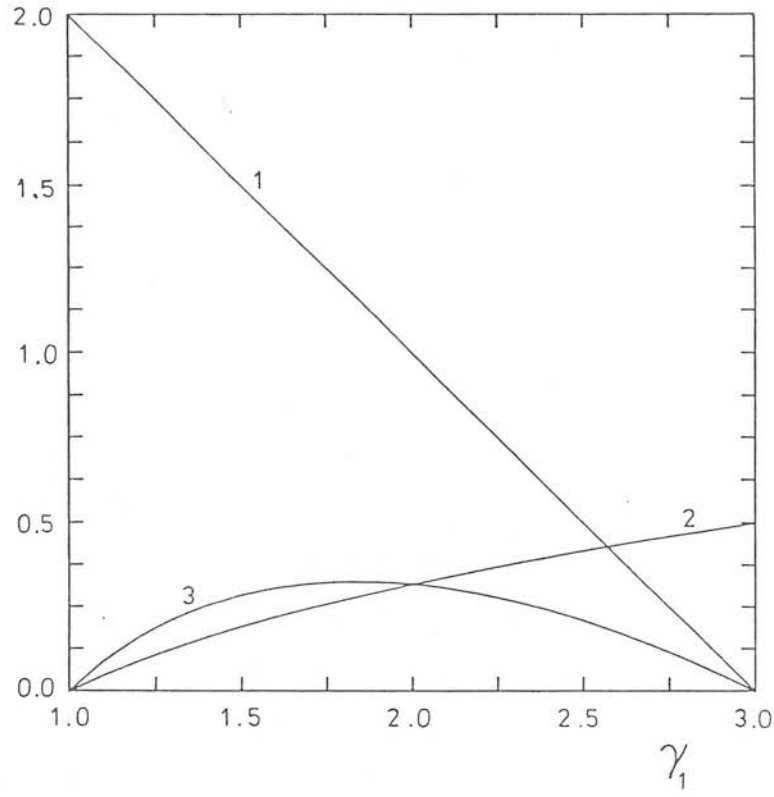

Figure 4.2. The effect of the assumed value of γ_1 upon the observed value of B.

1) $3 - \gamma_1$ as a function of γ_1

2) $1/I_{\gamma_1}$ as a function of γ_1

3) B_1/B_0 as a function of γ_1

that for which a reasonable value of B might be expected to give a measurable value of A. Subsequently, objects were rejected from the sample if the extinction towards them (as indicated by Burnstein and Heiles, 1982) was high. The number counts appeared to become seriously affected for extinctions $E(B-V) > 0.2$, accordingly all sources with values greater than this were excluded. This removed 9 sources from an initial composite sample (described below) of 93 sources; the limit corresponds approximately to a galactic latitude cut of $|b| \sim 10\text{-}15^{o}$.

Both these samples may be considered 100% complete, in the sense that all sources which satisfy the radio criteria have been identified and included in this analysis. On the basis of their magnitudes, only 3 sources without redshifts are expected to have $z < 0.15$. These sources have been included with redshifts estimated from the m-z relations of the parent samples.

To increase the numbers,sources from three other samples were then considered. The details of all of these samples, and the number of sources included are given in Table 4.2. The latter samples are as follows:

c) The Kuhr 1Jy sample. (Kuhr et al., 1981) This was an attempt to define an all-sky sample complete to 1Jy at 5GHz. Unfortunately, it suffers somewhat from a lack of optical data, so that the sample cannot be considered complete in the sense described above; it contains 47 sources with both identifications and redshifts, of which 5 are not already included.

d) The Parkes survey. This survey, at 2.7GHz, is radio-complete to 0.6Jy, south of $\delta = 25^{o}$. (Wall 1977). This survey is one of the basic source lists for the complete samples considered above; It

Table 4.2: The Radio-Source Samples Used

Sample	freq	S_{lim}	area covered	number included	comments
A) WP	2.7GHz	2.0Jy	all-sky	40 (40)	complete
B) Northern	2.7GHz	1.5Jy	dec > 10°	36 (11)	complete
C) Kuhr (1)	5.0GHz	1.0Jy	all-sky	47 (5)	incomplete
D) Parkes (1)	2.7GHz	0.6Jy	dec < 25°	36 (11)	incomplete
E) Kuhr (2)	5.0GHz	0.6Jy	all-sky	74 (17)	incomplete
			total number of sources	84	
F) Parkes (2)	2.7GHz	0.2Jy	dec < 25°	138	estimated z

contains an additional 11 sources not already included.

e) The Kuhr 0.6Jy sample. (Kuhr, 1979). This catalogue is an all-sky compilation of sources from the NRAO-MPIfR 5GHz surveys and the Parkes catalogue; it forms the finding list for the 1Jy complete sample. All sources in the appropriate redshift range from the catalogue were initially considered. Below S_5 = 0.6Jy, however the radio data became seriously incomplete; this flux-density limit was thus applied.

The composite sample formed from the above catalogues is given in Table 4.3. The low-frequency sample of Laing et al. (1983) - the 'revised 3CR' sample - was not used as a source list. However, there is a large overlap between this and the sample used here; sources in Table 4.3 which are also members of the Laing et al. sample are marked with an asterisk.

Finally, a number of sources from the Parkes catalogue (f) were considered. These were galaxies without known redshifts, for which the redshift was estimated from their magnitudes, assuming the m-log(z) relation found for the 47 sources with known redshifts (Fig. 4.3). Due to the likely error in these values, this was limited to sources with $z < 0.11$ ($m < 18$); a flux-density limit of 0.2Jy was also imposed. Due to the large number of sources involved, each source was not individually inspected for high extinction; instead a more conservative limit of $|b| > 25^{o}$ was imposed. This left a sample of 138 sources.

For the WP and Northern samples, high quality radio data are available. While some maps exist for the remaining sources, in general only flux densities at various frequencies are available. Thus for these sources, divisions can only be made in terms of

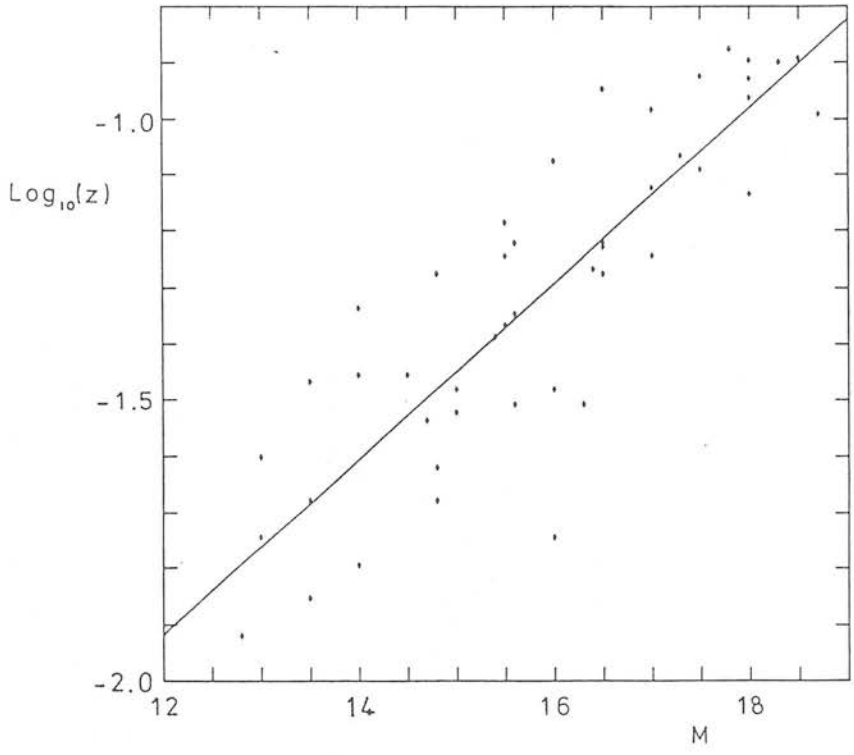

Figure 4.3. The M-log (z) relation for Parkes radio galaxies of known redshift. The solid line is the best least-squares fit, given by:

$$\log (z) = 0.156\ M - 3.80$$

Table 4.3: The Composite Radio Sample

IAU	other	type	mag	z	S		sample					
0034-01	3C15	G	15.3	0.073	2.56	0.79	A		C	D	E	
0036+03	4C03.01	G	13.5	0.015	1.10	1.01				D	E	
0055-01	3C29	G	14.1	0.045	3.46	0.76	A		C	D	E	
0055+30		G	12.5	0.016	1.21	0.04			C		E	
0104+32	3C31	G	12.2	0.017	3.53	0.84	A	B	C		E	*
0106+13	3C33	G	15.2	0.060	8.02	0.76	A	B	C	D	E	*
0111+02		G	16.3	0.047	0.61	-0.18					E	
0116+31	4C31.04	G	14.5	0.059	2.12	0.61	A	B	C		E	
0123-01	3C40	G	12.3	0.018	3.29	0.91	A		C	D	E	
0124+18	4C18.06	G	15.5	0.043	1.00	0.88				D	E	
0204+29	4C29.06	G	16.0	0.109	1.36	0.78					E	
0206+35	4C35.03	G	14.5	0.037	1.31	0.59					E	
0220+42	3C66B	G	12.8	0.022	5.23	0.54	A	B	C	D	E	*
0238+08	NGC1044	G	14.8	0.021	0.70	1.27				D		
0255+05	3C75	G	13.6	0.024	3.30	0.86	A		C	D	E	
0258+35	4C34.09	G	14.0	0.020	1.26	0.48					E	
0300+16	3C76.1	G	14.9	0.032	1.96	0.64		B	C	D	E	*
0305+03	3C78	G	12.8	0.029	5.34	0.64	A		C	D	E	
0314+41	3C83.1B	G	13.3	0.026	4.92	0.54	A	B	C		E	*
0316+41	3C84	G	11.9	0.017	9.64	-2.58	A	B	C		E	*
0325+02	3C88	G	14.0	0.030	3.18	0.79	A		C	D	E	
0331-01	3C89	G	15.5	0.139	1.41	0.92					E	
0338-21	0E-2639	Q	18.0	0.048	0.82	-0.22				D	E	
0356+10	3C98	G	14.4	0.031	5.80	0.92	A	B	C	D	E	*
0404+03	3C105	G	18.5	0.089	3.54	0.64	A		C		E	
0430+05	3C120	G	14.1	0.033	3.00	-1.71	A		C	D	E	
0453-20	OF-289	G	13.0	0.035	2.79	0.73	A		C	D	E	
0502-10	05-11	G	15.4	0.041	0.70	0.79				D		
0511+00		G	18.0	0.127	1.70	0.78			C	D	E	
(0634-20		G	16.8	0.056	2.20	0.18					E	)
0703+42	4C42.23	G	14.4	0.038*	1.69	0.85		B				
(0723-00		G	18.5	0.128	3.03	0.48				D	E	)
0734+80	3C184.1	G	17.0	0.118	1.90	0.67		B	C		E	*
0744+55	DA240	G	14.2	0.036	2.84	0.78	A	B			E	*
0755+37	3C189	G	14.9	0.043	1.79	0.55		B	C		E	
0802+24	3C192	G	15.5	0.060	3.30	0.71	A	B	C	D	E	*
0818+47	3C197	G	16.5	0.128	1.18	0.53					E	
0819+06	3C198	G	17.5	0.081	0.90	1.68				D		
0828+32	4C32.25	G	15.0	0.051	1.00	0.17					E	
0844+54	4C54.17	G	15.0	0.040	1.15	0.72					E	

Table 4.3: Continued

IAU	other	type	mag	z	S		sample
0915-11	Hyd A	G	14.8	0.065	23.50	0.90	A C D E
0936+36	3C223	G	17.1	0.137	2.09	0.78	A B C E *
0938+39	3C223.1	G	16.0	0.107	1.25	0.61	E
0945+07	3C227	G	16.3	0.086	4.30	0.82	A C D E
0945+73	4C73.08	G	14.7	0.058	1.70	0.80	B E *
1003+35	3C236	G	16.0	0.099	2.03	0.70	A B C E *
1101+38		G	13.1	0.030	0.77	0.09	E
1113+29	4C29.41	G	15.1	0.048	1.14	0.44	E
1142+19	3C264	G	12.8	0.021	3.27	0.53	A B C D E *
1215+03	4C04.41	G	17.0	0.075	1.21	1.34	D
1251+27	3C277.3	G	15.9	0.086	1.95	0.72	B C E
1251-12	3C278	G	13.5	0.015	4.50	0.93	A C D E
1319+42	3C285	G	16.1	0.079	0.00	0.00	E *
1321+31		G	13.9	0.016	0.70	-0.02	E
1340+05	4C05.47	G	17.8	0.133	1.10	0.56	D
1345+12	4C12.50	G	17.0	0.122	3.80	0.44	A B C D E
1350+31	3C293	G	14.3	0.045	2.93	0.73	A B C E *
1404+28	OQ208	G	14.0	0.077	1.81	-0.78	B C E
1414+11	3C296	G	12.2	0.024	2.73	0.76	A B C E *
1417-19	14-15	G	17.5	0.119	1.10	0.71	D
1441+52	3C303	G	17.3	0.141	1.57	0.81	B E *
1448+63	3C305	G	13.7	0.042	1.66	0.94	B E *
1452+16		G	14.0	0.046	0.80	0.93	D E
1502+26	3C310	G	15.3	0.054	3.10	1.46	A B C D E *
1511+26	3C315	G	16.8	0.108	2.10	0.77	A B C E *
1514+00		G	16.5	0.053	1.83	0.48	C D E
1514+07	3C317	G	13.5	0.035	2.20	1.40	A D E
1529+24	3C321	G	16.0	0.096	2.20	1.14	A B C E *
1557+70	4C70.19	G	14.0	0.032*	1.78	0.88	B
1559+02	3C327	G	15.9	0.104	5.04	0.95	A C D E
1615+35	NGC6109	G	14.9	0.030	0.00	0.00	E *
1637+82	NGC6251	G	13.0	0.024	2.17	0.70	A B E *
1652+39		G	14.0	0.033	1.40	0.02	C E
(1717-00	3C353	G	15.4	0.030	33.80	0.84	A C D E)
1803+78		G?	13.8	0.029*	2.36	-0.18	A B
1807+69	3C371	G	14.8	0.050	1.94	0.16	B C E
(1834+19		G	14.0	0.016	0.92	0.47	D)
(1836+17	3C386	G	16.0	0.018	4.20	1.01	D E *)
1842+45	3C388	G	15.7	0.091	3.15	0.94	A B C E *
1845+79	3C390.3	G	14.4	0.057	6.64	0.70	A B C E *

Table 4.3: Continued

IAU	other	type	mag	z	S		sample						
(1940+50	3C402	G	14.0	0.025	1.84	1.14					E	)	
(1949+02	3C403	G	15.4	0.059	3.68	0.73	A		C	D	E	)	
2045+06	3C424	G	17.5	0.127	1.24	1.05					E		
(2121+24	3C433	G	15.5	0.102	7.00	1.07	A	B	C	D	E	*)	
(2200+42	B1 Lac	Q	14.5	0.069	5.21	0.15	A	B	C		E	)	
2212+13	3C442A	G	13.7	0.026	0.00	0.00					E	*	
2221-02	3C445	G	15.8	0.056	3.46	0.70	A		C	D	E		
2229+39	3C449	G	13.2	0.017	2.50	0.95	A	B	C		E	*	
2243+39	3C452	G	16.0	0.081	5.94	0.97	A	B	C		E	*	
2244+36	4C36.47	G	16.0	0.081	1.13	0.75					E		
2247+11	4C11.71	G	12.0	0.026	1.40	0.20			C	D	E	*	
2300-18	OZ-102	G	18.3	0.126	0.98	0.16				D			
2335+26	3C465	G	13.2	0.029	4.00	1.03	A	B	C		E	*	

sources in brackets have too large values of E(B-V)

'*' indicates a member of the Laing et al. (1983) sample

spectral index and luminosity. The derivation of these quantities is complicated slightly for two reasons; firstly, the above samples are not all on exactly the same flux density scale. Secondly, some of the sources are variable, and not all measurements have been made at the same epoch. This has resulted in some of the sources having slightly different flux densities in the different catalogues. The first complication is inconsequential in comparison with the second, which we just have to accept; the result of this will be to broaden the distribution of α .

The values for all parameters used here are taken from the first sample in which the source appears, as given in Table 4.2.

4.6 : Results for Sources of Known Redshift

4.6.a Values of Agg*

4.6.a.(1) Values for Radio Sources

As a first step, it is instructive to consider the observed values of Agg* for the radio sources, before any corrections are applied.

Fig. 4.4.a shows the values of Agg*(1^{o}) for the 84 source composite sample, calculated using a 1^{o} counting radius, and normalised in an annulus 3-5^{o} from the source (c.f. LS Fig. 3). The values for the sources in common with LS are in excellent agreement. The diagram shows a similar result to that found by LS; little signal at low redshifts; generally larger values for $z \sim 0.02 - 0.05$, and a fall off to higher redshifts. Note however, that in this sample, there are many more sources with negative

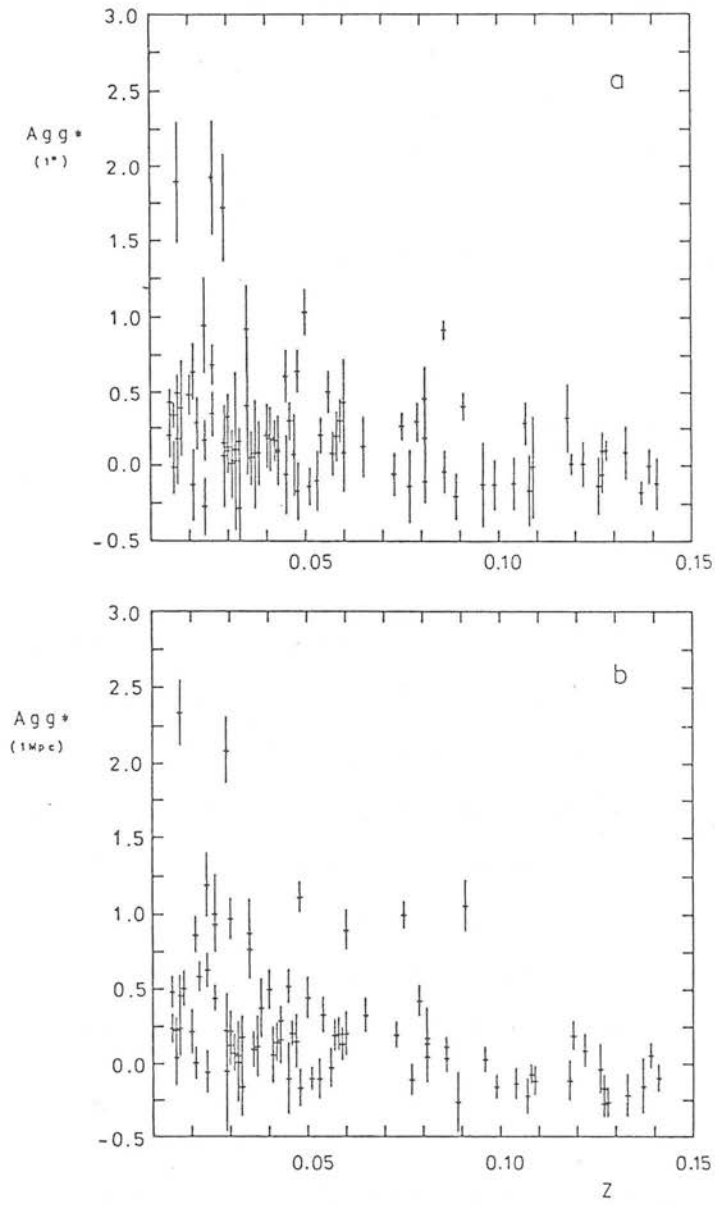

Figure 4.4. Agg* versus z for the composite radio sample:

a) calculated using a 1^{O} counting radius.

b) calculated using a 1Mpc counting radius.

values for Agg*(1^{o}) at low redshift.

Fig. 4.4.b shows the same plot for values calculated using a counting radius of θ = 1Mpc at the redshift of the source (Agg*(1Mpc)). While the general trends are similar, there are a number of differences. Firstly, the errors on the individual values are generally slightly smaller than using the 1^{o} method. Also, the values of Agg* for the lower redshift sources are somewhat larger. Finally, while at larger redshifts Agg*(1^{o}) tends to average around zero, Agg*(1Mpc) appears generally slightly negative.

Fig. 4.5 shows a plot of Agg*(1^{o}) versus Agg*(1Mpc); as these have both been calculated using identical background normalisations, all the scatter comes from the values of Nobs. The values of Agg*(1Mpc) for different background normalisations is shown in Fig. 4.6; it can be seen that in comparison with the above effect, the variations introduced by the background estimation are negligible. (This does not mean that the background inside the small area used in the summation is well known, simply that the mean background is.)

A plot of 1-Agg*(1Mpc)/Agg*(1^{o}) is shown in Fig. 4.7. It is difficult to detect a systematic variation between Agg*(1^{o}) and Agg*(1Mpc) with redshift; this is not too suprising in view of the large errors in both values. Some effects are noticeable, however. Firstly, in the range z = 0.07-0.1, for Agg*(1^{o}) 7 of the 13 sources have negative values. In comparison, Agg*(1Mpc) is negative for only 3 sources. This suggests that at higher redshifts, while the 1Mpc method may not be much less noisy, in individual cases it is actually detecting the presence of clustering which is not found using the 1 degree method. Secondly, as mentioned above, Agg*(1Mpc) appears generally negative above z ~ 0.1. The implications of this

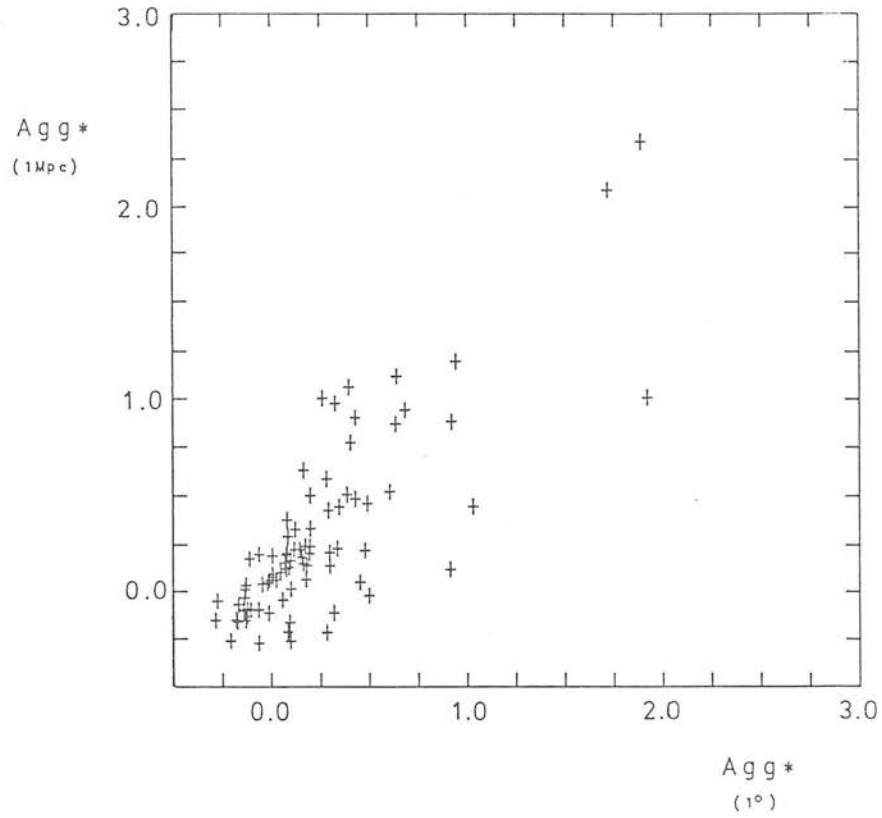

Figure 4.5. A comparison of the Agg* values obtained using a counting radius of θ = 1Mpc at the redshift of the source to those obtained using a constant radius of θ = 1 degree.

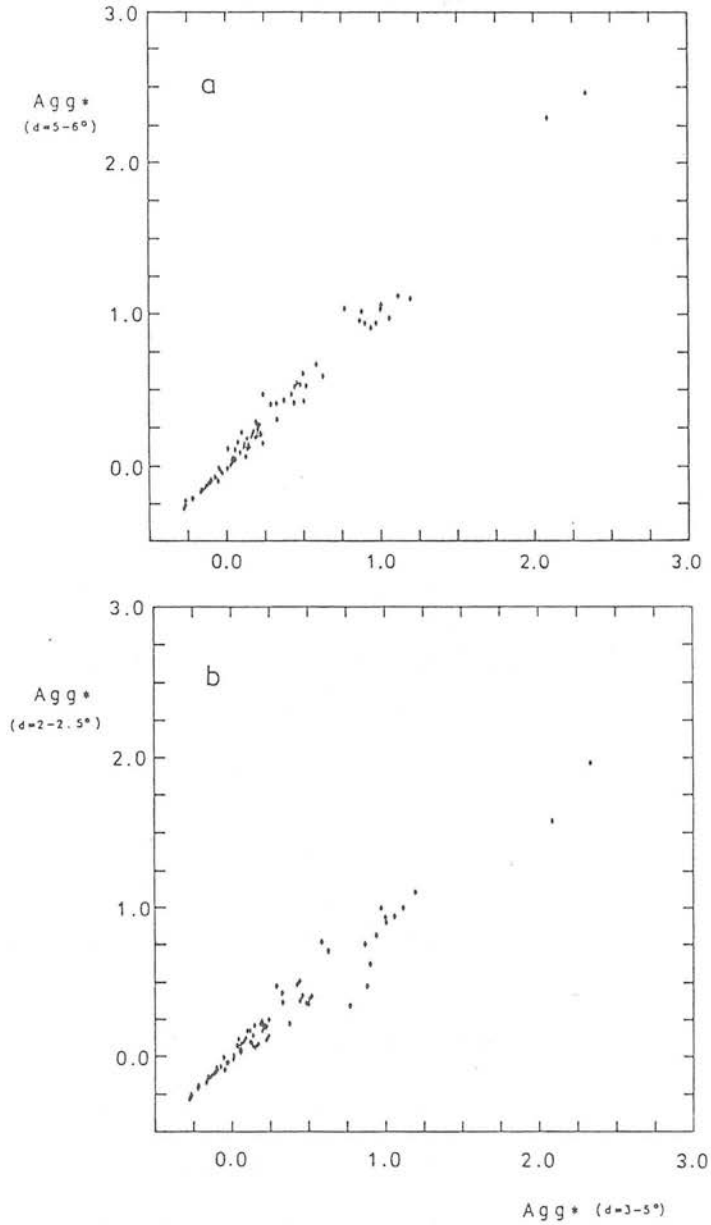

Figure 4.6. Agg* values calculated using different background normalisations. The standard values (normalised in an annulus d = 3-5 degrees) are compared to those obtained normalised using counts in an annulus of a) d = 5-6 degrees and b) d = 2-2.5 degrees.

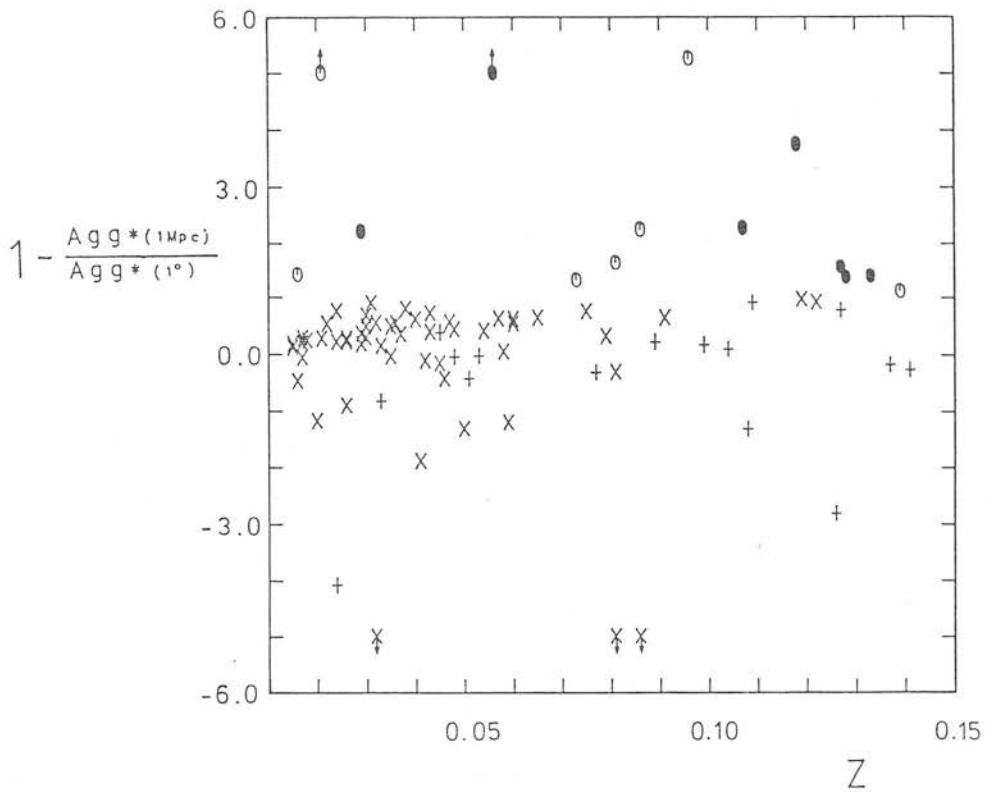

Figure 4.7. A comparison of Agg*(1°) with Agg*(1Mpc) as a function of redshift.

x = both measures positive

● = Agg*(1°) positive

o = Agg*(1Mpc) positive

\+ = both measures negative

result are not clear. Of the twelve sources with $z > 0.1$, and negative values of Agg*(1Mpc), for seven the corrected count of galaxies within the 1Mpc radius is less than 1. (In four cases, no galaxies were counted. This is clearly an "error" in the Lick counts, since the radio source at least should have been included. These are all radio-galaxies, with $m < 18$). Since the method automatically assumes that the source itself is present, and subtracts it in the determination of the number of neighbours, these sources have values of Agg* which are clearly spuriously low. (Although the "true" value may still be negative.) The presence of this effect in at least 30% of the sources with negative values suggests that the Lick counts are too unreliable to calculate values of Agg* for individual sources with $z > 0.1$. The fact that this effect is not obvious in the Agg*(1^{o}) measure is due to the much larger number of bins involved.

4.6.a.(2) Values for Abell Clusters

Finally, it is interesting to consider the results obtained for a sample of Abell clusters, as a comparison to the radio sources. It should be noted that Abell clusters are not necessarily representative of the typical environments of radio sources, but the knowledge that at least some of the radio sources are found in Abell clusters makes the comparison worth-while.

A sample of 107 Abell clusters was considered. These were chosen from the sample of Lier and van den Bergh (1977), with redshifts taken from the compilation of Sarazin et al. (1982). Clusters were included if they had at least two galaxies with measured redshifts which were not discrepant, as discussed by Sarazin et al. (i.e. the redshifts were in agreement, and also consistent with the cluster galaxy apparent magnitudes). In addition, clusters with $z > 0.1$ were

considered even if only one redshift was available. The value for Agg*(1Mpc) for this sample is shown in Fig. 4.8. A comparison of this with Fig. 4.4.b reveals two points. Firstly, the maximum values of Agg*(1Mpc) for radio galaxies at lower redshifts are similar to those Abell clusters of richness classes 0 and 1, although there are many sources with values less than this. Secondly, while the maximum values in the range $z < 0.1$ are similar for the radio sources and Abell class 1 clusters, there is a noticeable difference in the range 0.1-0.15; many Abell clusters still have positive values of Agg*(1Mpc). This suggests that while the data may not be good enough to obtain reliable values of B for high-redshift sources, it can at least indicate the absence of strong clustering around the sources, via a comparison such as this.

4.6.b Values of Bgg*

We will now discuss the values of Bgg* obtained for the various objects of different types. Henceforth, we will consider the value of Bgg* normalised by Bgg, the value expected for an 'average' galaxy, and denote this quantity, Bgg*/Bgg, simply as B.

4.6.b.(1) Values for Abell Clusters

A comparison of Agg* and B for Abell clusters of richness classes R=0,1 and 2 is shown in Fig. 4.9. Two points are of interest; firstly, the correction via X(z) appears to have been remarkably successful in "removing" the effect of varying redshift. Despite the uncertainties described above, this appears reasonably correct even out to $z \sim 0.15$. The second point to note is that, even amongst sources of the same richness class, there is a fairly large spread in the values of B, considerably more so that the formal errors described above. The weighted mean values of B for the

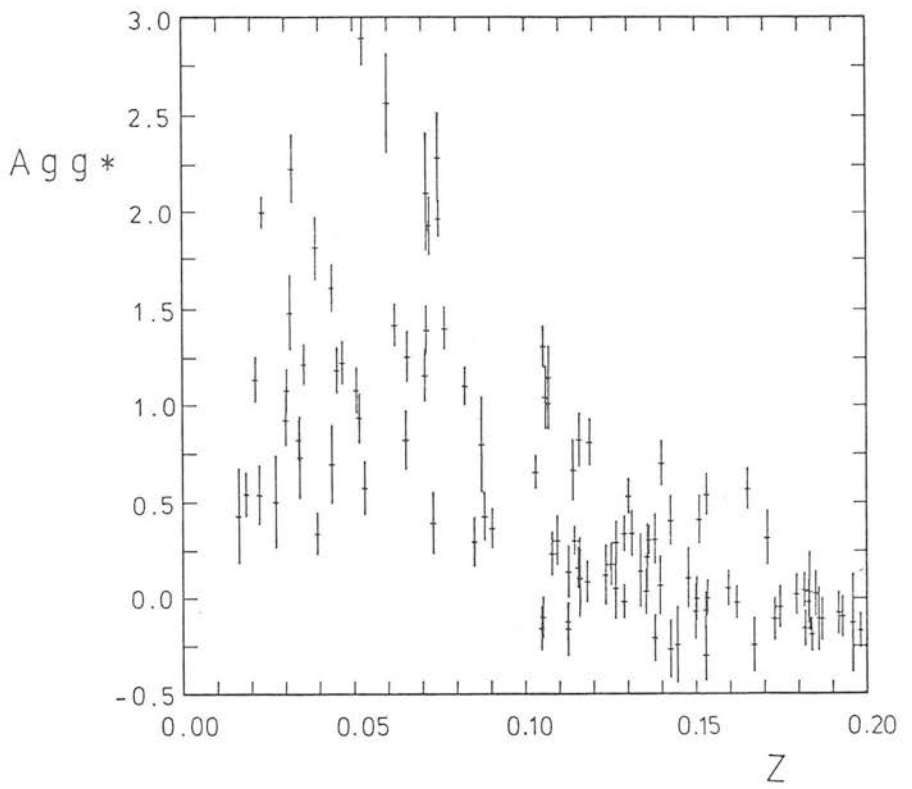

Figure 4.8. Values of Agg* for a sample of 107 Abell Clusters.

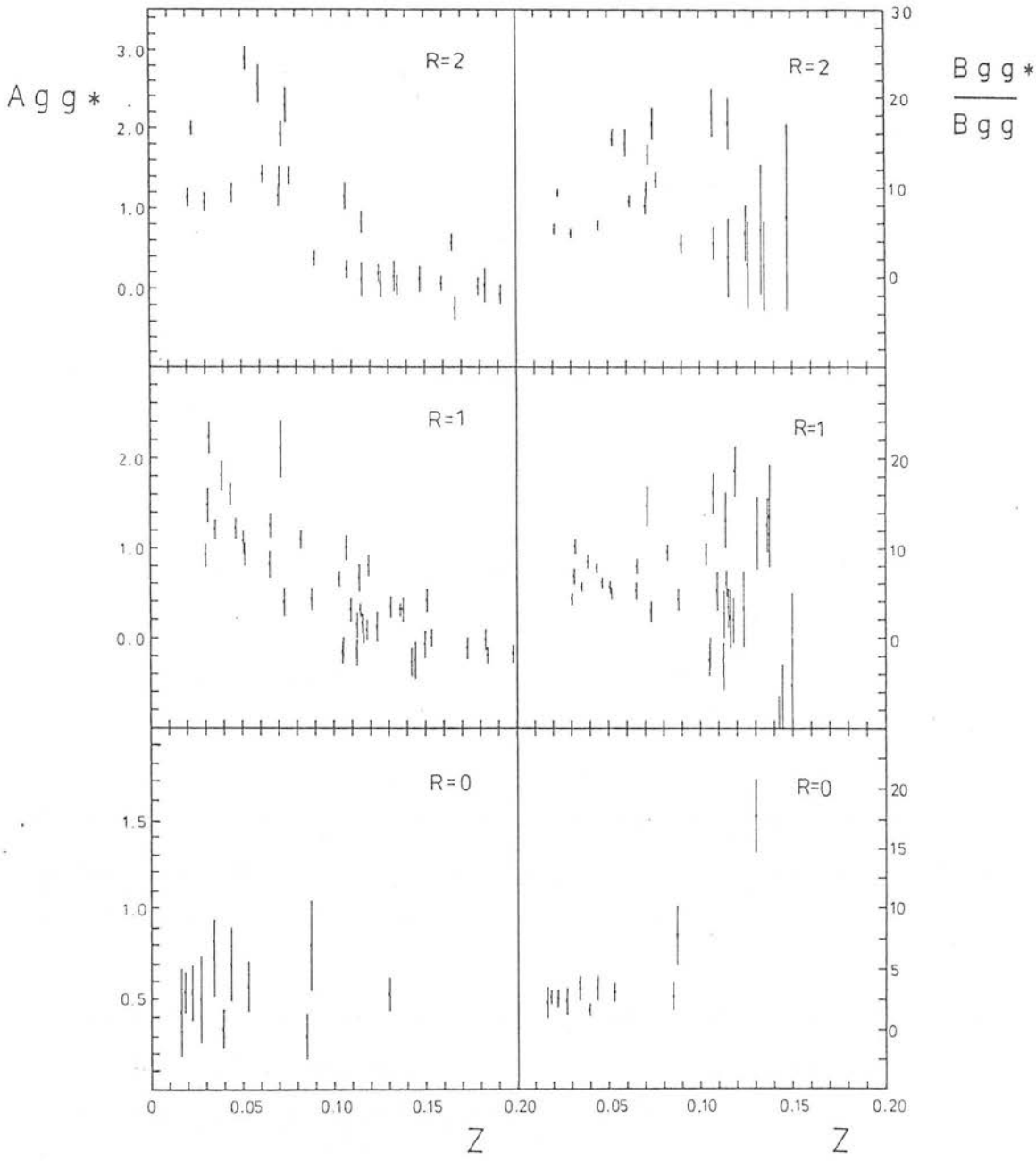

Figure 4.9. Values of Agg* and Bgg*/Bgg for Abell Clusters of richness classes R = 0, 1 and 2 showing the effects of the X(z) function. (Values of Bgg*/Bgg for sources with $z > 0.15$ have not been calculated.)

different richness classes, (calculated as described in Appendix B) for sources with $z < 0.1$ are,

$$R = 0 \quad \text{mean} = 2.8 \pm 0.3 \quad \sigma_{pop} = 0.5 \quad (11 \text{ sources})$$

$$R = 1 \quad \text{mean} = 6.8 \pm 0.7 \quad \sigma_{pop} = 2.6 \quad (15 \text{ sources})$$

$$R = 2 \quad \text{mean} = 9.7 \pm 1.2 \quad \sigma_{pop} = 4.2 \quad (13 \text{ sources})$$

4.6.b.(2) Values for the Composite Sample

In light of possible errors in Agg* for sources with $z > 0.1$, we will consider the values of B in more detail only for those sources with $0.015 < z < 0.1$. This sample contains a total of 69 sources, including one quasar. Excluding this leaves a sample of 68 radio galaxies. The value of B for these sources, along with radio morphological classifications are given in Table 4.4.

As a preliminary, we can now demonstrate empirically that any systematic effect caused by an incorrect assumption of γ is negligible. From equation 4.9, we can see that:

$$\text{Agg*} \propto 1/J \qquad (4.24)$$

hence

Table 4.4: Results for the 68-Source Sub-Sample ($z < 0.1$)

IAU name	other name	radio morphology		z	Agg* (1Mpc)	ΔAgg*	Bgg* (1Mpc)	B	ΔB
0034-01	3C15	I	*	0.073	0.197	0.084	57	1.42	0.60
0036+03	4C03.01	?	(5)	0.015	0.239	0.093	51	1.27	0.50
0055-01	3C29	I	*	0.045	0.520	0.110	102	2.55	0.55
0055+30		C	f.s.	0.016	0.043	0.187	9	0.22	0.98
0104+32	3C31	I	(8)	0.017	0.460	0.131	94	2.35	0.68
0106+13	3C33	IIg	(8)	0.060	0.901	0.130	210	5.25	0.75
0111+02		C	f.s.	0.047	0.152	0.176	31	0.77	0.88
0116+31	4C31.04	C	(8)	0.059	0.135	0.109	31	0.77	0.63
0123-01	3C40	I	*	0.018	0.505	0.115	101	2.53	0.57
0124+18	4C18.06	IIg	(3)	0.043	0.291	0.093	56	1.40	0.45
0206+35	4C35.03	?	(1)	0.037	0.119	0.202	22	0.55	0.95
0220+42	3C66B	I	(8)	0.022	0.585	0.098	112	2.80	0.47
0238+08	NGC1044	IIn	(3)	0.021	0.008	0.108	2	0.05	0.52
0255+05	3C75	I	*	0.024	1.196	0.206	225	5.63	0.98
0258+35	4C34.09	I	(9)	0.020	0.219	0.147	43	1.08	0.73
0300+16	3C76.1	I	(8)	0.032	0.011	0.270	2	0.05	1.25
0305+03	3C78	I	*	0.029	0.225	0.246	42	1.05	1.13
0314+41	3C83.1B	I	(8)	0.026	1.006	0.256	187	4.68	1.20
0316+41	3C84	I	(6)	0.017	2.337	0.209	478	11.95	1.08
0325+02	3C88	IIn	*	0.030	0.128	0.134	24	0.60	0.63
0356+10	3C98	IId	(8)	0.031	0.076	0.123	14	0.35	0.57
0404+03	3C105	IId	*	0.089	-0.264	0.205	-106	-2.65	2.08
0430+05	3C120	C	f.s.	0.033	-0.155	0.203	-29	-0.73	0.95
0453-20	OF-289	I	*	0.035	0.880	0.224	164	4.10	1.05
0502-10	05-11	?	(-)	0.041	0.061	0.186	12	0.30	0.90
0703+42	4C42.23	I	(8)	0.038	0.376	0.194	71	1.77	0.93
0744+55	DA240	IIn	(6)	0.036	0.101	0.118	19	0.47	0.55
0755+37	3C189	C	(8)	0.043	0.163	0.159	32	0.80	0.77
0802+24	3C192	IId	(8)	0.060	0.204	0.145	48	1.20	0.85
0819+06	3C198	IIn	(7)	0.081	0.138	0.094	47	1.17	0.80
0828+32	4C32.25	C	f.s.	0.051	-0.099	0.076	-21	-0.52	0.40
0844+54	4C54.17	I	(3)	0.040	0.500	0.130	95	2.38	0.63
0915-11	Hyd A	I	*	0.065	0.327	0.111	82	2.05	0.70
0945+07	3C227	IIg	*	0.086	0.036	0.087	14	0.35	0.82
0945+73	4C73.08	IIn	(6)	0.058	0.203	0.108	46	1.15	0.60
1003+35	3C236	IId	(8)	0.099	-0.157	0.081	-81	-2.03	1.05
1101+38		C	f.s.	0.030	0.223	0.132	41	1.02	0.60
1113+29	4C29.41	IIn	(9)	0.048	1.116	0.098	226	5.65	0.50
1142+19	3C264	I	(8)	0.021	0.867	0.118	167	4.18	0.57
1215+03	4C04.41	?	(2)	0.075	1.001	0.088	301	7.53	0.65

Table 4.4: Continued

IAU name	other name	radio morphology	z	Agg* (1Mpc)	ΔAgg*	Bgg* (1Mpc)	B	ΔB
1251+27	3C277.3	IIn (8)	0.086	0.116	0.062	44	1.10	0.57
1251-12	3C278	I *	0.015	0.482	0.103	103	2.58	0.55
1319+42	3C285	IIn (6)	0.079	0.424	0.101	138	3.45	0.82
1321+31		C f.s.	0.016	0.228	0.079	48	1.20	0.43
1350+31	3C293	I (6)	0.045	-0.101	0.243	-20	-0.50	1.20
1404+28	0Q208	C (8)	0.077	-0.107	0.104	-34	-0.85	0.80
1414+11	3C296	I (8)	0.024	-0.054	0.143	-10	-0.25	0.68
1448+63	3C305	I (6)	0.042	0.147	0.127	28	0.70	0.63
1452+16		? (4)	0.046	0.207	0.081	41	1.02	0.40
1502+26	3C310	IIn (8)	0.054	0.331	0.115	71	1.77	0.63
1514+00		IIn (2)	0.053	-0.101	0.135	-22	-0.55	0.73
1514+07	3C317	I *	0.035	0.770	0.196	143	3.58	0.93
1529+24	3C321	IId (8)	0.096	0.030	0.081	14	0.35	0.98
1557+70	4C70.19	I (8)	0.032	0.058	0.102	11	0.28	0.47
1615+35	NGC6109	I (6)	0.030	0.974	0.134	180	4.50	0.63
1637+82	NGC6251	I (6)	0.024	0.628	0.113	118	2.95	0.52
1652+39		C f.s.	0.033	0.181	0.138	34	0.85	0.65
1803+78		C (8)	0.029	-0.048	0.414	-9	-0.22	1.92
1807+69	3C371	C (8)	0.050	0.444	0.136	92	2.30	0.70
1842+45	3C388	IIn (8)	0.091	1.060	0.168	448	11.20	1.77
1845+79	3C390.3	IId (8)	0.057	0.194	0.101	43	1.08	0.57
2212+13	3C442A	I (6)	0.026	0.940	0.115	175	4.38	0.52
2221-02	3C445	IId *	0.056	-0.025	0.130	-5	-0.13	0.73
2229+39	3C449	I (8)	0.017	0.240	0.183	49	1.23	0.93
2243+39	3C452	IId (8)	0.081	0.047	0.172	16	0.40	1.45
2244+36	4C36.47	IIg (10)	0.081	0.172	0.202	58	1.45	1.70
2247+11	4C11.71	I (6)	0.026	0.442	0.083	82	2.05	0.40
2335+26	3C465	I (8)	0.029	2.089	0.220	386	9.65	1.02

references for radio morphology:

(1) Fanti et al., 1977.
(2) Fomalont, 1971.
(3) Fomalont et al., 1980.
(4) Hazard and Murdoch, 1977.
(5) Laing et al., 1970.
(6) Laing et al., 1984, and refs therein.
(7) Longair and Seldner, 1979.
(8) Peacock and Wall, 1982, and refs therein.
(9) Riley, 1975.
(10) Wilkinson et al., 1981.

$$Bgg^*/Bgg \propto X(z)/J \qquad (4.25)$$

The ratio $B_{\gamma=2.4}/B_{\gamma=1.77}$ for the 68 source sample is shown in Fig. 4.10. The absolute value of this ratio is not meaningful, since normalising Bgg* to the value for galaxies in general is not valid if we believe that is different for radio galaxies. This will not however affect the relative variation with z. The scatter in values apparent is due to the non-uniform area over which the integral has had to be performed, due to the binned nature of the data. It can be seen that both this, and the small systematic trend with z (due to the minimum bin size constraint) is negligible in comparison with the large variations in B from source to source.

We will now consider the relationship between B and the radio properties of individual sources.

The most interesting correlations we might wish to investigate are those between B and radio luminosity, morphology and spectral index. For all but five of these sources morphological classifications are available; they have been taken from a variety of sources, as indicated in Table 4.4. The dividing line between classifications is occasionally not well defined, although in most cases it is unambiguous; for the five sources without classifications, observations suggest that they are all extended.

The variations of B are most interestingly displayed in the B-log(P) plane, shown in Fig. 4.11 for the 68 source sample. The luminosity has been calculated here assuming $H_o = 50 kms^{-1} Mpc^{-1}$, $\Omega_o = 1$. The most obvious features of this diagram are as follows;

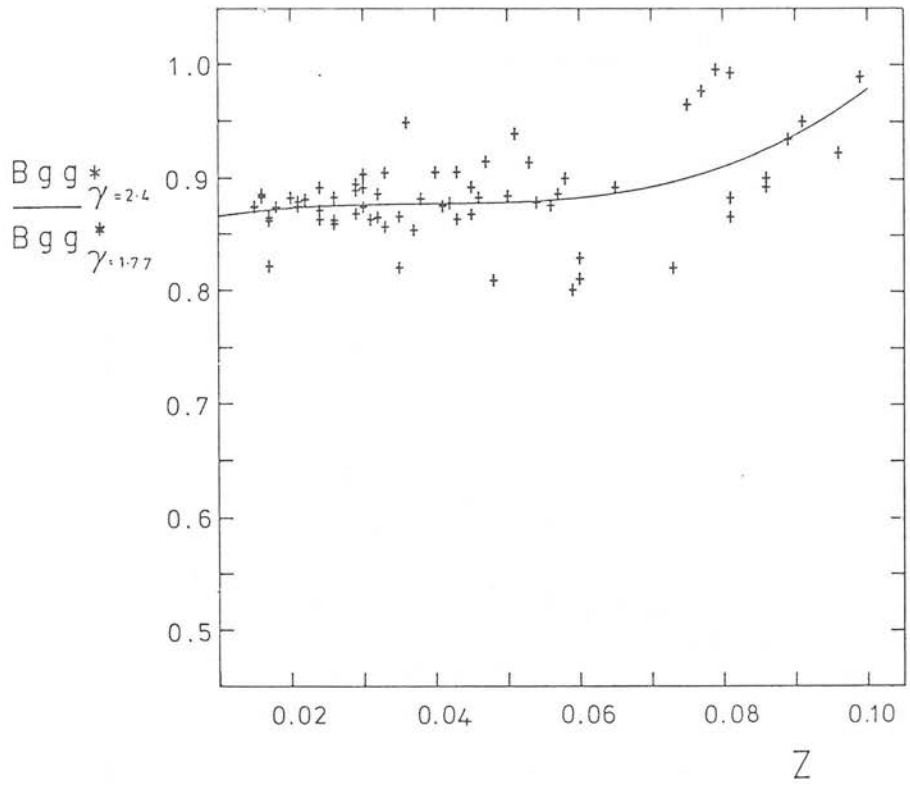

Figure 4.10. The ratio of the value of B calculated using $\gamma = 2.4$ to that calculated using $\gamma = 1.77$. The solid line is the best-fit polynomial to the data, which have been arbitrarily normalised.

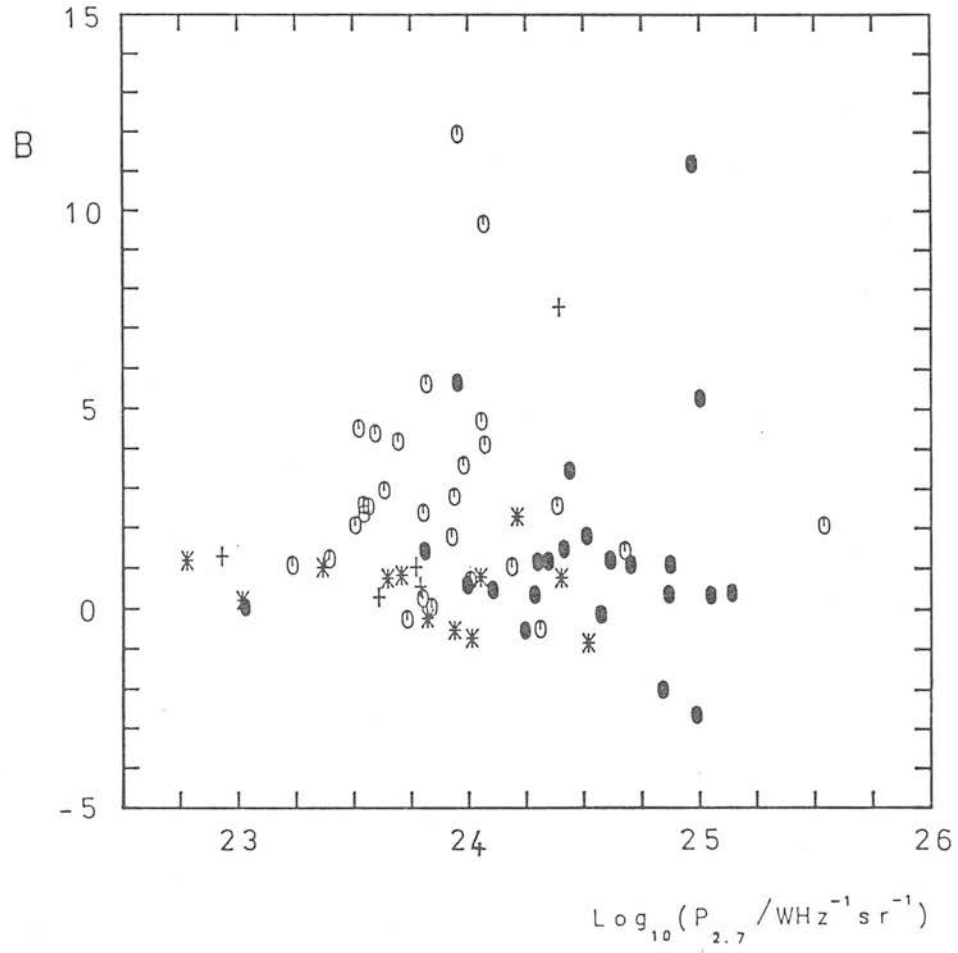

Figure 4.11. A plot of B versus 2.7GHz luminosity for the 68 source sample, differentiated according to source structure.

* = compact

o = FRI

● = FRII

\+ = unknown FR class

a) the compact sources have generally low values of B, with the majority having a value of ~ 1 or less.

b) For extended sources, while the well-known division in luminosity between FRI's and FRII's is evident at $P_{2.7} \sim 10^{24} WHz^{-1}sr^{-1}$, there is no obvious discontinuity in B. Although FRI sources appear to have on average rather higher values than the FRII sources, individual objects in each class show similar extremes of B.

c) whether we consider all sources, or only sources of one individual type, there appears to be a large scatter in B at all luminosities.

If this spread is real, it has important implications for the relationship between radio sources and their galactic environments. It is therefore important to try and ascertain the origin of the scatter.

The spread is certainly larger than the errors on individual objects, showing that it cannot be due simply to difficulties in determining the background counts. One possible hypothesis is that it could be due to the residual effects of the variation in the galactic extinction to objects of different galactic latitudes. However, inspection of the trend of B with |b| (Fig. 4.12) reveals no such effect. Also the effects of varying redshift, in moving the counts further down the cluster-luminosity function, with statistical variations in this function are not likely to be important, since objects of similar redshift show a wide range of B values. Finally, the effects of the plate-correction factors on the counts are much too small to cause such a large effect. We are thus lead to the conclusion that the scatter is certainly present in the

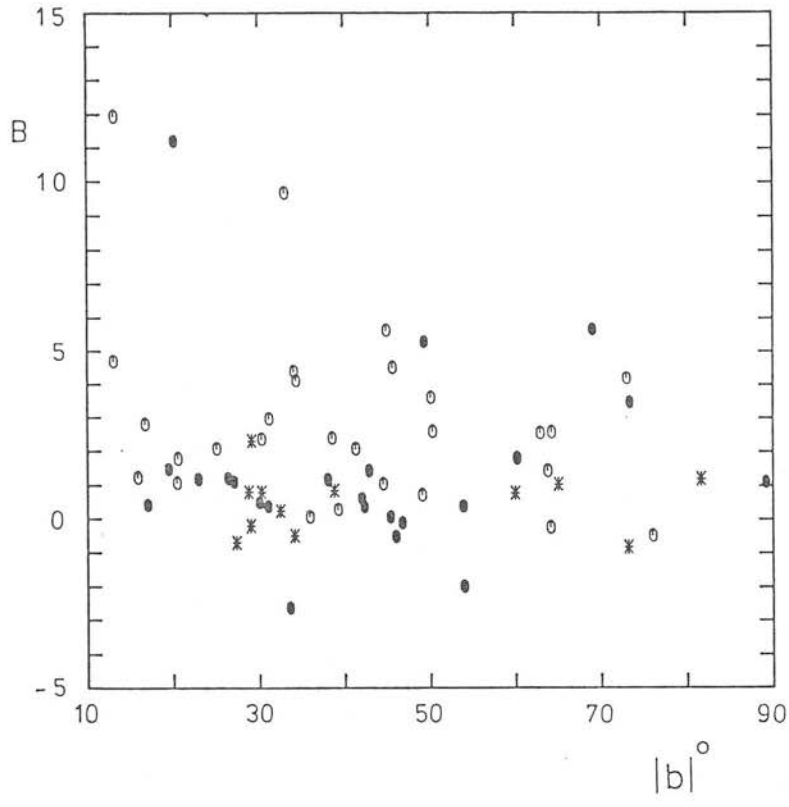

Figure 4.12. B as a function of galactic latitude for compact (*), FRI (o) and FRII (•) galaxies.

data, in the sense of being due to true variations in the galaxy populations around each source. To some extent, the effect may be caused by fluctuations in the number and space distribution of galaxies observed for different clusters which are 'similar' in other respects (e.g. in terms of their IGM densities). This would include the effects of non-spherical symmetry or variations in the power-law index. To test this hypothesis, the values of B were rederived for the 68 source sample using a 2Mpc counting radius. The values obtained, compared to the 1Mpc values are shown in Fig. 4.13. There are indeed some variations between the two measures for individual sources, however this does not appear to be large enough to account for all the variation between the values for different sources. A final possibility is that some sources may have a spuriously high value of Bgg*, due to chance superposition of background clusters. This possibility cannot be ruled out in the absence of redshift information; however, the discussion below indicates that it is not likely to be a problem for the vast majority of the sources. Thus it seems that simply on the basis of the observed values of B, there is a fairly large variation in the galaxy environments of individual sources of similar radio properties.

We will now try to quantify the effects discussed above. The main questions we wish to answer are; what are the mean values of B for the various radio classes, and, are these significantly different from class to class. A related question is what is the typical dispersion in the value of B within a specific class.

The computation of these quantities is made difficult by two effects. Firstly, the error in B is not constant for all sources. We therefore wish to apply some form of weighting in calculating the mean values. The second complication however, is the presence of

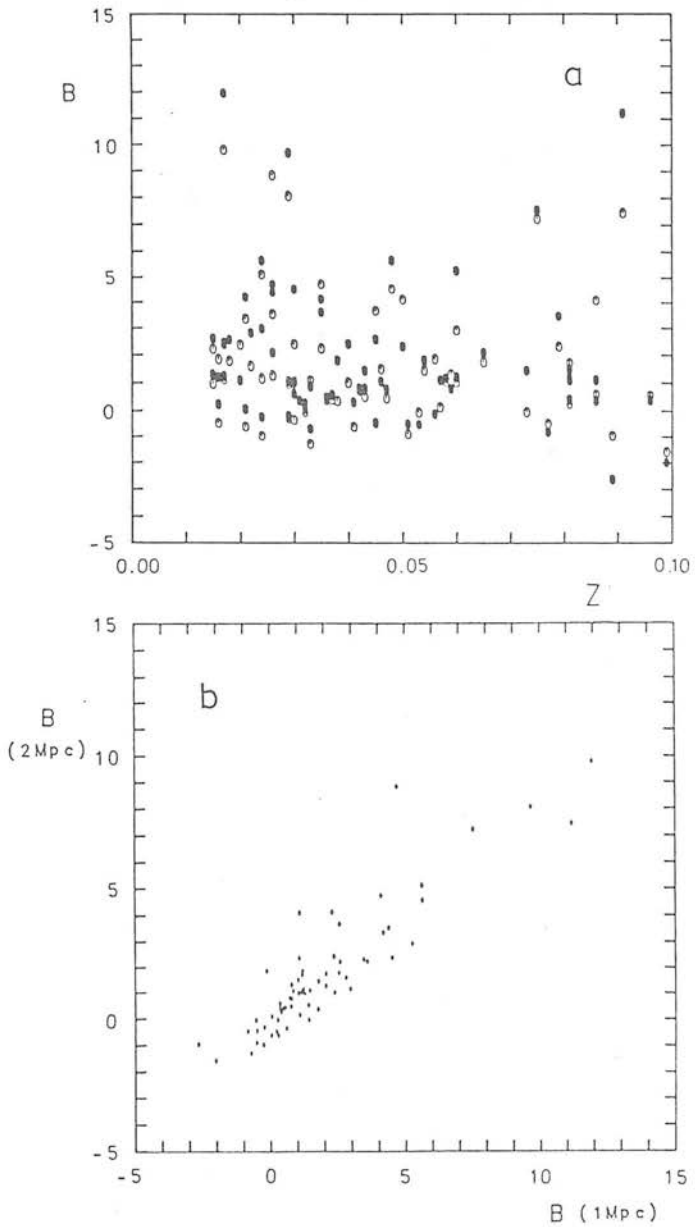

Figure 4.13. A comparison of the values of B obtained using counting radii of 1 and 2Mpc.

a) B(1mpc) (•) and B(2Mpc) (o) versus redshift

b) B(2Mpc) versus B(1Mpc)

this larger scatter in the distribution of values than would be expected simply from the size of the measurement errors. This problem, of combining weights for individual sources, with a true but unknown 'cosmic scatter' is one which occurs in many astrophysical situations; it is circumvented here using a method described in Appendix B. Henceforth, the means and their quoted errors will be calculated using this method, as will standard errors in the population, where given.

The mean values of B for the composite sample sources of each type, for $z < 0.1$, are as follows:

compact mean = 0.56 +/- 0.26 σ_{pop} = 0.57 (12 sources)

FR I mean = 2.89 +/- 0.51 σ_{pop} = 2.56 (28 sources)

FR II mean = 1.40 +/- 0.54 σ_{pop} = 2.43 (23 sources)

unknown mean = 2.16 +/- 1.36 σ_{pop} = 2.96 (5 sources)

The difference in the means between FRI and FRII sources is $\sim 2\sigma$. The corresponding values for the sources drawn from the WP and Northern samples, (which are 100% complete in the sense that all objects are identified and have redshifts) are insignificantly different from these values.

In investigating the distribution of B with morphological class (or luminosity), we must beware of possible systematic effects due to the redshift distribution of the sources. In a flux-limited

sample, to first order the most luminous sources appear at higher redshifts. To check for this effect, plots of B versus z for the three classes were inspected (Fig. 4.14). There is no evidence for any systematic redshift effects within the individual classes. As a final check, we note that the mean value of B for FRII sources with $z < 0.07$, a value which should avoid the faint-magnitude effects, and which covers a similar range to that over which the FRI sources lie, is also insignificantly different from the value for all FRII sources.

The plot of B versus z for the FRII sources reveals that four objects appear to have rather high values of B compared to the remainder; we might therefore suppose that these have been 'contaminated', in the sense discussed above. These sources were therefore considered in more detail.

1113+29 (4C29.41, B = 5.65) lies in the direction of the Abell cluster A1213. The redshifts of a number of members of this cluster have been obtained by Hintzen (1980), and these confirm that the radio source is indeed a true member. We may therefore have confidence in the value of B for this object.

Van den Bergh (1961) has noted the association of 0106+13 (3C33, B = 5.25) with Abell 150, a richness class 1, distance class 5 cluster. Leir and van den Bergh (1977) have estimated a redshift of $z = 0.093$ for the system, from the magnitudes of the first and tenth brightest cluster members. This is somewhat discrepant with the source redshift ($z = 0.06$), although not overwhelmingly so. However, the cluster centre is ~ 7 arcmin north of the radio galaxy, and Miller (private communication) has noted X-ray emission from this region consistent with being from a distant cluster. Thus the membership of the radio source is in some doubt. However, it will be

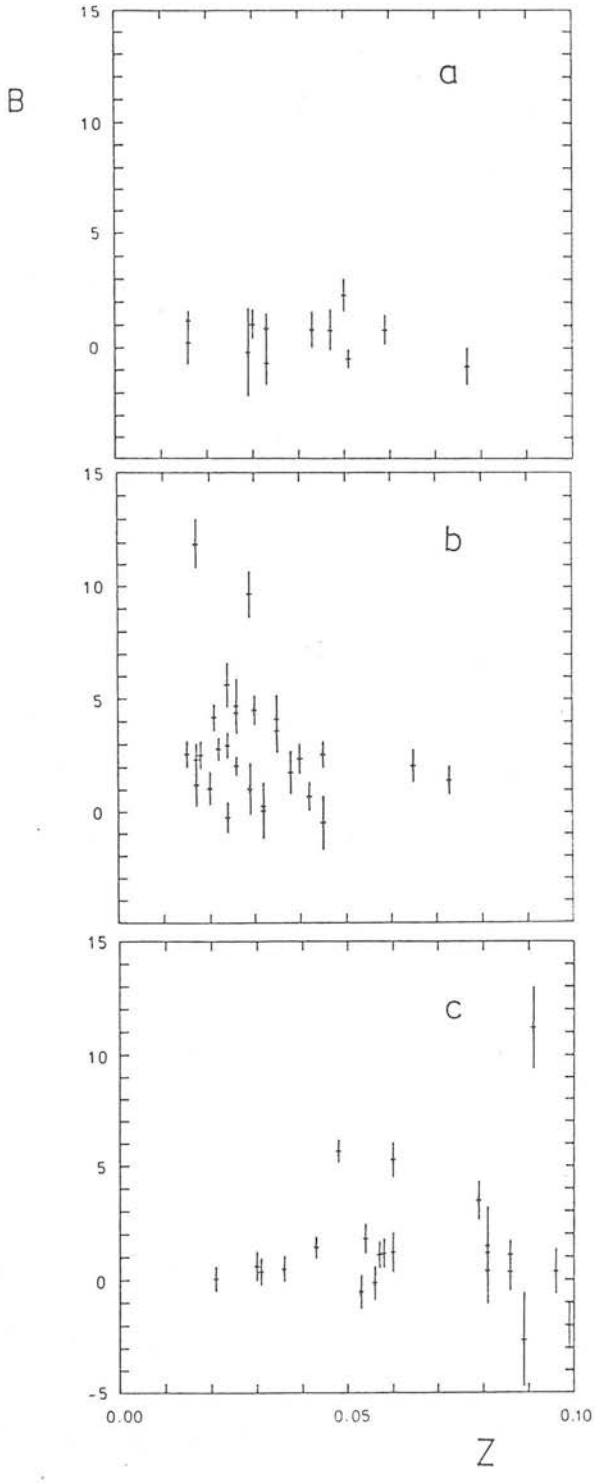

Figure 4.14. Plots of B versus redshift for a) Compact sources, b) FRI sources and c) FRII sources.

demonstrated in Chapter Six that a radio source's optical structure is well correlated with its cluster environment. 0106+13 is discrepant in this respect, with a much higher value of B than would be expected upon the basis of its optical structure; and this appears good evidence that it is not in fact physically associated with A150.

1319+42 (3C285, B = 4.5) and 1842+45 (3C388, B = 11.2) have both been noted as being members of small clusters (Sandage, 1967; Matthews et al., 1964), as would be expected from their observed values of B. However, in neither case has cluster membership been confirmed by redshift observations of other cluster members. We cannot therefore rule out the possibility that these are chance associations, although 1319+42 at least has a lower value of B than the (confirmed) value for 1113+29. If this were the case, then the range of B for FRII sources would be rather reduced; however the result for 1113+29 (and also, for example, known clusters around Cygnus A and 3C295) shows that FRII sources are not exclusively found in low-density environments.

Finally, the fact that of 35 sources (including the compact objects), which as a class exhibit low values of B, only three appear to have possibly erroneous values, indicates that the FRI values are unlikely to be affected.

From this analysis of the Lick data, there is little evidence for a large difference between FRII "classical" doubles, and the other FRII sources, as discussed by LS. The value of B versus z for FRII classical and non-classical doubles (as discussed by Longair and Riley 1979) is shown in Fig. 4.15. While the three highest values are exhibited by non-classical doubles (excluding 0106+13, which we note is a classical double), non-classical sources do also

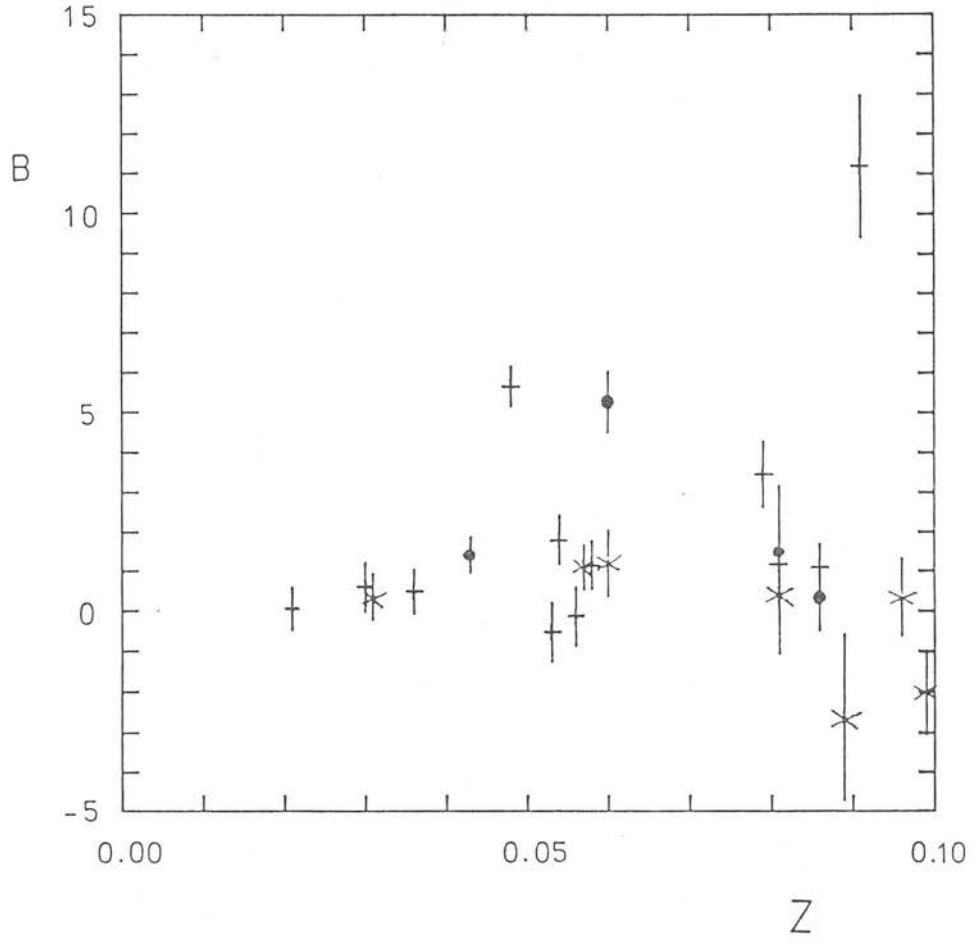

Figure 4.15. The values of B for "good" (•) "doubtful" (x) and "non" (+) classical double FRII sources.

appear in regions of unenhanced galaxy density. In fact, the result of LS was mainly due to 3C277.3 (~ 1.5° from the Coma cluster, but not associated with it) and the three high-redshift classical doubles, for which the values are uncertain. On the basis of the sources studied here, the difference between the two classes, as measured by their values of B, does not appear significant.

4.7 : Results for Estimated-Redshift Sources

A plot of B versus redshift for the estimated-z Parkes sample is shown in Fig. 4.16. At higher redshifts, there again appear a number of sources with spuriously low values of B, as discussed above. We may expect this effect to be aggravated by the estimated redshifts. Sources which have low (true) redshifts, with estimated redshifts which are too large will have erroneously high values of B, and vice-versa. However, since X(z) is a steepening function of z at higher redshifts, this effect will be worse for the high redshift sources for which the estimated redshift is too low. Also, when the sources become more distant than the limit of the Lick counts, Agg* will become negative, while the correction factor will still be large. In light of these effects, the sources with $z > 0.1$ will not be included further.

4.7.a B versus Spectral Index

Obviously, without radio maps we cannot classify these sources according to structure. We can however make use of two quantities which are known to be correlated with structure; spectral index and luminosity. Spectral index is correlated with structure in the sense that sources with flat spectra tend to be compact. WP have shown that for the Northern sample, very few extended sources have $\alpha_{2.7}^{5}$

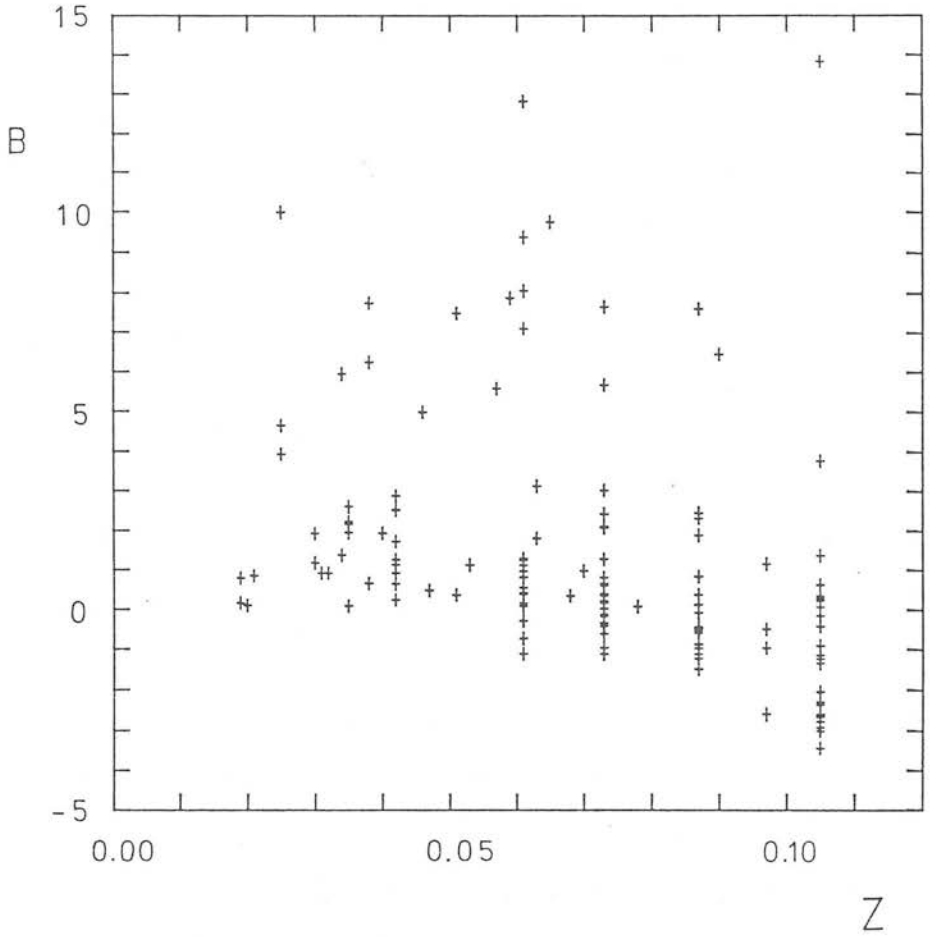

Figure 4.16. A plot of B versus redshift for the Parkes estimated-redshift sample.

less than 0.5. (The converse is not true however, in that compact sources may have steep spectra.) A plot of B versus α for the Parkes sample is shown in Fig. 4.17.a. There is a small difference in the means for the steep and flat spectrum sources, but this is not significant in view of the errors in these values. That there is no obvious segregation is not too suprising however when we consider the distribution of source numbers with α. The vast majority have $\alpha > 0.5$, and hence we can assume that a large fraction of these sources are extended. Only a small percentage of the extended sources would then need to have a value of α less than 0.5 to mask the correlation seen with structure. Compare for example the distribution of B with α for the 68 source sample, shown in Fig. 4.17.b.

4.7.b B versus Luminosity

The second correlation we can use is that between radio-luminosity and structure. As discussed in Chapter One, FR class is well correlated with luminosity, in the sense that low-luminosity sources tend to be FRIs, and high-luminosity sources FRIIs. This is obvious from Fig. 4.11, where the division is seen at $P_{2\ 7} \sim 10^{24} WHz^{-1}sr^{-1}$.

A plot of B versus log(P) for the estimated redshift sources is shown in Fig. 4.18.a for all sources with $\alpha > 0.5$. The distribution of sources is similar to that in Fig. 4.11, with sources of low P appearing to have high generally higher values of B, although again there is a wide spread at all luminosities. A plot of B versus log(P) for all sources is shown in Fig. 4.18.b; the distributions appear generally similar, although there are possibly rather more low-luminosity sources with small values of B in the estimated-z sample.

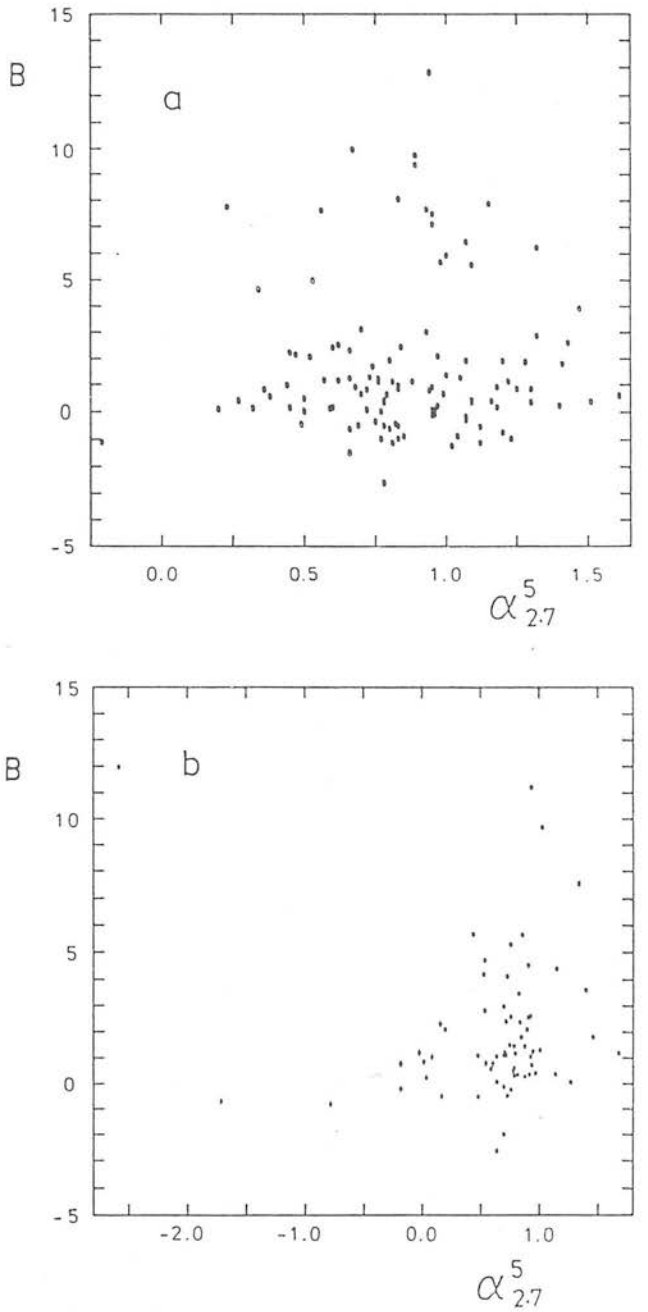

Figure 4.17 Plots of B versus spectral index ($\alpha^{5}_{2.7}$) for:

a) the Parkes estimated redshift sample, and

b) the 68 source sample (+ = compact, • = extended).

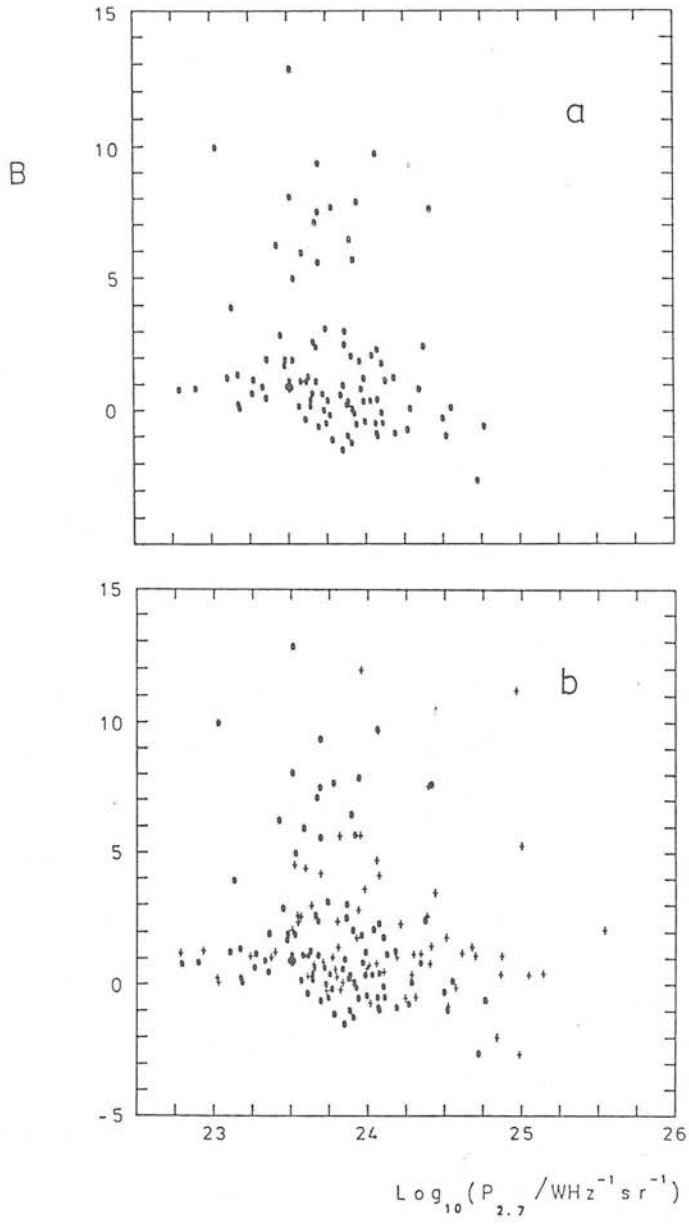

Figure 4.18. Plots of B versus 2.7GHz luminosity:

a) for the Parkes estimated-redshift sample source with $\alpha_{2.7}^{5} > 0.5$.

b) as a) with the extended sources from the 68 source sample also included.

The mean value for sources of low and high luminosity for the estimated z sample are:

$$\alpha > 0.5,\ P_{2.7} < 1.2\times10^{24}\mathrm{WHz}^{-1}\mathrm{sr}^{-1}\ \text{mean} = 2.00+/-0.33\ \sigma_{pop}=2.83 \quad (82)$$

$$\alpha > 0.5,\ P_{2.7} > 1.2\times10^{24}\mathrm{WHz}^{-1}\mathrm{sr}^{-1}\ \text{mean} = 0.62+/-0.55\ \sigma_{pop}=1.91 \quad (16)$$

The difference between these two means is again $\sim 2\sigma$, in the same sense as that for the 68 source sample. The mean for both high and low-luminosity sources appear somewhat lower however than the corresponding true-z values. This difference may be real, although it is difficult to imagine an effect which would cause it. There are two systematic effects which are present to some extent in the data and which would tend to cause this result. Firstly, there is the possibility that a number of the $\alpha > 0.5$ sources are in fact compact. If these do indeed have low values of B, then these would lower the the mean values of B. The distribution in luminosity for the sources known to be compact suggests that this might have a greater effect upon the estimated-redshift low-luminosity mean. Secondly, there are still a number of sources included for which no galaxies were observed in the Lick counts; these sources may well contribute a sufficiently large negative value of B to cause the difference in the estimated and true redshift means. This is a difficult effect to allow for. We cannot simply exclude these sources since presumably they do not have large values of B, or else some galaxies would have been counted. In other words, excluding sources at reasonable redshifts (i.e. values for which we know clustering is detectable) which have no observed counts, without excluding also those sources for which a positive count is observed will bias the results to a higher value. It is possible to get some estimate of the effect of these sources as follows. All the extended

sources in the 68 source sample have values of B which are compatible with a lower limit of ~ 1. (i.e. there is no evidence that any extended sources are in regions of galaxy density significantly less than average.) If we then replace all sources for which B is negative with the value B = 1, this should make a reasonable lower limit to the 'true' value of B for these sources. Performing this operation, we find for the mean values

$\alpha>0.5$, $P_{2.7} < 1.2\times10^{24}$ WHz $^{-1}$sr^{-1} mean = 2.31+/-0.30 σ_{pop} = 2.59

$\alpha>0.5$, $P_{2.7} > 1.2\times10^{24}$ WHz^{-1} sr^{-1} mean = 1.44+/-0.43 σ_{pop} = 1.41

These values are in much better agreement with those for the 68 source sample. In fact, if we assumed that for FRI sources, the typical lower value of B was slightly higher (as is reasonable from the 68 source results) even better agreement would result. Thus it seems likely that the values of B for the estimated redshift sample are consistent with those for the true-z sample, which serves to reinforce the trends observed in that sample.

4.8 : Summary

This chapter has extended the work of LS to include many more radio sources, and has considered in detail the sources of error in the measurement of clustering strength.

The results of the investigation have confirmed the major result of LS, that extended radio sources are on average in regions of enhanced galaxy density, and that FRI sources are in general in richer environments than the FRII sources. It has also produced the

new result that compact sources do not appear to be in significantly enhanced regions of galaxy density. From this analysis however, the distinct dichotomy between FRIs and FRIIs, inferred by LS, does not now seem to be as clear-cut. Nor do the class of FRII classical doubles, from their values of Bgg* alone, appear exceptional. These differences have some important consequences in the interpretation of the results. A discussion of this will be deferred at present however, until the results of the next chapter have been presented.

Chapter 5 : RADIO SOURCES AND CLUSTERING (2)

5.1 : Introduction

One of the initial aims of this project was to extend the work of LS to larger and deeper radio samples. A key requirement is thus deep plate material, and the availablilty of the SERC "J" and "Equatorial J" surveys, which together cover the whole of the southern sky, was a prime motivation for the instigation of the study. Unfortunately, it became clear during the course of the project that not all the desired plate material would be available in time for reduction. However, sufficient data were available to make useful progress in a number of areas. The aim of the work described in this chapter was two-fold; to obtain results for as many sources as possible for which optical and radio data were available, but which were not covered by the Lick counts; and to check the validity of the Lick count results where possible using superior galaxy samples.

In Section 5.2, the basic plate material used here is described, and in Section 5.3. the derivation of the galaxy samples is discussed. Section 5.4 describes the result of a 'Lick-type' analysis of the data, and a comparison of the results from the two different galaxy samples is presented in Section 5.5. Finally, in Section 5.6, the implications of the results of both this and the previous chapter are considered.

5.2 : The Schmidt Data

The combination of U.K. Schmidt plates and the COSMOS measuring machine is a powerful tool for pursuing statistical investigations. It has been used successfully not only for stellar work, but also for the production of faint number-magnitude counts (e.g. Shanks et al. 1984) and the correlation-analyses of deep galaxy samples (e.g. Hewett, 1983). The work described in this chapter is in principle similar to such projects, although operationally there are some important differences. The basic reduction process in all cases is similar; COSMOS produces a list of (x,y) co-ordinates for all "images" on the plate, together with various size, shape and magnitude parameters. These parameters are then used to select from the total sample of objects a subset consisting of all galaxies down to some fixed magnitude limit, upon which the subsequent analysis may be performed. It should be remembered that the fundamental limitations of such two dimensional samples described in Chapter Four - especially that of having to work "in projection" - are still present. The major advantages of using galaxy samples derived using COSMOS (apart from their depth and speed of definition) are the objective manner in which such samples may be derived, and the way in which any factors affecting the sample (e.g. stellar contamination) may be well determined.

The ideal plate material for an investigation using COSMOS would be a number of "A grade" plates for each field, possibly in more than one colour. (The UKST unit grade plates according to image quality and plate uniformity; "A grade" plates are those with no serious defects. Plates may be classified as "B grade" if they are of generally poorer quality, or if they suffer from a single major defect, such as large image size. The effects of plate quality for this investigation will be described below.) The southern sky,

however, consists of 600 Schmidt fields, so that the radio sources considered here are essentially distributed with only one source per field; it would thus be impractical to hope to obtain new plate material for each source. Accordingly, it was decided to work in the J passband (in which the greatest number of plates were already available) and to attempt to use existing plate material for as many sources as possible. A sub-set of the WP sample was initially considered, defined by the limits of the Schmidt telescope and AAT to the north, and the VLA to the south. This sample is therefore described by the criterion $+10^{o} > \delta > -45^{o}$, with the limit $0.015 < z < 0.25$ required in order for clustering to be detectable. The acquisition of plates was concentrated on this region, with preference being given to those sources not covered by the Lick survey. A number of the more southerly sources were also considered, but only one (0428-53) was finally reduced. This source will be included in the discussion of the sample. The complete sample, and the plate material used is given in Table 5.1. "A grade" original plates taken for survey purposes are not available for machine measurement; and the large number of "B grade" plates used here is a reflection of the policy of necessity adopted in selecting the plate material.

5.3 : Reduction of the COSMOS Data

All the plate were scanned using the COSMOS measuring machine, in its Image Analysis (IAM) Mode (see Stobie, 1982). The COSMOS measuring machine is basically a computer-controlled high-speed scanning microdensitometer. A flying-spot is produced by a cathode ray tube and focussed on the emulsion; the amount of transmitted light is measured and the resultant transmission value digitised to 8 bits (256 'T' values). The spot and pixel increment size are both

Table 5.1: The Sample

IAU	other	M	z	plate	grade (*)
0034-01	3C15	15.3	0.073	J8212C	BIE3
0035-02	3C17	18.0	0.220	J8212C	BIE3
0038+09	3C18	18.5	0.188	no plate	
0043-42		16.0	0.053	J2712C	A1
0055-01	3C29	14.1	0.045	J3725	BIE
0123-01	3C40	12.3	0.018	(Lick only)	
0131-36		13.0	0.030	J3596C	A1
0213-13	3C62	18.0	0.200*	J8039	BI3 (not reduced)
0255+05	3C75	13.6	0.024	(Lick only)	
0305+03	3C78	12.8	0.029	(Lick only)	
0325+02	3C88	14.0	0.030	J6397	A
0349-27	OE-283	15.8	0.066	J2576	BI3
0356+10	3C98	14.4	0.031	(Lick only)	
0404+03	3C105	18.5	0.089	(Lick only)	
0428-53		13.2	0.039	J1893	BI3
0430+05	3C120	14.1	0.033	(Lick only)	
0442-28	OF-271	17.4	0.151*	J4737C	A2 (not reduced)
0453-20	OF-289	13.0	0.035	J5614	BU3
0518-45	Pic A	16.0	0.035	J2715	BE1
0521-36		16.8	0.062	J5542	BE2
0625-35	OH-342	14.0	0.055	J3885C	A3 (low gal lat)
0806-10	3C195	17.8	0.182*	J9002	BI4 (low gal lat)
0915-11	Hyd A	14.8	0.065	J3817	BI
0945+07	3C227	16.3	0.086	(Lick only)	
1251-12	3C278	13.5	0.015	(Lick only)	
1514+07	3C317	13.5	0.035	(Lick only)	
1559+02	3C327	15.9	0.104	(Lick only)	
1648+05	Her A	16.9	0.154	J9223	A (not reduced)
1717-00	3C353	15.4	0.030	J5194	BX2 (low gal lat)
1949+02	3C403	15.4	0.059	J8648	BI4 (low gal lat)
2058-28	OW-297.8	14.6	0.038	J640C	A1
2104-25	OX-208	15.8	0.037	J754	BISP2
2211-17	3C444	18.0	0.153	J1746	A
2221-02	3C445	15.8	0.056	(Lick only)	
2314+03	3C459	17.6	0.220	J9440	BI (not reduced)
2331-41		18.0	0.200*	J2413C	A1 (not reduced)

(*) A, B = overall grade. I, E etc. indicate specific defects (e.g. I = large images, E = elliptical images). A numeric qualifier indicates a survey plate. For more details, see U.K.S.T. Handbook.

variable over a range of 8,16 or 32 microns. In the IAM mode the plate is raster scanned, with the cathode ray producing a scan parallel to the X direction 128 pixels wide, while the plate carriage drifts in the Y direction. Prior to measurement, a transmission to intensity conversion is set up from measurements of the plate step wedge. During the course of measurement, a grid of 'sky background' transmission values is obtained from the median value of histograms from successive grids of 128 x 128 pixels. These sky values are then median filtered in the Y direction. The transmission value corresponding to a user specified percentage cut above sky is then calculated, and only the pixels with transmission values less than this are retained. In the subsequent off-line Image Analysis, adjacent pixels are connected to form images. A number of parameters, basically calculated from the unweighted and intensity-weighted moments of the pixel distribution are then calculated. These image parameters are the basis for subsequent analysis.

All plates used here were scanned using a 32 micron spot, and 16 micron pixel size. A threshold cut of typically 7-10% above sky was used, although this was increased somewhat (to ~ 20%) at lower galactic latitudes, to reduce spurious merging. The 'whole plate' (usually 24 x 24 cm) was scanned, with the area limits chosen to include the radio source and as much surrounding area as possible. The standard COSMOS IAM 'quality-control' package was inspected for each measure; this provides a background plot, image dot plots and a number of two-parameter plots, and allows for the detection of contaminated areas (e.g. bright stars) and 'field effects'. Subsequent analysis was carried out using independent software.

A major factor in the reduction of the COSMOS data is the requirement to distinguish between stars and galaxies. Initially it

was envisaged that star/galaxy separation, as decribed for example by Hewett (1983), would be applied to the whole of the measured area. This method uses the COSMOS IAM parameters, which provide basic information about the image intensity profiles, to descriminate between the different types of object on the plate. Since "single stars" form a well defined reference point for image structure, in practice the procedure generally consists of separating "single stars" from "other objects". An ordering parameter is used to rank images by size or magnitude; different image types are then separated on the basis of a second image parameter. The parameters used here are defined in Table 5.2; they consist of image area, central surface brightness (CSB), and occupation index (OI). Other classification parameters may be formed from the IAM output, however the positions of objects in different two-parameter plots are not independent (since they are formed from the same image profile), and the parameters given in Table 5.2 are generally the most efficient for a given magnitude interval.

The derivation of a galaxy sample using machine based star/galaxy separation is thus as follows. For a given magnitude, all stars will have identical intensity profiles, apart from minor telescopic effects. The image parameters derived thus lie in a narrow range - with a small dispersion due to plate and measurement noise. Other images (galaxies, blended stars, etc.) have different intensity profiles, and hence image parameters, and will therefore fall away from the "stellar locus" of images in a two-parameter plot. The "galaxy" sample is thus considered to consist of all images lying further away than a given threshold from this locus. The threshold may be defined interactively, using eye-classifications of a sub-set of the objects to define the boundary. Alternatively some form of purely automatic method may be used, such as fitting a gaussian to the distribution of the second

Table 5.2: COSMOS Image Parameters Used for Star/Galaxy Separation.

parameter	definition
cosmag	$-2.5 \log \Sigma(Ii - Isky)/(Isky/pixarea)$ calculated from IAM parameter 9 ($-250\log \Sigma(Ii-Isky)$ and 10 (Isky at centroid)
log(area)	log (area in pixels) calculated from IAM parameter 7 (area in pixels)
Central Surface Brightness (CSB)	log((Imax - Isky)/Isky) calculated from IAM parameter 8 (min. transmission) converted to intensity via T-I look-up table and 10 (Isky at centroid)
Occupation Index	(delta(X)*delta(Y))/area calculated from IAM parameters 3,4,5 and 6 (minimum and maximum X and Y values) and 7 (area in pixels)

Ii	=	Intensity of i'th pixel.
Imax	=	Intensity of brightest pixel in image.
Isky	=	Sky background pixel intensity.
Pixarea	=	Area of one pixel in square arcsec.
Area	=	Area of image above threshold (units = pixels).
delta(X), delta(Y)	=	Maximum extent of image above threshold in X and Y directions (units = 0.1microns).

parameter across the stellar locus for successive increments of magnitude. In this case images more than a fixed number of standard deviations from the mean are included.

In applying these machine based classification methods, a number of points should be noted.

Firstly, none of the IAM parameters provides a good separation at both bright and faint magnitudes. For example, occupation index is only useful at bright magnitudes, where stars have appreciable diffraction spikes. In the intermediate range, the CSB parameter is of little use, due to saturation of the images; parameters utilising information from the low surface brightness regions (e.g. log(area)) are more effective. Conversely, at the fainter magnitudes, the signal to noise of the lsb parameters decreases rapidly. Objects are more reliably classified here using the central surface brightness parameter, due to the greater signal to noise of the central image pixels. The combination of classifications from a number of different parameters is not generally useful, due to the non-poisson nature of many noise sources. The approach used here will be to use only the parameters in Table 5.2, choosing the one most appropriate at a given magnitude range for each plate.

Secondly, the IAM output is not sufficiently detailed to remove blended images (double stars, etc) from the "galaxy" sample, without removing a significant fraction (>10%) of galaxies with asymmetric profiles. This is an important point, as typically 5-10% of all images brighter than m ~ 21 are merged by COSMOS, even at high galactic latitudes. This has a significant effect on the construction of a galaxy sample; a related point is the effect of the ratio of stellar to galaxy number density as a function of magnitude. At brighter magnitudes, the separation between "single

stars" and galaxies may be good in terms of the percentage of stars successfully placed in the stellar sample. However, when the number density of stars is high, compared to that of galaxies, a small loss of stars from the stellar sample (either due to noise or merging) can lead to a large contamination of the galaxy sample.

Thirdly, many COSMOS measures have shown serious "field-effects", evidenced as a variation in the position of the stellar locus with the local sky intensity. Detailed investigations by Hewett (1983) have shown that the major cause of this effect may be explained by a non-linearity in the COSMOS density approximation at high density. A real sky background variation thus results in a change in the magnitude of the images. The non-linearity modifies the profiles of bright saturated images most severely; low surface brightness components of images are not affected. Thus this effect is most important for stars of intermediate brightness, and causes major difficulties in performing star/galaxy separation based on the position of the stellar locus.

Finally, at the faintest magnitudes (below ~ 1-2 cosmos magnitudes above sky) the stars begin to "spread-out" in parameter space, and galaxies merge into the stellar locus. All images tend to have similar profiles, and any separation made using the IAM parameters can be correct only in a statistical sense. Classification by eye however, using the same plate material, is no more successful in this region.

In summary, while the above techniques are reliable (in the absence of field-effects), they cannot be considered 100% efficient. Blended images, plate flaws and so on will tend to lie in the galaxy sample, and in general cannot be removed using machine methods. When the stellar number density is high, a threshold set sufficiently low

to include all galaxies will include a substantial fraction (in terms of galaxy number density) of stars. It is therefore important that the true content of the galaxy and stellar samples derived using machine based methods are thoroughly checked by visual examination of a number of images.

In this investigation, such difficulties were compounded for a number of reasons.

a) the presence of field effects on some measures, (often since objects were fairly near the corners of plates, in regions of rapidly varying sky) meant that a global star/galaxy separation would be made more difficult using purely measure-based methods.

b) the availability of only one plate for each source meant that spurious images could not be rejected by plate-matching.

c) the poorer quality plates used for many of the fields meant that any separation relying on the measured COSMOS parameters was less reliable than it would have been had survey quality material been available. Experince suggests (UKSTU handbook) that a change of seeing from 2 to 4 arcseconds (sufficient to result in a B grade plate on image considerations alone) changes the plate limiting magnitude by ~ 0.8 magnitudes, and raises the limiting magnitude for star-galaxy separation by ~ 1.0 magnitudes. Since in the majority of cases, survey quality film copies were available, eye-classification could be reliably made below the limit which would have been set had only the measured plate been available.

d) the comparatively low galactic latitude of many of the sources meant that the problems of stellar contamination was much greater than in corresponding sample defined at higher latitudes.

e) finally, for many of the low redshift sources, comparatively shallow samples were required, which again meant that stellar contamination would be more serious.

As these requirements for a high degree of control over stellar contamination, together with the desire to achieve a high success rate for the galaxy classifications would have required a considerable calibration effort for any purely machine-based technique, it was decided to expend this effort in a more profitable manner, by classifying completely a number of "control areas" for comparison with the radio source.

Software was written to read images from tape to disk, extract various subsets of these images, and plot them either in the form of finding charts or two-parameter plots. A circular region around the source, with a radius corresponding to 1Mpc was then extracted, and a similar process performed for each of a number ($\sim$ 5-9) of comparison areas, of identical size. These were placed at random on the measured area, with no reference to the plate, but with the provisos that a) they were more than $\sim 2^{\circ}$ away from the radio position; b) that they did not lie on any bright star or other contaminated region (as indicated by the quality-control data); and c) for those plates which were suspected of showing possible field-effects, regions with similar sky intensity were chosen where possible.

Each of these areas was then analysed in an identical manner. A preliminary (conservative) star/galaxy separation was performed, by defining a separation line on the appropriate two-parameter plot (cosmag versus c.s.b, log(a) or occupation index) for each magnitude range. All the images surviving this selection were then checked visually, usually on the "A grade" film copy of the field. All contaminating images were rejected, and any galaxies erroneously merged by COSMOS were assigned a magnitude by comparison with similar galaxies in the field. This method had the advantage of combining both machine-based and visual techniques, with the

classification of large numbers of "definite" stars being avoided, but with the ability to reject spurious images, which could not have been detected on the basis of the machine measurement alone, being retained.

It should be noted that for the majority of the sources, the magnitude limit was such that this separation was unambiguous; no galaxies present on the plate were rejected by the initial cut, and the requirement for supplementary classification was to remove the large number (in terms of the galaxy density) of merged stars, etc. For the more distant sources, no attempt was made to perform any separation within ~ two magnitudes of the plate limit; comparisons with other experienced users showed excellent consistency to this limit.

These classified areas formed the basis for further analysis. The detailed distribution of galaxies (with no error in classification) was available for the vicinity of each radio galaxy; while the background number density was available from the control regions. As no magnitude calibration was available for the fields, all work was performed initially in terms of cosmag. The results from galaxy samples defined in such a manner were then characterised for the later stages of analysis by their number density, rather than magnitude limit.

5.4 : Lick-Type Analysis

In this section, we will consider the results of a "Lick-type" analysis of the COSMOS data, as peformed for the sample of galaxies in Chapter Four. This provides a similar B parameter for the sources, so that they may be considered in the other analyses, for

which the majority of sources only have Lick based values.

Using the program described in Chapter Four, it is possible to calculate the H(z) function for a variety of lower magnitude (=number density) limits. The variation of H(z) as a function of cosmag, for three different redshifts is shown in Fig. 5.1. The corresponding background number-density is also shown. It is possible to calculate from these quantities the expected number of galaxies within 1Mpc of the radio galaxy, given an assumed value of Bgg*. The values for a range of limiting magnitude are given in Table 5.3. Naively, we might expect the 'best' magnitude limit to be that which minimises the H(z) function. In the presence of random variations in the background however, we must also take into account the total number of galaxies within the area. For example, taking as a simple measure of this effect a poisson variation in the expected background count, we can see that the deeper value for the $z = 0.075$ case would give a more significant value, despite the fact that H(z) is larger. The choice of limiting magnitude is further complicated by the fact that at low redshifts ($z \lesssim 0.03$) the minimum H(z) occurs at such a high value that the background would be difficult to measure. Conversely at higher redshifts ($Z \gtrsim 0.2$), limitations due to difficulties in star/galaxy separation prevent the minimum H(z) from being reached. In practice, a sufficiently deep value for the lower limit was used, in consideration of the above points, so that a higher limit could be subsequently imposed if desired. This value was chosen without explicit reference to the distribution in magnitude of the galaxies in the radio source field, so that the possibility of "biassing" the result to fluctuations in the cluster luminosity function was avoided.

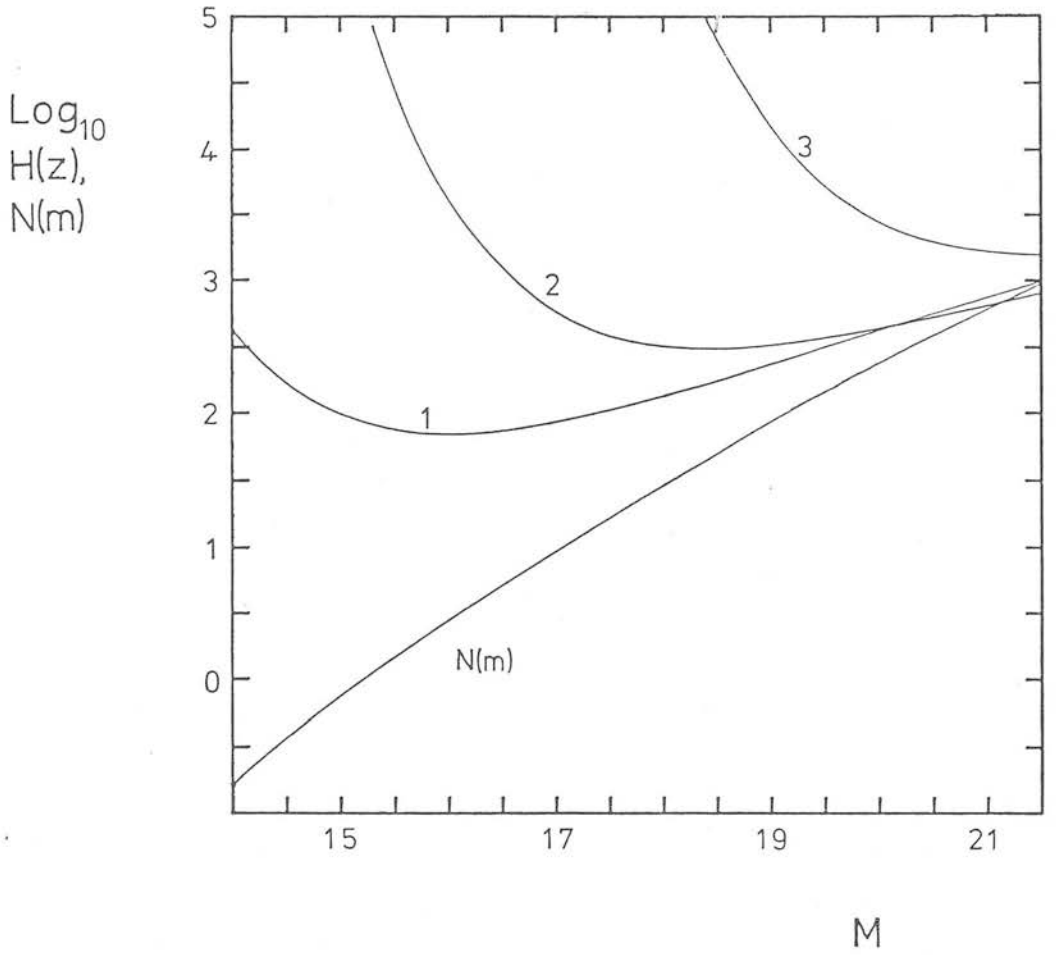

Figure 5.1. The variation of H(z) with limiting cosmos magnitude for z = 0.03 (1), 0.075 (2) and 0.20 (3). Also shown is the integral number N(m) of galaxies brighter than the limiting magnitude.

Table 5.3: Expected Number of Galaxies Within 1Mpc for a Variety of Source Redshifts. Bgg* = 80.

	cosmag	background (per sq.dg.)	H(z)	Agg*	background number	excess due to cluster
z = 0.03	-6.5	3	70	1.143	1	4.5
	-4.5	30	140	0.571	10	23
	-3.0	150	320	0.250	50	50
z = 0.075	-5.5	10	580	0.138	0.6	0.6
	-4.0	50	310	0.258	3.3	6
	-2.5	250	440	0.182	17	22
z = 0.20	-3.0	150	5300	0.015	2	0.4
	-2.0	400	2000	0.040	5	2.8
	-1.0	900	1500	0.053	12	9

5.4.a Calculation of A

The value of A, and its error was obtained from the reduced areas in an identical manner to that used for the Lick analysis. The mean count of the comparison areas was used to define the expected number of background sources within the corresponding area around the radio source, and the excess calculated by subtracting this from the observed count. The error in this quantity was taken from the r.m.s. of the comparison areas. The mean value in these areas was also used to calculate the value of Ng, and the value of A was then calculated using Eqn. 4.9 above.

5.4.b Conversion to B

Again, the conversion from A to B for the Schmidt plate data was performed in a similar manner to that for the Lick count data. The conversion program was run with appropriate values for the thresholding parameters (sky background, percentage-cut and seeing) and galactic extinction for each plate. The value of H(z) appropriate to the number density of the galaxy sample was then calculated. The value of Bgg* thus obtained may be converted to a ratio using the same value of Bgg (40) as used for the Lick counts.

5.4.c Results

It soon became apparent that sources at galactic latitudes much less than $|b| \sim 25^{o}$ would be difficult if not impossible to reduce using these methods, simply due to the extremely high number density of stellar images. This meant that 0625-35 1717-00 had to be excluded from the analysis. Also, while 1648+05, 1949+02 and 2314+03 had plate material available, this came too late for the sources to be included in the analysis. Excluding also the estimated-redshift

objects, this leaves a sample of 15 sources, for which values of B, as derived from Schmidt-plates, were available.

The value of B for these sources, with their errors, are given in Table 5.4. For the majority of sources, the analysis was repeated for galaxy samples of varying depth. Also given in Table 5.4 are the observed and expected numbers of galaxies within 1Mpc of the source, and the corresponding background number density. Since the galaxy number-density increases rapidly with magnitude, these samples are approximately independent; the agreement between the B values obtained is a reassuring check on the validity of the method. For the remaining discussion, the mean value of each source will be used in any calculations.

5.4.d Investigations of More Detailed Fitting

With the much greater quantity of data available for each source from the COSMOS measures as compared with the Lick counts (in particular the positions of each galaxy), we might consider the possibility of more detailed fitting methods to derive parameters to quantify the clustering. To consider this point, data for two sources are presented in more detail. These sources (2058-28 and 2104-25) are both FRI galaxies, and have values of B typical for objects in the richer cluster environments. A second factor in the choice of these sources was that they both lie at a comparatively low redshift, increasing the number of galaxies observable above the plate limit, and simplifying the problems of image classification. They are thus the 'best' examples of sources for which more detailed analysis might be appropriate.

The fields of these galaxies are shown in Fig. 5.2 and Fig. 5.3. Figs. 5.2 and 5.3(a) are direct photographs (taken from the film

Table 5.4: Results Obtained Using U.K. Schmidt Plates

IAU namd	Z	Area arcmin	Area sq. deg.	Cosmag	Ng	obs no.	exp no.	A	H(z)	Bgg*	<Bgg*>	<B>	Lick(1) Bgg*	Lick(2) Bgg*
0034-01	0.073	8.9	0.0699	-2.0	295	24	20.6	0.017	475	8±30	21±15	0.53±0.38	57±24	64±23
				-2.5	150	17	10.6	0.072	365	26±22				
				-3.0	90	11	6.4	0.080	315	25±25				
0035-02	0.220	3.4	0.0098	-2.0	295	5	2.9	0.025	3305	85±95	85±95	2.13±2.38		
0043-42	0.053	11.2	0.0546	-2.5	330	25	18.0	0.056	485	27±28	17±20	0.43±0.50		
				-3.5	92	7	5.0	0.034	265	9±12				
0055-01	0.045	13.4	0.1573	-4.0	123	27	19.3	0.067	285	19±26	19±18	0.48±0.45	102±22	45±25
				-5.0	36	10	5.7	0.114	165	19±26				
0131-36	0.030	20.1	0.3538	-3.0	89	58	31.6	0.214	250	54±24	47±11	1.18±0.28		
				-4.0	23	24	8.1	0.487	120	59±19				
				-5.0	10	10	3.7	0.385	85	33±18				
0325+02	0.030	20.1	0.3538	-3.5	19	17	6.8	0.364	115	42±15	51±12	1.28±0.30	22±25	44±24
				-4.5	5	10	1.9	0.981	70	68±20				
0349-27	0.066	10.1	0.0885	-3.0	263	33	23.3	0.059	435	26±24	33±15	0.83±0.38		
				-4.0	45	9	4.0	0.156	245	38±19				

Table 5.4: Continued

IAU name	Z	Area arcmin	Area sq. deg.	Cosmag	Ng	obs no.	exp no.	A	H(z)	Bgg*	<Bgg*>	<B>	Lick(1) Bgg*	Lick(2) Bgg*
0428-53	0.039	15.7	0.2140	-3.0	175	152	37.5	0.662	335	600±60	440±35	11.00±0.88		
				-4.0	46	91	9.8	1.800	530	350±45				
0453-20	0.035	16.8	0.2457	-3.5	185	86	45.5	0.200	360	70±30	58±13	1.45±0.33	164±42	50±25
				-4.5	80	45	20.2	0.272	225	60±20				
				-5.5	30	20	7.5	0.353	140	50±20				
0518-45	0.035	16.8	0.2457	-3.5	80	44	19.6	0.275	225	62± 8	49± 6	1.23±0.15		
				-4.5	23	13	5.6	0.281	130	36± 8				
				-5.0	13	11	3.2	0.490	100	49±18				
0521-36	0.062	10.1	0.0885	-2.0	510	60	45.3	0.047	605	28±15	38± 9	0.95±0.23		
				-3.0	85	16	7.5	0.156	275	43±11				
0915-11	0.065	10.1	0.0885	-3.0	110	42	9.8	0.499	310	155±30	160±30	4.00±0.75	82±28	65±20
				-4.0	28	16	2.5	0.785	230	180±70				
2058-28	0.038	15.7	0.2140	-3.0	80	59	17.0	0.524	225	118±26	109±17	2.73±0.43		
				-4.0	28	27	6.0	0.730	140	102±22				
2104-25	0.037	16.2	0.2296	-3.0	78	74	17.8	0.698	225	155±35	175±25	4.38±0.63		
				-4.0	27	43	6.1	1.378	135	190±32				
2211-17	0.153	4.5	0.0175	-2.5	492	18	8.6	0.081	970	80±40	105±35	2.63±0.88		
				-3.0	183	11	3.2	0.177	1120	200±80				

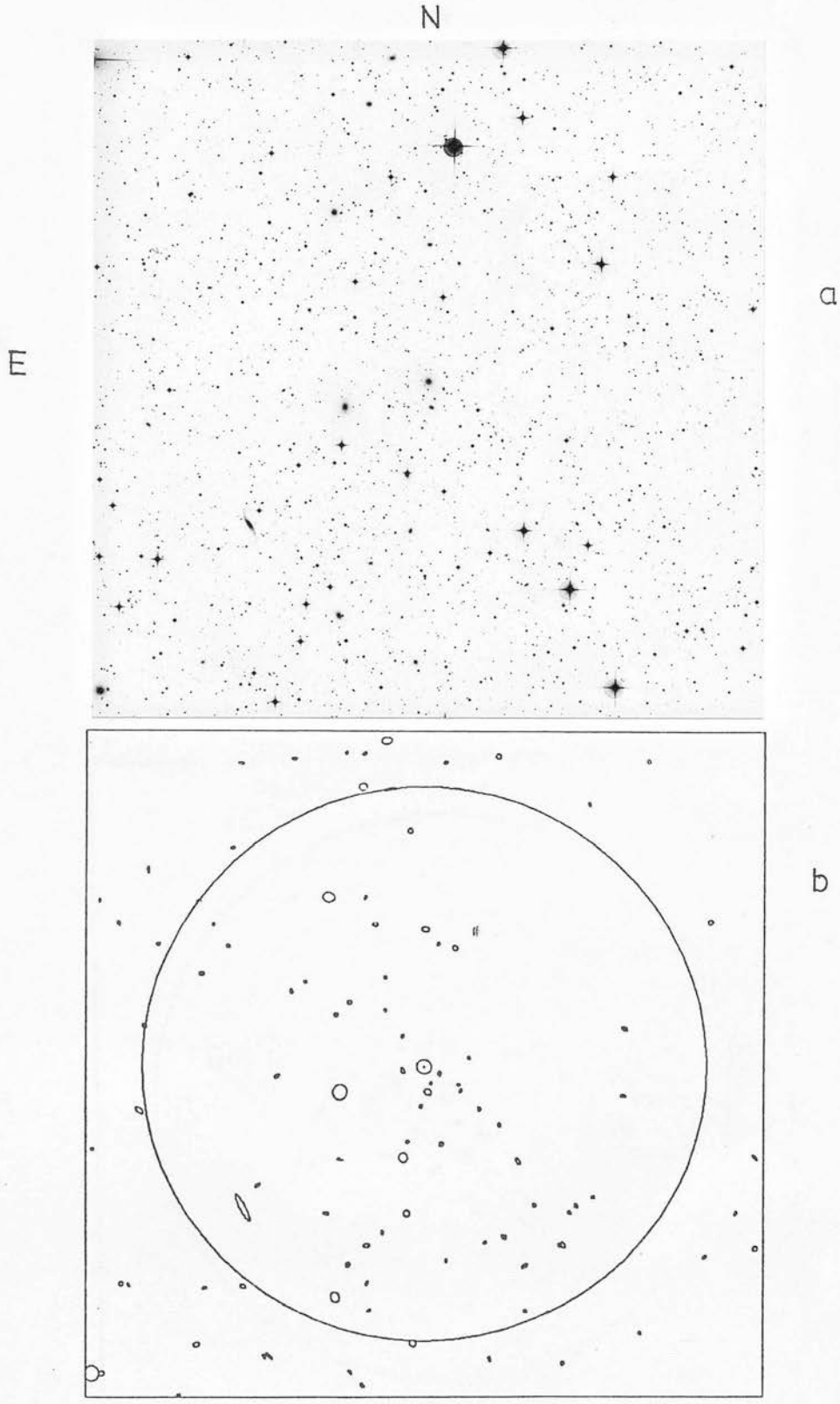

Figure 5.2. The field of 2058-28. a) A region of half-side 1.2Mpc from the U.K. Schmidt film copy at 3x magnification (22 arcsec per mm.), b) An ellipse plot of the same area, with only galaxies greater than three cosmos magnitudes above sky included.

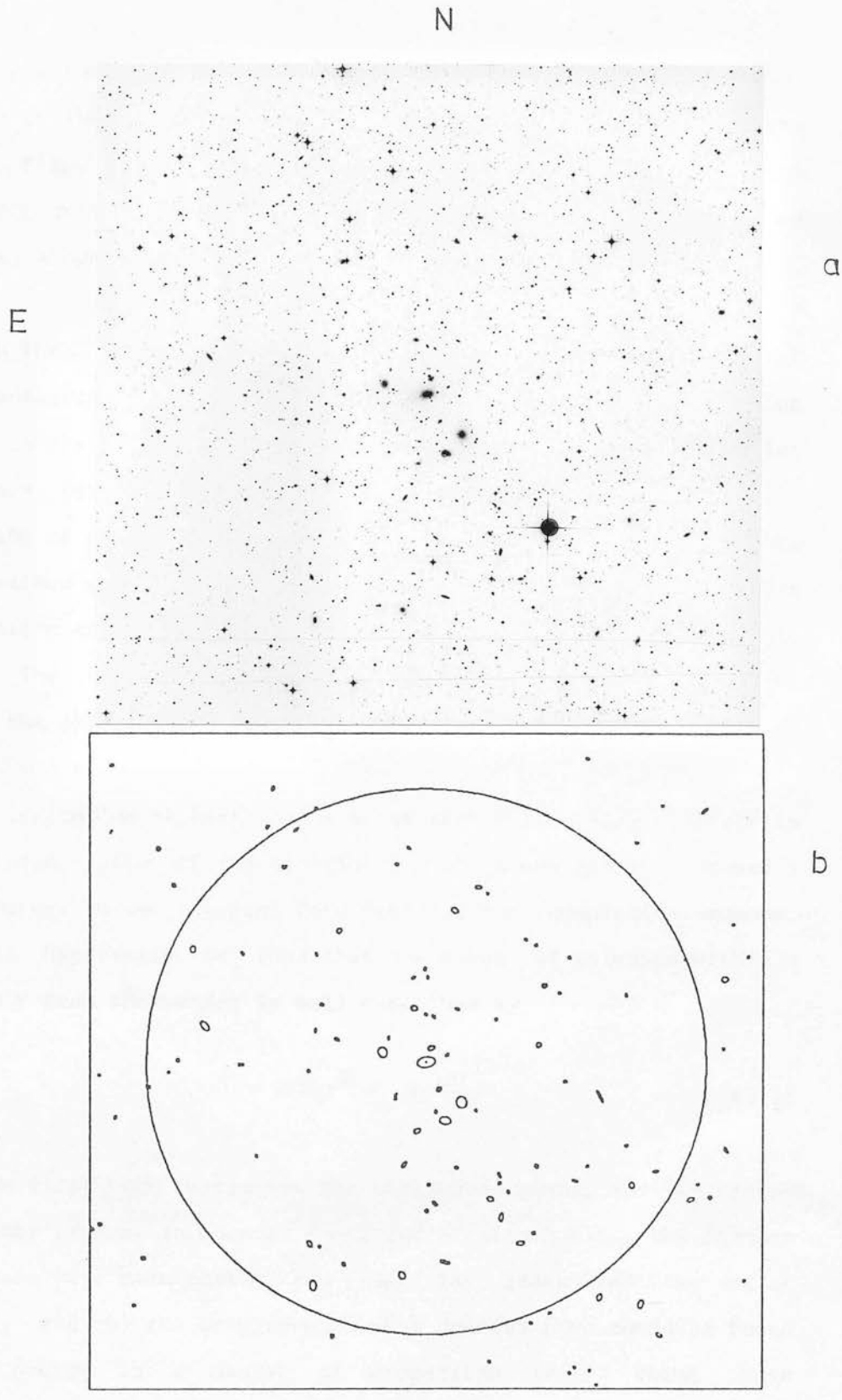

Figure 5.3. As Figure 5.2 for 2104-25.

copies used for image classification) of regions of half-side 1.2Mpc centred on the source. The results of the image classifications are shown in Figs. 5.2 and 5.3(b). These are ellipse plots of the same area, with only galaxies with a cosmag greater than three magnitudes above sky shown.

With these individual galaxy positions, it is possible to test the hypothesised distributions of objects within the counting radius. In what follows, we will not attempt to define an angular dependence for the galaxy distribution, i.e. we will retain the assumption of circular symmetry. Rather than perform ringcounts, to make maximum use of each data point we will consider the cumulative distribution of the galaxies with increasing distance from the radio source. The two-sided Kolmogorov-Smirnov test may then be used to compare the observed and predicted distributions.

The assumption of Section 5.4.a. is that a power-law fall-off is a good description of the distribution of excess galaxies around a radio source. In the integral form suitable for cumulative counts, our null hypothesis is thus that the number of galaxies within a distance r from the source is well described by

$$n(<r) = 2\pi Ngr^2 + Ng\,\frac{Ar^{(2-\delta)}}{2-\delta} \qquad (5.1)$$

where the first term represents the background count, and the second the cluster excess. In Chapter Four, and Section 5.4.a., the further assumptions were made that a) the power law index had the value $\delta = 0.77$, and b) the background number density (Ng) could be found from the counts in a number of comparison areas. Using these assumptions the value of A is fixed by the total number of galaxies observed in the counting region. The relevant values of these parameters for 2058-28 and 2104-25, for this magnitude limit, were

presented in Table 5.4. They are reproduced here in Table 5.5, labelled hypothesis A. The predicted distributions, using these values, are shown in Fig. 5.4 and Fig. 5.5, along with the observed counts for each source.

The goodness of fit of the hypothesed distribution to the data may be measured by the value of the Kolmogorov-Smirnov statistic D. This is defined by

$$D = \max(|N_{obs} - N_{pred}|) \qquad (5.2)$$

i.e. the maximum vertical difference between the observed and predicted distributions. The significance of a given value of D, for N points, is tabulated by Conover (1971). For 2058-28, the maximum difference between the two curves occurs at $\theta = 0.221^{o}$ (0.83Mpc), with a normalised value of D = 0.138. This is less than the $1-\alpha$ quantile for $\alpha = 0.2$ (for 56 points), and hence we conclude that the difference between the two distributions is not significant. For 2104-25 the value of the statistic is D = 0.133. For 74 objects, this lies between then $1-\alpha$ quantiles for $\alpha = 0.1$ and 0.2. While this is a more significant deviation than that found for 2058-28, it is still not sufficient to disprove the null hypothesis.

Although our null hypothesis (that the cluster excess may be described by a $\delta = 0.77$ power-law) is not disproven, we might wish to see whether a different value of δ (e.g. > 0.77) provides a better representation to the data. In theory it should be possible to obtain the 'best' values for A, δ and Ng simultaneously, by finding those values which minimise the KS statistic. We might hope in this way to find the 'true' background number of galaxies in the area, as well as the form of the cluster distribution. In practice for these sources, allowing δ, A and Ng to vary in a truely

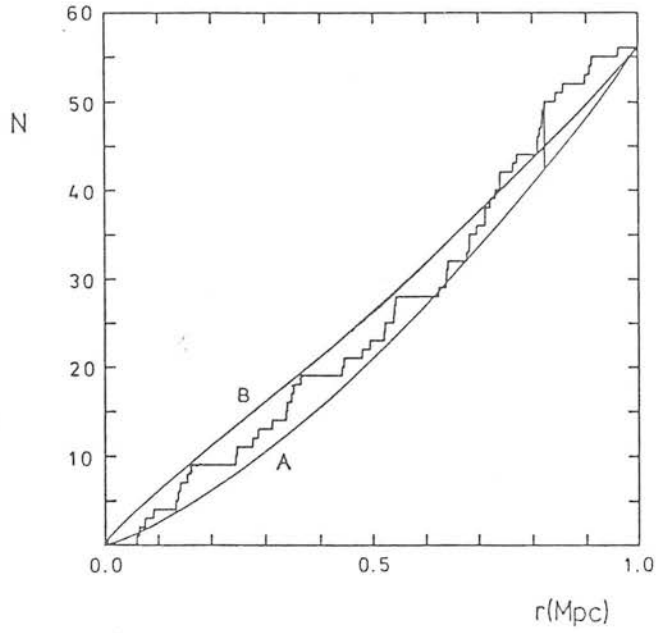

Figure 5.4 The observed and predicted cumulative number of galaxies within a distance corresponding to r Mpc at the redshift of the source for 2058-28. The parameters for the predicted curves are given in Table 5.5.

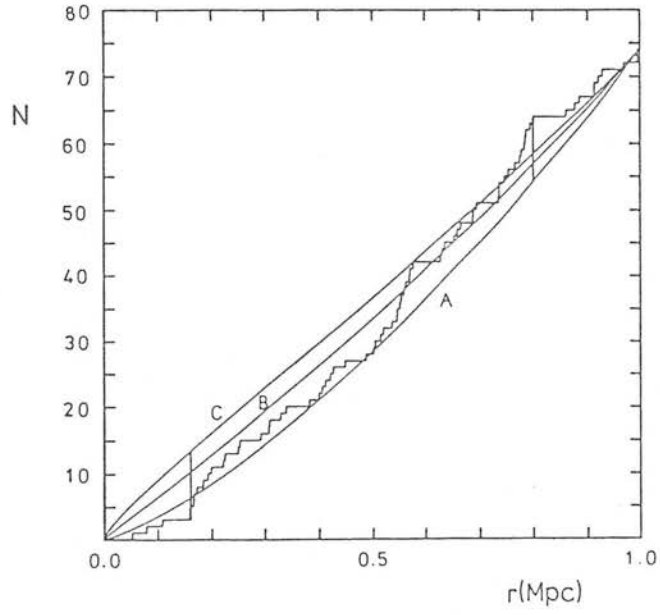

Figure 5.5 As Figure 5.4 for 2104-25.

Table 5.5: Best-Fit Parameters to Cumulative Distributions for 2058-28 and 2104-25

		Ng	δ	A	D	θ (Mpc)
2058-28:	A) δ, Ng fixed, A from integral number	74	0.77	0.524	0.138	0.83
	B) Ng fixed, best-fit values of A and δ	74	1.17	0.207	0.093	0.83
2104-25:	A) δ, Ng fixed, A from integral number	77	0.77	0.698	0.133	0.80
	B) Ng fixed, best-fit values of A and δ	77	1.05	0.370	0.097	0.16
	C) δ, Ng fixed, A from integral number	77	1.20	0.258	0.139	0.16

arbitrary manner gives a spurious result, for the following reason. At large radii, the observed number of galaxies is dominated by the background. Thus the shape of the curve at reasonably large values of r is fixed, and only the normalisation may be changed, via Ng. The excess numbers due to the cluster may dominate at low r, and hence the form of the curve may be altered via A and δ in this region. However, for both these sources, the region of worst 'mis-fit' is at the larger values of r. The fitting routine may only alter the form of the curve to improve the fit here by making A so large, and Ng so small, that the cluster contribution still dominates, even at this distance. This results in a good fit, but a spuriously low value for Ng.

We may still investigate the 'best-fit' values obtained by varying A and δ simultaneously, with Ng fixed (hypothesis B). (The results obtained by constraining Ng within a reasonable range around the mean value are essentially identical.) These values, together with the value of the KS statistic are also given in Table 5.5, and shown in Fig 5.4 and 5.5. The values of δ obtained in this manner ($\sim$ 1.1) do appear slightly higher: however the goodness of fit at low r is not significantly better than for the δ = 0.77 case. A fit with δ = 1.2 - case C - to 2104-25 (c.f. 2058-28) gives a comparable fit to that for δ = 0.77, although the mis-fit here is worst at a low value of r.

In summary, we can conclude that for these sources at least, using this form to parameterise the distribution of excess galaxies in the region, with δ fixed at 0.77, does appear to be a reasonably correct procedure. The analysis has shown that the presence of a significant contribution from the background would be a potential cause of severe difficulty, if attempts were made to fit both δ and A simultaneously to less rich systems. While it would be possible to

consider different forms for the galaxy excess (e.g. isothermal sphere models), again the same difficulties would arise. In addition, the limited number of sources for which such information would be available would in any case make it less useful. For the remainder of this work therefore, we will continue to parameterise the degree of clustering about the radio sources simply by the value of A, the amplitude of the correlation function fitted assuming $\delta = 0.77$.

5.5 : Comparison with the Lick Results

Five sources reduced using the COSMOS data were also accessible to the Lick catalogue. The values obtained by the analysis of Chapter Four are also given in Table 5.4, column 13. At first sight, there appears to be some discrepancy (up to ~ x 5) in the results obtained by the two methods. This is explicable however, in terms of the background normalisation used. For the Lick results, all counts were normalised by the number of galaxies in an annulus 3-5 degrees away from the source. For the COSMOS data this is not possible, due to the limitations of plate area, the maximum distance here is ~ 2.5 degrees. If the source is in a region of generally enhanced galaxy density, this results in a spuriously high normalisation being used, with a resultant value of Bgg* too low. The value of Bgg* obtained using the Lick counts, but reducing them in the same manner as that used for the COSMOS data, are given in Table 5.4, column 14. In this case, the values of Bgg obtained are from a normalisation using as nearly as possible the identical areas used in the COSMOS analysis. It can be seen that these values are in much better agreement. The largest discrepancy now comes from 0915-11, which is at low galactic latitude, and therefore less reliable.

This result does have some implications for the COSMOS derived values, since it suggests that indeed in some cases the background normalisation is not being correctly evaluated. This is a problem which cannot be readily circumvented with the present data. However, it should not be serious for the higher redshift sources, since the metric distance used in these cases should be large enough to avoid any large-scale clustering. While the effect cannot be ruled out in the remainder of the sources, it should be noted that both 0055-01 and 0453-20 are in the vicinty of rich Abell clusters, whose presence was noted during the course of the reduction. No such enhancements were obvious for the other sources, suggesting that the derived values should not be seriously in error.

In the remaining discussion, the COSMOS values will be used for 0034-01, 0325+02 and 0915-11, since these are probably more reliable than the Lick values, while the Lick values will be used for 0055-01 and 0453-20, for which the COSMOS values are obviously in error.

We can now consider a global comparison between the Lick and COSMOS reduced sources in the sample. The Lick values used are for the WP sample sources between $+10^{o} > \delta > -23^{o}$, given in Table 5.1. As discussed, the sources reduced using COSMOS data were designed to complete this sample to $z = 0.25$ and $\delta = -45^{o}$. Also included is 0428-53, which is one of a random subset of more southerly sources for which optical observations (Chapter Six) were made. The values of Bgg* for these sources, together with morphological classifications, are given in Table 5.6, and a plot of Bgg*/Bgg versus z shown in Fig. 5.6. It can be seen that there is no systematic difference between the sources reduced by the different methods. A plot of Bgg*/Bgg versus 2.7GHz luminosity is shown in Fig. 5.7 for the extended sources, and is in good agreement with the same plot for the 68-source sample of Chapter Four (Fig 4.11). Thus

Table 5.6: Bgg* Values for the Sample

IAU name	other name	FR class	M	z	Bgg*	B
0034-01	3C15	I	15.3	0.073	21	15
0035-02	3C17	I	18.0	0.220	85	95
0038+09	3C18	II	18.5	0.188	-	
0043-42		II	16.0	0.053	17	20
0055-01	3C29	I	14.1	0.045	102	22
0123-01	3C40	I	12.3	0.018	101	23
0131-36		II	13.0	0.030	47	11
0213-13	3C62	II	18.0	0.200*	-	
0255+05	3C75	I	13.6	0.024	225	39
0305+03	3C78	I	12.8	0.029	42	45
0325+02	3C88	II	14.0	0.030	51	12
0349-27	OE-283	II	15.8	0.066	33	15
0356+10	3C98	II	14.4	0.031	14	23
0404+03	3C105	II	18.5	0.089	-106	83
0428-53		I*	13.2	0.039	440	35
0430+05	3C120	C	14.1	0.033	-29	38
0442-28	OF-271	II	17.4	0.151*	-	
0453-20	OF-289	I	13.0	0.035	164	42
0518-45	Pic A	II	16.0	0.035	49	6
0521-36		I	16.8	0.062	38	9
0625-35	OH-342	I	14.0	0.055	-	
0806-10	3C195	II	17.8	0.182*	-	
0915-11	Hyd A	I	14.8	0.065	160	30
0945+07	3C227	II	16.3	0.086	14	33
1251-12	3C278	I	13.5	0.015	103	22
1514+07	3C317	I	13.5	0.035	143	37
1559+02	3C327	II	15.9	0.104	-71	55
1648+05	Her A	II	16.9	0.154	-	
1717-00	3C353	II	15.4	0.030	-	
1949+02	3C403	II	15.4	0.059	-	
2058-28	OW-297.8	I	14.6	0.038	109	17
2104-25	OX-208	I	15.8	0.037	175	25
2211-17	3C444	II	18.0	0.153	105	35
2221-02	3C445	II	15.8	0.056	-5	29
2314+03	3C459	II	17.6	0.220	-	
2331-41		II	18.0	0.200*	-	

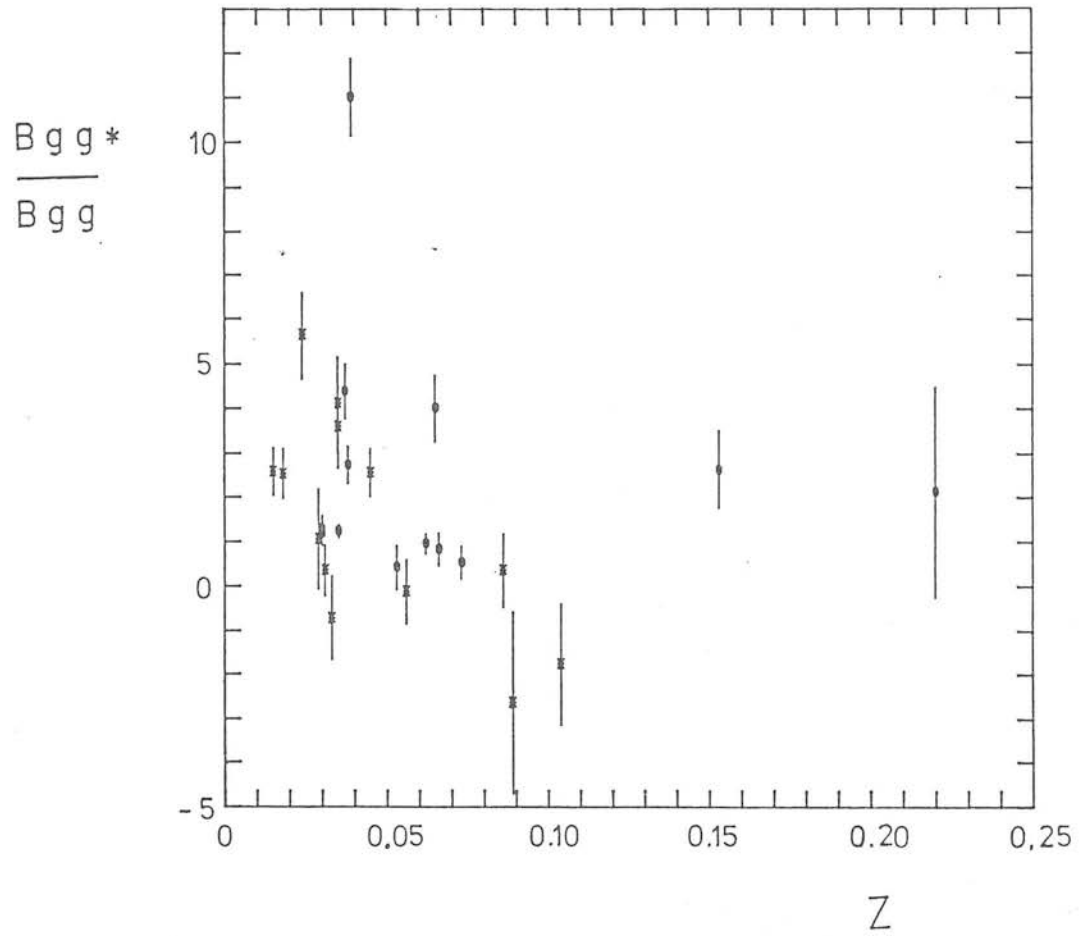

Figure 5.6 A plot of Bgg*/Bgg versus z for sources reduced using U.K. Schmidt data (•) and Lick count data (*).

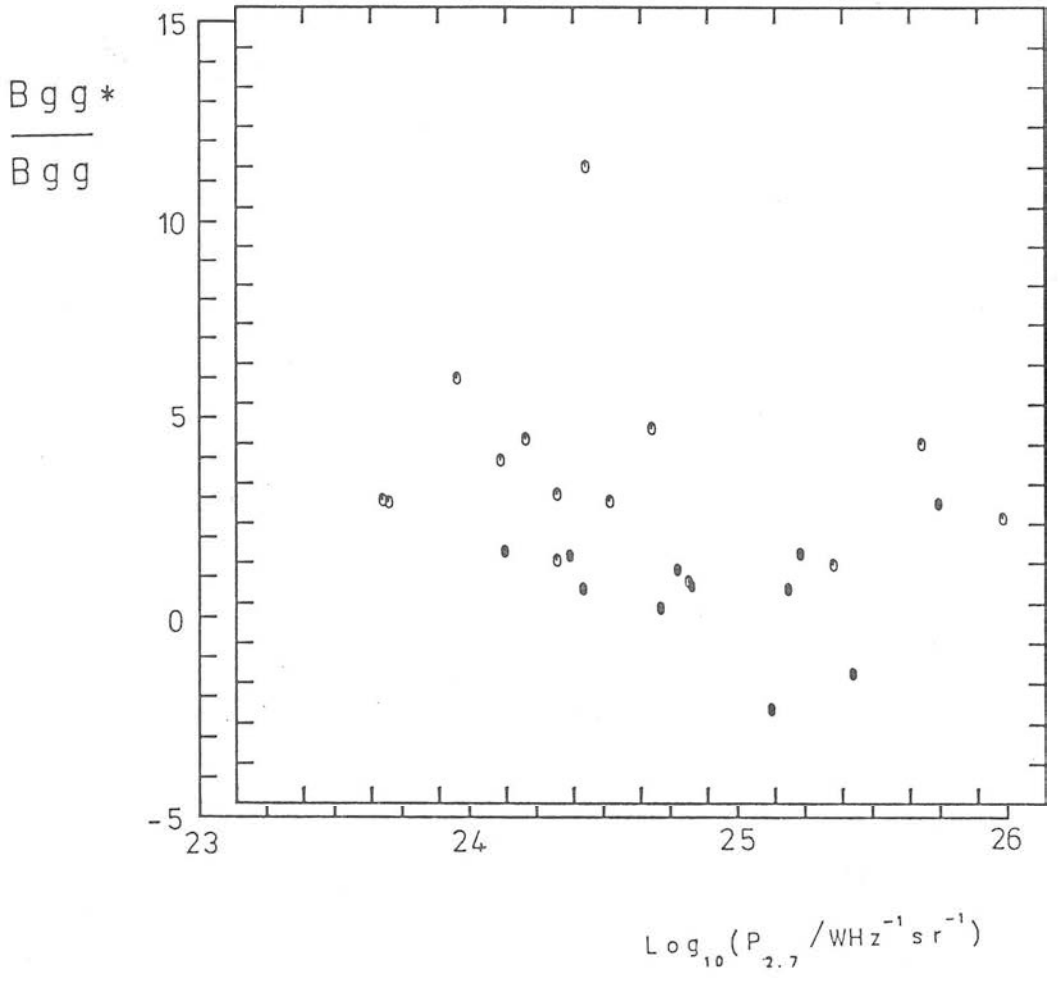

Figure 5.7. Bgg*/Bgg versus 2.7GHz luminosity for FRI (o) and FRII (•) sources.

the COSMOS results, as well as providing values for the sources not covered by the Lick counts, provide a reassuring check on the validity of the Lick values, despite the possibilty of unquantified systematic effects in those data.

5.6 : Discussion

We may summarise the main work of the last two Chapters as follows:

a) The cluster environments for members of a complete sample of radio galaxies have been derived from the Lick counts; detailed consideration having been given to the various sources of error affecting these measurements. The sources have been divided according to morphological type, and the range of values for each class illustrated. The mean value and the dispersion for each class have also been calculated, in such a way as to allow for variations in the measurement error from source to source; careful internal checks have also been made to ensure that these mean values do not suffer from any systematic effects introduced by the method.

b) the trends displayed by the main sample have been confirmed by consideration of an independent sample of estimated-redshift sources. Taking radio luminosity as a good indicator of morphological type, the results for this sample are in good agreement with those for the sources of known redshift.

c) A number of sources have also been reduced using galaxy samples derived from U.K. Schmidt plates. These have again shown values consistent with the main 68-source sample.

We can thus be confident that the values obtained are an accurate measure of the local galaxy excess in the vicinity of each source.

Let us now discuss the results for the different types of radio galaxy.

5.6.a Implications for Compact Sources

An important new result of this analysis is that compact radio sources do not appear in regions of enhanced galaxy density. While the mean value of Bgg*/Bgg for compact sources is marginally less than one; even if a real effect this would not in itself indicate that compact sources are abnormally 'un-clustered'. Since the average Bgg for galaxies in general includes galaxies found in clusters, and since if a radio galaxy is in a cluster it appears to be extended, it seems reasonable to suppose that compact sources may be equated with 'normal' galaxies which do not happen to lie in reasonably rich clusters. However, there is a significant difference in environment between the compact and extended sources, and this has some implications for the nature of these objects. The emission process for these sources is not well understood; however VLBI observations have shown that many of these objects have a one-sided jet structure, on scales $\ll$ 1 arcsec, and this naturally suggests the possibility of a 'relativistic beaming' model for these sources. In such a model, a source is assumed to emit low-luminosity, oppositely-directed jets, with Lorentz factors $\gamma \sim 5$. When one of these jets lies within an angle $\sim 1/\gamma$ of the line of sight, its emission is greatly enhanced, and the object is observed as a compact source. This not only provides a natural explanation for the one-sided jet structure, but also implies that compact sources should have 'unbeamed counterparts', in which the jets are directed

~ transversely to the line of sight.

An initial form of this model was proposed by Scheuer and Readhead (1979), who suggested that flat-spectrum radio-loud quasars might be the beamed counterparts of radio-quiet quasars. However, the detection of low-surface-brightness emission surrounding flat-spectrum quasars (Browne et al., 1982; Fomalont and Johnson, 1980) argues against this model, since this emission should also be detected in searches for radio emission from optically-selected quasars.

In a more recent form, Orr and Browne (1982) have suggested that flat and steep-spectrum quasars may be unified by this scheme. They used such a model to predict the proportion of flat-spectrum objects in samples defined at various frequencies; this depends upon the core Lorentz factor, and they found good agreement with the data for $\gamma \sim 5$, resulting in maximum enhancements of about 1000, for sources close to the line of sight.

The luminosities of the objects for which Orr and Browne proposed their hypothesis (e.g. 3CR quasars) are much greater than those of the sources investigated here, but we can still consider how such a model might be applied to the sources under study. Inspection of Fig. 4.11 shows that the majority of the FRII sources have total luminosities rather greater than those of the compact objects. they cannot therefore be considered as candidates for the unbeamed sources, since, if this were the case, the extended (unbeamed) emission from the objects would still be visible. Hence the only candidates for the unbeamed objects are the lower-luminosity FRI sources. However, if we compare the cluster environments for these two classes of object, the value for FRI sources is ~ 5 times that for the compact objects. This result is

not expected in the unified scheme, where the only difference between the beamed and unbeamed sources is their orientation with respect to the line of sight.

Since a galaxy's local environment is not obviously related to the source alignment, this can be considered strong evidence against such a unified model. While this result does not necessarily rule out the Orr and Browne hypothesis for more luminous objects (although these would have to be a different class of object from that considered here), similar results have been found for these sources. For example, in a spectroscopic survey of galaxies in fields around 27 high-luminosity quasars, Stockton (1978,1980) found that 10 of the 14 galaxies associated with the quasars were in the fields of known steep-spectrum objects, while only 1 was associated with a known flat-spectrum object. (The other 3 were with unknown-spectrum objects.) In addition, correlations between X-ray and other properties for various classes of active nuclei (Miller, 1983a) have also produced evidence against the unified scheme.

5.6.b Implications for Extended Sources

The main results for extended sources may be summarised as follows. The more complex (FRI) sources are typically found in regions of significantly enhanced galaxy density. The FRII sources are not on average found in such dense regions, in fact they appear to differ in their cluster environments only marginally from galaxies drawn at random from the whole population. These results are in agreement with those of Longair and Seldner, although the quantitative values have changed somewhat. The mean values obtained here are rather smaller than those of LS; this discrepancy is not due to the Bgg normalisation values used, and in fact the LS value (Bgg = 68, for H_o = 50kms^{-1}Mpc^{-1}) is slightly higher than that used

here. As the Agg* values obtained using $\theta = 1^{o}$ are in excellent agreement, the difference must be due to the different forms of the H(z) function used; it is thus perhaps remarkable that the ratio of FRI:FRII values has remained essentially unchanged. As discussed in section 4.6.b, a significant difference has not been found here between classical double and 'other' FRII sources; for a sample size ~ twice that of LS. Indeed the LS result was due in large part to a number of high-redshift ($z > 0.085$) sources, and also to 1251+27 (3C277.3) which in their analysis was seriously affected by the nearby Coma cluster.

In their analysis of the results LS made the implicit assumption, from the facts discussed above, that there was a good 1:1 correspondence between source morphology and cluster environment, with a division between classical double galaxies, which exist in regions of low galaxy density, and all other extended sources, which are found in high-density regions. This lead them to the conclusion that the sources which could become classical doubles were those which were isolated, but had their own sufficiently dense gaseous haloes to provide the supposedly required source confinement.

This simple picture no longer seems entirely applicable. While the typical environments of FRI and FRII sources do appear different, the distinction is by no means well defined. Although the majority of FRII sources appear to have Bgg*/Bgg ~ 1, some of these objects do exist in high galaxy-density environments. Conversely, there are a number of FRI sources with low Bgg*. Thus this analysis suggests that rather than a division at a specific source structure, there is a continuous relationship between source complexity and cluster environment. In this context, it is suggestive that the five 'most-distorted' FRI galaxies, from the sample of Chapter Three,

all have higher than average values of Bgg*. (It is also interesting to note that four of these five objects exhibit double nuclei.) The classical double sources are now no longer special in this respect, but merely represent one end of a continuum of cluster environment. We may therefore postulate that in all cases it is the presence of some IGM, rather than an intrinsic gaseous atmosphere which provides the required confinement for the radio source. This is in agreement with the work of Miller (1983), who did not find any evidence for extended X-ray emission associated with the 3CR sources observed by him.

It is interesting at this stage to consider the question of why the observed correlation between radio structure and cluster strength is so poor - although of course it should be remembered that no well-ordered ranking by structure, apart from the FR division, has been employed. One simple reason is that Bgg*, the global density within 1Mpc, may not be directly related to the physical process causing the correlation. For example, structure upon scale less than 1Mpc may be important; recent work on the cluster environments of quasars (Yee and Green, 1984; Stockton, 1984) suggests that the groups associated with these objects are significantly more compact than typical rich clusters. Alternatively, if it is the velocity of the galaxy through the IGM which is important, the occurance of one or more near neighbours may have a greater effect than the general galaxy density at larger distances from the source.

In this respect, it is worth noting the work of Stocke (1979). In his analysis, Stocke considered the environments of a sample of 53 radio galaxies with $z < 0.15$, mainly drawn from the 3CR sample. He used as measures of the local galaxy density simple combinations of d_i and r_i, (d_i = projected major diameter, r_i = projected

distance from radio galaxy of the ith galaxy) with only galaxies within 1Mpc, and with angular diameters between 5 and 30kpc at the redshift of the source being included in the statistics. Unfortunately numerical values were not presented, and Stocke's interpretation of radio structure is rather different from that used here (for example, he states that 'only five sources were either single or had structures too complex to be described as "classical doubles" '). However, one of the most convincing relations presented by him is that between the distance to the closest neighbouring galaxy and the bending angle, ϕ, where ϕ is the deviation of one radio lobe from a line drawn between the position of the optical galaxy and the second lobe. This angle is only larger than $\sim 10^{\circ}$ (i.e. the source would almost certainly be classed FRI) for objects with neighbours within 50kpc of the optical galaxy.

Finally, there is of course the possibilty that the local environment is only indirectly related to the process which causes the difference between FRI and FRII sources. If we believe that the relevant process is that of galaxy merging, then we would expect this to occur more frequently in high-density regions; this would then cause an apparent correlation between the cluster environment and the radio source structure. A consideration of these topics is given in more detail in Chapter Seven.

Chapter 6 : SURFACE PHOTOMETRY OF SOUTHERN RADIO GALAXIES

6.1 : Introduction

The results of the previous chapters confirm that the environment is clearly related to the nature of the radio-activity and structure of active galaxies. As this has only been simply measured in terms of galaxy number densities however, it is not obvious from the results what is the exact physical cause of the relationship. For example, the correlation may be a result of the presence of a more dense IGM in these regions, but alternately it may be due to encounters with near neighbours, or even galaxy mergers, which would be expected to occur more frequently in richer systems. In this chapter, the results of a programme of surface photometry, for the low-redshift sample of galaxies considered in Chapter Five, are presented. Such a study provides complementary information to that of the previous chapters, in that it investigates the nature of the host galaxies themselves. This will enable us to compare their intrinsic properties with the more global ones of their surroundings as a whole.

6.1.a Galaxy Merging - the (M_V- α) Diagram

Galaxy merging has been the subject of considerable interest both theoretically and observationally, not least because it is a possible mechanism to explain the absolute magnitude distribution of first-ranked cluster ellipticals. The remarkably small scatter in magnitude found in these objects is seen as evidence that some special formation or evolutionary process is operating in the rich environment (Sandage 1976, Dressler 1978). Observational support for

this effect comes from a number of studies, perhaps the most direct being those into the relationship between luminosity and structural parameters for these objects.

The majority of the work in this field has been performed in terms of the dimensionless structure parameter α, introduced by Gunn and Oke (1975). This is defined by

$$\alpha_{\gamma} = \left. \frac{\delta \log L(r)}{\delta \log r} \right|_{\gamma} \qquad (6.1)$$

where L(r) is the luminosity enclosed within r, and γ, the sampling radius, is usually chosen (for historical reasons) to be 19.2kpc ($H_o = 50 kms^{-1} Mpc^{-1}$). If I(r) is the surface brightness at r, then this may be simply shown to be equivalent to

$$\alpha_{\gamma} = \left. \frac{2\pi r^2 I(r)}{L(r)} \right|_{\gamma} \qquad (6.2)$$

i.e. twice the ratio of the mean surface brightness at γ to the mean surface brightness within γ. With this dimensionless size parameter, the magnitude parameter used is Mv_{γ}, the absolute magnitude within an aperture of metric size γ. (Henceforth the value γ = 19.2kpc will be assumed, and the subscript γ dropped.) Clearly, for a galaxy which can be described by a simple analytic form (e.g. a de Vaucouleurs profile) α is directly related to the appropriate characteristic size parameter. For example, for $\alpha > 0.25$, α varies approximately linearly with logRe, where Re is the de Vaucouleurs half-light radius.

Studies of the Mv and α parameters for samples of first-ranked cluster galaxies (e.g. Hoessel, 1980) have demonstrated a relationship between Mv and α, in the sense that galaxies with larger values of α have brighter absolute metric magnitudes. This is

consistent with theories of galaxy merging (e.g. Hausman and Ostriker, 1978) - the characteristic radius swells as the galaxy has to accomodate the different specific binding energy of the consumed galaxy. Support for this hypothesis comes from the fact that many first-ranked cluster galaxies show multiple nuclei; presumably a clear indicator of merging, since it is difficult to imagine other mechanisms for their production. For example, Hoessel (1980) found that in his sample of 108 Abell clusters, 28% of the galaxies exhibited such multiple nuclei. He pointed out that a close collision between a cluster member and the brightest galaxy is expected once every 10^9 yrs, for a typical cluster, and that simulations of the merger process yield an expected duration for each merger of $\sim 2.5 \times 10^8$ years. Thus the observed fraction of multiple systems is consistent with the expected frequency, if all mergers result in a detectable multiple system at some stage. Additional support comes from the observation of a weak correlation between α and Bautz-Morgan class, in the sense that α is highest for type I clusters. This is also in agreement with theoretical predictions, which suggest that merging occurs at a faster rate in richer, denser systems. Similar results have been found by Schneider et al. (1983) for an extended sample of Abell clusters, and also by Thuan and Romanishin (1981), for a sample of 'cD' galaxies in poor clusters (from Morgan et al.,1975, (MKW) and Albert et al. 1977 (AKW)). Results for the latter sample suggest that even more mergers have taken place here than for the Abell cluster objects, consistent with theoretical models if these galaxies are in systems with low velocity dispersions and hence high central galaxy densities.

Clearly, since they are simply related for galaxies which obey a de Vaucouleurs profile, the (M_V- α) relation must translate directly into a similar relation in the characteristic brightness-size plane. Indeed, Hoessel found that his relation was identical to the

(unexplained) Be-logRe relation found by Kormendy (1977) for elliptical galaxies in the Virgo cluster. He therefore suggested that all ellipticals may be formed by the homologous mergers of smaller systems. There are however, a number of arguments against this (see Kormendy 1982); and it should be borne in mind that the observed (Mv- α) correlation may simply be an extension of the Kormendy relation at lower luminosities. Even if this should turn out to be the case, however, (Mv- α) studies provide a useful means of comparison for the optical structure of different types of galaxy, and for galaxies in differing environments.

We wish to investigate the relationship between the giant elliptical galaxies that are host to the powerful radio sources, and the giant elliptical galaxies found in both Abell clusters and also in the poorer AMW and MKW clusters. If α can be taken as a measure of the degree of merging that has taken place, then these measurements will indicate the importance of this evolutionary process in the radio galaxies. This is of importance not only in terms of understanding the radio-source phenomenon itself, but also in interpreting the infrared Hubble diagram for these sources (Lilly and Longair 1982, 1984) in terms of the combination of both evolutionary and cosmological effects.

A preliminary investigation in this area has been made by Lilly, McLean and Longair (LML, 1984), who made α parameter measurements for 10 powerful FRII galaxies. The results of their study were as follows. Firstly it was clear that the radio-galaxies form an (Mv-α) relation which is continuous with that of the Abell clusters. Equally clear however, was the fact that these galaxies do not cover the same range of values of Mv and α as the Abell, AMW and MKW cluster galaxies. Even though radio activity of this sort is known to occur generally in luminous systems, the galaxies of LML

are not amongst the most luminous elliptical galaxies in the Universe. This difference must be related either directly or indirectly to the environment of the radio galaxy, and could possibly be caused by different dynamical histories.

The work of LML is extended, in this chapter, through the study of a larger number of radio galaxies for which the results of the previous chapters may be utilised in furthering the analysis. By making observations of Mv and α for luminous elliptical galaxies selected on the basis of their radio properties alone, without direct regard to their environment, but with detailed information on that environment available, we will be able to examine the hypothesis that the Mv- α relation is indeed caused by the merging process - a drawback of previous investigations is that the samples used have consisted of galaxies selected directly by their environment. We will also be able to assess the importance of this evolutionary process upon the nature of the radio source. In addition, the data are of sufficiently high quality to enable a number of other parameters to be derived (for instance, the ellipticity, and the presence of isophotal twisting and multiple nuclei).

Most importantly, the availability of radio structural data and spectral information will also allow correlations between these and the optical structure to be investigated. Combined with the results of the last Chapters, we will be in a position to assess the relative importance of global environment (via Bgg*) and immediate surroundings (via Mv and α).

6.2 : Method

6.2.a The Observations

The observations described here were made on the nights of the 9th, 10th and 11th of December 1983, using the Anglo-Australian 3.9m Telescope (AAT) with the R.G.O. CCD camera at prime focus. Weather condtitions were very variable, ranging from complete cloud cover to conditions of excellent seeing and transparency. The sources observed were drawn from the complete sub-set of the WP sample ($10^{o} > \delta > -45^{o}$), for which both high-quality radio data and clustering information was available; the basic source list consisted of all radio galaxies with redshifts $z < 0.25$ which lay within the accessible R.A. range.

The initial aim of the programme was to observe all of the prime sample in the appropriate R.A. range in U,Bj,V and R. The desirability of observations in more than one colour was two-fold. Variations of the parameters with colour would firstly indicate the presence of stellar colour gradients in the galaxies and secondly indicate any comtamination from an optically active nucleus. Also, the availiblity of a large sample of radio galaxies at low redshift with measured UBVR magnitudes would have provided an extremely useful baseline to investigate changes in the spectral energy distributions of radio galaxies at high redshifts. Studies of the colours of these objects (Lilly and Longair 1982, 1984) have shown that most radio galaxies at $z \sim 1$ appear to have substantial excesses of ultra-violet flux density. This has been interpreted as being caused by massive stars in a very young stellar population, although these conclusions have in the main been drawn from a comparison with the spectral energy distributions of nearby radio-quiet galaxies. The available U photometry for radio galaxies

is severely limited, and certainly does not cover a complete sample of such radio galaxies (Sandage, 1972). U photometry would have been of considerable interest, since this is the region of the spectrum which is redshifted into the red in these objects.

Unfortunately, due the loss of time to cloud this could not be achieved, and the final data set consists of R observations of all but one object, with Bj observations of a number of the lower redshift sources. The list of sources defined by the R.A. range available is given in Table 6.1. Those sources for which only R observations were made are marked with an asterisk, while 0404+03 was not observed at either wavelength. Care was taken to match sources of appropriate redshift to the seeing as far as possible, and in cases where initial observations had been made in non-photometric conditions, repeat observations were made of shorter exposure to determine the magnitude zero-point. Some additional sources outside the declination range of the main sample were also observed, to fill in gaps in the R.A. distribution; these are also given in Table 6.1. Both these sources, and the sources for which Bj observations were made, were chosen purely on operational grounds, with no reference to their radio or other properties.

6.2.b Initial Reduction

Besides observations of the programme sources, observations were made of standard stars, and various other calibration procedures carried out.

A number of dark current exposures (1000sec exposures with the shutter closed) were taken, and bias exposues (0sec dark exposures) were also taken at frequent intervals throughout the run. These bias frames were found to remain constant throughout the run, at a mean

Table 6.1: The Sample

IAU	other	M	Z
0034-01	3C15	15.3	0.073
0035-02	3C17	18.0	0.220
* 0038+09	3C18	18.5	0.188
0043-42		16.0	0.053
0055-01	3C29	14.1	0.045
0123-01	3C40	12.3	0.018
* 0131-36		13.0	0.030
* 0213-13+	3C62	18.0	0.200
0255+05	3C75	13.6	0.024
0305+03	3C78	12.8	0.029
0325+02	3C88	14.0	0.030
0349-27	OE-283	15.8	0.066
** 0404+03	3C105	18.5	0.089
0430+05	3C120	14.1	0.033
* 0442-28+	OF-271	17.4	0.151
0453-20	OF-289	13.0	0.035
0518-45	Pic A	16.0	0.035
0521-36		16.8	0.062
0625-35	OH-342	14.0	0.055
* 0806-10+	3C195	17.8	0.182
0915-11	Hyd A	14.8	0.065
0945+07	3C227	16.3	0.086
1251-12	3C278	13.5	0.015
* 1318-43	NGC5090	14.5	0.011
* 1333-33	IC4296	11.1	0.013
* 2211-17	3C444	18.0	0.153
2221-02	3C445	15.8	0.056
* 2314+03	3C459	17.6	0.220
* 2331-41+		18.0	0.200

IAU	other	M	Z
* 0106+13	3C33	15.2	0.060
* 0356+10	3C98	14.4	0.031
0428-53		13.2	0.039
* 0620-52		14.5	0.051
0625-53		13.0	0.054
0802+24	3C192	15.5	0.060
2356-61		16.0	0.096

* only R observations
** not observed
\+ estimated redshift

level of ~ 90 counts, with some very weak structure. Accordingly, the mean of all the bias frames was found, and this mean frame used to subtract the bias level from each exposure. The dark-current exposures were found to have effectively zero signal after subtracting the bias level, and the dark current was thus determined to be negligible.

Sets of flat-fields were taken at the start and end of each night, using the inside of the dome illuminated by a tungsten lamp. For each set of flat-fields, a number of exposures were made of varying length, and with varying degrees of illumination.

The flat-field frames were found to be excellently constant within a single set of exposures; and linear within the noise over a wide range of exposure levels. The flat-fields did however vary slightly from night to night, with large scale variations over the chip on the order of one percent. This variation was also observed in the astronomical exposures, in the sense that an exposure taken on one night, normalised with the flat-field of another night showed similar structure. Variation between the sets of start and end-of-night flat-field exposures was also visible, but only at the $< 1\%$ level. Since no flat-fields were taken during the course of the run, it was not feasible to try and interpolate between flat-fields. Accordingly, each set was simply averaged, and the unweighted average of start and end-of-night was taken as the flat-field for that particular night. This was found to remove the small-scale structure completely, and to leave large scale variations of at most a few tenths of a percent. The only exception to this appeared to be the astronomical exposures taken at the very start and end of each night, when it was not completely dark, and also some exposures taken near the moon, for which the flat-fields were slightly worse.

Finally, the R exposures suffer from the addition of "fringes", a pattern of thin-film interference caused by night-sky lines. these were removed by subtraction of suitable multiples of a "fringe-frame", a zero-mean exposure of a blank area of sky.

6.2.c Photometric Calibration

The data obtained here do not require extremely accurate photometric calibration, accuracies of a few percent for the radio galaxy being sufficient. Accordingly a fairly simple calibration procedure was followed.

Six standard stars were selected from the work of Graham (1982), covering the observable R.A. range. These had V magnitudes covering the range 13th to 15th mag, and colours (B-V) of ~ 0.5 to 0.8. These were observed where possible at the start, middle and end of each night. In addition, four more standards from Landolt (1983), with magnitudes ~ 12th to 13th mag were observed, extending the colour range to (B-V) of ~ -0.3. Finally three more standards from Graham (1982) were available for measurement on the CCD fields of two of the primary standards. These were in the range 16th to 17th magnitude. Whilst these were not included in the main reductions, a comparison of their magnitudes is a good test of the calibration at fainter magnitudes, especially since they were observed for abnormally short exposure times.

The quoted magnitudes of the standards were all in the Johnson BV, Cousins R systems. The observational passbands used here are those defined by the B,Bj and R filters of the AAT. (Bj is a passband designed to simulate the SERC photographic J passband.) The observed magnitudes of the standards were derived using the aperture photometry program of STARLINK. Variations in the size of the

aperture and the position of the sky region chosen were found to have a negligible effect on the observed magnitude. A profile fitting routine was also used to obtain magnitudes; this allows a profile of the form

$$I = A \exp(-0.5 \left(\frac{r'}{\sigma} \right)^{\gamma}) \qquad (6.3)$$

(where σ is the profile width, r' the effective radial distance, and γ a radial fall-off parameter (=2 for a Gaussian)) to be fitted to all stellar images in the field, with the best fit then scaled to the individual images. Due to the small number of stars in many of the frames, the shapes of the fit were determined here solely by the standard.

A comparison of these two methods showed excellent agreement, and indicated an internal rms of ~0.02 mag. In fact, for the B and Bj magnitudes, departures from the expected values at fainter magnitudes indicated that the profile-fitting values were less reliable than the aperture values. Since profile fitting is not strictly correct for frame to frame calibration, only the aperture magnitudes were considered for subsequent analysis.

The standard transformation equations for the AAT are

$$r - R = A_1 + 0.1X \qquad (6.4)$$

$$b - B = A_2 + 0.27X - 0.086\ (B-V) \qquad (6.5)$$

where r, b (and v, b_j over) are the observed (instrumental) magnitudes

$$v - V = A_3 + 0.157X + 0.069(B-V) \qquad (6.6)$$

where A_i = constant, X = sec(z), z = zenith distance. (Gilmore, Pence, private communication).

The latter two were combined to provide a J equation

$$bj - Bj = A_4 + 0.24X - 0.043\ (B-V) \qquad (6.7)$$

Using the colour equation obtained by Blair and Gilmore (1983),

$$Bj = B-0.28\ (B-V) \qquad (6.8)$$

These equations were used to correct the exposures for varying airmass, while the observations of the standard stars were used to define the magnitude zero-points. Typical r.m.s. errors in the standard stars using these equations were a few percent.

6.2.d Derivation of the Mv- α Parameters

The derivation of these (Mv- α) parameters from the fully-reduced images was performed (by S. Lilly) in an essentially similar manner to that of LML. Firstly, the nucleus of the image was found by fitting a Gaussian profile to the central image pixels. All stars, companion galaxies and small multiple nuclei were then replaced by a corrected intensity as in LML; i.e. if they lay less than 2γ from the centre, by a 180 degree rotation about the nucleus, otherwise by a locally determined mean sky value (plus noise). The sky background was determined by fitting a gaussian to the top of the histogram of pixel values in an annulus between 3 and 4γ from the nucleus. For successive increments of radius, the

enclosed luminosity was then calculated simply by the summation of all pixels with centres less than the appropriate distance from the centre, and the subtraction of the sky value. A small correction was applied, to account for rounding effects, by multiplying by πr^2 and dividing by the total pixel area. The metric magnitude was then obtained simply from the intensity within the appropriate radius (19.2kpc). The slope of the growth curve at γ, ($\equiv \alpha$), was found by fitting a parabola to the log(enclosed luminosity) at adjacent radii.

The observed R magnitudes (corrected for the effects of galactic extinction using the data of Burnstein and Heiles, 1982) were converted to absolute V magnitudes as follows. Firstly, the apparent magnitudes were converted to zero-redshift absolute magnitudes using the K-corrections of Pence (1976). These absolute R magnitudes were then transformed to V magnitudes assuming a (V-R)j colour of 0.86 (Sandage, 1973) and a colour transformation

$$(V-R)c = 0.73(V-R)j - 0.03 \qquad (6.9)$$

(Bessell, 1979).

The aim of this procedure was not to obtain V magnitudes per se; indeed these may be incorrect for the broad-line galaxies with significant non-thermal components. However, the constant ΔM applied to all the galaxies will not change their relative position in the 'observed' ($Mv-\alpha$) plane, and the use of V magnitudes facilitates comparisons with other workers.

As the last step, a small seeing correction was applied to α, as described in LML. This procedure simply consists of modelling the effect of seeing, by degrading model galactic profiles with various

gaussian seeing profiles. The observed α and seeing FWHM can then be used to obtain the true α value. The correction is small, and certainly for $z < 0.1$ the error is negligible.

No attempt was made to obtain a value of α for the unknown redshift objects, due to the uncertainty of the estimated redshift. None of these objects appeared unusual in any of their characteristics however, and the omission of them from the results should not have any serious consequences.

6.3 : Results

The majority of the sources observed here exhibit simple structures typical of giant elliptical galaxies. Within the central tens of kpc from the nucleus they show symmetrical, smoothly decreasing isophotes, generally near circular, and centred on the position of peak surface brightness. This will be referred to as the 'nucleus', although the possible contribution of any non-stellar component in these objects varies widely. In terms of their Mv-α parameters, these objects show generally similar properties to the first-ranked ellipticals in Abell clusters. Typical examples of the sources, covering a range of α, are shown in Fig. 6.1. The galaxies of this type account for 28 of the 35 sources observed; the values of Rc, and the derived values of Mv, α_r and α_j are given in Table 6.2.

The remainder of the sources exhibit more interesting light distributions. 0131-36 (NGC612) is unusual for a radio galaxy: in addition to a dominant bulge, it has a stellar disk component and a dust-lane (see Ekers et al., 1978). 2211-17 (3C444), although as one of the higher redshift objects poorly resolved, shows evidence for a

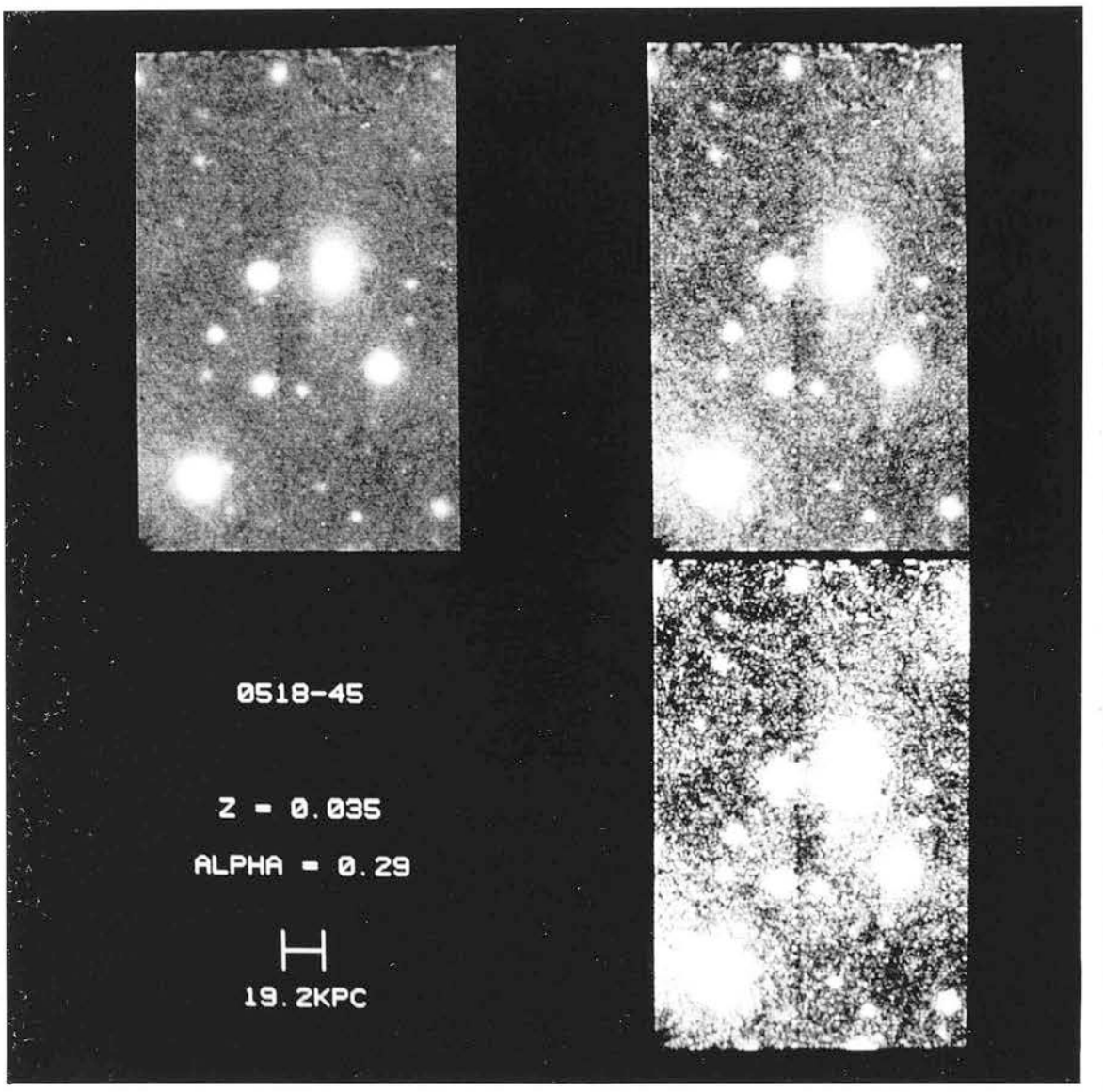

Figure 6.1.a. The fully reduced R CCD frame of 0518-45. The same image is displayed at three different intensity levels. Clockwise from left, pure-black to pure-white ranges from:

1) 90% of sky to 5% of peak object intensity
2) 95% of sky to 2% of peak object intensity
3) 98% of sky to 1% of peak object intensity

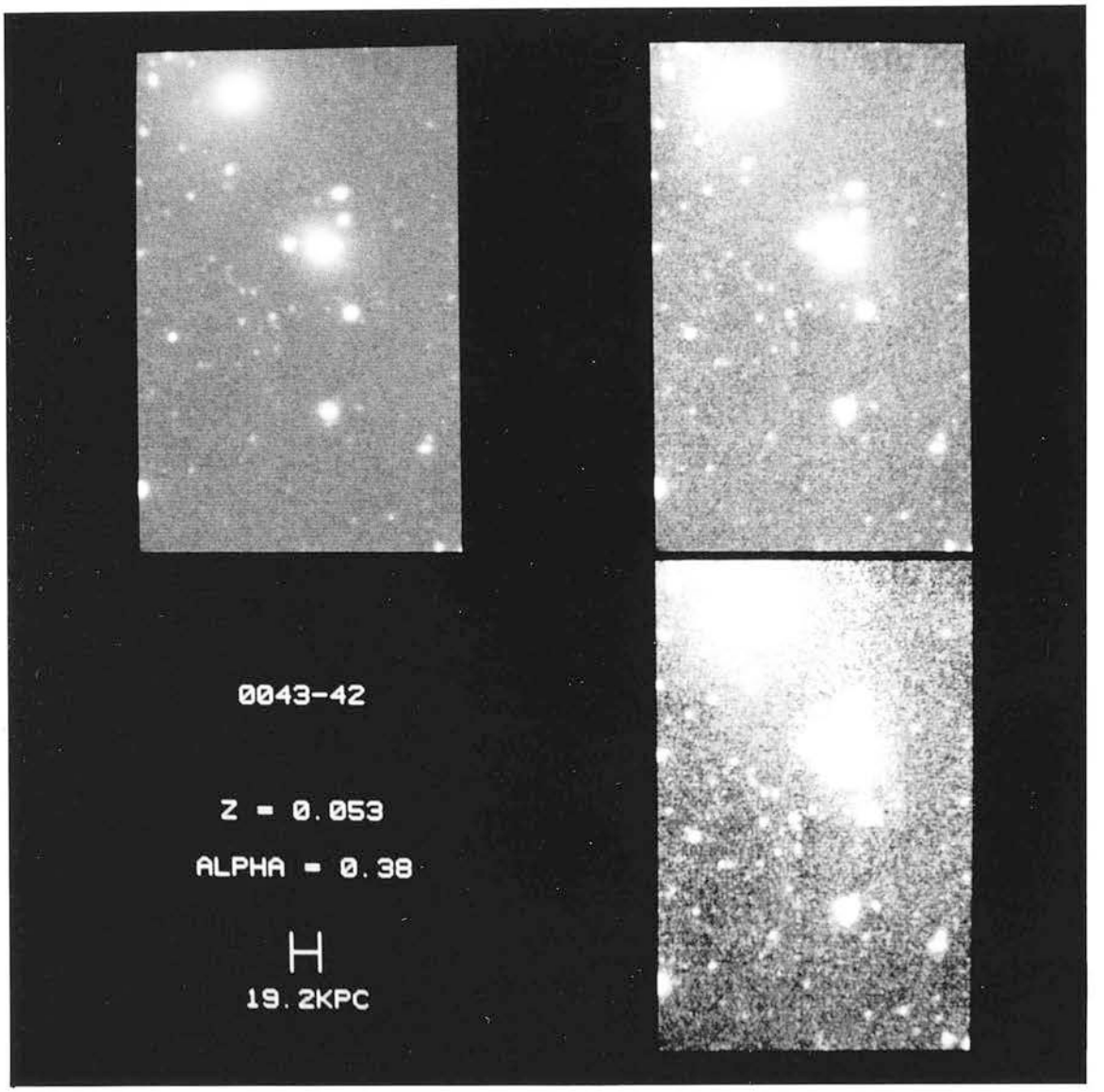

Figure 6.1.b. As (a) for 0043-42.

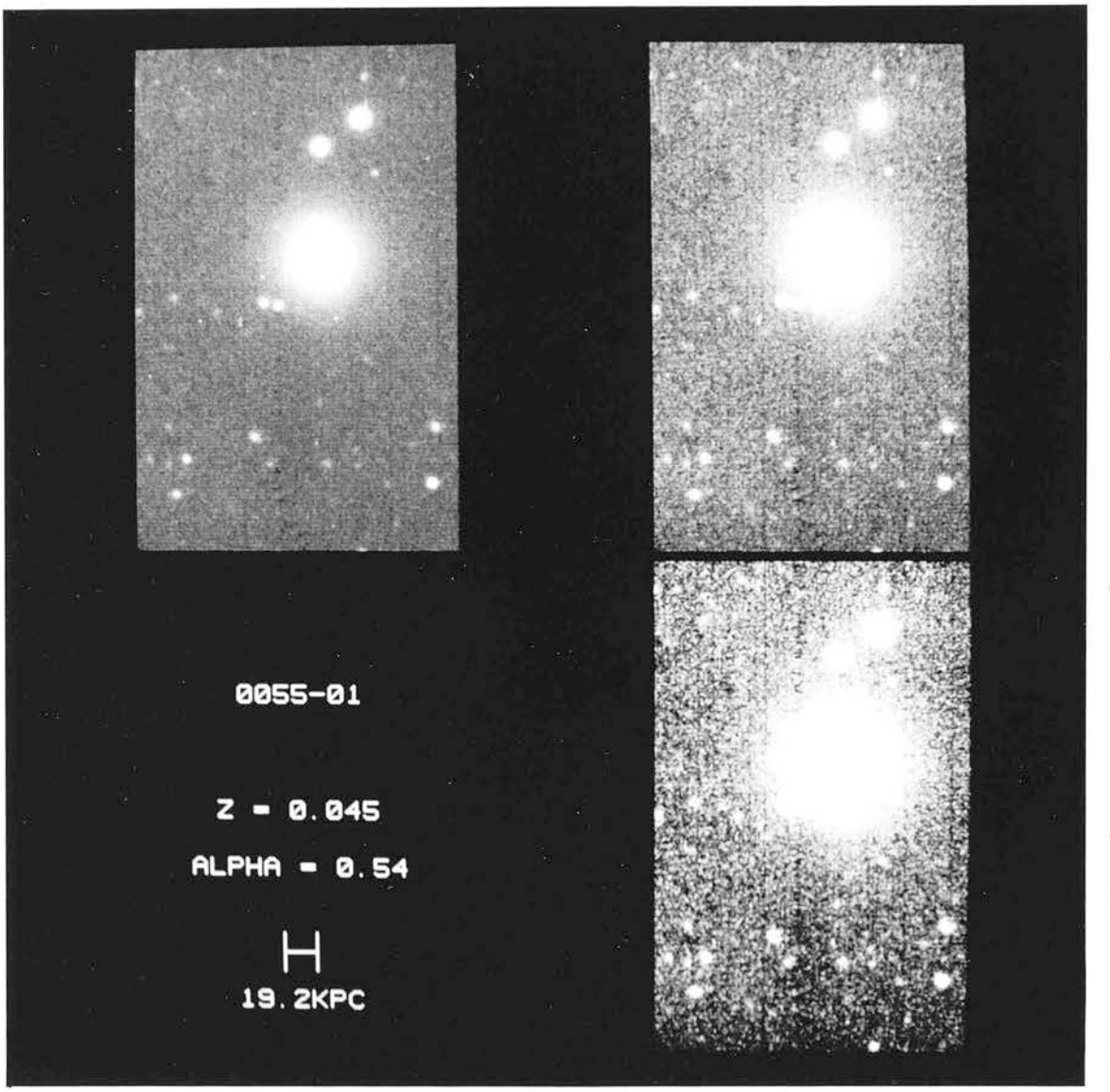

Figure 6.1.c. As (a) for 0055-01.

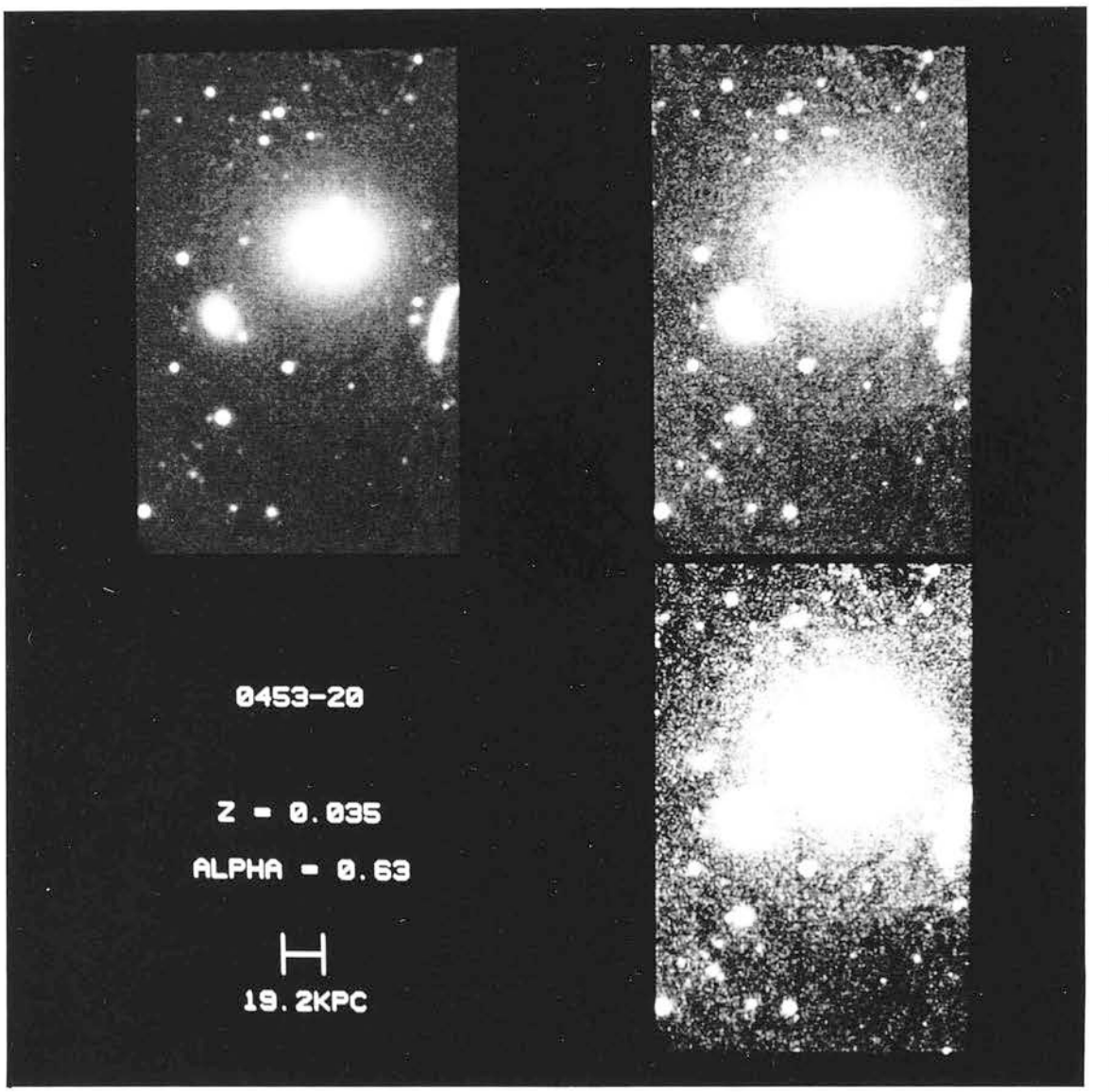

Figure 6.1.d. As (a) for 0453-20.

Table 6.2: The (Mv $-\alpha$) Measurements

IAU	Z	Rc	(Bj-Rc)	α_{δ_3}	α_R	Mv	Mvt	Bgg*	Radio *	Spectra +	
0034-01	0.073	15.03	1.52	0.39	0.41	-22.72	-23.18	21	I	B	(7)
0035+02	0.220	17.80	-	-	0.38	-22.63	-23.04	85	I?	A	(15)
0038+09	0.188	18.50	-	-	0.43	-21.52	-22.01	N/A	IId	A	(12)
0043-42	0.053	15.56	1.58	0.40	0.38	-21.45	-21.86	17	IIg	B?	(14)
0055-01	0.045	13.70	1.45	0.50	0.54	-22.95	-23.67	102	I	B	(7)
0106+13	0.060	14.95	-	-	0.44	-22.35	-22.86	210	IIg (4)	A	(9)
0123-01	0.018	-	-	-	-	-	-	101	I	B	(5)
0131-36	0.030	12.77	-	-	0.55	-22.99	-23.73	47	IIn	B	(8)
0255+05	0.024	-	-	-	-	-	-	225	I	B	(7)
0305+03	0.029	12.20	1.44	0.51	0.54	-23.47	-24.19	42	I	B	(15)
0325+02	0.030	13.52	1.39	0.66	0.64	-22.23	-23.19	51	IIn	B	(15)
0349-27	0.066	15.58	1.14	0.79	0.62	-21.94	-22.85	33	IId	A	(4)
0356+10	0.031	14.07	-	-	0.32	-21.75	-22.06	14	IId (4)	A	(1)
0428-53	0.039	-	-	-	-	-	-	440	I (1)	B	(5)
0430+05	0.033	13.04	0.90	0.18	0.23	-22.92	-22.83	-29	U	BLRG	(11)
0453-20	0.035	13.19	1.36	0.64	0.63	-22.90	-23.83	164	I	B	(6)
0518-45	0.035	14.71	1.14	0.28	0.29	-21.38	-21.66	49	IId	A	(2)
0521-36	0.062	14.18	1.11	0.17	0.22	-23.20	-22.98	38	I	BL Lac	(3)
0620-52	0.051	13.41	-	-	0.77	-23.51	-24.86	N/A	I? (3)	B	(13)
0625-35	0.055	13.93	1.42	0.50	0.56	-23.18	-23.94	N/A	I	B	(6)
0625-53	0.054	-	-	-	-	-	-	N/A	I? (2)	B	(5)
0802+24	0.060	15.10	1.36	0.36	0.35	-22.21	-22.57	48	IId (4)	A	(1)
0915-11	0.065	14.14	1.37	0.78	0.85	-23.35	-24.99	160	I	B	(5)
0945+07	0.086	15.72	1.24	0.27	0.28	-22.41	-22.44	14	IIg	BLRG	(10)
1251-12	0.015	-	-	-	-	-	-	103	I	B	(7)
1318-43	0.011	10.68	-	-	0.59	-22.86	-23.69	N/A	I	B?	(16)
1333-33	0.013	10.35	-	-	0.55	-23.55	-24.29	N/A	I	B	(6)
2211-17	0.153	16.86	-	-	0.85	-22.65	-24.29	105	IIn	B	(7)
2221-02	0.056	14.95	1.65	0.20	0.20	-22.20	-22.04	-5	IId	BLRG	(10)
2314+03	0.220	17.25	-	-	0.24	-23.18	-23.08	N/A	IId	BLRG	(15)
2356-61	0.096	15.65	1.47	0.57	0.59	-22.74	-23.57	N/A	IId (1)	A	(5)

* Radio structures from Chapter Three except:

(1) Christiansen et al., 1981.
(2) Hunstead, 1972.
(3) Large, 1981.
(4) Peacock and Wall, 1982 and refs therein.

\+ Optical Spectra from:

(1) Costero and Osterbrock 1980.
(2) Danziger et al. 1977
(3) Danziger et al. 1979
(4) Danziger et al. 1984
(5) Danziger and Goss, 1983.
(6) Fosbury, private communication
(7) Gilmore, private communication
(8) Goss et al., 1980.
(9) Koski, 1978.
(10) Osterbrock et al., 1976.
(11) Phillips and Osterbrock, 1975.
(12) Smith et al., 1976
(13) Tritton, 1972.
(14) Whiteoak, 1972.
(15) Yee and Oke, 1978.
(16) no reference

double nucleus, with the central peak of surface brightness being accompanied by a second less-bright peak. Values of α have been derived for both these sources, and they appear to lie sensibly in the (Mv- α) plane; the values for these sources are also given in the Table.

The final five sources (0123-01,0255+05,0428-53,0635-53 and 1251-12) are perhaps the most interesting in the sample. Well resolved, they all exhibit double (optical) structure, with in each case two distinct "nuclei" embedded in the more extensive outer isophotes. "Contour" plots of the CCD frames of these objects, with increasing intensities being represented alternately by black and white, are shown in Fig. 6.2. Two obvious features of interest are the large extent to which the isophotes may be traced, and the displacement of both nuclei from the centres, as defined by these outer isophotes. In terms of the later discussion, it is interesting that all these sources fall into the FRI category.

Clearly, for these more pathological objects, the definition of α is both difficult to apply, and conceptually less useful. Accordingly no attempt was made to derive α for these sources. Instead, the (Mv- α) diagram for the remaining sources will first be discussed, and the relationship of these more unusual sources, and their implications for the (Mv- α) diagram, considered later.

6.3.a The (Mv- α) Diagram

The (Mv- α) diagram for all the reduced sources is shown in Fig. 6.3. Some general features of the diagram may immediately be noted. Firstly, the sources observed here exhibit a similar range of properties as found for the Abell cluster samples of Hoessel and Schneider et al. (Fig. 6.4, reproduced from LML). The more extreme

Figure 6.2.

"Contour" plots of the R CCD frames of the five double nuclei galaxies, produced by replacing increasing intensity levels alternately by black and white. The sky has been subtracted, and the peak intensity levels of the objects normalised to 100.

Contour levels are:

a) 0123-01 0.075,0.75,1.5,2.5,3,4,6,8,12,20,40,75
b) 0255+05 0.075,0.75,1.5,2.5,3,4,6,8,12,20,40,75
c) 0428-53 0.075,0.75,1.5,2.5,3,4,6,8,12,20,40,75
d) 0625-53 0.075,0.75,1.5,2.5,3,4,6,8,12,20,40,75
e) 1251-12 1.5,5,8,12,15,20,25,50,75

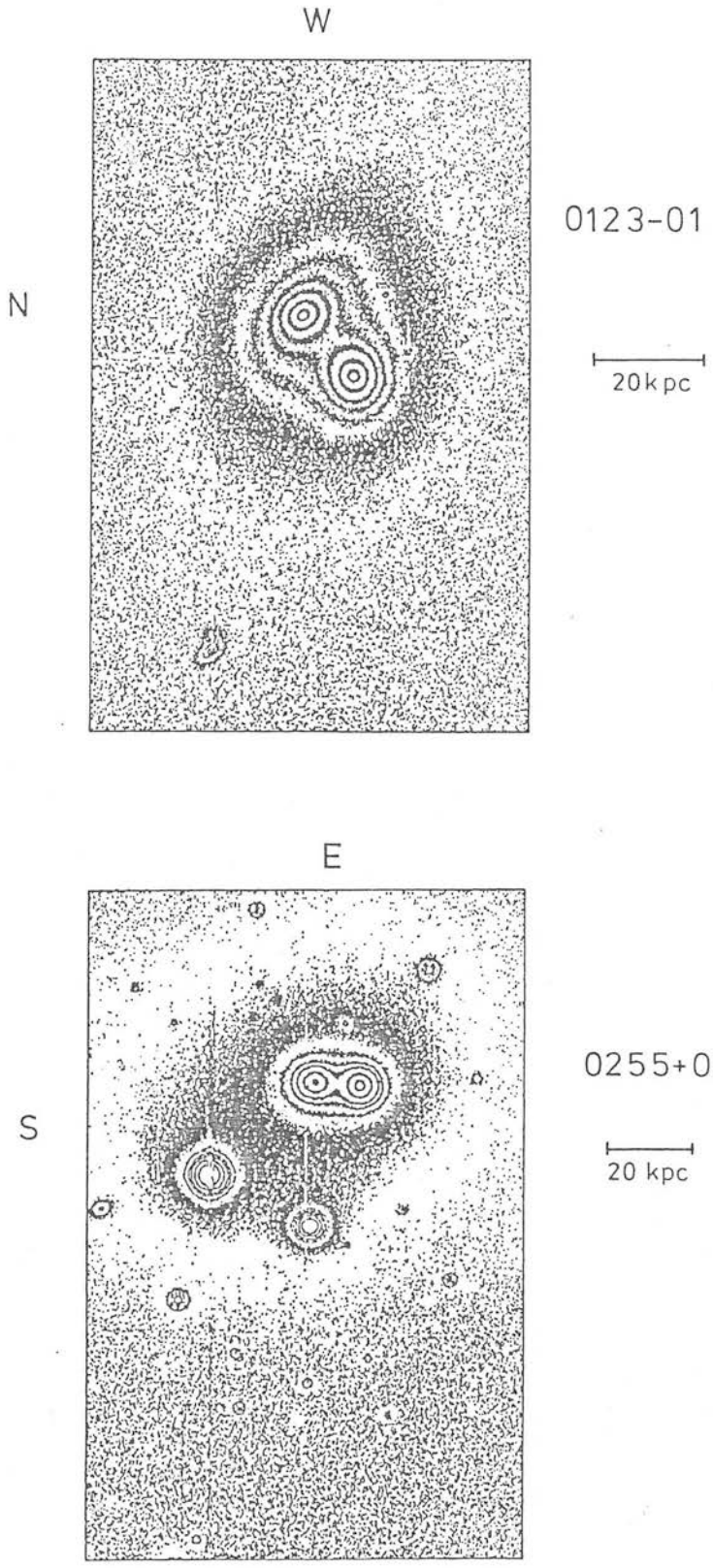
W
N
0123-01
20kpc
E
S
0255+05
20 kpc

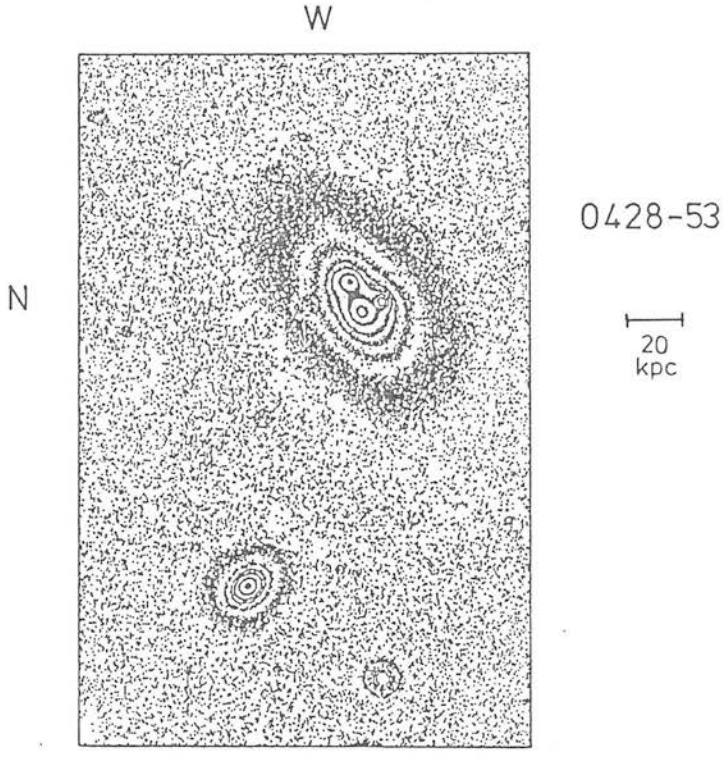
W
N
0428-53
20
kpc

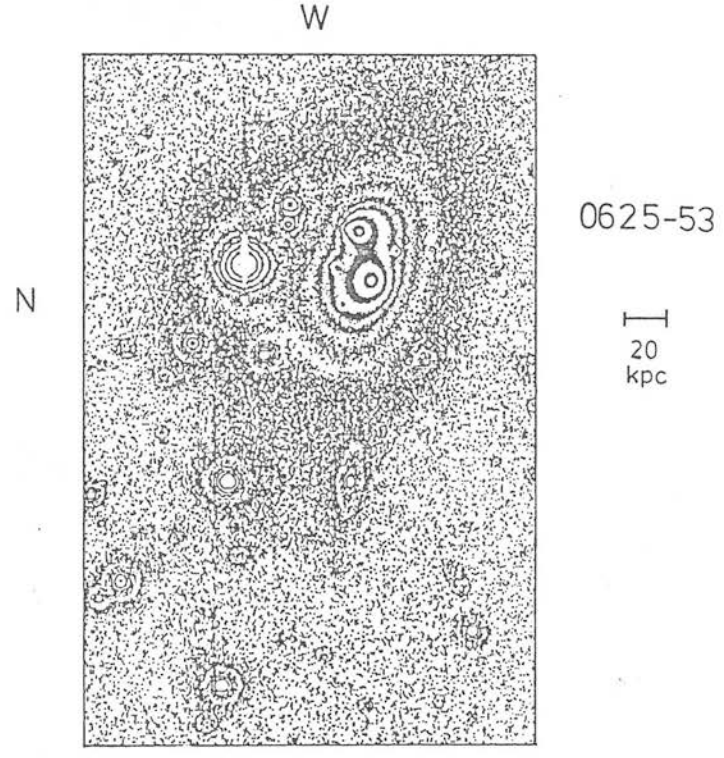
W
N
0625-53
20
kpc

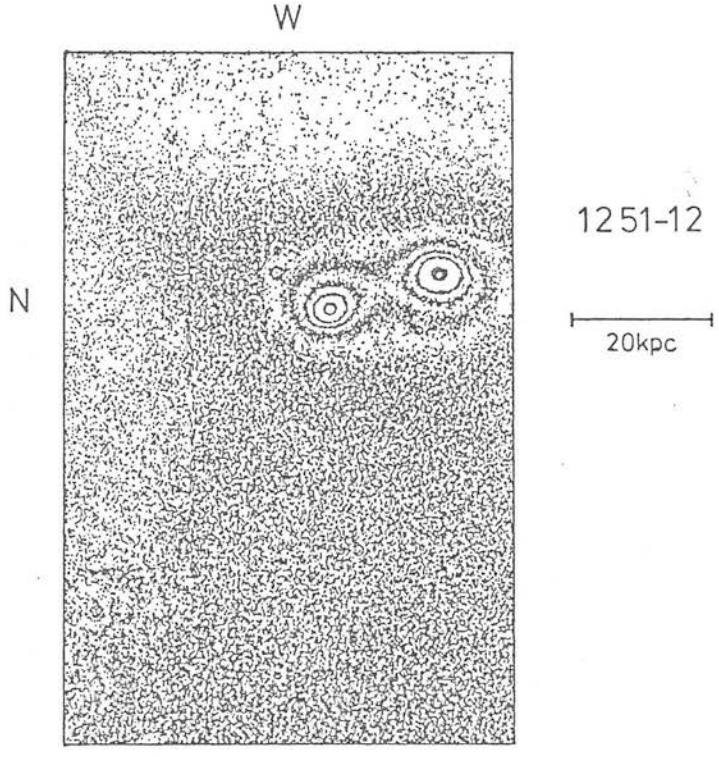
W
N
1251-12
20kpc

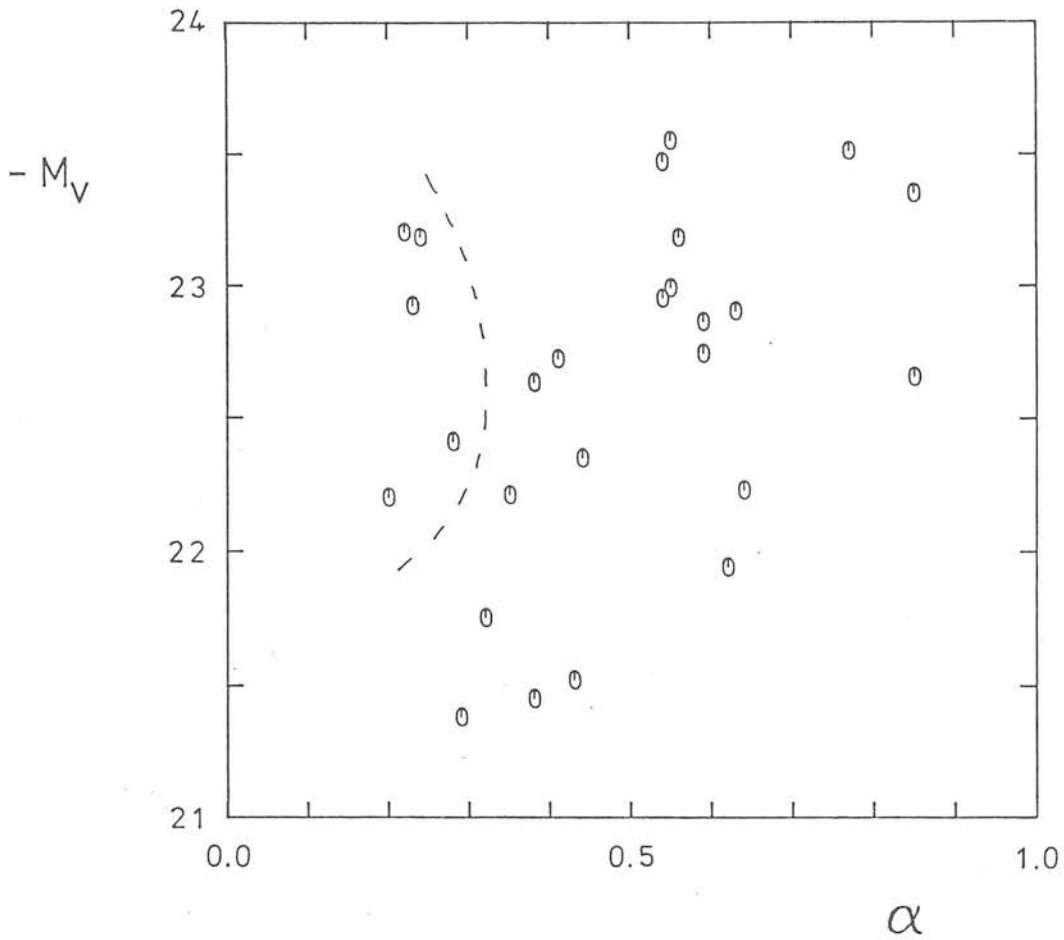

Figure 6.3. The (Mv - α) Diagram. The sources to the left of the dashed line are the broad-line radio galaxies.

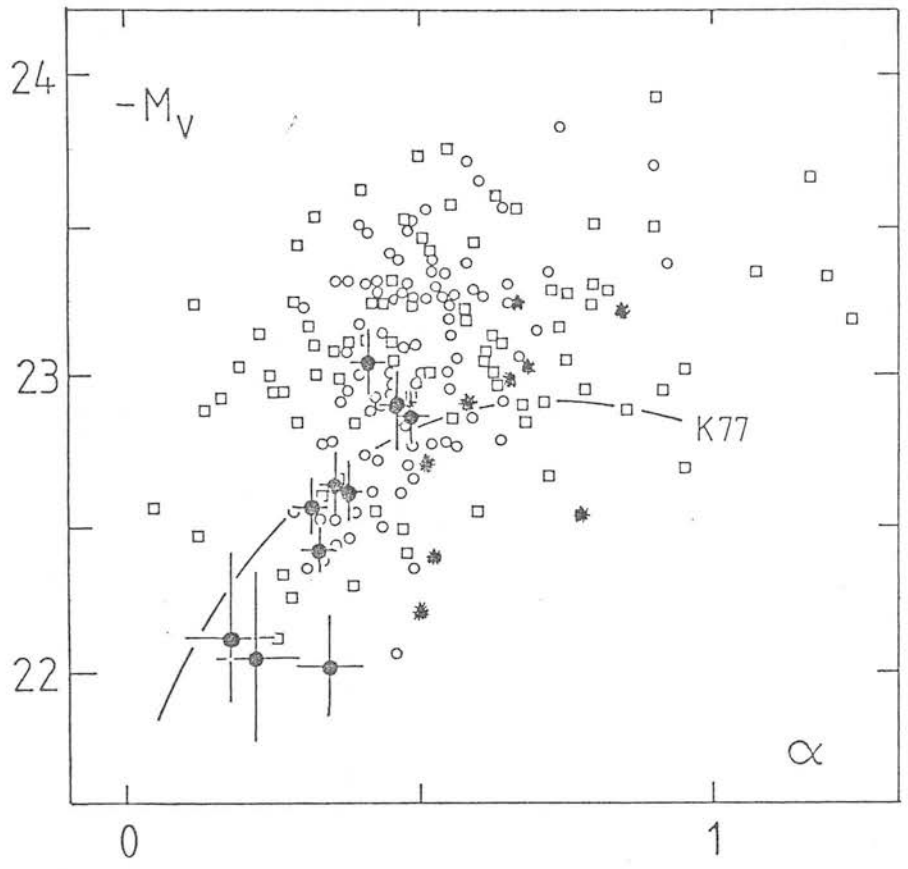

Figure 6.4. The (Mv- α) Diagram illustrating the results of previous workers (reproduced from LML).

o = 1st ranked Abell cluster galaxies from Hoessel (1980)
□ = 1st ranked Abell cluster galaxies from Schneider et al. (1983)
* = cD galaxies in poor clusters from Thuan and Romanishin (1981)
● = 3C radio galaxies from LML (1984)

The dashed curve is the equivalent in the (Mv- α) plane of the Be-logRe relation of Kormendy (1977).

values of α (> 1.0) demonstrated by some of the Schneider et al. objects are not found, although this may be due to the smaller sample size used here. Our sources do appear to have slightly fainter magnitudes however, with a number of objects (with small α)having Mv > -22.

The trend of Mv with α here appears similar to that for the Abell cluster galaxies; the larger galaxies generally having brighter metric magnitudes. This is in contrast to the behaviour of the LML sample. Our sample, which contains galaxies exhibiting radio structures of all types 'fills-in' the top-right corner of the (Mv- α) diagram, which was avoided by the classical-double sample of LML. This immediately demonstrates that galaxies of different radio type are also different in terms of their optical properties. The sources of higher α (> 0.5) do appear to have values of Mv greater than predicted by the Kormendy relation for normal ellipticals, although this effect is not large.

An important point to note in inspecting the (Mv- α) diagram is the effect of the addition of a nuclear component on the parameters. This affects both Mv and α, as can be seen from the definition of α in terms of ratios of surface brightness. The magnitude of this effect depends upon the relative strengths of the stellar and non-stellar components, but its result is to move a galaxy to lower α and brighter Mv. This is graphically indicated if we consider the positions of the broad-line radio-galaxies on Fig. 6.3. These are the galaxies which would be expected to have the strongest nuclear components; they all lie to the extreme top-left corner of the diagram. If allowance is made for this effect, the correlation between Mv and α for the sample appears even more pronounced.

It is possible to investigate the importance of this effect by

comparing the colour of the galaxy with the ratio of α_J to α_R; this is shown in Fig. 6.5 for all the sources for which these parameters are available. Although the numbers are small, the two bluest objects are indeed 0430+05 (a compact broad-line galaxy) and 0521-36 (a Bl-Lac object) and these do have $\alpha_J < \alpha_R$, as expected. Also, the non broad-line galaxies all appear to have normal colours, and α_J/α_R ~1, suggesting that they are not strongly affected by any nuclear component. There is one obviously discrepant object on this diagram, 0349-27. The reason for this is not clear, although the image is rather near the edge of the CCD frame, and may have been affected by this. The source position in the (Mv-α) plane does not appear discrepant, suggesting that it is the Bj image which is at fault, and the R image results have been included in the following discussions.

6.3.b The Relationship between Radio Structure and (Mv-α).

We can now consider the relationship between a galaxy's radio structure, and its position on the (Mv-α) diagram. For all sources taken from the main sample, radio data have been presented in Chapter Three. For the remaining sources, Cambridge synthesis maps are available for 0106+13,0356+10 and 0802+24. 0428-53 and 2356-61 have low resolution Fleurs synthesis maps (Christiansen et al. 1977). 0620-52 and 0625-53 have no synthesis maps available, however, data from the Molonglo telescope suggests that although they are both extended, they do not exhibit double structure (Large, 1981; Hunstead, 1972). As in previous chapters, the simplest division we can make for these sources in terms of their radio morphology is into FR class. This classification is given for all the sources in Table 6.2, and the (Mv-α) diagram with the various classes indicated is shown in Fig. 6.6. A clear distinction between the different types of source is obvious. The FRI sources are

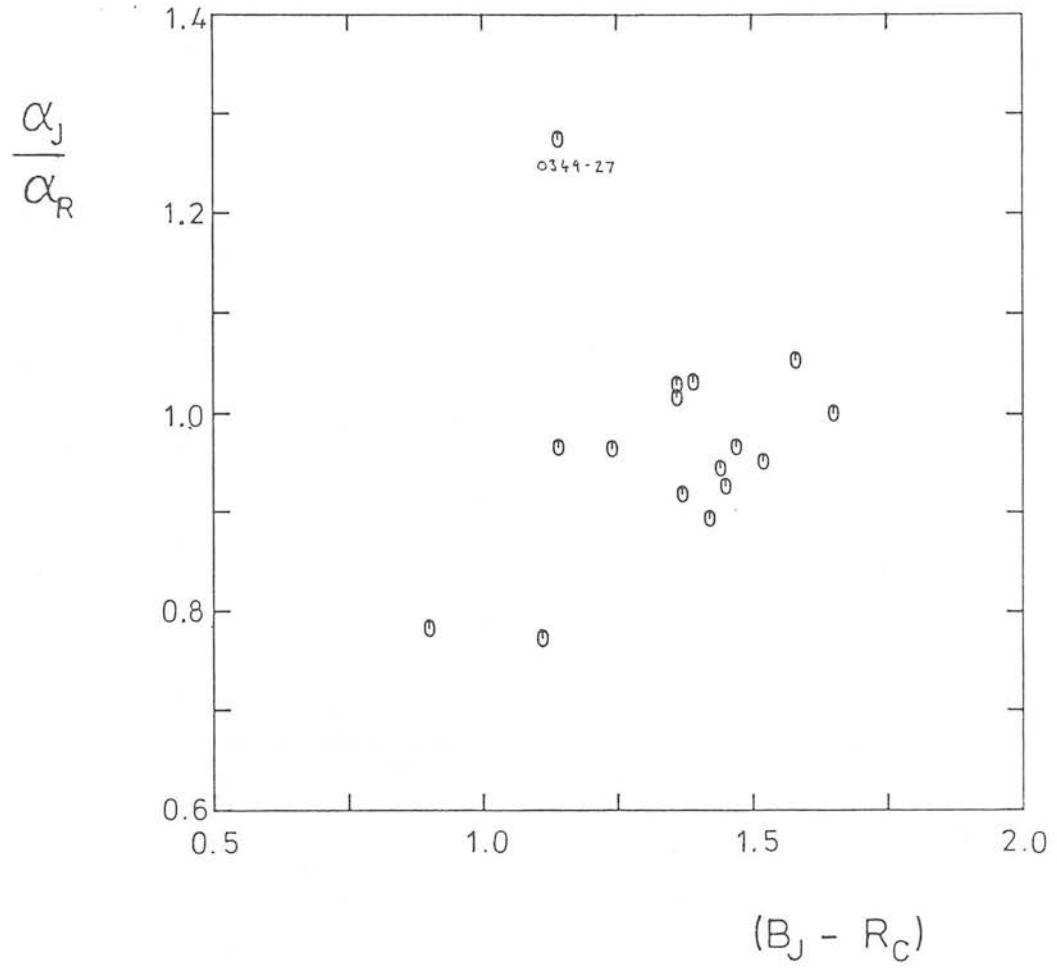

Figure 6.5. The ratio α_J / α_R as a function of $(B_J - R)$ colour.

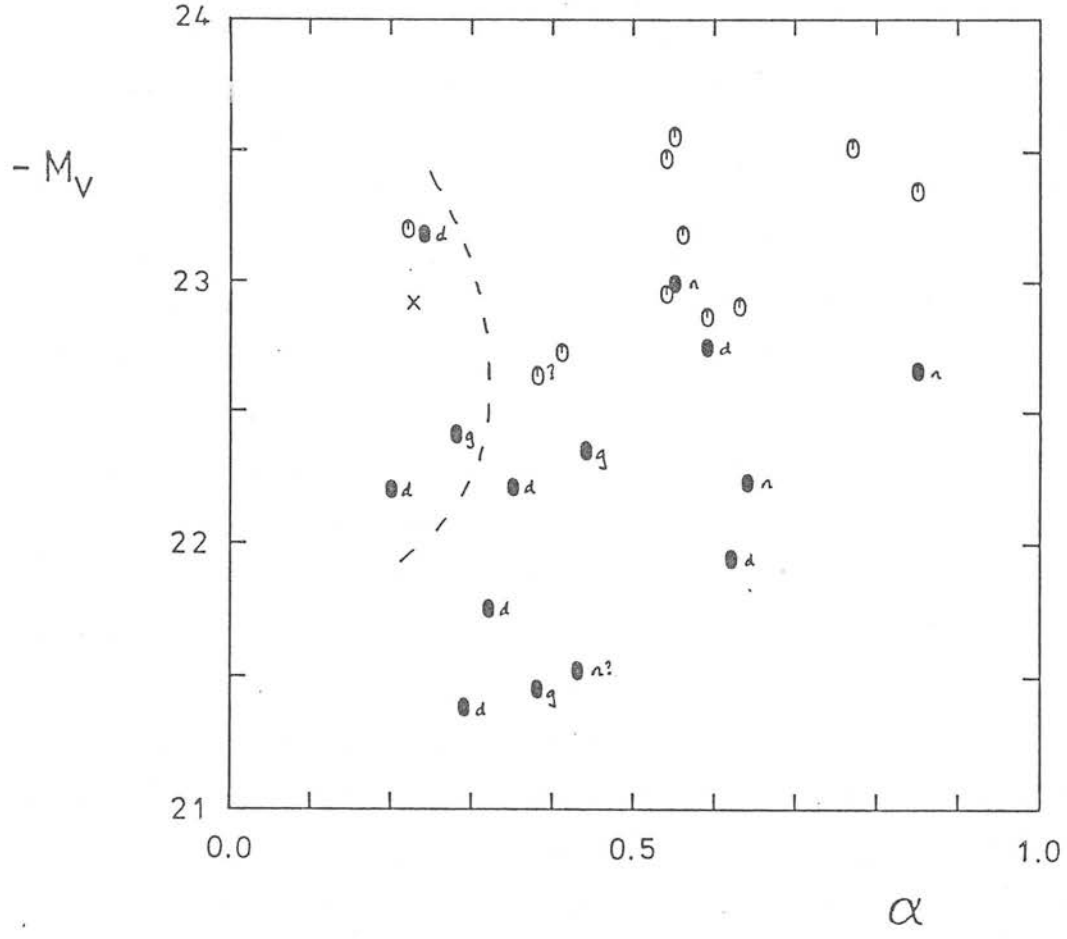

Figure 6.6. The (Mv $-\alpha$) Diagram with source morphology indicated.

(o) = FRI sources
(●) = FRII sources
(x) = compact sources

bright, and have large characteristic radii, while the FRII sources are both fainter and have smaller α. It is difficult to be more quantitative, in terms of radio structure, within the FR classes. However, the following points can also be made. Firstly, the 'classical-double' sources appear the most extreme FRIIs in terms of their (Mv-α) position, lying generally to the very bottom-left hand corner, although this is a rather subjective judgement; FRII sources which lie near the dividing line in (Mv-α) tend to be the less well-defined examples of this class. Secondly, the extended sources with broad-lines, which we assume would lie in the lower left hand corner of the diagram in the absence of any nuclear component, also exhibit FRII morphologies. Finally, it is interesting to note that the five sources with multiple nuclei, not plotted on this diagram, are all FRI sources.

Although a galaxies position on the (Mv-α) plane is amenable to physical interpretation, both Mv and α in isolation are rather arbitrary parameters. Perhaps a more meaningful quantity is the total magnitude of the source, Mvt; this may be simply calculated for the galaxy by assuming a de Vaucouleurs form for the surface brightness profile. Fig. 6.7 show the line in the (Mv-α) plane of fixed total magnitude, for varying α, and also the effect of the addition of a varying non-thermal component. Since these lines are fortuitously ~ parallel, we may decompose the broad-line radio galaxies, assuming that they have underlying stellar components similar to the other sources, and obtain an estimate of the total magnitude of all the objects. The value of Mvt computed is such a manner is also given in Table 6.2.

We may now compare this quantity with the radio luminosity of the sources, calculated as in chapter Four. This is shown in Fig. 6.8, with the sources again divided according to FR class, and with

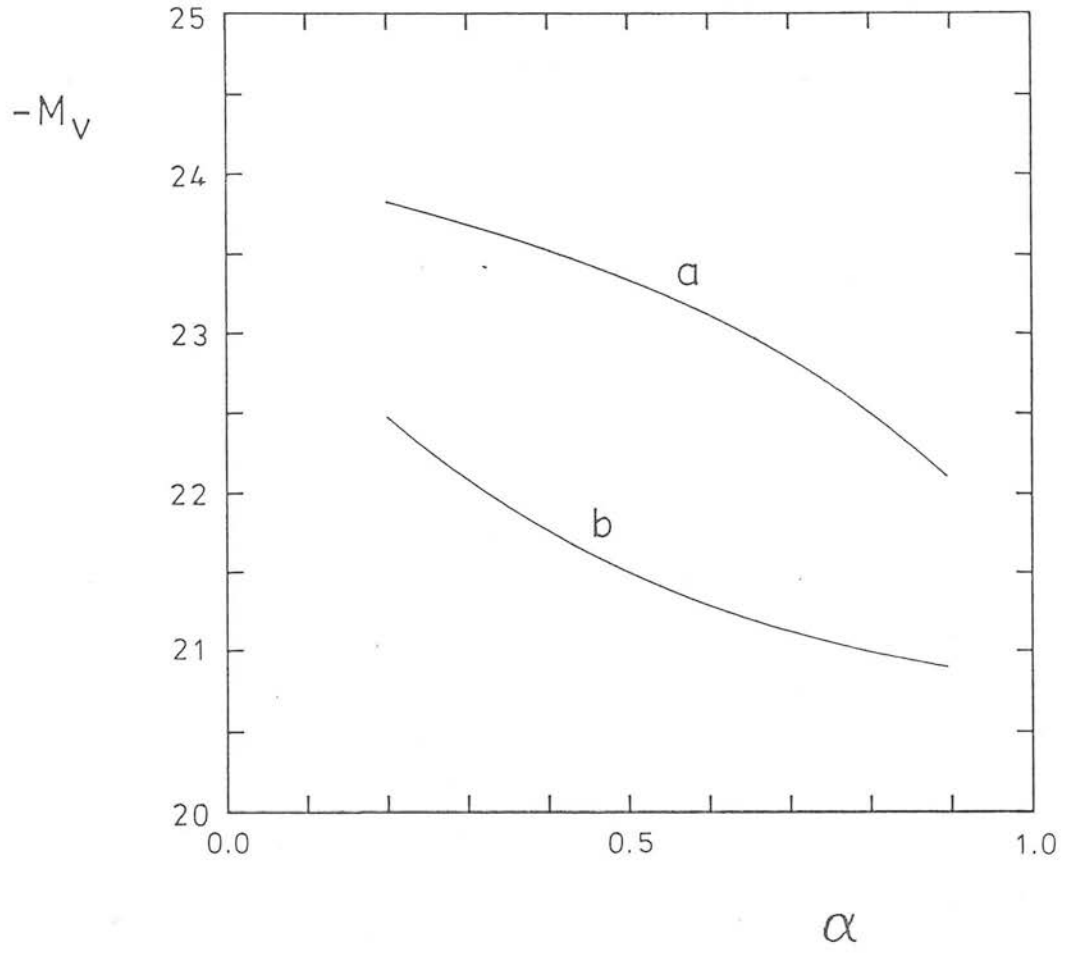

Figure 6.7. The variation of Mv with α :

a) For a fixed total magnitude.

b) For the addition of an increasing unresolved non-thermal component. (L(r) in equation 6.2 is increased, without changing I(r)). The effect is to move a galaxy to progressively smaller α and brighter Mv; i.e. a galaxy with a 'true' α of 0.9 would be moved along curve (b) to the left by the presence of an increasing non-thermal component.

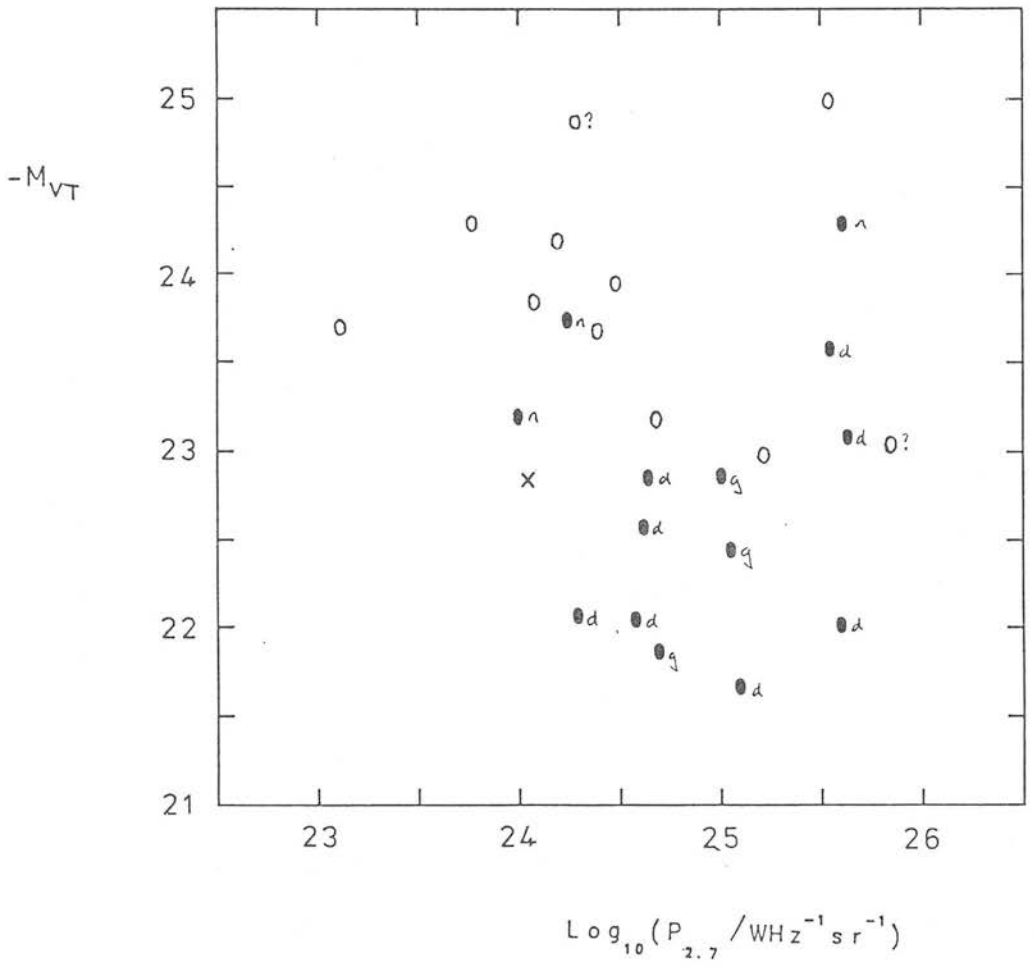

Figure 6.8. A plot of total magnitude versus 2.7GHz luminosity for FRI (o) FRII (●) and compact (x) sources.

the classical doubles indicated. It is interesting to compare this diagram with Fig. 5.7, the plot of Bgg* versus log(P) for approximately the same sample.

6.3.c The Relationship between Optical Spectra and (Mv-α)

The second important area to explore is the relationship between optical spectral type, and optical structure. The optical spectra available for the sources form a much less homogeneous data-set than the radio data. However, reasonably complete spectral data have been obtained for the majority of the sources; information for a number was kindly supplied by Drs. G. Gilmore and R. Fosbury, while others have been the subject of investigations by Osterbrock and collaborators, and Danziger and collaborators (see Table 6.2 for references). Spectra for the remainder have been taken from a variety of sources, also given in Table 6.2.

In view of the inhomogeneity in the data, a simple classification approach as used by Hine and Longair was adopted; objects were classified either as broad-line sources, as sources exhibiting strong narrow emission lines such a [OII]3727, [OIII]4959,5007, [NeIII]3869 (type A), or as sources with weak or no emission lines (type B). This definition does not correspond exactly to that of Hine and Longair, since not only the [OII] line was considered (e.g. sources noted in original references as having 'strong lines' were so classified here). However, the classification scheme is broadly similar. There is an obvious lack of quantitative information in these classifications, but for the majority of the sources they are fairly reliable. In particular, it is unlikely that any broad-line galaxies have been missed. Only two sources are seriously lacking in data; no information has been obtained for 1318-43, while 0043-42 has only the original photographic redshift

reference available. Presumably, for this source emission lines of [OIII] and H β would have been observed, if present. No emission lines were noted as having been used in the redshift determination however, and so this source has been tentatively classified as type B. 0518-45 (Pictor A) has been included in the narrow emission line class, although it does show some evidence for broad lines. This unusual object has been discussed by Danziger et al. (1977), and it is possible that much of the emission is not photo-ionised by a non-stellar nucleus.

The (Mv- α) diagram with this subdivision is shown in Fig. 6.9. Not suprisingly, since we know that FR class and spectral type are related, this diagram appears similar to Fig. 6.6. However, if anything, the division is more obvious here, with almost no overlap between the different spectral types. For example, it is interesting that one of the less-typical FRII sources, 2211-17, shows no evidence for strong lines, and this classification is more in line with its position on the (Mv- α) diagram; 0325+02 and 0131-36, which have no evidence for hot-spots, and are class B galaxies, also have comparatively large Mv and α.

6.3.d Relationship between (Mv- α) and Clustering

The final relationship we will consider is that between the cluster environment of the source, as measured by Bgg*, and the values of Mv and α. The values of B are taken from Table 5.3, although no values are available for the majority of the southern sources, since these were chosen at random from a much larger sample of possible candidates.

A plot of Bgg* versus for the sample is shown in Fig. 6.10. It can be seen that there is a good correlation between these

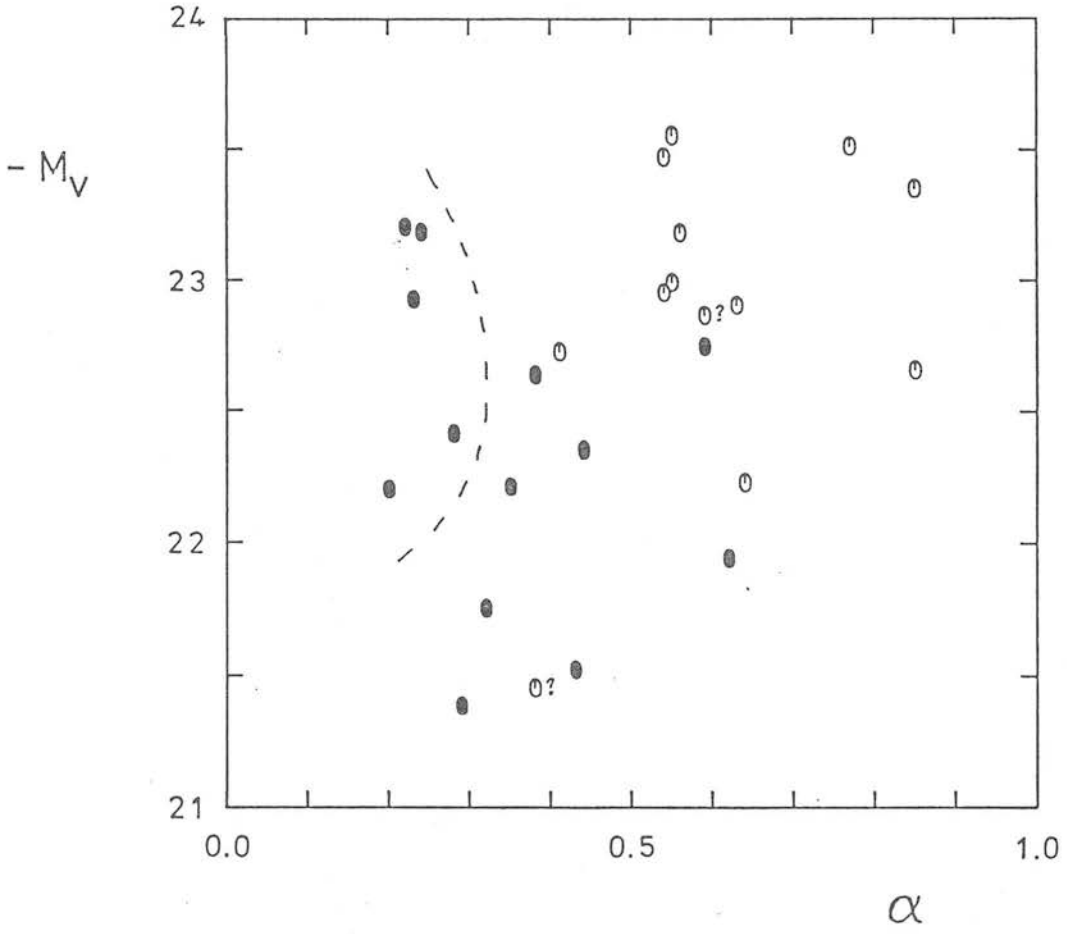

Figure 6.9. The (Mv - α) Diagram with source spectral type indicated.

(●) class A galaxies
(o) class B galaxies

The broad-line radio galaxies lie to the left of the dashed line.

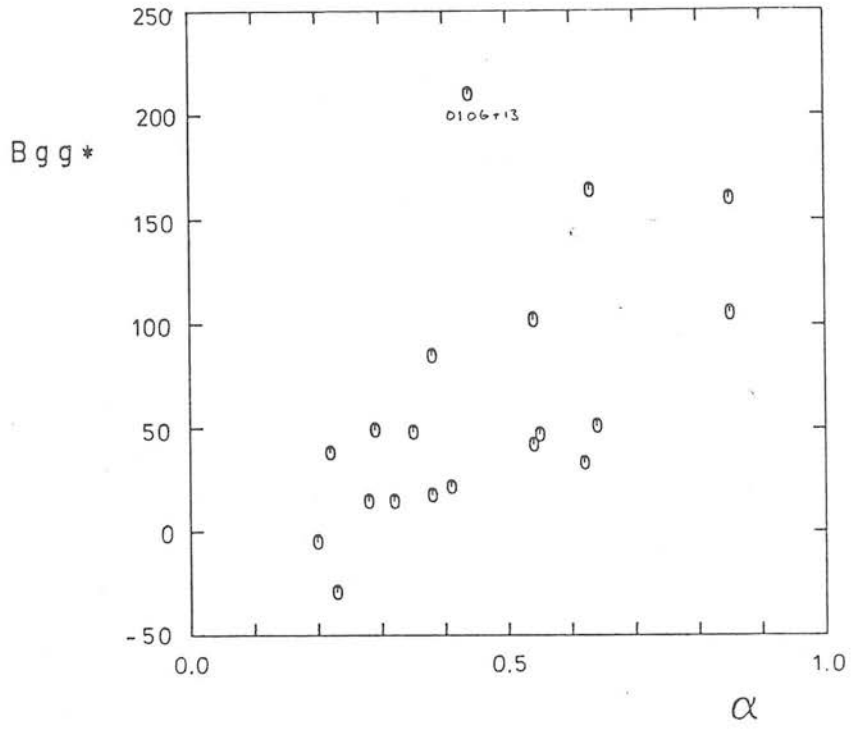

Figure 6.10. A plot of Bgg* versus α .

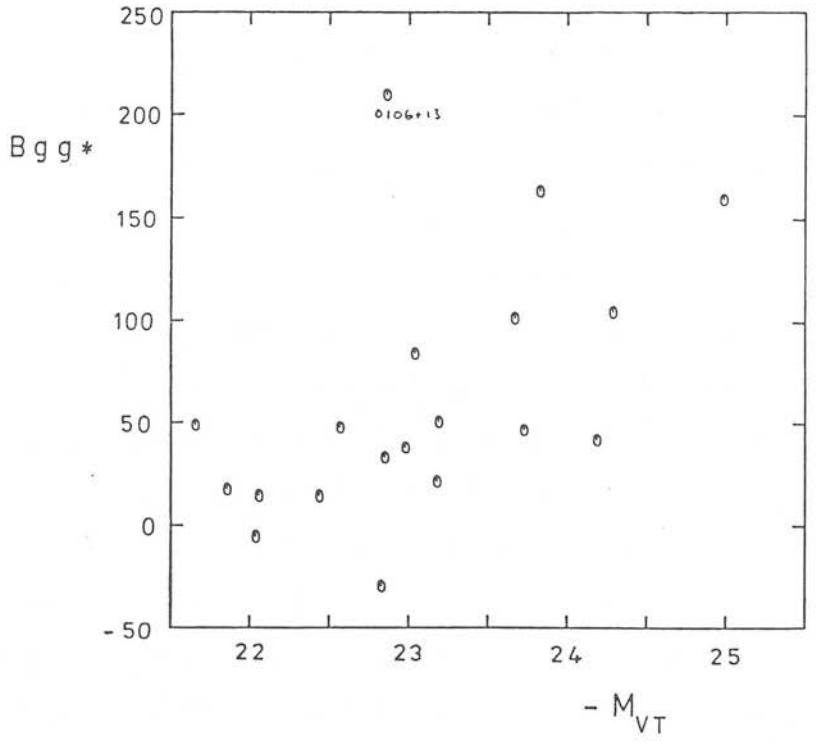

Figure 6.11. A plot of Bgg* versus Mvt.

quantities; sources of high α appear in rich cluster environments, while those with low α have comparatively few close neighbours. A similar result is obtained for the correlation of Bgg* with Mvt (Fig. 6.11), the advantage of this representation being that the broad-line radio galaxies have been 'corrected' in this plot for their non-thermal component. One source, 0106+13 (3C33) appears to have a rather large value of Bgg* for its Mvt. It was suggested in Section 4.6.b that in fact this source might have a spuriously high value of Bgg*, due to contamination of the galaxy counts by a nearby cluster. It's position on this plot does seem to confirm this; and also demonstrates that the position of a galaxy in the (Mv-α) plane is perhaps a pointer to its galaxy environment which is less susceptible to error than Bgg*.

6.3.e The Double-Nuclei Objects

As has been discussed above, the incidence of multiple nuclei in first-ranked Abell cluster galaxies (e.g. Hoessel 1980) has often been cited as one of the most direct pieces of evidence that the process of merging is taking place. However, recent observational studies have shown a number of these systems to have high relative relative velocities (e.g. Wirth et al., 1982) and some theoretical work has suggested that other properties of cD galaxies (their central location and extended envelopes) may be a result of dynamical processes that occured during cluster formation (Merritt, 1984). Indeed, image processing studies of multiple nuclei have shown that in many cases there is little evidence that these 'nuclei' are actually interacting with the envelope of the cD (Lauer, private communication). It is therefore of special interest that a number of the sources observed here do show unequivocal evidence of merging. These are the five 'dumb-bell' systems, contour plots for which have been shown in Fig. 6.2.

Two of these objects, 0625-53 and 1251-12, are especially striking. In each case the centres of progressively fainter isophotes in each of the two galaxies in the dumb-bell system move along axes tangential to the centre of mass, and the effect is seen in opposite directions in the two components of each system (Fig. 6.12). This suggests a picture in which the envelopes of the two galaxies have felt the strongest effects of the interaction, while the nuclei still orbit the centre of mass relatively unaffected. In the case of 0625-53, the isophotes also show a tidal distortion towards the centre of mass, indicated by the 'x' shaped cross-over of the isophotes at the centre of the bridge. Note that for 1251-12, and also for 0123-01, which both have compact emission, this is associated with only one of the nuclei, and the other does not appear to be active.

While the other three systems are not quite so dramatic, their surface brightness distributions are still noteworthy. In each case, both nuclei are symmetrically displaced from the centre of the outer isophotes, which again appear to be centred upon the approximate centre of mass of the system. This appears most pronounced for 0255+05, for which the outer isophotes are almost spherical. It seems highly likely that the end result of this interaction will be a system which appears spherically symmetric, with a magnitude typical of a bright cD galaxy, and indeed all of these objects appear excellent examples of a current merger.

We can now consider how these objects are related to the remainder of the sample. As noted, all the objects exhibit FRI emission. In fact, as discussed in Chapter Three, those with high resolution maps available (0123-01, 0255+05, 1251-12) appear amongst the most complex of the sources observed. 0255+05 and 1251-12 also exhibit definite 'head-tail' structure, consistent with the parent

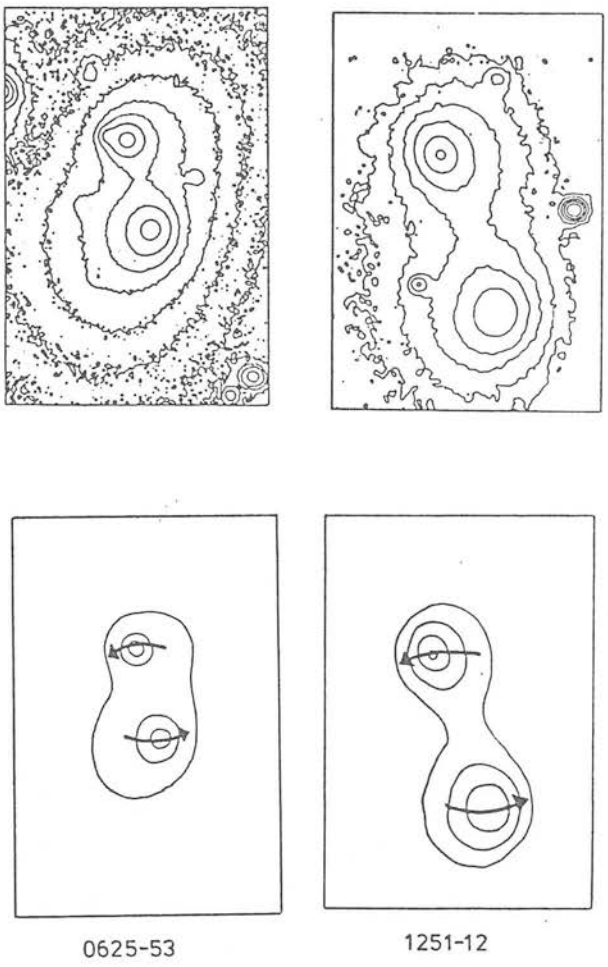

Figure 6.12. A schematic illustration of the inner isophotes of 0625-53 and 1251-12.

galaxy being accelerated by the interaction. In terms of their environment, these five sources also show comparatively high values of Bgg*; and we might therefore expect their dynamical histories to have been similar to the other FRI sources, which also lie in rich environments. The fact that these are the sources which show large Mv and α is compelling evidence that this may be taken as indicative of a history of galaxy merging in these systems.

6.4 : Conclusions

The results of this chapter have provided a number of important insights into the properties of giant elliptical galaxies.

Firstly, considered as a whole, the sample provides good evidence that the process of galaxy merging is occuring in the centres of rich clusters. Support for this fact comes from the result that, for a sample of galaxies selected solely upon the basis of their radio properties, there is a good correlation between the local galaxy denisty within 1Mpc of the source, and the source structure, as measured by Mv and α. Sources with large Mv and α have Bgg*/Bgg $\sim$ 2-4, typical of Abell clusters, while sources which have Bgg*/Bgg $\sim$ 1 have values of $\alpha \sim 0.3$, that suggested by Hoessel (1980) to be appropriate for galaxies which have not undergone merging. Of course, the observed relationship may be interpreted as a result of an independent Bgg*-Mvt relation, with the (Mv-α) correlation simply being an extension of that of Kormendy (1977). However, a convincing argument for the merging hypothesis is the presence of five obvious double-nuclei galaxies in the sample. The fact that all these systems exhibit FRI emission, which naturally places them in the top-right corner of the (Mv-α) diagram, is strong evidence that the other sources are the remnants of less

recent mergers.

In terms of both radio structure, and optical spectral type, the (Mv- α) diagram exhibits a clear division; FRII/Class A objects have low Mv and α, while FRI/Class B objects have large Mv and α. In fact, the spectral-class/morphological-type correspondence appears even more convincing if we consider an equivalence between classical double sources and strong emission line objects; while the number of non-classical double FRII sources is small, their position in the (Mv- α) plane is consistent with this division. Although a small point, it is also worthwhile to note that the position of the broad-line radio galaxies is consistent with them being identical to the narrow-line galaxies in terms of their optical morphologies, (and hence environments) apart from the addition of an unresolved non-thermal component in the nucleus.

The above discussion is in complete accord with the hypothesis of LML that the classical double sources observed by them are not the same in terms of their optical properties as the lower-luminosity radio sources which gave rise to the original cD classification. They have discussed the importance of this for e.g. Hubble diagrams using classical-double sources to fill in the high-redshift regions. Here we are concerned with the physical origin of the difference between the different classes of radio source. Superficially, the division between FRI and FRII sources, in the (Mv- α) plane, which may be made almost perfectly by a line of total magnitude, suggests that it might be the presence of merging which is important. However, we should note that although the division by Bgg* is perhaps not quite as good, the value of Bgg* is much more susceptible to contamination, and random errors in the observable quantities. The close connection between environment and merging, noted above, means that a division between FRI and FRII

sources will occur in both measures, regardless of which is the most fundamental. This problem will be discussed in the next chapter, which draws together the results obtained in the thesis as a whole.

Chapter 7 : GENERAL SUMMARY AND DISCUSSION

The main results of this thesis, apart from the optical and radio data presented in Chapters Two and Three, may be summarised as follows:

1) there is a definite correlation between the local galaxy density within 1Mpc and the structure of extended radio sources. FRI galaxies appear in regions of generally enhanced galaxy density, while FRII sources on average lie in regions of galaxy density typical of that for galaxies in general. In terms of Bgg*, there is no definite distinction between "classical" and "non-classical" double FRII sources, although the non-classical doubles may span the range between FRI and classical-double FRII sources.

2) Compact radio sources do not appear in regions of enhanced galaxy density. This is strong evidence against 'unified' models for these objects.

3) The local environment of a galaxy is closely related to its total magnitude, and its position in the ($Mv - \alpha$) plane. Good evidence that the observed correlation between Mv and α is caused by the merging of galaxies is the fact that five of the sixteen FRI galaxies (which all lie in the bright Mv, high α region of the diagram) exhibit interacting double nuclei.

4) The relation between radio morphology and spectral type occurs here as essentially a 1:1 correspondence; FRI galaxies have weak or absent emission lines, while FRII galaxies exhibit strong emission line spectra. There is slight evidence (supported by their position in the ($Mv - \alpha$) diagram) that the FRII non-classical

doubles should be classed with the FRI galaxies in this respect.

One immediate point is that correlations between all of the properties di cussed above will appear if any small sub-set of them are physically related. Thus for example, the correlation between FR class and spectral type may arise if both are independently correlated with the galaxy's environment. The questions to be answered are; which are the fundamental relations giving rise to the observed correlations, and how are these relations explained in terms of basic physical processes.

Firstly, we may consider the relationship between merging and environment, and their possible effects upon radio source structure. We would expect (and indeed observe) that mergers have occured more often in regions of high galaxy density. This makes it difficult to determine whether it is the presence of merging, or simply the environment alone which is responsible for the observed division between FRI and FRII sources.

The presence of a concurrent merger can be ruled out as a pre-requisite for all FRI sources, since the majority of the FRI galaxies do not exhibit evidence for a continuing occurance of the process. Mergers may be important however, if the conditions inside a merger remnant which are important for the radio-emission process have changed in comparision to galaxies which have not undergone merging (e.g.mergers are more 'bloated'). However, good direct evidence to support the argument that it is the environment that is important is the absence of any FRII type emission from second or third-ranked cluster members (McHardy, 1979); these are galaxies which would have low Mv and α ,but high Bgg*. We will therefore base the following discussion upon the hypothesis that the merging process (as discussed in Chapter Six) is not the main cause of the

FRI/FRII division, but is simply a result of the differing galaxy environments for the two classes of object.

We thus return to the question of how the environment may modify the observed form of the radio emission; and what causes the difference in the optical emission line strengths between the two types of object. Again, this latter effect may be caused by the same physical process which causes the FRI/FRII morphological division, or it may be due to an unrelated correlation with other properties of the source. In this respect, it is worth noting the results of Miller (1983b, see also Fabbiano et al. 1984). He performed an X-ray survey of a complete sample of 3CR radio-galaxies, and considered a number of correlations which were present in this sample. The sources studied consisted of all 3CR galaxies with $S_{178} > 10$ Jy, $V < 18$, $|b| > 10^{o}$ and $\delta > 10^{o}$. This provided a sample of 43 sources, all but one with $z < 0.2$, of which 40 were observed with the Einstein satellite, in a variety of programmes. Twenty-six sources were detected, data for twenty-one of which were available for analysis.

The poor angular resolution of the X-ray observations made it difficult to distinguish with certainty the exact source of emission. Rich clusters of galaxies are known to be sources of X-ray emission, so that this would be expected for radio galaxies within clusters, regardless of any intrinsic emission. However all the FRII sources appeared unresolved with the IPC, and upper limits on the size of the X-ray emitting regions were smaller than the radio angular size for three of the largest sources. This suggests that the dominant X-ray emission in these galaxies does not arise from the radio lobes, or from any hot gas which is extended on the scale of the lobes. The overall conclusion was that the X-ray emission from isolated galaxies is dominated by emission from an active

nucleus, and that radio galaxies in clusters of galaxies probably also have nuclear X-ray emission.

In terms of radio structure, Fabbiano et al. found that the FRII sub-sample tended to include higher X-ray luminosity sources than the FRI sample. While this difference was not large, they noted that the true distribution of X-ray luminosities would be biassed by the presence of cluster emission, as described above. As the majority of sources affected in this way are FRI sources, allowance for this effect would tend to separate the two classes even further. Not suprisingly, the distribution of X-ray luminosity for the sample between class A and B sources was similar to that for the FR division. Fabbiano et al. noted that the galaxies with the broadest permitted lines tended to have the highest X-ray luminosities; there was also a strong correlation between the X-ray luminosity and the nuclear component radio luminosity for the sources in the sample. The most obvious interpretation for this is that the X-rays are emitted from the active nucleus, although there need not be a direct link between the radio and X-ray emission.

Finally, Fabbiano et al. considered the relationship between the nuclear radio luminosity of the radio galaxies, and their total luminosity. Due to difficulties in isolating the core luminosities of FRI sources (since many have jets extending into the core) the results were based upon correlations in the FRII subsample, although the correlations were also indicated in the FRI sub-sample. They found that there did appear to be a correlation between the core radio luminosity and the total radio luminosity, in the sense that more radio powerful galaxies had stronger cores. Such a correlation has also been found by Burns and Gregory (1982) for a sample of 4C radio galaxies in poor clusters, including both FRI and FRII sources.

We therefore have a general picture where FRII galaxies are luminous, have simple well defined double structure, strong nuclear activity, as evidenced by radio and X-ray emission, strong optical emission lines, and fairly typical local galaxy environments. FRI sources on the other hand have lower luminosities, weaker core activity, with weak or absent emission lines, and lie in regions of generally enhanced galaxy density.

A possible explanation for these differences may lie with the strength of the nuclear activity. We might suppose that a stong 'central engine' will produce stable beams, capable of transmitting large amounts of kinetic energy per second to the hot-spots. The most powerful sources are those in which the beams are able to transmit this energy to the extremities of the source; the classical doubles. Less powerful beams produce less powerful hot-spots, so that a larger fraction of the radiation comes from the more diffuse radio-emitting region accumulated over the life-time of the source. Miller et al. (1985) have shown that the static thermal pressure of the IGM is insufficient to provide the required confinement for these sources; and we might expect such sources to occur irrespective of the presence or otherwise of a dense IGM. If this were so, then we would expect these sources to have clustering properties typical of ordinary galaxies; some may occur in rich clusters, but this is neither required for, nor rules out, the formation of such sources.

In a source with still weaker beams, the beam might break up because of instabilities and entrainment at its edges, with increased magnetic fields and the acceleration of relativistic particles leading to a 'switching on' of radio emission, and the production of an FRI source. Birkinshaw et al. (1978) have suggested this process to explain the observed correlation between the total

radio luminosity of the source, and the distance from the nucleus of the first rapid increase in brightness for FRI sources. In the weaker sources, the first bright regions of radio emission are observed closer to the nucleus, as we would expect if this mechanism were operating.

This hypothesis provides a possible explanation for the low luminosity and complex morphology associated with the weak core activity in these sources. As there are no radio-emitting hot-spots in these sources, the emission come solely from the diffuse regions. If these are allowed to expand freely then the source will suffer adiabatic losses, and its luminosity decrease. We might thus postulate that a certain density of IGM is required to contain such sources, if they are to remain visible, and this is (generally) found in the regions of enhanced galaxy density; thus explaining the observed difference between the clustering properties of FRI and FRII sources.

The alternative to the suggestion that it is the core activity which is the dominant mechanism in 'deciding' upon the type of source is that the difference in morphology between FRI and FRII sources is due to interactions of the beams with the surrounding environment. The simplest hypothesis is that the beams are either distorted or disrupted by interactions with the environment, and are thus unable to supply energy to the hot-spots. This distortion may be due to the ram pressure of the IGM as the source moves within a cluster, or simply due to the acceleration of the parent galaxy through the gravitational effects of near neighbours (as for example has been suggested for 3C31 by Blandford and Icke, 1978). In the dynamical-bending model, the active galaxy is assumed to be moving with $v > 1000 kms^{-1}$ through the intracluster gas, and the radio emitting regions are swept backwards by the associated ram pressure.

In this model, the wide-angle trails (bent doubles) are supposed to be an intermediate category, between the head-tails and normal double sources, in which the motion of the galaxy causes distortion to a lesser degree. Unfortunately, while the head-tail source are nearly always associated with non-dominant, presumably rapidly moving galaxies (Simon, 1978; McHardy, 1979), bent double sources are identified almost invariably with nearly stationary, dominant D or cD galaxies. These sources therefore present serious difficulties for such a model, and an alternative is to invoke a passive mechanism for bending, such as bouyancy or large-scale mass motions (Burns, 1981; Burns et al., 1982). However, while any of these mechanisms may be working to cause the complex morphology often seen in cluster radio sources, the existence of relaxed but undistorted FRI sources, such as 0055-01, or the 'narrow edge-darkened doubles', such as 1333-33 are difficult to account for by such methods. Thus it seems that intrinsic beam strengths may be an important factor in determining source morphology, irrespective of the cluster environment.

There are two potential problems with the picture suggested above. The first is that there are a number of high-luminosity sources (with strong central components) which exhibit FRI structure, and conversely some weaker sources which exhibit FRII type morphology. These would violate a simple model where the 'stability' of the beam is directly proportional to the strength of the source. (There are also a number of FRII sources without strong cores in our sample.) Also, we have the difficulty of explaining the observed emission-line properties of the sources. The line-strengths of these objects appear to be much better correlated with the radio structure than with the radio core luminosity. For example, while Hine and Longair (1979) find that the cores of class B objects are generally of lower luminosity than those of class A objects, much of

this correlation is due to the separate correlation of both with the total radio luminosity. For a fixed (intermediate) range of total luminosity, the distribution of core luminosity for both class A and class B objects is rather similar. This would therefore suggest that either the optical activity is a better measure of the power of the 'central engine' than the core radio luminosity, or that some other factor is causing the correlation between radio structure and optical activity.

A candidate for this process is again interaction with the source environment. Gunn and Gott (1972) have suggested that ram-pressure of the IGM might strip the galaxy of its interstellar gas; alternatively, the gas may be lost due to thermal evaporation by a hot IGM (Cowie and Singaila, 1977). That some form of gas removal is occuring for galaxies in clusters has been demonstrated by Gilser (1979), who showed that emission lines are less common for cluster ellipticals in general, as compared to field galaxies. Thus we might expect that in some cases, interactions with the IGM could both prevent the formation of a classical-double source, by distortion of the beams, and also remove the line-emitting gas from the galaxy, in accordance with observations.

7.1 : Suggestions for Future Work

The investigations described in this thesis have of necessity made use of fairly crude measures of the various properties of the sources, with a simple structural classification, the description of the cluster environment by a single parameter, and a rather basic and subjective spectral division. There are thus a number of areas where further investigations would be desirable.

Perhaps the most pressing requirement is for homogenous optical spectra for all the members of the sample, with quantitative and absolute measurements of emission line strengths. This would allow a confirmation that the mechanism for line formation is indeed photo-ionization by a non-thermal continuum, and also for a correlation of line strengths with other forms of nuclear activity to be made. We would then be in a position to make a more definite statement as to whether the emission-line strength is simply related to the core activity in the source, or whether it is significantly modified by the cluster environment.

Multi-object spectroscopy of the fields of a number of sample members would also be of interest. At an immediate level, such observations would allow unambiguous foreground object removal, as well as providing cluster velocity dispersions and the velocity of the radio source relative to the cluster. Together with minimum pressure estimates from the radio data, this would enable IGM densities to be estimated, and thus allow an investigation into the possible magnitude of any ram-pressure effects. Long-slit spectra of the double-nuclei objects would also be of interest, to allow relative velocities to be obtained for the nuclei and the envelopes.

A detailed study in such a manner, for a small number of objects, would compliment the statistical analyses described in this thesis. Especially useful would be the detailed comparison of different objects selected to be as similar as possible in one property. For example, we might compare high-B FRII galaxies with FRI galaxies in similar environments; or the sources with the most extreme values of α at a given value of B. A knowledge of the X-ray properties of these systems (e.g. from the Einstein data-bank) would provide further information on environment; and detailed galaxy distributions would allow for a comparison of the relative

importance of global/local cluster properties.

Finally, an extension of these studies to higher redshifts would be of interest. This would be especially desirable in order to search for any changes in the environments of the classical double sources, which might provide a physical explanation for the observed cosmological evolution of the radio source population.

REFERENCES

Adgie, R.L., Crowther, J.H. & Gent, H., 1972. Mon. Not. R. astr. Soc., 159, 233.

Albert, C.E., White, R.A. & Morgan, W.W., 1977. Astrophys. J., 211, 309.

Anguita, C. & Pedreros, M., 1977. Astron. J., 82, 102.

Arp, H. & Bertola, F., 1971. Astrophys. J., 163, 195.

Bahcall, N.A., 1977. Ann. Rev. Astr. Astrophys., 15, 505.

Bautz, L.P. & Morgan, W.W., 1970. Astrophys. J., 162, L149.

Bessell, M.S., 1979. P.A.S.P., 91, 589.

Birkinshaw, M., Laing, R., Scheuer, P. & Simon, A., 1978. Mon. Not. R. astr. Soc., 185, 39P.

Blair, M. & Gilmore, G., 1982. P.A.S.P., 94, 742.

Blandford, R.D. & Icke, V., 1978. Mon. Not. R. astr. Soc., 185, 527.

Blandford, R.D. & Rees, M.J., 1974. Mon. Not. R. astr. Soc., 169, 395

Bolton, J.G., Clarke, M.E. & Ekers, R.D., 1965. Aust. J. Phys. 18, 627.

Bolton, J.G. & Ekers, J., 1966. Aust. J. Phys., 19, 559.

Bolton, J.G., Gardner, F.F. & Mackey, M.B., 1964. Aust. J. Phys., 17, 340.

Bolton, J.G. & Kinman, T.D., 1966. Astrophys. J., 145, 951.

Bozyan, E.P., 1979. Astron. J., 84, 910.

Browne, I.W.A., Orr, M.J.L., Davies, R.J., Foley, A., Maxlow, T.W.B. & Thomasson, P., 1982. Mon. Not. R. astr. Soc., 198, 673.

Burbidge, G. & Crowne, A.H., 1979. Astrophys. J. Suppl., 40, 583.

Burns, J.O., 1981. Mon. Not. R. astr. Soc., 195, 523.

Burns, J.O. Eilek, J.A. & Owen, F.N., 1982. in "Extragalactic Radio Sources, IAU Symp 97", p45. ed Heeschen, D.S. & Wade, C.M., Reidel, Dordrecht.

Burns, J.O. & Gregory, S.A., 1982. Astron. J., 87, 1245.

Burns, J.O. & Owen, F.N., 1977. Astrophys. J., 217, 34.

Burnstein, D. & Heiles, C., 1982. Astron. J., 87, 1165.

Burbidge, E.M. & Burbidge, G.R., 1972. Astrophys. J., 172, 37.

Christiansen, W.N., Frater, R.H., Watkinson, A., O'Sullivan, J.D. & Lockhart, I.A., 1977. Mon. Not. R. astr. Soc., 181, 183.

Clarke, M.E., Bolton, J.G. & Shimmins, A.J., 1966. Aust. J. Phys., 19, 375.

Conover, W.J., "Practical Non-Parametric Statistics", J Wiley & Sons.

Costero, R. & Osterbrock, D.E., 1977. Astrophys. J., 211, 675.

Cowie, L.L. & Songaila, A., 1977. Nature, 226, 501.

Danziger, I.J., Fosbury, R.A.E., Goss, W.M., Bland, J. & Boksenburg, A., 1984. Mon. Not. R. astr. Soc., 208, 589.

Danziger, I.J., Fosbury, R.A.E., Goss, W.M., & Ekers, R.D., 1979. Mon. Not. R. astr. Soc., 188, 415.

Danziger, I.J., Fosbury, R.A.E. & Penston, M.V., 1977. Mon. Not. R. astr. Soc., 189, 41P.

Danziger, I.J. & Goss, W.M., 1983. Mon. Not. R. astr. Soc., 202, 703.

de Ruiter, H.R., Willis, A.G. & Arp, H.C., 1977. Astron. & Astrophys. Suppl., 28, 211.

de Vaucouleurs, G., de Vaucouleurs, A. & Corwin, H.G., 1976. "Second Reference Catalogue of Bright Galaxies", University of Texas Press, Austin.

Dressler, A., 1978. Astrophys. J., 222, 23.

Ekers, R.A., Goss, W.M., Kotanyi, C.G. & Skellern, D.J., 1978. Astron. Astrophys., 69, L21.

Ellis, R.S., 1982. In "The Origin and Evolution of Galaxies", ed. Jones, S.J.T. & Jones, J.E., Reidel, Dordrecht.

Fabbiano, G., Miller, L., Trinchieri, G., Longair, M., & Elvis, M., 1984. Astrophys. J., 277, 115.

Fanaroff, B.L. & Riley, J.M., 1974. Mon. Not. R. astr. Soc., 167, 31P.

Fomalont, E.B., 1971. Astron. J., 76, 513.

Fomalont, E.B. & Moffet, A.T., 1971. Astron. J., 76, 5.

Goss, W.M., Danziger, I.J., Fosbury, R.A.E. & Boksenburg, A., 1980. Mon. Not. R. astr. Soc. 190, 23P.

Graham, J.A., 1982. P.A.S.P., 94, 244.

Griffin, R.F., 1963. Astron. J., 68, 421.

Groth, E.J. & Peebles, P.J.E., 1977. Astrophys. J., 217, 385.

Gunn, J.E. & Gott, J.R., 1972. Astrophys. J., 176, 1.

Gunn, J.E., Hoessel, J.G., Westphal, J.A., Perryman, M.A.C. & Longair, M.S., 1981. Mon. Not. R. astr. Soc., 194, 111.

Gunn, J.E., & Oke, J.B., 1975. Astrophys. J., 195, 255.

Hausman, M.A. & Ostricker, J.B., 1978. Astrophys. J., 224, 320.

Hawkins, M.R.S., 1981. Mon. Not. R. astr. Soc., 194, 1013.

Hewett, P., 1983. Ph.D. Thesis, University of Edinburgh.

Hewitt, A. & Burbidge, G., 1980. Astrophys. J. Suppl., 43, 57.

Hine, R.G., & Longair, M.S. 1979. Mon. Not. R. astr. Soc., 188, 111.

Hintzen, P., 1980. Astron. J., 85, 626.

Hoessel, J.G., 1980. Astrophys. J., 241, 493.

Hoskins, D.G., Murdoch, H.S. Adgie, R.L., Crowther, J.H. & Gent, H., 1974. Mon. Not. R. astr. Soc., 166, 235.

Hunstead, R.W., 1971. Mon. Not. R. astr. Soc., 152, 277.

Hunstead, R.W., 1972. Mon. Not. R. astr. Soc., 157, 367.

Hunstead, R.W., Murdoch, H.S., Condon, J.J. & Phillips, M.M., 1984. Mon. Mot. R. astr. Soc., 207, 55.

Jenkins, C.J., Pooley, G.G. & Riley, J.M., 1977. Mem. R. astr. Soc., 84, 61.

Johnson, H.L. & Sandage, A., 1956. Astrophys. J., 124, 379.

Kormendy, J., 1977. Astrophys. J., 218, 333.

Kormendy, J., 1982. In "Morphology and Dynamics of Galaxies", ed. Martinet, L. & Mayor, M., 12th Adv. Course, SAAS-FEE, Geneva Obs.

Koski, A.T., 1978. Astrophys. J., 223, 56.

Kuhr, H., Witzel, A., Pauliny-Toth, I.I.K. & Nauber, U., 1981. Astr. Astrophys. Suppl. Ser., 45, 367.

Kuhr, H., Nauber, U., Pauliny-Toth, I.I.K. & Witzel, A., 1979. M.P.I.f.R. Preprint No. 55.

Laing, R.A., Riley, J.M. & Longair, M.S. 1983. Mon. Not. R. astr. Soc., 204, 151.

Landolt, A.U., 1983. Astron. J., 88, 439.

Large, M.I., Mills, B.Y., Little, A.G., Crawford, D.F. & Sutton, J.M., 1981. Mon. Not. R. astr. Soc., 194, 693.

Leir, A.A. & van den Bergh, S., 1977. Astrophys. J. Suppl., 34, 381.

Lilly, S.J. & Longair, M.S., 1982. Mon. Not. R. astr. Soc., 199, 1053.

Lilly, S.J. & Longair, M.S., 1984. Mon. Not. R. astr. Soc., 211, 833.

Lilly, S.J., McLean, I.S. & Longair, M.S., 1984. Mon. Not. R. astr. Soc., 209, 401.

Longair, M.S. & Riley, J.M., 1979. Mon. Not. R. astr. Soc., 188, 625.

Longair, M.S. & Seldner, M., 1979. Mon. Not. R. astr. Soc., 189, 433.

Lu, P.K., 1970a. Astron. J., 75, 1161.

Lu, P.K., 1970b. Astron. J., 75, 1165.

Lu, P.K., 1974. Astron. J., 79, 453.

Maltby, P.T., Matthews, T.A. & Moffet, A.T., 1963. Astrophys. J., 137, 153.

Matthews, T.A., Morgan, W.W. & Schmidt, M., 1964. Astrophys. J., 140, 35.

McHardy, J., 1979. Mon. Not. R. astr. Soc., 188, 495.

Merritt, D., 1984. Astrophys. J., 276, 26.

Miley, G., 1980. Ann. Rev. Astron. Astrophys., 18, 165.

Miller, L. 1983a. in "VLBI and Compact Radio Sources, IAU Symp 110", p. 189. ed Fanti, R., Kellermann, K. & Setti, G. Reidel, Dordrecht.

Miller, L. 1983b. PhD. Thesis, Cambridge University.

Miller, L., Longair, M.S., Fabbiano, G., Trinchieri, G. & Elvis, M., 1985, Mon. Not. r. astr. Soc., in press.

Mills, B.Y., 1960. Aust. J. Phys., 13, 550.

Mills, B.Y., Slee, O.B. & Hill, E.R., 1958. Aust. J. Phys. 11, 360.

Morgan, W.W., Kayser, S. & White, R.A., 1975. Astrophys. J. 199, 545.

Moseley, G.F., Brooks, C.C. & Douglas, J.N., 1970. Astron. J., 75, 1015.

Orr, M.J.L. & Browne, I.W.A., 1982. Mon. Not. R. astr. Soc., 200, 1067.

Osterbrock, D.E., 1978. Phys. Scripta, 17, 137.

Osterbrock, D.E., Koski, A.T. & Phillips, M.M., 1976. Astrophys. J., 206, 898.

Pauliny-Toth, I.I.K., 1977. In "Radio Astronomy and Cosmology IAU Symp. 74", p.63, ed D.L. Jauncey, D. Reidel, Dordrecht.

Peacock, J.A., & Wall, J.V., 1981. Mon. Not. R. astr. Soc., 194, 331.

Peacock, J.A., & Wall, J.V., 1982. Mon. Not. R. astr. Soc., 198, 843.

Peebles, P.J.E., 1980. "The Large Scale Structure of the Universe", Princeton University Press, Princeton.

Pence, W., 1976. Astrophys. J., 203, 39.

Perley, R.A., 1982. Astron. J., 87, 859.

Perley, R.A., Fomalont, E.B. & Johnson, K.J., 1980. Astron. J., 85, 649.

Phillips, M.M. & Osterbrock, D.E., 1975. P.A.S.P., 87, 949.

Prestage, R.M. & Peacock, J.A., 1983. Mon. Not. R. astr. Soc., 204, 355.

Radevich, M.R. & Kraus, J.D., 1971. Astron. J., 76, 683.

Sandage, A., 1953. Astron. J., 58, 61.

Sandage, A., 1967. Astrophys. J., 150, L145.

Sandage, A., 1972. Astrophys. J., 178, 25.

Sandage, A., 1973. Astrophys. J., 183, 711.

Sandage, A., 1976. Astrophys. J., 205, 6.

Sarazin, C.L., Rood, H.J. & Struble, M.F., 1982. Astron. Astrophys. 108, L7.

Savage, A., 1976. Mon. Not. R. astr. Soc., 174, 259.

Schechter, P., 1976. Astrophys. J., 203, 297.

Scheuer, P.A.G. & Readhead, A.C.S., 1979. Nature, 277, 182.

Schilizzi, R.T., 1975. Mem. R. astr. Soc., 79, 75.

Schilizzi, R.T., Lockhart, I.A. & Wall, J.V., 1972. Aust. J. Phys., 25, 545.

Schilizzi, R.T. & McAdam, W.B., 1975. Mem. R. astr. Soc., 79, 1.

Schmidt, M., 1977. Astrophys. J., 217, 358.

Schneider, D.P., Gunn, J.E., & Hoessel, J.G., 1983. Astrophys. J., 268, 476.

Seldner, M., Siebers, B., Groth, E.J. & Peebles, P.J.E., 1977. Astr. J., 82, 249.

Shaffer, D.B., 1978. Astron. J., 83, 209.

Shane, C.D. & Wirtanen, C.A., 1967. Publ. Lick Obs., 22, Pt 1.

Shanks, T., Stevenson, P.R.F. & Fong, R., 1984. Mon. Not. R. astr. Soc., 206, 767.

Simkin, S.M., 1976. Astrophys. J., 204, 251.

Simon, A.J.B., 1978. Mon. Not. R. astr. Soc., 184, 537.

Smith, H.E. & Spinrad, H., 1980. P.A.S.P., 92, 553.

Smith, H.E., Spinrad, H. & Smith, E.O., 1976. P.A.S.P., 88, 621.

Stobie, 1982. Cosmos User Manual.

Stocke, J., 1979. Astrophys. J., 230, 40.

Stockton, A., 1978. Astrophys. J., 223, 747.

Stockton, A., 1980. in "Objects of High Redshift, IAU symp. 92", p. 89. ed. Abell, G.O. & Peebles, P.J.E., Reidel, Dordrecht.

Stockton, A., 1984. Invited Review Paper at the Third Asian-Pacific Regional Meeting of the IAU, Kyoto, Japan.

Sullivan, C. & Argue, A.N., 1980. Mon. Not. R. astr. Soc., 193, 921.

Thuan, T.X., & Romanishin, W., 1981. Astrophys. J., 248, 439.

Tritton, K.P., 1972. Mon. Not. R. astr. Soc., 158, 277.

Ulvestad, J., Johnston, K., Perley, R. & Fomalont, E., 1981. Astron. J. 86, 1010.

Van den Bergh, S., 1961. Astrophys. J., 134, 970.

Wall, J.V., 1977. In "Radio Astronomy and Cosmology, IAU Symp. 74", p. 55, ed D.L. Jauncey, D. Reidel, Dordrecht.

Wall, J.V. & Peacock, J.A., 1985. Mon. Not. R. astr. Soc., in press.

Westerlund, B.E. & Smith, C.F., 1966. Aust. J. Phys., 19, 181.

Wills, D. & Wills, B.J., 1966. Astrophys. J. Suppl., 31, 143.

Wirth, A., Smarr, L. & Gallagher, J.S., 1982. Astron. J., 87, 602.

Whiteoak, J.B., 1972. Aust. J. Phys., 25 233.

Wyndham, J.D., 1965. Astron. J., 70, 384.

Yee, H.K.C. & Green, F.R., 1984. Astrophys. J., 280, 79.

Yee, H.K.C. & Oke, J.B., 1978. Astrophys. J., 226, 753.

Zwicky, F. & Humason, M.L., 1964. Astrophys. J., 139, 269.

APPENDIX A: THE 233-SOURCE ALL-SKY SAMPLE

Table A.1 Contains the 233 source all-sky sample of Wall and Peacock (1985). The key to the columns is as follows:

(1) IAU name.

(2) Other name.

(3) & (4) Right Ascension (1950) and uncertainty in seconds of time. A C indicates that the position is the mid-point of a double source without a central component, in which case the error is given by (6).

(5) & (6) Declination (1950) and uncertainty in arcsec.

(7) Reference for position.

(8), (9) & (10) Flux densities at 1.4, 2.7 and 5GHz.

(11) Spectral index $\alpha^{5}_{2.7}$, defined in the sense $S_{\nu} \propto \nu^{-\alpha}$.

(12) Optical classification.

(13) V magnitude.

(14) Redshift; * indicates and estimate

Table A.1. The Wall and Peacock All-Sky Sample.

(1)	(2)	(3)	(4)	(5)	(6)	(7)	(8)	(9)	(10)	(11)	(12)	(13)	(14)
IAU	Name	R.A.		Dec.			S(1.4)	S(2.7)	S(5.0)		ID	V	z
0003-00	3C2	00 03 48.84	0.03	-00 21 06.0	0.4	24	3.54	2.40	1.41	0.86	Q	19.4	1.037
0008-42		00 08 21.30	0.01	-42 09 50.6	0.1	1	5.40	2.47	1.31	1.03	EF		1.600*
0022-42		00 22 15.42	0.01	-42 18 40.7	0.1	1	3.02	2.84	1.77	0.77	EF		1.600*
0023-26	OB-238	00 23 18.91	0.01	-26 18 49.3	0.1	1	9.00	5.80	3.76	0.70	G	19.5	0.398*
0034-01	3C15	00 34 30.56	0.02	-01 25 37.8	0.4	4	4.30	2.56	1.57	0.79	G	15.3	0.073
0035-02	3C17	00 35 47.18	0.02	-02 24 09.5	0.3	4	6.25	4.04	2.59	0.72	G	18.0	0.220
0038+09	3C18	00 38 14.57	0.12	09 46 56.1	4.1	6	4.26	3.00	1.62	1.00	G	18.5	0.188
0039-44		00 39 46.86	0.27	-44 30 28.6	2.4	7	4.30	2.08	1.17	0.93	G	18.5	0.251*
0040+51	3C20	00 40 19.99	C	51 47 08.1	5.0	8	10.79	6.51	4.18	0.72	G	19.0	0.350
0043-42		00 43 54.50	0.20	-42 24 01.0	3.0	5	9.10	5.00	2.93	0.87	G	16.0	0.053
0045-25	NGC253	00 45 05.60	0.20	-25 33 37.0	3.0	5	6.30	3.52	2.40	0.62	G	7.0	.0010
0055-01	3C29	00 55 01.57	0.02	-01 39 39.4	0.3	4	5.22	3.46	2.16	0.76	G	14.1	0.045
0104+32	3C31	01 04 39.17	0.02	32 08 44.3	0.6	8	5.22	3.53	2.10	0.84	G	12.2	0.017
0105-16	3C32	01 05 48.78	0.07	-16 20 21.1	1.2	7	3.80	2.25	1.14	1.10	G	20.1	0.525*
0106+13	3C33	01 06 14.94	C	13 04 26.4	24.0	9	12.59	8.02	5.03	0.76	G	15.2	0.060
0114-21	OC-224	01 14 25.95	0.01	-21 07 55.0	0.1	1	4.10	2.23	1.24	0.95	EF		1.600*
0116+31	4C31.04	01 16 47.25	0.01	31 55 05.8	0.1	1	2.54	2.12	1.46	0.61	G	14.5	0.059
0117-15	3C38	01 17 59.84	0.14	-15 35 57.3	2.1	7	4.70	2.72	1.56	0.90	G?	21.0	0.794*
0123-01	3C40	01 23 26.00	C	-01 36 20.0	40.0	25	6.42	3.29	1.88	0.91	G	12.3	0.018
0123+32	3C41	01 23 54.70	C	32 57 38.7	2.3	11	3.49	2.26	1.46	0.71	G	22.0	0.794
0131-36		01 31 43.54	0.02	-36 44 57.2	1.3	28	7.10	5.60	4.08	0.51	G	13.0	0.030
0133+20	3C47	01 33 40.42	0.01	20 42 10.6	0.5	12	3.68	2.00	1.16	0.88	Q	18.1	0.425
0133+47	OC457	01 33 55.11	0.01	47 36 12.8	0.1	1	2.17	2.22	3.26	-0.62	Q	18.0	0.860
0134+32	3C48	01 34 49.83	0.01	32 54 20.5	0.1	1	15.29	9.08	5.37	0.85	Q	16.2	0.367
0157-31	OC-397	01 57 58.51	0.11	-31 07 50.6	1.5	7	3.70	2.37	1.44	0.81	Q?	19.6	2.032*
0159-11	3C57	01 59 30.27	0.07	-11 47 00.2	1.3	7	2.90	2.00	1.35	0.64	Q	16.4	0.669
0202+14	4C15.05	02 02 07.40	0.01	14 59 51.0	0.1	1	3.40	3.00	2.30	0.43	G?	22.1	1.202*
0208-51		02 08 56.97	0.02	-51 15 07.5	0.2	4		3.56	3.21	0.17	Q	17.5	1.003
0210+86	3C61.1	02 10 45.20	C	86 05 08.2	18.0	9	6.06	3.77	1.68	1.31	G	19.0	0.186
0212+73		02 12 49.94	0.01	73 35 40.1	0.1	1		2.39	2.20	0.13	Q?	19.5	1.928*
0213-13	3C62	02 13 11.61	0.14	-13 13 24.0	3.6	7	5.00	2.79	1.77	0.74	G	18.0	0.200*
0220+42	3C66B	02 20 01.73	0.02	42 45 54.6	0.3	13	10.25	5.23	3.75	0.54	G	12.8	0.022
0235-19	OD-159	02 35 24.90	0.07	-19 45 29.3	1.2	7	4.40	2.41	1.41	0.87	G?	20.3	0.575*
0237-23	OD-263	02 37 52.79	0.01	-23 22 06.3	0.1	1	7.02	4.90	3.30	0.64	Q	16.6	2.223
0240-00	NGC1068	02 40 07.09	0.04	-00 13 30.7	0.6	24	4.87	3.13	1.93	0.78	G	9.0	.0041
0252-71		02 52 26.50	0.60	-71 16 43.0	4.0	5	5.90	3.10	1.54	1.14	G	18.0	0.200*
0255+05	3C75	02 55 05.10	0.50	05 50 44.0	8.0	6	6.22	3.30	1.94	0.86	G	13.6	0.024
0305+03	3C78	03 05 49.05	0.01	03 55 13.1	0.1	1	7.24	5.34	3.60	0.64	G	12.8	0.029
0307+16	3C79	03 07 11.35	0.02	16 54 36.8	1.0	14	4.59	2.50	1.41	0.93	G	18.5	0.256
0314+41	3C83.1B	03 14 56.79	0.02	41 40 32.6	0.3	14	9.35	4.92	3.53	0.54	G	13.3	0.026
0316+16	CTA21	03 16 09.14	0.01	16 17 40.4	0.1	1	7.60	4.77	2.93	0.79	G?	22.0	1.259*
0316+41	3C84	03 16 29.56	0.01	41 19 51.9	0.1	1	12.76	9.64	47.20	-2.58	G	11.9	0.017
0320-37	For A	03 20 46.80	0.30	-37 23 06.0	4.0	27		98.00	71.00	0.52	G	5.1	.0057
0325+02	3C88	03 25 18.90	0.40	02 23 22.0	0.4	6	4.85	3.18	1.95	0.79	G	14.0	0.030
0336-01	CTA26	03 36 58.95	0.01	-01 56 16.9	0.1	1	2.30	2.02	2.30	-0.21	Q	18.4	0.852
0347+05	4C05.16	03 47 06.97	0.11	05 42 35.2	2.6	7	3.25	2.00	1.24	0.78	G?	19.4	0.380*
0349-27	OE-283	03 49 36.90	2.40	-27 52 50.0	30.0	25	5.20	2.89	2.01	0.59	G	15.8	0.066
0356+10	3C98	03 56 10.49	C	10 17 16.4	25.0	8	9.56	5.80	3.29	0.92	G	14.4	0.031
0403-13	OF-105	04 03 14.20	0.20	-13 16 21.0	3.0	5	3.30	3.15	3.24	-0.05	Q	17.2	0.571
0404+76	4C76.03	04 04 00.13	0.16	76 48 52.5	0.2	15		4.05	2.79	0.60	G	22.2	1.380*
0404+03	3C105	04 04 48.07	0.04	03 32 49.7	0.6	24	4.93	3.54	2.39	0.64	G	18.5	0.089
0405-12	OF-109	04 05 27.45	0.05	-12 19 32.4	0.7	3	2.80	2.35	1.81	0.42	Q	17.1	0.574
0407-65		04 07 58.09	0.14	-65 52 49.2	1.3	7	15.00	6.50	3.28	1.11	Q?	18.0	0.871*
0409-75		04 09 58.94	0.31	-75 14 57.1	2.0	7	13.50	7.23	4.25	0.86	G?	21.5	1.000*
0410+11	3C109	04 10 54.85	0.01	11 04 39.5	0.5	14	4.09	2.50	1.77	0.56	G	17.9	0.306
0420-01		04 20 43.54	0.01	-01 27 28.8	0.1	1	1.70	2.15	2.14	0.01	Q	17.8	0.915
0428-53		04 28 00.00	2.00	-53 56 00.0	20.0	27	5.83	3.84	3.40	0.20	G	13.2	0.039
0428+20	OF247	04 28 06.86	0.01	20 31 09.1	0.1	1	3.81	3.18	2.30	0.53	G	20.0	0.219
0430+05	3C120	04 30 31.60	0.01	05 14 59.5	0.1	1	5.48	3.00	8.60	-1.71	G	14.1	0.033
0433+29	3C123	04 33 55.30	C	29 34 18.8	2.0	12	45.67	27.57	16.20	0.86	G	19.9	0.218

Table A.1. Continued.

(1)	(2)	(3)	(4)	(5)	(6)	(7)	(8)	(9)	(10)	(11)	(12)	(13)	(14)
IAU	Name	R.A.		Dec.			S(1.4)	S(2.7)	S(5.0)		ID	V	z
0438-43		04 38 43.18	0.01	-43 38 53.1	0.1	1	6.80	6.20	7.00	-0.20	Q	18.8	2.852
0440-00	OF-67	04 40 05.29	0.01	-00 23 20.6	0.1	1	3.18	3.73	3.13	0.28	Q	18.5	0.844
0442-28	OF-271	04 42 37.40	0.50	-28 15 18.0	7.0	6	7.10	3.84	2.16	0.93	G	17.4	0.151*
0451-28	OF-285	04 51 15.13	0.01	-28 12 29.3	0.1	1	2.50	2.38	2.50	-0.08	Q	18.5	2.564
0453-20	OF-289	04 53 14.13	0.15	-20 38 56.4	2.0	7	4.70	2.79	1.78	0.73	G	13.0	0.035
0453+22	3C132	04 53 42.05	C	22 44 43.4	1.0	8	3.25	2.10	1.13	1.01	G	19.0	0.214
0454-46		04 54 24.19	0.03	-46 20 38.5	0.2	4	2.60	2.36	2.04	0.24	Q	18.0	0.858
0500+01	OG3	05 00 45.18	0.01	01 58 53.8	0.1	1	2.21	2.47	1.85	0.47	EF		1.000*
0518+16	3C138	05 18 16.53	0.01	16 35 26.9	0.1	1	8.88	7.10	4.04	0.92	Q	17.9	0.759
0518-45	Pic A	05 18 23.00	0.50	-45 49 44.0	6.0	27	66.00	29.00	15.00	1.07	G	16.0	0.035
0521-36		05 21 12.90	0.06	-36 30 16.5	1.1	7	18.60	12.50	9.23	0.49	G	16.8	0.062
0528+13	OG147	05 28 06.76	0.01	13 29 42.2	0.1	1	2.19	2.97	3.86	-0.43	Q?	19.5	1.928*
0537-44		05 37 21.00	0.01	-44 06 46.8	0.1	1	2.70	3.84	3.80	0.02	Q	15.5	0.894
0538+49	3C147	05 38 43.51	0.01	49 49 42.8	0.1	1	22.05	13.14	8.18	0.77	Q	16.9	0.545
0605-08	OH-10	06 05 36.03	0.01	-08 34 20.3	0.1	1	2.50	2.70	3.39	-0.37	Q?	18.0	0.871*
0605+48	3C153	06 05 44.46	0.04	48 04 49.0	0.4	24	4.01	2.33	1.35	0.89	G	18.5	0.277
0620-52		06 20 34.30	0.40	-52 39 42.0	4.0	5	3.40	2.10	1.23	0.87	G	14.5	0.051
0625-53		06 25 19.23	0.12	-53 39 25.5	1.6	7	6.70	3.70	1.80	1.17	G	13.0	0.054
0625-35	OH-342	06 25 20.80	0.20	-35 27 20.0	3.0	5	4.50	2.90	2.09	0.53	G	14.0	0.055
0637-75		06 37 23.42	0.07	-75 13 37.4	0.2	4	6.70	4.51	5.49	-0.32	Q	15.8	0.651
0651+54	3C171	06 51 11.05	0.05	54 12 50.4	0.4	24	3.66	2.02	1.16	0.90	G	18.8	0.238
0735+17	OI158	07 35 14.13	0.01	17 49 09.3	0.1	1	1.92	2.00	2.05	-0.04	Q	14.9	0.424
0736+01	OI61	07 36 42.51	0.01	01 44 00.2	0.1	1	2.89	2.30	2.06	0.18	Q	16.5	0.191
0742+10	OI471	07 42 48.47	0.01	10 18 32.5	0.1	1	3.17	3.74	3.57	0.08	EF		2.000*
0743-67		07 43 22.19	0.05	-67 19 09.1	0.3	4	5.30	2.74	1.51	0.97	Q	16.4	0.395
0744+55	DA240	07 44 34.82	0.07	55 56 28.3	0.6	29		2.84		0.78	G	14.2	0.036
0802+24	3C192	08 02 32.31	C	24 18 54.9	10.0	8	4.89	3.30	2.13	0.71	G	15.5	0.060
0806-10	3C195	08 06 29.90	0.06	-10 19 09.7	1.4	7	3.40	2.49	1.60	0.72	G	17.8	0.182*
0809+48	3C196	08 09 59.42	0.04	48 22 07.2	0.4	24	13.85	7.75	4.35	0.94	Q	17.6	0.871
0814+42	OJ425	08 14 51.67	0.01	42 32 07.7	0.1	1	2.48	2.24	1.68	0.47	Q	16.9	0.486*
0825-20	OJ-242	08 25 03.49	0.06	-20 16 25.9	1.0	7	3.70	2.10	1.18	0.94	Q	18.0	0.871*
0831+55	4C55.16	08 31 04.38	0.01	55 44 41.4	0.1	1	8.04	7.54	5.60	0.48	G	17.5	0.242
0834-20	OJ-257.5	08 34 24.60	0.01	-20 06 30.4	0.1	1	3.50	4.15	3.42	0.31	Q	19.0	2.752
0834-19	OJ-158.1	08 34 56.15	0.03	-19 41 25.4	0.4	2	4.60	2.50	1.51	0.82	G?	20.7	0.692*
0836+71	4C71.07	08 36 21.56	0.01	71 04 22.5	0.1	1		3.15	2.57	0.33	Q?	16.5	0.394*
0842-75		08 42 10.73	0.26	-75 29 36.3	1.6	7	4.30	2.15	1.38	0.72	Q	18.9	0.524
0851+20	OJ287	08 51 57.25	0.01	20 17 58.4	0.1	1	1.59	3.42	2.61	0.44	Q	14.0	0.306
0858-27	OJ-297	08 58 31.70	0.30	-27 56 33.0	4.0	5	2.20	2.00	1.38	0.60	Q?	16.2	0.336*
0859-25	OJ-299	08 59 36.63	0.13	-25 43 38.8	1.7	7	5.80	3.30	1.70	1.08	G	21.0	0.794*
0859-14	OJ-199	08 59 54.94	0.01	-14 03 38.9	0.1	1	3.10	2.93	2.29	0.40	Q	16.6	1.327
0906+43	3C216	09 06 17.25	0.04	43 05 59.4	0.4	24	3.76	2.42	1.78	0.50	Q	18.5	0.668
0915-11	Hyd A	09 15 41.50	0.30	-11 53 06.0	7.0	6	37.40	23.50	13.50	0.90	G	14.8	0.052
0917+45	3C219	09 17 50.70	0.02	45 51 44.2	0.1	10	8.02	4.40	2.29	1.06	G	17.3	0.174
0923+39	4C39.25	09 23 55.32	0.01	39 15 23.5	0.1	1	2.52	4.60	8.90	-1.07	Q	17.9	0.699
0936+36	3C223	09 36 50.86	0.03	36 07 34.7	0.7	14	3.35	2.09	1.29	0.78	G	17.1	0.137
0945+07	3C227	09 45 07.80	0.50	07 39 09.0	5.0	6	7.40	4.30	2.60	0.82	G	16.3	0.086
0951+69	M82	09 51 41.95	0.01	69 54 57.5	0.1	16	7.94	5.66	3.94	0.59	G	8.4	.0014
0954+55	4C55.17	09 54 14.36	0.01	55 37 16.4	0.1	1	3.52	2.63	2.27	0.24	Q	17.7	0.909
0958+29	3C234	09 58 57.38	0.01	29 01 37.4	0.2	14	5.35	2.96	1.54	1.06	G	17.1	0.185
1003+35	3C236	10 03 05.39	0.01	35 08 48.0	0.2	8	3.24	2.03	1.32	0.70	G	16.0	0.099
1005+07	3C237	10 05 22.02	0.03	07 44 58.6	0.4	24	6.25	3.50	1.93	0.97	G?	21.3	0.912*
1015-31	OL-327	10 15 53.39	0.01	-31 29 11.3	0.1	1	3.50	2.22	1.32	0.84	G?	20.2	0.550*
1017-42		10 17 56.23	0.12	-42 36 21.9	1.3	7	4.10	2.33	1.20	1.08	Q?	19.0	1.479*
1040+12	3C245	10 40 06.00	0.03	12 19 15.1	0.4	24	3.06	2.00	1.41	0.57	Q	17.3	1.029
1055+01	4C01.28	10 55 55.32	0.01	01 50 03.5	0.1	1	3.10	3.02	3.07	-0.03	Q	17.7	0.888
1127-14	OM-146	11 27 35.67	0.01	-14 32 54.4	0.1	1	6.20	6.50	7.25	-0.18	Q	16.9	1.187
1136-13	OM-161	11 36 38.51	0.08	-13 34 05.4	1.1	3	4.10	2.80	1.88	0.65	Q	17.8	0.554
1142+19	3C264	11 42 29.58	0.02	19 53 02.7	0.4	17	5.78	3.27	2.36	0.53	G	12.8	0.021
1148-00	4C-00.47	11 48 10.13	0.01	-00 07 13.3	0.1	1	2.90	2.58	1.95	0.45	Q	17.6	1.982
1151-34	OM-386	11 51 49.44	0.01	-34 48 47.2	0.1	1	6.40	4.18	2.74	0.69	Q	17.5	0.258

Table A.1. Continued.

(1)	(2)	(3)	(4)	(5)	(6)	(7)	(8)	(9)	(10)	(11)	(12)	(13)	(14)
IAU	Name	R.A.		Dec.			S(1.4)	S(2.7)	S(5.0)		ID	V	z
1157+73	3C268.1	11 57 49.30	C	73 17 26.5	4.0	8	7.04	4.05	2.63	0.70	G	22.0	0.970*
1203+64	3C268.3	12 03 54.08	0.03	64 30 18.5	0.1	12	3.53	2.00	1.16	0.88	G	19.0	0.371
1216+06	3C270	12 16 51.20	1.00	06 06 13.0	6.0	6	17.50	12.80	9.04	0.56	G	10.4	.0069
1222+13	M84	12 22 31.58	0.02	13 09 50.7	1.5	8	6.24	4.30	2.72	0.74	G	8.7	.0028
1226+02	3C273	12 26 33.25	0.01	02 19 43.3	0.1	1	38.84	38.90	40.00	-0.05	Q	12.8	0.158
1228+12	Vir A	12 28 17.56	0.01	12 40 02.0	0.3	18	214.00	120.00	67.60	0.93	G	8.7	.0038
1245-19	ON-176.2	12 45 45.22	0.01	-19 42 57.5	0.1	1	5.50	3.94	2.47	0.76	G?	19.5	0.398*
1246-41	NGC4696	12 46 03.27	0.15	-41 02 21.4	1.7	7	4.10	2.21	1.33	0.82	G	11.2	.0090
1251-12	3C278	12 51 59.60	0.50	-12 17 08.0	6.0	6	6.80	4.50	2.54	0.93	G	13.5	0.015
1253-05	3C279	12 53 35.84	0.01	-05 31 08.0	0.1	1	10.40	11.20	16.10	-0.59	Q	17.8	0.538
1254+47	3C280	12 54 41.36	C	47 36 32.1	1.3	12	5.08	2.86	1.53	1.02	G	22.0	0.996
1306-09	OP-10	13 06 02.20	0.20	-09 34 33.0	3.0	5	4.40	2.80	1.88	0.65	G?	20.5	0.631*
1308-22	3C283	13 08 57.40	0.03	-22 00 46.7	0.4	2	5.40	2.43	1.09	1.30	G?	21.5	1.000*
1318-43	NGC5090	13 18 14.00	C	-43 26 57.0	30.0	25	5.86	3.09	1.71	0.96	G	14.5	0.011
1322-42	Cen A	13 22 32.23	C	-42 45 25.0	40.0	26		128.00	61.00	1.20	G	7.0	.0008
1323+32	4C32.44	13 23 57.92	0.01	32 09 43.0	0.1	1	4.56	3.35	2.31	0.60	G?	19.0	0.316*
1328+25	3C287	13 28 15.93	0.01	25 24 37.4	0.1	1	6.72	4.60	3.08	0.65	Q	17.7	1.055
1328+30	3C286	13 28 49.66	0.01	30 45 58.6	0.1	1	14.78	10.38	7.48	0.53	Q	17.3	0.849
1333-33	IC4296	13 33 47.18	0.07	-33 42 39.8	0.9	3	11.96	10.06	6.19	0.79	G	11.1	0.013
1345+12	4C12.50	13 45 06.17	0.01	12 32 20.3	0.1	1	5.01	3.80	2.89	0.44	G	17.0	0.122
1350+31	3C293	13 50 03.23	0.03	31 41 32.6	0.4	24	4.42	2.93	1.87	0.73	G	14.4	0.045
1355-41		13 55 56.83	0.12	-41 38 16.7	1.5	7	4.60	2.49	1.40	0.93	Q	16.0	0.313
1358+62	4C62.22	13 58 58.36	0.01	62 25 06.7	0.1	1	4.32	2.69	1.77	0.68	G	20.2	0.525*
1409+52	3C295	14 09 33.50	0.04	52 26 13.0	0.4	24	22.18	11.94	6.48	0.99	G	20.1	0.461
1414+11	3C296	14 14 26.36	0.04	11 02 18.6	1.2	19	4.32	2.73	1.71	0.76	G	12.2	0.024
1416+06	3C298	14 16 38.77	0.03	06 42 20.9	0.4	2	5.66	2.70	1.52	0.93	Q	16.8	1.439
1424-41		14 24 46.73	0.07	-41 52 54.4	1.0	3	3.50	2.63	2.12	0.35	Q?	17.5	0.668*
1453-10	OQ-190	14 53 12.32	0.07	-10 56 51.0	1.5	7	3.70	2.50	1.41	0.93	Q	17.4	0.940
1458+71	3C309.1	14 58 56.64	0.01	71 52 11.2	0.1	20	8.50	5.36	3.33	0.77	Q	16.8	0.904
1502+26	3C310	15 02 46.88	0.02	26 12 35.4	0.7	8	7.67	3.10	1.26	1.46	G	15.3	0.054
1504-16	OR-107	15 04 16.42	0.01	-16 40 59.3	0.1	1	2.70	2.30	1.96	0.26	Q	18.5	0.876
1508-05	4C-05.64	15 08 14.98	0.01	-05 31 49.0	0.1	1	3.90	2.50	2.33	0.11	Q	17.0	1.191
1510-08	OR-107	15 10 08.90	0.01	-08 54 47.6	0.1	1	3.00	3.00	3.25	-0.13	Q	16.3	0.361
1511+26	3C315	15 11 30.81	0.02	26 18 39.4	0.4	8	3.87	2.10	1.31	0.77	G	16.8	0.108
1514+07	3C317	15 14 17.08	0.07	07 12 16.2	1.9	7	5.35	2.20	0.93	1.40	G	13.5	0.035
1514-24	Ap Lib	15 14 45.28	0.01	-24 11 22.6	0.1	1	2.70	2.10	1.94	0.13	Q	15.0	0.049
1518+04	4C04.51	15 18 44.73	0.03	04 41 05.5	0.4	24	4.01	2.20	1.00	1.28	EF		1.600*
1529+24	3C321	15 29 33.50	0.03	24 14 26.5	1.0	8	3.59	2.20	1.09	1.14	G	16.0	0.096
1547-79		15 47 39.15	0.41	-79 31 42.4	2.1	7	4.00	2.28	1.35	0.85	G	18.0	0.200*
1549-79		15 49 28.38	0.21	-79 05 17.8	0.3	4	6.20	4.02	4.50	-0.18	G	18.8	0.288*
1559+02	3C327	15 59 58.60	2.00	02 06 24.0	30.0	25	8.95	5.04	2.81	0.95	G	15.9	0.104
1600+33	4C33.38	16 00 11.91	0.01	33 35 09.6	0.1	1	2.36	2.26	1.51	0.65	EF		2.000*
1602+01	3C327.1	16 02 12.96	0.02	01 25 58.7	0.3	4	4.07	2.14	1.11	1.07	G	20.5	0.480*
1607+26	CTD93	16 07 09.29	0.01	26 49 18.6	0.1	1	4.43	3.04	1.56	1.08	G?	21.0	0.794*
1609+66	3C330	16 09 13.90	C	66 04 22.8	6.0	8	6.98	3.76	2.35	0.76	G	20.3	0.549
1610-77		16 10 51.75	0.10	-77 09 52.6	0.3	4	5.00	3.37	5.55	-0.81	Q	19.0	1.710
1611+34	OS319	16 11 47.92	0.01	34 20 19.8	0.1	1	2.92	2.45	2.67	-0.14	Q	17.5	1.401
1622-25	OS-237.8	16 22 44.11	0.01	-25 20 51.5	0.1	1	1.60	2.27	2.20	0.19	G?	21.9	1.202*
1633+38	4C38.41	16 33 30.63	0.01	38 14 10.1	0.1	1	2.01	2.53	4.08	-0.78	Q	18.0	1.814
1634+62	3C343	16 34 01.08	0.01	62 51 41.6	0.1	1	5.17	2.71	1.50	0.96	Q	20.6	0.988
1637-77		16 37 05.50	0.90	-77 09 55.0	4.0	5	6.50	3.77	2.58	0.62	G	16.0	0.043
1637+62	3C343.1	16 37 55.31	0.01	62 40 34.3	0.1	1	4.66	2.26	1.20	1.03	G	20.7	0.750
1637+82	NGC6251	16 37 56.95	0.01	82 38 18.5	0.1	30		2.17		0.70	G	13.0	0.024
1641+39	3C345	16 41 17.61	0.01	39 54 10.8	0.1	1	6.30	6.08	10.90	-0.95	Q	16.0	0.594
1641+17	3C346	16 41 34.55	0.04	17 21 20.6	0.5	24	3.64	2.20	1.34	0.80	G	17.2	0.161
1648+05	Her A	16 48 40.10	0.50	05 04 28.0	5.0	6	44.43	24.60	12.41	1.11	G	16.9	0.154
1704+60	3C351	17 04 03.51	0.07	60 48 31.3	0.6	9	3.52	2.05	1.21	0.86	Q	15.3	0.371
1717-00	3C353	17 17 56.80	0.20	-00 55 49.0	4.0	5	56.22	33.80	20.20	0.84	G	15.4	0.030
1733-56		17 33 20.40	1.20	-56 32 26.0	10.0	27	8.40	5.20	3.32	0.73	G?	17.0	0.126*
1740-51		17 40 27.00	0.30	-51 43 25.0	2.0	5		4.60	2.95	0.72	G	19.2	0.347*

Table A.1. Continued.

(1)	(2)	(3)	(4)	(5)	(6)	(7)	(8)	(9)	(10)	(11)	(12)	(13)	(14)
IAU	Name	R.A.		Dec.			S(1.4)	S(2.7)	S(5.0)		ID	V	z
1741-03	OT-68	17 41 20.62	0.01	-03 48 48.9	0.1	1	1.00	3.05	3.63	-0.28	Q?	18.5	1.135*
1803+78		18 03 39.18	0.01	78 27 54.3	0.1	1		2.36	2.63	-0.18	G?	13.8	0.029*
1814-63		18 14 46.13	0.20	-63 47 00.9	1.6	7	14.20	7.50	4.29	0.91	G	16.0	0.063
1828+48	3C380	18 28 13.54	0.04	48 42 40.5	0.4	24	14.11	10.00	6.19	0.78	Q	16.8	0.691
1832+47	3C381	18 32 24.40	C	47 24 36.5	7.0	14	3.79	2.33	1.29	0.96	G	17.5	0.161
1839-48		18 39 27.10	0.30	-48 39 39.0	3.0	5	3.70	2.00	1.26	0.75	G	16.5	0.100*
1842+45	3C388	18 42 35.45	0.02	45 30 21.6	0.2	12	5.57	3.15	1.77	0.94	G	15.7	0.091
1845+79	3C390.3	18 45 37.57	0.04	79 43 06.4	0.1	21	12.33	6.64	4.32	0.70	G	14.4	0.057
1928+73	4C73.18	19 28 49.35	0.01	73 51 44.9	0.1	1		3.42	3.34	0.04	Q	15.5	0.360
1932-46		19 32 18.91	0.12	-46 27 23.9	1.2	7	13.40	6.54	3.47	1.03	G	18.9	0.302*
1934-63		19 34 47.65	0.14	-63 49 34.7	1.6	7	16.00	11.10	6.45	0.88	G	18.4	0.183
1938-15	OV-164	19 38 24.80	0.20	-15 31 34.0	4.0	5	6.90	3.80	2.29	0.82	G?	21.5	1.000*
1939+60	3C401	19 39 38.84	0.05	60 34 32.6	0.5	8	4.75	2.79	1.52	0.99	G	19.1	0.201
1949+02	3C403	19 49 44.13	0.09	02 22 41.5	2.1	7	5.85	3.68	2.35	0.73	G	15.4	0.059
1954-55		19 54 18.90	0.40	-55 17 42.0	4.0	5	7.00	3.74	2.31	0.78	G	16.3	0.060
1954-38		19 54 39.06	0.01	-38 53 13.3	0.1	1	1.59	2.00	2.00	0.00	Q	17.5	0.630
2008-06	OW-15	20 08 33.70	0.01	-06 53 01.8	0.1	1	3.65	2.20	1.33	0.82	G?	21.6	1.047*
2021+61	OW637	20 21 13.30	0.01	61 27 18.1	0.1	1	2.20	2.17	2.31	-0.10	G	19.5	0.227
2032-35	OW-354	20 32 37.20	0.12	-35 04 29.6	1.4	7	6.40	3.70	1.88	1.10	G?	21.5	1.000*
2052-47		20 52 50.13	0.03	-47 26 19.6	0.2	4	3.00	2.20	2.45	-0.17	Q	17.8	1.489
2058-28	OW-297.8	20 58 39.50	2.50	-28 13 15.0	30.0	25	6.70	3.10	1.96	0.74	G	14.6	0.038
2104-25	OX-208	21 04 25.30	2.50	-25 37 58.0	30.0	25	12.00	7.30	4.23	0.89	G	15.8	0.037
2106-41		21 06 19.39	0.01	-41 22 33.4	0.1	1	1.98	2.11	2.28	-0.13	Q?	20.0	2.512*
2121+24	3C433	21 21 31.00	C	24 51 36.0	10.0	12	11.68	7.00	3.62	1.07	G	15.5	0.102
2128+04	OX46	21 28 02.61	0.01	04 49 04.3	0.1	1	3.98	3.12	2.07	0.67	EF		2.000*
2128-12	OX-148	21 28 52.67	0.01	-12 20 20.6	0.1	1	1.80	2.00	2.00	0.00	Q	16.0	0.501
2134+00	OX57	21 34 05.21	0.01	00 28 25.1	0.1	1	3.13	7.60	12.38	-0.79	Q	18.0	1.936
2135-14	OX-158	21 35 00.10	0.30	-14 46 27.0	4.0	5	3.00	2.00	1.36	0.63	Q	15.5	0.200
2135-20	OX-258	21 35 01.32	0.01	-20 56 03.7	0.1	1	3.78	2.49	1.50	0.82	G	19.4	0.380*
2145+06	4C06.69	21 45 36.08	0.01	06 43 40.9	0.1	1	2.97	3.10	4.57	-0.63	Q	16.5	0.990
2150-52		21 50 48.17	0.18	-52 04 23.9	1.8	7	4.20	2.10	1.17	0.95	G?	22.2	1.380*
2152-69		21 52 58.60	0.80	-69 55 50.0	8.0	5	30.39	19.27	12.44	0.71	G	14.0	0.027
2153+37	3C438	21 53 45.42	C	37 46 13.1	2.0	8	6.70	3.26	1.54	1.22	G	19.2	0.290
2200+42	B1 Lac	22 00 39.36	0.01	42 02 08.6	0.1	1	4.60	5.21	4.75	0.15	Q	14.5	0.069
2203-18	OY-106	22 03 25.73	0.01	-18 50 17.1	0.1	1	6.20	5.20	4.24	0.33	Q	19.0	0.618
2211-17	3C444	22 11 42.51	0.07	-17 16 33.7	1.2	7	7.90	4.52	2.08	1.26	G	18.0	0.153
2221-02	3C445	22 21 15.50	2.00	-02 21 16.0	30.0	25	5.59	3.46	2.25	0.70	G	15.8	0.056
2223-05	3C446	22 23 11.05	0.04	-05 12 17.4	0.7	3	6.00	4.40	4.31	0.03	Q	18.4	1.404
2229+39	3C449	22 29 07.60	0.03	39 06 03.4	0.6	19	3.62	2.50	1.39	0.95	G	13.2	0.017
2230+11	CTA102	22 30 07.80	0.01	11 28 22.8	0.1	1	6.01	5.30	3.50	0.67	Q	17.5	1.037
2243+39	3C452	22 43 32.81	0.01	39 25 27.6	0.2	14	10.53	5.94	3.26	0.97	G	16.0	0.081
2243-12	OY-172.6	22 43 39.80	0.01	-12 22 40.3	0.1	1	2.54	2.74	2.38	0.23	Q	17.3	0.630
2245-32	OY-376	22 45 51.53	0.01	-32 51 42.2	0.1	1	1.37	2.01	1.80	0.18	Q	18.6	2.268
2250-41		22 50 12.25	0.15	-41 13 44.4	1.7	7	5.20	2.34	1.27	0.99	G	19.0	0.316*
2251+15	3C454.3	22 51 29.52	0.01	15 52 54.3	0.1	1	11.84	10.00	23.30	-1.37	Q	16.1	0.860
2314+03	3C459	23 14 02.27	0.03	03 48 55.2	0.4	24	4.17	2.36	1.30	0.97	G	17.6	0.220
2326-47		23 26 33.72	0.02	-47 46 51.8	0.2	4	2.82	2.34	2.46	-0.08	Q	16.0	1.299
2331-41		23 31 45.37	0.13	-41 42 02.5	1.3	7	5.70	2.66	1.52	0.91	G	18.0	0.200*
2335+26	3C465	23 35 58.95	0.01	26 45 16.4	0.1	22	7.51	4.00	2.12	1.03	G	13.2	0.029
2342+82		23 42 06.35	0.02	82 10 01.3	0.1	23		2.33	1.30	0.95	EF		1.000*
2345-16	OZ-176	23 45 27.69	0.01	-16 47 52.6	0.1	1	1.20	4.08	3.47	0.26	Q	18.0	0.600
2352+49	OZ488	23 52 37.79	0.01	49 33 26.8	0.1	1	2.93	2.21	1.77	0.36	G	19.0	0.237
2356-61		23 56 30.00	C	-61 11 30.0	36.0	27	23.70	10.22	4.43	1.36	G	16.0	0.096

APPENDIX B: A Method of Finding the Weighted Mean of a Set of Measurements in the Presence of "Cosmic Scatter"

Assume we have a set of values x_i, which are drawn from a distribution of mean μ, and variance σ, but which have in addition individual measurement errors σ_i. We wish to find the appropriate values of the weights, w_i to calculate the weighted mean of the set of values.

We will use normalised weights, $\Sigma w_i = 1$.

Assume that w_i and $(x_i - \mu)$ are uncorrelated, so that $\langle x \rangle = \mu$.

We wish the variance of $\bar{x}$.

Now:

$$\bar{x}^2 = \sum_i \sum_j w_i w_j x_i x_j \qquad \text{(B.1)}$$

$$\begin{aligned} \langle x_i x_j \rangle &= \mu^2 , \quad i = j \\ &= \mu^2 + \sigma^2 + \sigma_i^2 , \quad i = j \end{aligned} \qquad \text{(B.2)}$$

hence

$$\begin{aligned} \langle \bar{x}^2 \rangle &= \mu^2 \left((\Sigma w_i)^2 - \Sigma w_i^2 \right) \\ &+ \Sigma w_i^2 \left(\mu^2 + \sigma^2 + \sigma_i^2 \right) \end{aligned}$$

$$= \mu^2 (\Sigma w_i)^2 + \Sigma w_i^2 (\sigma^2 + \sigma_i^2) \qquad \text{(B.3)}$$

so the variance of $\bar{x}$

$$< \bar{x}^2 > - < \bar{x} >^2 = \Sigma\, w_i^2 \, (\sigma^2 + \sigma_i^2) \qquad \text{(B.4)}$$

To find the minimum variance, $\partial / \partial w_i = 0$. But we need to keep the normalisation, and hence set

$$\frac{\partial}{\partial w_i} \quad \frac{\Sigma\, w_i^2 \, (\sigma^2 + \sigma_i^2)}{\Sigma\, w_i} = 0. \qquad \text{(B.5)}$$

$$\Rightarrow \quad \frac{2\, \Sigma\, w_i \, (\sigma^2 + \sigma_i^2)}{\Sigma\, w_i} - \frac{\Sigma\, w_i \, (\sigma^2 + \sigma_i^2)}{\Sigma\, w_i} \qquad \text{(B.6)}$$

and so the weights

$$w_i \propto \frac{1}{\sigma^2 + \sigma_i^2} \qquad \text{(B.7)}$$

and

$$\bar{x} = \frac{\Sigma\, \dfrac{x_i}{\sigma^2 + \sigma_i^2}}{\Sigma\, \dfrac{1}{\sigma^2 + \sigma_i^2}} \pm \frac{\sqrt{\Sigma\, \dfrac{1}{\sigma^2 + \sigma_i^2}}}{\Sigma\, \dfrac{1}{\sigma^2 + \sigma_i^2}} \qquad \text{(B.8)}$$

Thus we have a formula to calculate the weighted mean, given the known measurement errors, and the value of σ. We can calculate σ as follows.

The weighted r.m.s. is given by:

$$\overline{x^2} = \Sigma\ w_i\ (\ x_i - \bar{x}\ )^2 \qquad (B.9)$$

$$= \Sigma\ w_i x_i^2 - \bar{x}^2 \qquad (B.10)$$

Hence:

$$< \overline{x^2} > = \Sigma\ w_i\ (\ \mu^2 + \sigma^2 + \sigma_i^2\ ) - (\ \mu^2 + \Sigma w_i^2\ (\sigma^2 + \sigma_i^2) \qquad (B.11)$$

$$= (\ w_i - w_i^2\ )\ (\ \sigma^2 + \sigma_i^2\ ) \qquad (B.12)$$

Thus the process is as follows. Assume an initial guess for the weights (e.g. $w_i = 1/n$). Then we can calculate an initial value of $\bar{x}$. This allows us to obtain a value of σ from equation B.12. This may then be used to obtain an improved value of the weights, and the process repeated until the value of σ converges. The final mean and error, along with the value of the 'cosmic scatter' can then be calculated from B.8.